CLIMATE TRENDS, VARIABILITY AND EXTREMES IN THE ADRIATIC REGION BASED ON KILOMETRE–SCALE MODELLING

Tojčić, Iva

University of Zagreb

Faculty of Science
Department of Geology

Iva Tojčić

CLIMATE TRENDS, VARIABILITY AND EXTREMES IN THE ADRIATIC REGION BASED ON KILOMETRE–SCALE MODELLING

DOCTORAL DISSERTATION

Zagreb, 2024

Faculty of Science
Department of Geology

Iva Tojčić

CLIMATE TRENDS, VARIABILITY AND EXTREMES IN THE ADRIATIC REGION BASED ON KILOMETRE–SCALE MODELLING

DOCTORAL DISSERTATION

Supervisor: Dr. Cléa Lumina Denamiel

Zagreb, 2024

Sveučilište u Zagrebu

Prirodoslovno–matematički fakultet
Geološki odsjek

Iva Tojčić

KLIMATSKI TRENDOVI, VARIJABILNOST I EKSTREMI U JADRANSKOM PODRUČJU NA TEMELJU MODELIRANJA NA KILOMETARSKOJ SKALI

DOKTORSKI RAD

Mentorica: dr. sc. Cléa Lumina Denamiel

Zagreb, 2024

This doctoral dissertation was written as part of the University Postgraduate Doctoral Study in Oceanology at the Department of Geology, Faculty of Science, University of Zagreb, under the supervision of Dr. Cléa Lumina Denamiel. The research was carried out in the Laboratory for physical chemistry of aquatic systems of the Ruđer Bošković Institute as part of the project "Numerical modelling of the Adriatic-Ionian decadal and inter-annual oscillations: from realistic simulations to process-oriented experiments" (ECMWF Special Project) and with the financing of the Croatian Science Foundation (DOK-2021-02-7189).

ACKNOWLEDGEMENTS

I would like to express my deepest gratitude to my mentor, Clea, who has devoted countless hours working with me and teaching me all the wonders of programming and modelling. Her guidance and expertise have been invaluable on this journey, and I am profoundly grateful for her support and time.

Velika zahvala i profesoru Ivici Vilibiću, koji je vjerovao u moje sposobnosti i pružio mi priliku da zakoračim u svijet znanosti na njegovom projektu, na samom početku moje karijere.

Hvala članovima povjerenstva za ocjenu ovog doktorskog rada, profesorima Belušiću, Kovaču i Vilibiću, na njihovim komentarima i sugestijama, koje su značajno doprinijele kvaliteti konačne verzije rada.

Najveće hvala mojoj mami i bratu, koji su mi tijekom cijelog školovanja pružali bezuvjetnu podršku i vjerovali u mene na svakom koraku. Bili ste moj vjetar u leđa i neizmjerno sam zahvalna i sretna što ste uvijek našli vremena i razumijevanja za mene i sve moje priče o ispitima, prezentacijama, rokovima i ostalim brigama s kojima se doktorand susreće. Znali ste kako mi olakšati, utješiti me i motivirati. Hvala vam što ste uvijek bili tu za mene i omogućili mi da ispunim svoje ciljeve. Sigurna sam da je tata ponosan na sve nas, jer je ovo naš zajednički uspjeh.

Važnu ulogu na ovom putu imao je i moj Dario, kojem se zahvaljujem na nesebičnoj podršci, strpljenju, savjetima i ohrabrenju u trenucima kada su izazovi izgledali nepremostivo. Hvala ti što si uvijek bio moj oslonac.

Hvala i mojoj kolegici i prijateljici, Petri, s kojom sam diskutirala probleme na koje sam naišla tijekom istraživanja i svladavala tremu prije važnih ispita i konferencija na kojima smo zajedno sudjelovale, a koja je cijeli ovaj proces učinila lakšim i zabavnijim.

Naposljetku, hvala svim mojim prijateljima i prijateljicama, mojoj baki, Tanji i maloj Ivani, što su svaki moj dosadašnji uspjeh i korak na ovom putu slavili kao svoj, razumjeli kada nisam imala vremena za druženje zbog posla i učenja i koji su vjerovali u mene kada sam i sama sumnjala hoću li uspjeti *dogurati* do kraja. Bili ste u pravu, uspjela sam! Hvala vam na podršci.

University of Zagreb
Faculty of Science
Department of Geology

Doctoral thesis

CLIMATE TRENDS, VARIABILITY AND EXTREMES IN THE ADRIATIC REGION BASED ON KILOMETRE–SCALE MODELLING

Iva Tojčić

ABSTRACT

This thesis explores the novel application of an ultra-high-resolution atmosphere-ocean model, Adriatic Sea and Coast (AdriSC), to simulate the complex climate of the Adriatic region. The kilometre-scale resolution of AdriSC allows for the precise simulation of local processes such as bora dynamics and dense water formation, which are crucial in shaping the regional climate. The model proves effective in capturing the BiOS–driven variability in the Adriatic Sea, previously unaddressed by coarser resolution models. Extensive and profound changes in trends, variability, and extremes in the Adriatic region, due to ongoing and projected future climate variations, are identified and quantified: (1) strong land-sea contrasts in the atmosphere, (2) intensification of the heatwaves and most likely of the extreme rainfalls and droughts, (3) dense water formation in the northern Adriatic likely to be strongly reduced, (4) potential intensification of the surface saline lake effect during summer, (5) southern Adriatic cyclonic gyre likely to be shrinking and intensifying, and (6) strengthening of the vertical stratification over the SAP. Given the potential negative impact of these climate events for environment, humans, and for various economic sectors, understanding, and predicting these changes is crucial for policymakers and local communities to develop effective adaptation and mitigation strategies. Consequently, the AdriSC climate simulation might be eventually generalized by implementing and running an ensemble of kilometre-scale atmosphere-ocean models under more climate scenarios in the Adriatic region, but in a smart way taking into account an extensive computational demand that such simulations require.

(190 pages, 60 figures, 9 tables, 293 references, original in English)
Keywords: Adriatic region, far-future climate, extreme warming, kilometre-scale atmosphere-ocean modelling

Supervisor: Dr. Cléa Lumina Denamiel
Reviewers: Prof. Danijel Belušić
Dr. Žarko Kovač
Dr. Ivica Vilibić

Sveučilište u Zagrebu
Prirodoslovno–matematički fakultet
Geološki odsjek

Doktorski rad

KLIMATSKI TRENDOVI, VARIJABILNOST I EKSTREMI U JADRANSKOM PODRUČJU NA TEMELJU MODELIRANJA NA KILOMETARSKOJ SKALI

Iva Tojčić

SAŽETAK

Ova disertacija istražuje primjenu združenog atmosfersko-oceanskog modela ultra-visoke rezolucije, Adriatic Sea and Coast (AdriSC), za simulaciju složene klime jadranskog područja. Kilometarska razlučivost AdriSC modela omogućuje vjerodostojnu simulaciju lokalnih procesa poput dinamike bure i stvaranja guste vode, koji su ključni za oblikovanje regionalne klime atmosphere i mora. Model se pokazao učinkovitim u reproduciranju varijabilnosti u Jadranskom moru uzrokovanoj Jadransko-jonskom bimodalnom oscilacijom (BiOS), što prijašnji modeli, s grubljom razlučivosti, nisu postigli. Identificirane su i kvantificirane sveobuhvatne i značajne promjene u trendovima, varijabilnosti i ekstremima u jadranskom području zbog aktualnih i predviđenih budućih klimatskih promjena: (1) snažni kontrasti kopno-more u atmosferi, (2) intenzifikacija toplinskih valova i posljedično ekstremnih oborina i suša, (3) smanjenje stvaranja guste vode u sjevernom Jadranu, (4) potencijalno jačanje efekta površinskih slanih jezera tijekom ljeta, (5) smanjenje obujma uz istovremeno jačanje južnojadranskog ciklonalnog vrtloga, te (6) jačanje vertikalne stratifikacije u Južnojadranskoj kotlini. S obzirom na negativne učinke takvih klimatskih promjena na ljude i različite gospodarske sektore, razumijevanje i predviđanje ovih promjena ključno je za donositelje odluka i lokalne zajednice kako bi razvili učinkovite strategije prilagodbe i ublažavanja. Stoga je preporuka ovaj prototip kilometarskog klimatskog modela primijeniti i za analize ansambla klimatskih simulacija za više scenarija klimatskih promjena u jadranskom području, pri tom primijenjujući "pametnu" optimizaciju računalnih resursa koje ovakve simulacije zahtijevaju.

(190 stranica, 60 slika, 9 tablica, 293 literaturna navoda, jezik izvornika: engleski)

Ključne riječi: jadransko područje, buduća klima, ekstremno zagrijavanje, modeliranje atmosfere i mora na kilometarskoj skali

Mentorica: dr. sc. Cléa Lumina Denamiel

Ocjenjivači: prof. dr. sc. Danijel Belušić
izv. prof. dr. sc. Žarko Kovač
dr. sc. Ivica Vilibić

Table of contents

1. INTRODUCTION

1.1 Adriatic atmosphere–ocean interactions and climate

The Adriatic is a region of high complexity, both in terms of its geography and the number of environmental processes at play — ranging from long–term processes on larger spatial scales (e.g. Adriatic Sea thermohaline circulation) to short–term processes which vary on smaller spatial scales (e.g. bora windstorms). Similarly to the other Mediterranean regions, the Adriatic is also a known hotspot in terms of multiple strong climate hazards and high vulnerability under global warming (IPCC 2022). This section provides a brief overview of the Adriatic basin geography, main physical processes, and the projected impact of climate change over the entire region.

1.1.1 Geography

The Adriatic Sea, the northernmost area of the Mediterranean Sea (Fig. 1), is a semi–enclosed basin deeply incised into the European mainland. Its climate is strongly affected by the complex orography, the land–sea contrasts, the intense air–sea interactions, and a range of both large and small–scale complex dynamical processes. The Adriatic Sea has an area of approximately 138 600 square kilometres with a mean depth of 240 metres, holding a volume estimated at around 35 000 cubic kilometres (Cushman–Roisin et al. 2001). The complex geomorphology of this elongated basin (870 km long and about 200 km wide; Fig. 1) includes (1) more than 1200 islands, islets, ridges, and rocks, mostly located along the northeastern coastline; (2) mountain ranges surrounding the basin — i.e. Alps in the north, Apennines in the west, and Dinarides in the east; and (3) bathymetries evolving from a shallow shelf (30 m on average) in the north to, in the middle Adriatic, a shallow pit (up to approximately 280 m) known as the Jabuka Pit and a 170–m deep sill known as the Palagruža Sill and, in the south, a very deep pit (up to approximately 1200 m) known as the Southern Adriatic Pit (SAP).

Another important characteristic of the Adriatic basin is that it contributes to about one–third of the total Mediterranean river freshwater influx. Milliman et al. (2016) claim that only a few coastal seas in the world are as dominated by as many small mountainous rivers as the Adriatic Sea: Alpine rivers (the Po, Adige, Brenta, Piave and Tagliamento rivers) to the northwest, Apennine rivers to the west, and Albania mountainous rivers in the southeast. A total of 35 rivers drains into the Adriatic basin. The Po River is by far the largest Adriatic river (i.e. draining 74 000 km^2 and having an average flow of 1 500 m^3/s) and with the Drini (Albania; 20 000 km^2) and the Adige (northeast Italy; 12 000 km^2), collectively drain

approximately 60 % of the Adriatic basin. Further, the Po River in the north, and rivers Drim, Semani and Vijose in the south (Artegiani et al. 1997a, b) are significant sources of nutrients and freshwater loads in the Adriatic (Chiaudani et al. 1980, Gilmartin et al. 1990).

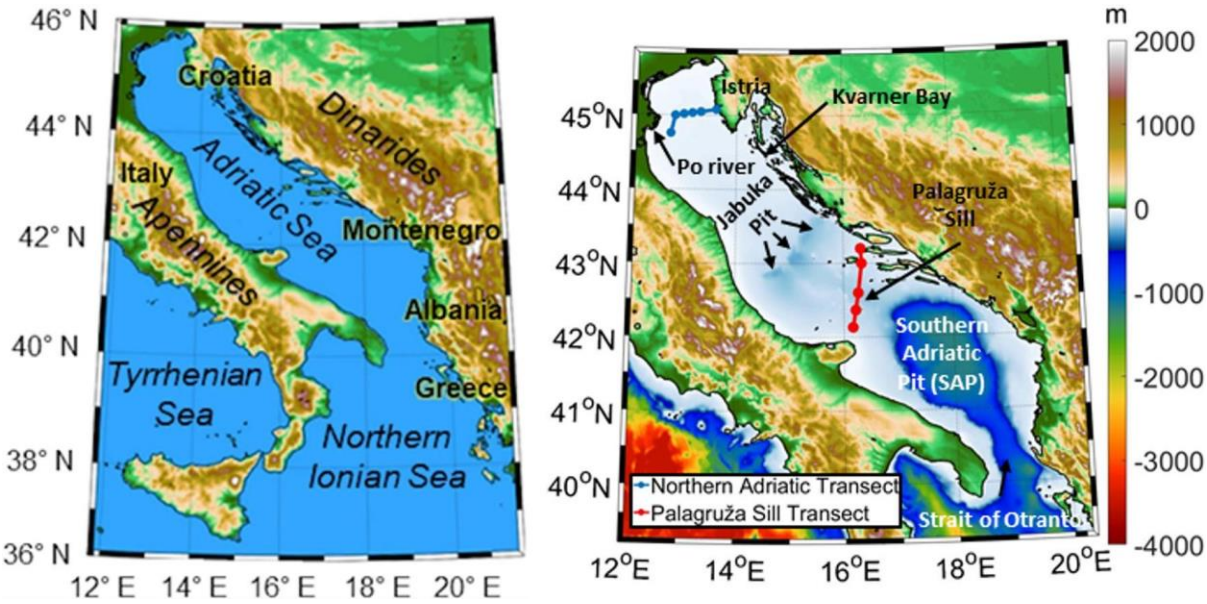

Figure 1. Orography (left panel) and bathymetry (right panel) of the Adriatic basin.

The distinctive and geographically complex Adriatic region is characterised by a diverse climate resulting from strong atmosphere–ocean interactions and topographical variations. The most important climate modifiers over the Adriatic basin are the Adriatic Sea and the orography of the Dinarides and Alps due to their shape, altitude, and position concerning the predominant air currents, the openness of the northeastern parts towards the Pannonian Plain, and the diversity of vegetation. The Adriatic region's unique climate includes coastal Mediterranean conditions, mountainous influences, and distinct atmospheric phenomena. The coastal regions of the Adriatic region present a Mediterranean climate, with hot, dry summers and mild, wet winters. Conversely, regions like the Alps, Apennines, and Dinarides extend their mountainous climate even to coastal areas due to long coastal ridges such as Velebit Mountain, which generates the downslope bora winds (Grisogono and Belušić, 2009). Moving further inland, the continental climate prevails with greater precipitation during the warm seasons compared to the cold ones (Gajić–Čapka et al. 1993).

1.1.2 Atmospheric dynamics

The Adriatic region is located between the subtropical high–pressure zone and the mid–latitude westerlies belt, and experiences seasonal shifts in atmospheric conditions (Orlić et al. 1992). The westerlies dominate most of the year, bringing frequent cyclones and anticyclones.

In summer, the subtropical high–pressure zone prevails, reducing disturbances from the westerlies. The Adriatic's global radiation varies seasonally, with air temperatures peaking in July and reaching their lowest in January (Furlan 1977). The air temperatures exhibit seasonal fluctuations of about 20 °C over the entire basin, while the north–south temperature differences range from about 3.5 °C in May to about 7 °C in November (Artegiani et al. 1997). Relative humidity is minimal in summer and the highest in autumn, with significant synoptic variations: the humidity can be lowered by 60–70 % during windstorms (Škreb et al. 1942). Cloud cover and precipitation also follow seasonal patterns, with maximum precipitation in late autumn and minimum in summer. Inland areas receive more precipitation (about 1,000 mm/year) than coastal stations (approximately 400 mm/year) (Orlić et al. 1992). Orographically driven extreme windstorms, particularly the bora and sirocco winds, strongly influence the Adriatic region. On the one hand, bora events are cold and dry winds originating from the northeast. They are associated with extreme heat losses and significantly impact the northern Adriatic waters by increasing evaporation, seawater density, and heat loss (Dorman et al. 2006). They mostly occur between December and March and affect specific areas such as the Kvarner Bay (Fig. 1). The typical duration of bora events is about two days, but may reach a week, while having substantial variability at daily, hourly and sub–hourly timescales (Belušić et al. 2004; Grisogono & Belušić 2009; Stiperski et al. 2012). On the other hand, sirocco events are associated with warm, dry, and often dusty winds that originate from North Africa. These winds have a distinct influence on the climate of the Adriatic region, bringing warmth and altering temperature and humidity conditions.

1.1.3 Ocean dynamics

1.1.3.1 Water masses

Five main types of water masses can be found in the Adriatic Sea (Cushman–Roisin et al. 2001): Adriatic Surface Water (AdSW), Ionian Surface Water (ISF), Levantine Intermediate Water (LIW), Northern Adriatic Dense Water (NAddW) and the south Adriatic Deep Water (AdW). Each of these water masses exhibits distinctive characteristics (Viličić 2014), and they have been first systematically classified by these characteristics by Mira Zore Armanda (Zore, 1963). AdSW significantly cools in winter but is not recognisable by characteristic temperature and salinity values. ISW is also subjected to seasonal atmospheric changes (i.e. exchange of heat fluxes) that are associated with a relatively wide range of temperature (18–23 °C) and salinity (38.77–38.93) as found during several Adriatic cruises in July/2004, May/2005 and

October/2005 (Budillon et al. 2010). LIW is defined by a salinity greater than 38.75 and temperatures equal to 14 °C. It extends into the southern Adriatic from the Ionian Sea at a depth between 40 and several hundred metres (Vilibić & Orlić 2002). The flow speed in this layer changes from year to year and depends on the atmospheric pressure gradient and water density gradient in the eastern Mediterranean as well as atmospheric and oceanic oscillations such as the North Atlantic Oscillation (Hurrell 1995) or the Ionian Oscillation (Civitarese et al. 2010). NAddW has temperature between 12.3 and 12.5 °C and salinity of 38.3–38.4 (Manca & Giorgetti 1999). It forms throughout the northern Adriatic during the winter action of the bora winds (Vilibić & Supić 2005; Mihanović et al. 2013). This water rapidly sinks in the area of the convergent Istrian front (Peters et al. 2007), spreads in the subsurface layer, and fills the Jabuka Pit and the Southern Adriatic Pit (SAP). In the deep part of the SAP, this water transforms into AdW with a potential density anomaly greater than 29.18 kg/m³, a temperature below 13 °C, and a salinity of 38.60 (Manca & Giorgetti 1999). The production of AdW is subject to interannual variabilities — some winters witness a rich production while others observe minimal formation (Cushman–Roisin et al. 2001) — and significantly impacts the characteristics of the water masses in the Eastern Mediterranean (Gačić et al. 2010).

1.1.3.2 Thermohaline circulation

The Adriatic thermohaline circulation arises from the interaction between thermal and haline forcing, influencing the local circulation features and current patterns (Artegiani et al. 1997a; Cushman–Roisin et al. 2001). The general surface circulation in the Adriatic occurs in a counterclockwise direction, with water flowing along the Croatian coast (i.e. Eastern Adriatic Current) and exiting on the Italian side through the Otranto Strait (i.e. Western Adriatic Current). Surface inflow currents are more intense along the eastern coast in winter, while surface outflow currents are more intense along the western coast in summer. The Eastern Adriatic Current transports warmer and saltier water along the eastern coast of the Adriatic from the eastern part of the Mediterranean and the Ionian Sea (Zore–Armanda 1969). Deviations from this main pattern have been observed and include the presence of smaller clockwise–rotating eddies during the warmer months, with the outgoing branch of the circulation being more pronounced than the incoming one. In the deeper layers, the prevailing circulation is counterclockwise, with the incoming current dominant in the intermediate layer and the outgoing current at the bottom. These currents, while not high in speed (up to 20 cm/s; Vilibić et al. 2023), are associated with surface and coastal flows of heat, leading to changes in salinity and temperature.

1.1.3.3 Air–sea interactions

Artegiani et al. (1997a) compared and discussed several climatological wind datasets and calculated the climatological heat budget of the basin with bulk formulas. They concluded that, first, the heat budget at the surface is dominated by the incoming shortwave heat fluxes balanced by longwave and latent heat energy losses and, second, the basin has average heat loss of 19–22 W/m^2. Consequently, heat from the northern Ionian is imported through the Otranto Strait which is known to play an important role in the heat storage balance of the Adriatic basin. The Adriatic is also a dilution basin, where freshwater influx from precipitation and continental runoff surpasses the loss due to evaporation. In particular, freshwater river runoff clearly affects the salt balance of the Adriatic surface layer during spring and summer (Artegiani et al. 1997a) while the main salt introduction into the Adriatic is through the Strait of Otranto. Every two to four years, the entire volume of the Adriatic is renewed through exchanges with the Mediterranean through the Strait of Otranto, a process accelerated by river discharge and submarine groundwater outflow (Franić 2005; Vilibić & Orlić 2002).

During orographically–driven windstorms, the Adriatic experiences well–developed surface wind–driven currents that can exceed 50 cm/s (Poulain & Raicich 2001). On the one hand, extreme bora events also drive the sea surface cooling, the mixing of the water column, the NAddW dynamics and, ultimately, the formation of the AdW, the densest water in the Mediterranean (Poulain & Raicich 2001; Artegiani et al. 1997a; Pullen et al. 2007; Orlić et al. 2007; Janeković et al. 2014; Ličer et al. 2016; Denamiel et al. 2020b). During bora events, the cooling occurs at hourly to daily timescales, rapidly impacting the vertical ocean structure in shallow areas already homogenised during the late autumn and winter seasons (Franco & Michelato 1992; Artegiani et al. 1997a) and taking out heat from the sea at rates up to 2000 W/m^2 for the most extreme events (Janeković et al. 2014). In the following days to weeks, a strong thermohaline circulation develops in the Adriatic–Ionian basin and can last for months (Orlić et al. 2007). Therefore, sea surface cooling during wintertime bora may be considered as a proxy for the dense water formation and the associated thermohaline circulation, which have, for example, a critical impact on the ocean biogeochemistry (e.g. Conan et al. 2018). On the other hand, extreme sirocco winds are associated with extreme waves (up to 4 m of significant wave height, Pomaro et al. 2017) and storm surges in the northern Adriatic (Bajo et al. 2019; Denamiel et al. 2020a), which particularly affect the Venice Lagoon (Trigo & Davies 2002; Cavaleri et al. 2010) and can move large boulders (weighting up to a ton) along the Croatian coastline (Biolchi et al. 2019a,b). Sirocco windstorms are also known to strongly

impact the channels between the coast and islands open to the southeast along the Croatian coastline (Brzović & Strelec Mahović 1999; Grisogono & Belušić 2009).

1.1.3.4 Adriatic–Ionian water exchanges

In terms of interchanges of water masses with the saltier and warmer Ionian Sea, the persistence of substantial decadal oscillations — known as the Adriatic–Ionian Bimodal Oscillating System (BiOS; Gačić et al. 2010; Mihanović et al. 2015; Denamiel et al. 2022) — is the main driver of the Adriatic circulation (Lionello et al. 2006). A decade ago, Gačić et al. (2010) proposed the first explanation of the physical mechanisms driving the BiOS, more than half a century after the existence of quasi–decadal variability of salinity and water masses in the Adriatic was noticed (Buljan 1953; Buljan and Zore–Armanda 1976). This explanation provides a scientific framework which connects the quasi-decadal reversals of the Northern Ionian Gyre (NIG) circulation to the salinity variability and the dense water formation in the Adriatic Sea. Namely, the southern Adriatic Sea salinity is decreased by the advection of the less–saline Modified Atlantic Water during the anticyclonic phase of the NIG and increased by the advection of the highly–saline Levantine/Eastern Mediterranean waters during the cyclonic phase of the NIG. Additionally, the reversals from anticyclonic to cyclonic (or cyclonic to anticyclonic) of the NIG are explained by the decreased (or increased) density of the Adriatic dense water outflow in the northern Ionian Sea, where the isopycnal surfaces are deepened (or raised) and thus the upper water layer is stretched (or squeezed) leading to a change in vorticity and hence a NIG reversal. Later, the BiOS regimes have also been connected to the salinity variability and the dense water formation of the Aegean basin (Krokos et al. 2014; Theocharis et al. 2014; Velaoras et al. 2014; Reale et al. 2017) and wind stress curl variability over the Ionian Sea (Pinardi et al. 2015; Eusebi Borzelli & Carniel 2023).

1.1.4 Impact of climate change

The impact of climate change is already felt in the Adriatic region. Air temperatures are already exhibiting an increase in the present climate, with more pronounced warming in summer and less in winter (Ogrin 2015; Radilović et al. 2020). Precipitation patterns are also shifting in various regions, with results by Gajić–Čapka et al. (2014) indicating general weak trends in precipitation extremes. However, more significant annual and seasonal changes are seen in the mountainous and coastal hinterland regions, where drying tendencies occur, especially during the summer season while the mainland experiences a higher amount of precipitation. In the ocean, sea surface temperatures are following seasonal atmospheric trends

but with somewhat higher rates, increasing at approximately 0.4−0.5 °C over recent decades, as observed through *in–situ* and satellite measurements (Bonacci et al. 2021). Recent trends at the Adriatic's longest surveyed transect, the Palagruža Sill (Fig. 1), indicate weakened thermohaline circulation and increased salinity in the surface and intermediate layers (Vilibić et al. 2013).

One of the prominent projections for the Adriatic far–future climate is a general increase in air temperatures associated with more frequent and prolonged heatwaves (Darmaraki et al. 2019). This warming is a consistent result of climate models, and could have implications for various economic sectors, including agriculture and tourism (Oplanić et al. 2023, Climate Risk Profile:Croatia, 2021). Climate models also project changes in precipitation patterns over the entire Adriatic region. While some areas may experience increased rainfall and the risk of more intense storms, others might face decreased precipitation, leading to increased drought conditions. Finally, climate projections suggest that sea–levels in the region will rise substantially which can lead to increased coastal erosion, saltwater intrusion into freshwater sources, and potential flooding in low–lying coastal areas, particularly in the Venice Lagoon (Ramieri 2000).

1.2 Adriatic atmosphere–ocean climate modelling

Geoscientific models are essential for the understanding of the complex atmosphere–ocean dynamics, interactions, and climate. However, the Adriatic orographic characteristics, land–sea interactions, and air–sea dynamics create an environment that challenges atmosphere–ocean climate modelling: the finer the spatial and temporal resolutions of the atmosphere–ocean models, the more accurately represented the Adriatic basin processes but the higher the numerical cost (Prein et al. 2015). This section presents, analyses, and discusses the different numerical strategies used to study the atmosphere–ocean processes within the Adriatic basin.

1.2.1 Adriatic Sea modelling challenges

In the last decades, many studies have focused on the numerical modelling of the Adriatic thermohaline circulation (Umgiesser et al. 2022). Initial efforts involved ocean models with resolutions up to 3 kilometres, concentrating on dense water formation within the northern Adriatic shelf and the SAP (Bergamasco et al. 1999; Beg–Paklar et al. 2001; Mantziafou & Lascaratos 2004, 2008). At the time, the atmospheric fields used to force these ocean models were primarily climatological data and datasets from the European Centre for Middle–range

Weather Forecast (ECMWF; May 1982; Artegiani et al. 1997a). However, these early efforts faced many challenges, as the ECMWF reanalyses, due to their coarse resolution, could not accurately simulate the extreme bora events driving the dense water formation in the northern Adriatic Sea (Cavaleri & Bertotti 1997). Subsequent studies revealed that modifications were needed to better represent the ocean dynamics during bora events, such as increasing wind speeds by up to 60 % (Mantziafou & Lascaratos 2004). More recently, several studies have proven that only high–resolution limited–area models can represent the complex Adriatic atmosphere–ocean dynamics during extreme events (e.g. Pasarić et al. 2007; Prtenjak et al. 2010; Janeković et al. 2014, Ricchi et al. 2016; Cavaleri et al. 2010; Denamiel et al. 2021a). In particular, kilometre–scale limited–area models have been used to simulate various ocean processes driven by extreme conditions in the Adriatic Sea, including waves, storm surges, sea surface cooling, water column mixing, dense water formation, and long–term thermohaline circulation during severe bora and sirocco windstorms (Cavaleri et al. 2010; Ricchi et al. 2016; Carniel et al. 2016).

Despite these advancements, certain challenges persist, including errors associated with the representation of river discharges and open boundary conditions. Outdated river climatologies have been used in numerous Adriatic modelling studies, resulting in significant overestimation of river discharges in the northeastern Adriatic (Janeković et al. 2014). These climatologies have been shown to prevent dense water formation in the coastal eastern Adriatic and decrease ocean density in the northern Adriatic shelf (Mihanović et al. 2013; Vilibić et al. 2016). Errors related to open boundaries, especially at the Strait of Otranto, have also been documented, leading to an underestimation of salinity (Janeković et al. 2014). Furthermore, improper parameterization of vertical mixing and diffusion can affect the performance of Adriatic models, and data assimilation procedures have been suggested to improve ocean modelling solutions (Janeković et al. 2020).

1.2.2 Global and regional climate modelling

In terms of climate change, state–of–the–art coupled atmosphere–ocean Global and Regional Climate Models (GCMs and RCMs) have significantly advanced our understanding of global and regional climate patterns. However, these models often have relatively coarse spatial resolutions, which make them less suitable for assessing climate change impacts at a local scale (Christensen et al. 2007). Historically, single atmospheric GCMs (with resolutions of the order of hundreds of kilometres) and RCMs (with typical resolutions of 7 to 50 km) have

been used in the Mediterranean Sea and most particularly in the Adriatic Sea in a wide range of impact studies such as the assessment of future wind (e.g. Bellafiore et al. 2012), wave (e.g. Lionello et al. 2012a; Benetazzo et al. 2012) and storm surge (e.g. Lionello et al. 2012b) climates. In particular, Pasarić and Orlić (2004) studied bora and sirocco in the Adriatic Sea, finding potential decreases in their numbers and intensities following a coarse–resolution GCM not necessarily capable of capturing the spatial characteristics of these extreme events while Pašičko et al. (2012) suggested an increase in wind speed over the Adriatic coastal regions by the mid–21st century, using one RCM and one greenhouse gas scenario. Regarding the air–sea interactions, Bellafiore et al. (2012) assessed two RCMs over the Adriatic and recommended a larger ensemble of RCMs for a more robust climate change signal while Benetazzo et al. (2012) forecasted reduced wave severity by the 21st century's end due to bora and sirocco variations, acknowledging the need for further research to distinguish their distinct roles.

More recently, two different ensembles of RCMs projecting climate change under various greenhouse gas emissions have become available in the Mediterranean region as part of the Coordinated Regional Climate Downscaling Experiment (CORDEX) initiative (https://esg–dn1.nsc.liu.se/search/cordex, last visited 15 November 2023) which coordinates the production of climate change projections at the regional scale (Giorgi et al. 2019). The EURO–CORDEX ensemble at 0.11° resolution (Coppola et al. 2021) with 14 different RCMs driven by 8 Coupled Model Intercomparison Project (CMIP) 5 global climate models and the Med–CORDEX ensemble (e.g. Ruti et al. 2016) mostly composed of atmosphere–land–ocean models at 7 to 50 km resolution. These ensembles have thus been used to better characterise the atmosphere–ocean dynamics (e.g. Belušić Vozila et al. 2019; Ivušić et al. 2021; Baronetti et al. 2022; Parras–Berrocal et al. 2023) and the climate–related hazards (i.e. flooding, extreme wave conditions, coastal vulnerability and erosion processes; e.g. Torresan et al. 2019) in the Adriatic basin. In particular, Parras–Berrocal et al. (2023) analysed the REMO–OASIS–MPIOM model results (Sein et al. 2015) of the Med–CORDEX ensemble and found that the projected dense water formation could be reduced by 75 % in the Adriatic Sea by the end of the century due to hydrographic changes in surface and intermediate water that strengthen the vertical stratification, hampering vertical mixing and thus convection.

1.2.3 Kilometre–scale climate modelling

Within the Adriatic basin, the need to bridge the gap between large– or medium– scale modelling studies and local–scale climate impacts has become increasingly apparent (Torresan

et al. 2019). Indeed, until now, the RCMs developed over the entire Mediterranean Sea within the Med–CORDEX initiative (e.g. Ruti et al. 2016) formed the foundation for assessing the future Adriatic Sea conditions under global warming. However, these RCM horizontal resolutions, of the order of 10 km, have been proven to be insufficient to resolve the complex Adriatic dynamics in both the atmosphere (Denamiel et al. 2021a) and the ocean (Pranić et al. 2023). The Med–CORDEX RCMs thus struggle to reproduce many Adriatic coastal processes including the extreme bora events (Denamiel et al. 2021a) and the BiOS (Dunić et al. 2019; Pranić et al. 2021).

Kilometre–scale atmospheric climate models have emerged as a promising solution, offering a better representation of the topography, coastline, and air–sea interactions in the Adriatic area when compared to GCMs and RCMs (Kotlarski et al. 2014). These high–resolution models excel at capturing critical phenomena like orographically influenced variations in precipitation, wind patterns, and surface energy balance, which hold great significance for coastal and mountainous regions in the Adriatic area (Gutowski et al. 2020; Vautard et al. 2013; Güttler et al. 2015; Estournel et al. 2021; Rummukainen, 2016). In particular, due to their extreme computational costs, the Pseudo–Global Warming (PGW; Schär et al. 1996, 2020) method for future climate projections was used for simulations ranging from few days during extreme events to 31–year periods.

It is only recently that the PGW approach was extended to the ocean (Denamiel et al. 2020a) and implemented in the first (sub–) kilometre–scale atmosphere–ocean climate model in the world: the Adriatic Sea and Coast (AdriSC) modelling suite (Denamiel et al. 2019, 2021b). The AdriSC model uses a modular approach to accurately represent the processes governing the atmospheric and oceanic circulations at various temporal and spatial scales in the Adriatic and northern Ionian Sea. A first module produces hourly results at up to 3 km in the atmosphere and 1 km in the ocean and can be used for long–term simulations. Till now, two 31–year long AdriSC simulations have been performed, an evaluation run during the 1987–2017 period forced by reanalysis products (hereafter historical conditions) and an extreme warming run during the 2070–2100 period for a Representative Concentration Pathways (hereafter RCP) 8.5 greenhouse gas scenario downscaling a single model of the Med–CORDEX ensemble. A second module allows further downscaling of these basic module results to 1.5 km in the atmosphere and to a few metres along the eastern Adriatic coastline for short–term simulations (i.e. 1.5 days) during extreme events (e.g. bora, sirocco, etc.). Several short–term AdriSC numerical experiments (Denamiel et al. 2020a,b) have been used to derive the local impact of

climate change on extreme windstorm events in the Adriatic under moderate and extreme warming (i.e. RCP 4.5 and RCP 8.5, respectively).

1.3 Short outline of the dissertation

Due to the complex orography and bathymetry of the Adriatic basin, the main hypothesis of this thesis is that the impact of climate change in this region can only be described with complex (sub–) kilometre–scale atmosphere–ocean models such as the AdriSC modelling suite. Since the AdriSC model has already been successfully validated throughout the Adriatic basin based on a large dataset of *in–situ* measurements and remote sensing products (Denamiel et al. 2021b; Pranić et al. 2021), the goal of this PhD study is to analyse the results of the AdriSC simulations for historical conditions (1987–2017) and far–future moderate and extreme warming conditions (RCP 4.5 and RCP 8.5; 2070–2100) to assess the local impact of climate change in the Adriatic coastal areas. This research will first demonstrate the added value of the kilometre–scale approach used within the AdriSC modelling suite in the context of modelling the Adriatic atmosphere–ocean dynamics, interactions, and climate. Then, it will quantify the impact of climate change on both extreme events with short–term simulations and the Adriatic atmosphere–ocean trends and variability with long–term simulations.

The thesis presents several key chapters, each contributing to a comprehensive understanding of the Adriatic basin's future climate and extreme event dynamics.

Chapter 2 initiates the research by introducing the AdriSC modelling suite and outlining the methodology for simulating climate change in the Adriatic with the pseudo–global warming approach. Then, the chapter introduces the different atmosphere–ocean short–term and long–term simulations — e.g. choice of extreme events, setup of the simulations, observations used to demonstrate the added value of the kilometre–scale approach — used in the thesis. Finally, the chapter presents the different methods used to analyse the AdriSC climate simulations.

Chapter 3 further examines the benefits of kilometre–scale modelling in the Adriatic region for two different cases. Case 1 focuses on modelling extreme bora events, exploring their sensitivity to atmospheric model horizontal resolution, and the representation of the bora dynamics, and air–sea interactions. Case 2 investigates the BiOS–driven variability in the Adriatic Sea, evaluating long–term monitoring transects and assessing interannual to decadal variability in the sea's thermohaline circulation. The chapter concludes with a comprehensive discussion.

Then, in Chapter 4, the impact of climate change on the far–future extreme bora events associated with air–sea heat transfers and sea surface cooling is assessed. The chapter concludes with a discussion of the findings and their implications in terms of the impact of climate change on extreme bora events.

Chapter 5 presents a detailed analysis of the atmosphere and ocean trends, variability, and extremes under historical (1987–2017) and far–future (RCP 8.5, 2070–2100) climate conditions. The implications of these changes are discussed, particularly their effects on the atmosphere–ocean dynamics in the Adriatic region, and compared to previous studies, all while acknowledging limitations.

Finally, Chapter 6 offers conclusions, highlighting the novelty of using an ultra–high–resolution atmosphere–ocean model for simulating the Adriatic climate. It discusses the challenges associated with running and analysing such models, particularly in handling enormous data volumes. It emphasizes the importance of informed policy strategies, regional planning, and adaptive measures in light of projected climate changes in the Adriatic region, as well as the need for further research and validation, particularly in areas where findings differ from past results.

2. MODELS, SIMULATIONS AND METHODS

2.1 Adriatic Sea and Coast (AdriSC) modelling suite

The AdriSC modelling suite, as described by Denamiel et al. (2019), has been developed to accurately represent the processes governing the atmospheric and oceanic circulation at various temporal and spatial scales in the Adriatic and northern Ionian seas. This suite comprises two modules: a basic module used to reproduce the Adriatic Sea baroclinic circulation at deep–sea and coastal scales and a specialised extreme event module to better simulate atmospherically–driven extreme events.

2.1.1 Basic module

The basic module (Fig. 2, green frame) of the AdriSC modelling suite is based on the Coupled Ocean–Atmosphere–Wave–Sediment Transport (COAWST) modelling system (Warner et al. 2010). It uses the Model Coupling Toolkit (MCT; Larson et al. 2005) and the Spherical Coordinate Remapping and Interpolation Package (SCRIP) to dynamically couple (online coupling) the Weather Research and Forecasting (WRF; Skamarock et al. 2005) atmospheric model, the Regional Ocean Modeling System (ROMS; Shchepetkin and McWilliams, 2009) ocean model, and the Simulating Waves Nearshore (SWAN; Booij et al. 1996) wave model. In this configuration (Fig. 2 and Table 1), the Adriatic atmospheric processes, depending on both local orography and Mediterranean regional forcing, are represented with a 3 km grid (266 x 361 grid points) encompassing the entire Adriatic and northern Ionian seas. Additionally, the AdriSC WRF 3 km grid is nested in a 15 km outer grid (140 x 140 grid points) approximately covering the central Mediterranean basin. In the ocean, the exchanges of the Adriatic Sea with the Ionian Sea are captured with a 3 km grid identical to the atmospheric domain, while an additional nested 1 km grid (676 x 730 grid points) more accurately represents the complex geomorphology of the Adriatic Sea. The vertical discretisation of the grids is achieved via terrain–following coordinates: 58 levels refined in the surface layer for the atmosphere (Laprise 1992) and 35 levels refined near both the sea surface and bottom floor for the ocean (Shchepetkin & McWilliams 2009). A digital terrain model (DTM) incorporating offshore bathymetry from ETOPO1 (Amante & Eakins 2009), nearshore bathymetry from navigation charts CM93 2011, topography from the GEBCO 30 arcsec grid 2014 (Weatherall et al. 2015), and coastline data generated by the Institute of Oceanography and Fisheries (Split, Croatia) is providing the high–resolution orography, bathymetry, and coastline of all the AdriSC grids.

2.1.1.1 Atmospheric model setup

The AdriSC WRF model physics and parameterisations are based on the configuration of Adriatic high–resolution WRF models described by Kehler–Poljak et al. (2017): Morrison 2 moment scheme microphysics scheme (Morrison et al. 2005), Mellor–Yamada–Janjić (MYJ) Planetary Boundary Layer (Janjić 1994), Dudhia (Dudhia 1989) and RRTM (Mlawer et al. 1997) short and longwave radiation schemes, Eta surface–layer scheme (Janjić 1994), and five–layer thermal diffusion scheme for soil temperature (Dudhia 1996). As the spatial extension of the ocean grids does not entirely cover the WRF 15 km atmospheric domain, the sea surface temperature (SST) from the ROMS grids is not prescribed to the AdriSC WRF models. This approach avoids any potential discontinuities along the border between the two–way nested WRF 15 km and WRF 3 km atmospheric grids and optimises the balance between the AdriSC model efficiency and accuracy by reducing the exchanges between the different grids. Consequently, the only grid exchanges in the basic module consist in the AdriSC WRF 3 km model providing atmospheric fields (i.e. horizontal wind at 10 m, temperature at 2 m, relative humidity at 2 m, mean sea–level pressure, downward shortwave radiations, longwave radiations, rain and evaporation) to the AdriSC ROMS–SWAN 3 km and 1 km models.

Table 1 Summary of the AdriSC modelling suite main features. Adapted from Denamiel et al. (2019).

	Basic module				Extreme event module	
	Atmosphere		Ocean		Atmosphere	Ocean
Models	WRF		ROMS–SWAN		WRF	ADCIRC–unSWAN
Number of domains	2		2		1	1
Resolution	15 km	3 km	3 km	1 km	1.5 km	5 km to 10 m
Initial and boundary conditions	External forcing		External forcing		WRF 3 km	ROMS–SWAN 1km
Frequency of outputs	Hourly				1–min	

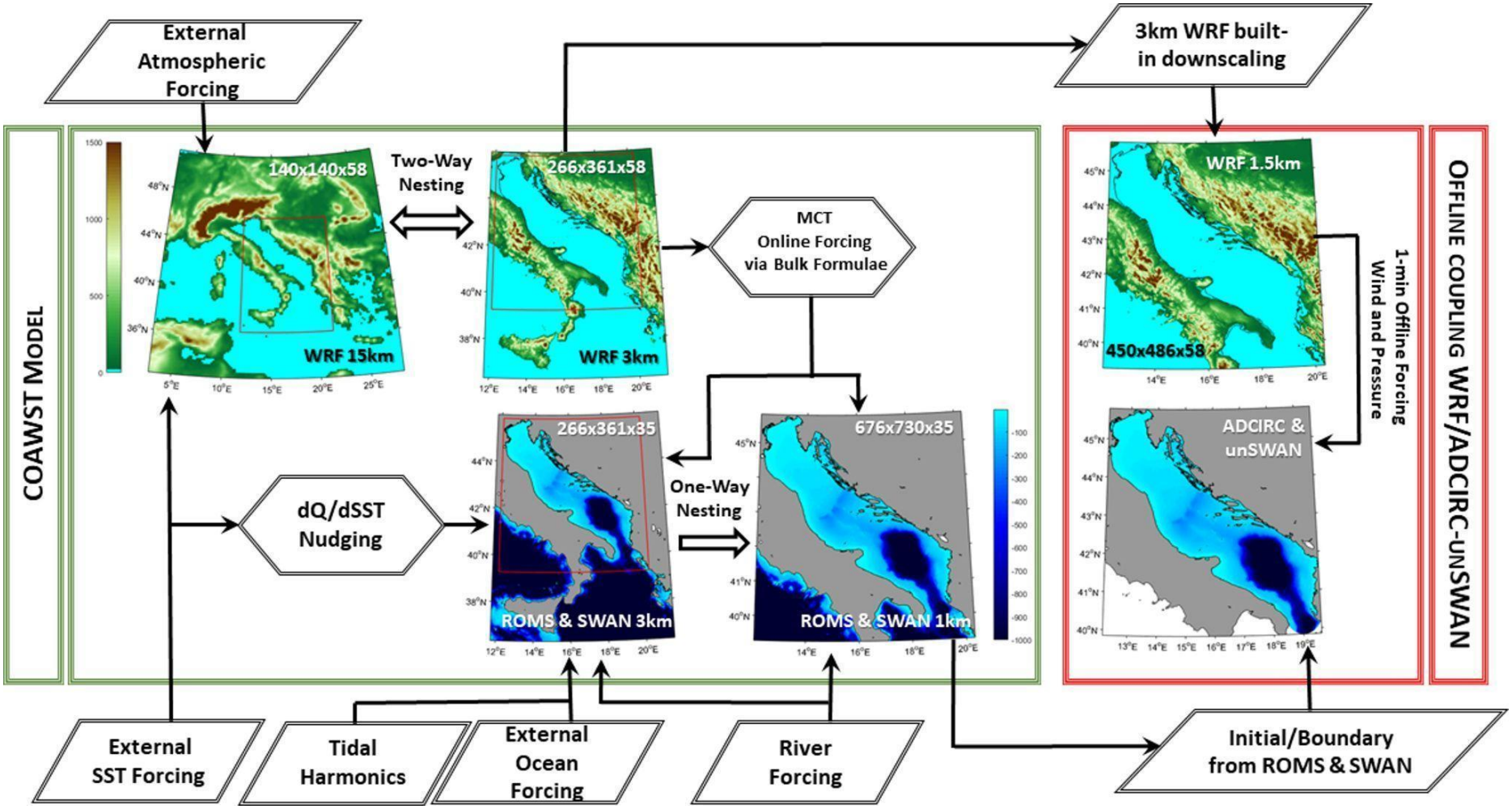

Figure 2. Flow chart of the AdriSC modelling suite representing the coupling between the different models (in green COAWST within the basic AdriSC module, in red WRF/ADCIRC–unSWAN within the extreme event AdriSC module), their grids (plotted with topography/bathymetry data) and their forcing. Adapted from Denamiel et al. (2019).

2.1.1.2 Ocean–wave model setup

The setup of the AdriSC ROMS models encompasses four main features. First, for all AdriSC ROMS grids, the bathymetry (with a minimum depth of 2 m) is smoothed with a linear programming (LP) method (Dutour Sikirić et al. 2009) in order to minimise the roughness factors while keeping the DTM bathymetric features and reducing the horizontal pressure gradient errors generated by the use of terrain–following coordinates with steep bathymetric gradients. In the basic module configuration, 35 vertical layers — transformed (Vtransform=2) and stretched (Vstretching=4) following Shchepetkin and McWilliams (2009) — are used with increased resolution at the surface (Θs=6) and bottom (Θb=2) as well as a thickness of 50m (hc=50).

Second, the tidal forcing used in all simulations consists of eight tidal constituents (M2, S2, N2, K2, K1, O1, P1, Q1) extracted from the Mediterranean Sea and Black Sea (2011) 1/30º regional solution of the OTIS. The tidal constituents used were previously found to adequately reproduce the tidal dynamics in the Adriatic Sea (Cushman–Roisin & Naimie 2002; Janeković & Kuzmić 2005). Concerning the river forcing, 54 river flows in total (only 49 for the 1 km grid) are imposed over at least six grid points each (and 18 grid points for the Po River delta), with river mouths located along the coastline of the Italian peninsula, Sicily, Croatia, Slovenia, Albania, Montenegro, and Greece. The monthly climatology of the river flow is acquired from the RivDis database (Vörösmarty et al. 1996) and several other studies (Pano & Abdyli 2002; Malačić & Petelin 2009; Pano et al. 2010; Janeković et al. 2014; Ljubenkov 2015) whereas the river flow interannual variability is obtained from Ludwig et al. (2009). Additionally, the river flows are linearly distributed between the first 20 sigma vertical levels — i.e. the discharge is multiplied by weights ranging from 20/210 at the surface, to 19/210 at the first sigma level below the surface, to zero at the 20th sigma level below the surface.

Third, on the one hand, the high optical water clarity in shallow parts of the Adriatic such as the eastern Adriatic Sea creates warming SST trends linked to the absorption of the shortwave radiation reaching the seafloor, while, on the other hand, the low optical water clarity along the Italian coast due the muddy waters of the Po River plume tends to produce opposite trends. A dQ/dSST procedure, which is described in detail in the study of Denamiel et al. (2019), is thus used to solve this problem by minimising the corrections of the heat fluxes produced by WRF while making sure that no artificial SST trends are generated in the shallow

parts of the ROMS grids. In brief, this method imposes a heat flux correction through the calculation of the kinematic surface net heat flux sensitivity to the SST of reference.

Finally, concerning the configuration of the physical options for the ROMS models, the barotropic velocities, surface elevations, and baroclinic fields at the open boundaries are imposed with the Flather (Flather 1976), Chapman (Chapman 1985), and Orlanski (Orlanski 1976) conditions. Additionally, the baroclinic structure is relaxed — with a minimum folding time of 3 days — towards the fields provided by the ocean forcing (Marchesiello et al. 2001). The relaxation occurs in two different nudging areas: (1) a 10–grid–point–wide zone along the open boundaries and (2) a zone covering the bathymetry deeper than 2000 m but only for the temperature and salinity in order to minimise the numerical diapycnal mixing. A sponge area of 10 grid points (identical to the first nudging area) also ensures that the horizontal viscosities are smoothly interpolated from values 4 times bigger at the open boundaries than inside the domain. Last, the tracer advection is provided with the Multidimensional Positive Definite Advection Transport Algorithm (MPDATA; Smolarkiewicz & Grabowski 1990), while the horizontal momentum advection uses a fourth–order centred scheme and the turbulence closure scheme follows the GLS gen framework (Umlauf & Burchard 2003).

Concerning the AdriSC SWAN models, the third generation SWAN model is used with backward space and time propagation schemes, default initial condition, dissipation from whitecapping by Komen et al. (1984) and Madsen bottom friction (Madsen et al. 1988).

2.1.2 Extreme event module

This module model domains (Fig. 2, red frame) are chosen to represent atmospherically–driven extreme sea–level events (Table 1). A 1.5 km atmospheric grid (450 × 486 grid points) covering the entire Adriatic region provides a good representation of the orography of the main Croatian islands and the Adriatic region complex coastal topography. For the ocean, an unstructured mesh with a resolution ranging from about 5 km in the deepest part of the Adriatic to 10 m along the Croatian coastline (286 336 nodes, 513 340 triangular elements with 477 islands and islets included) is used. Given the spatial and temporal resolution of the available atmospheric and oceanic forcing for the Adriatic, the direct use of the 1.5 km atmospheric grid and the unstructured ocean mesh to reproduce extreme events would definitely lead to a misrepresentation of the conditions driving the extreme events. However, using the hourly results produced by the 3 km atmospheric and 1 km ocean grids to force the extreme event module allows for a better representation of the short–term extreme events, as the initial and

boundary conditions already include high temporal and spatial variabilities. The extreme event module thus downscales the atmospheric and ocean results obtained with the basic module by coupling offline the AdriSC WRF model (1.5 km grid) with the barotropic version (2DDI) of the unstructured ADvanced CIRCulation (ADCIRC; Luettich et al. 1991) model fully coupled with the unstructured SWAN (unSWAN) model (Dietrich et al. 2012). In more details, the hourly results from the AdriSC WRF 3 km grid obtained with the basic module are first downscaled offline to the AdriSC WRF 1.5 km grid covering the Adriatic Sea. Then, the hourly sea surface elevation from the ROMS 1 km grid, the 10–min spectral wave results from the SWAN 1 km grid (or hourly forcing from external forcing from other wave models in case the SWAN model was not used within the basic module) and finally the 1–min 10 m wind and surface atmospheric pressure results from the AdriSC WRF 1.5 km model are used to force the unstructured mesh of the ADCIRC and unSWAN models. Finally, within the extreme event module, the SWAN model receives forcing from the AdriSC WRF 1.5 km (i.e. wind fields) and AdriSC ADCIRC (i.e. ocean barotropic currents, sea–level and friction) models every minute.

The setup of the AdriSC WRF 1.5 km model is similar to the one used in the basic module while the 2DDI–ADCIRC model simulates wetting–drying processes in low–lying areas and imposes zero land boundary flux. In addition, the computation of the bottom stresses of the AdriSC ADCIRC ocean model accounts for the spatial distribution of the sediment grain size at the bottom of the Adriatic Sea extracted from the Adriatic Seabed database (Jenkins et al. 2005) and the wave effects. The third generation unSWAN model is used as described in the section above.

2.1.3 Compilation and performances

The COAWST, WRF and ADCIRC–unSWAN models were compiled with the Intel 17.0.3.053 compiler, the PNetCDF 1.8.0 library and the MPI library (mpich 7.5.3) on the now retired ECMWF's CRAY High–Performance Computer (HPC). In addition, ecFlow 4.9.0, the workflow package used by all ECMWF operational suites, was set up to run all AdriSC simulations automatically and efficiently in a controlled environment. In terms of workload, no hyperthreading was used and the AdriSC basic was optimally run on 260 CPUs, with both the WRF and ROMS grids decomposed into 10 x 13 tiles (Denamiel et al. 2019). The AdriSC WRF 1.5 km model was run on 210 CPUs (14 x 15 tiles) while the AdriSC ADCIRC–SWAN model was run on 100 CPUs. Despite this optimal configuration of the models that maximised

the running time of each individual model and the time used to exchange data between the different grids, the AdriSC basic module ran at extreme computational cost and about 18 months were needed to complete each 31–year long simulation. It should also be noted that running separately the WRF 1.5 km and ADCIRC–unSWAN models from the AdriSC extreme event module is, respectively, 9 and 6 times slower than running the coupled atmosphere–ocean basic module.

2.2 Pseudo–Global Warming (PGW) methodology

The principle of the PGW simulations — as first introduced by Schär et al. (1996) and described in detail by Rasmussen et al. (2011), Kröner et al. (2017) and Brogli et al. (2019a, b) — is to impose an additional climatological change (e.g. a temperature change ΔT representative of the increase in temperature between past and future climate) to the forcing used to produce the evaluation runs.

2.2.1 Downscaled RCM fields

One of the specific aims of the Med-CORDEX experiment (e.g. Ruti et al. 2016) is to provide coupled ocean–atmosphere regional model results. The RCMs of the Med–CORDEX ensemble are thus based on several numerical models running in coupled or uncoupled mode and forced by different Global Climate Models (GCMs). However, when the AdriSC climate model was implemented, a reported issue with the CNRMCM5 CMIP5 GCM forcing for the historical run put in question the reliability of this product.

Consequently, the only coupled results publicly available — with high enough temporal and spatial resolutions for the historical period (1950–2005) and the two climate scenarios RCP 4.5 and RCP 8.5 (2006–2100) — were those of the LMDZ4–NEMOMED8 RCM model (Hourdin et al. 2006; Beuvier et al. 2010) forced by the IPSL–CM5A–MR GCM model (simulations r1i1p1). These results are defined as two continuous LMDZ4–NEMOMED8 simulations (1950–2100) extending the historical run with either the RCP 4.5 or RCP 8.5 runs and are used to force the AdriSC PGW simulations.

2.2.2 PGW in the atmosphere

For the atmosphere, as described in many previous studies (Pan et al. 2011; Kendon et al. 2014; Tolle et al. 2014; Argueso et al. 2014; Rasmussen et al. 2014; Ban et al. 2015; Prein et al. 2015; Fosser et al. 2016; Kendon 2017), the ERA–Interim (ERA–I; Dee et al. 2011) 0.75°

resolution air temperature $\left(T^{ERAI}\right)$, relative humidity $\left(RH^{ERAI}\right)$ and horizontal wind velocities $\mathbf{V}^{ERAI}=\left(V_x^{ERAI},V_y^{ERAI}\right)$ defined on 37 atmospheric pressure levels (p) are modified between 1000 hPa and 70 hPa with respectively $\Delta T\left(t_{c\lim},x,y,p\right)$, $\Delta RH\left(t_{c\lim},x,y,p\right)$ and $\Delta\mathbf{V}=\left(\Delta V_x\left(t_{c\lim},x,y,p\right),\Delta V_y\left(t_{c\lim},x,y,p\right)\right)$ derived from RCP 4.5 & 8.5 by subtracting the atmospheric results from the 1987–2017 period to those of the 2070–2100 period and producing 6–hourly three–dimensional climatologic changes for the 366 days of the year $\left(t_{c\lim}\right)$. The WRF 15-km boundary and initial conditions of the PGW simulations (T^{SCEN}, RH^{SCEN}, V_x^{SCEN} and V_y^{SCEN}) are thus given by:

$$
\begin{aligned}
T^{SCEN}\left(t,x,y,p\right)&=T^{ERAI}\left(t,x,y,p\right)+\Delta T\left(t_{c\lim},x,y,p\right)\\
RH^{SCEN}\left(t,x,y,p\right)&=RH^{ERAI}\left(t,x,y,p\right)+\Delta RH\left(t_{c\lim},x,y,p\right)\\
V_x^{SCEN}\left(t,x,y,p\right)&=V_x^{ERAI}\left(t,x,y,p\right)+\Delta V_x\left(t_{c\lim},x,y,p\right)\\
V_y^{SCEN}\left(t,x,y,p\right)&=V_y^{ERAI}\left(t,x,y,p\right)+\Delta V_y\left(t_{c\lim},x,y,p\right)
\end{aligned}
\qquad (1)
$$

In order to adjust the height of the surfaces of constant pressure to the temperature and relative humidity changes, the geopotential – depending on the virtual temperature T_v^{SCEN}, the ERA-Interim geopotential ϕ^{ERAI} at the reference pressure $p_{ref}=1000hPa$ and the gas constant R, is recalculated as follows:

$$
\phi^{SCEN}\left(t,x,y,p\right)=\phi^{ERAI}\left(t,x,y,p_{ref}\right)-\int_{p_{ref}}^{p}\frac{RT_v^{SCEN}}{p}dp \qquad (2)
$$

Finally, the 2-m air temperature change ΔT_S derived from SCEN 4.5 and SCEN 8.5 runs is used to adjust the ERA-Interim surface (ground and 2-m air) temperatures $\left(T_S^{ERAI}\right)$ such as:

$$T_S^{SCEN}(t,x,y) = T_S^{ERAI}(t,x,y) + \Delta T_S(t_{clim},x,y) \quad (3)$$

2.2.3 PGW in the ocean

The developed methodology for the ocean follows the principles of the PGW for the atmosphere. In this study, the Mediterranean Forecasting System (MFS) 1/16° resolution (Simoncelli et al. 2019; hereafter MEDSEA) ocean temperature $\left(T^{MEDSEA}\right)$, salinity $\left(S^{MEDSEA}\right)$ and currents $\left(V_x^{MEDSEA}, V_y^{MEDSEA}\right)$ defined on 72 unevenly spaced vertical levels (z), are thus modified with respectively $\Delta T(t_{clim},x,y,z)$, $\Delta S(t_{clim},x,y,z)$ and $\Delta \mathbf{V} = \left(\Delta V_x(t_{clim},x,y,z), \Delta V_y(t_{clim},x,y,z)\right)$ derived from RCP 4.5 & 8.5 ocean results to produce daily climatologic changes (t_{clim}) for the 366 days of the year. The ROMS 3–km boundary and initial conditions of the PGW simulations (T^{SCEN} and S^{SCEN}) are thus given by:

$$\begin{aligned}
T^{SCEN}(t,x,y,z) &= T^{MEDSEA}(t,x,y,z) + \Delta T(t_{clim},x,y,z) \\
S^{SCEN}(t,x,y,z) &= S^{MEDSEA}(t,x,y,z) + \Delta S(t_{clim},x,y,z) \\
V_x^{SCEN}(t,x,y,z) &= V_x^{MEDSEA}(t,x,y,z) + \Delta V_x(t_{clim},x,y,z) \\
V_y^{SCEN}(t,x,y,z) &= V_y^{MEDSEA}(t,x,y,z) + \Delta V_y(t_{clim},x,y,z)
\end{aligned} \quad (4)$$

In the ocean, the static stability depends on the density (ρ) and the vertical variations of the local potential density (σ_n) such as:

$$E(x,y,z) = -\frac{1}{\rho(x,y,z)}\frac{\delta\sigma_n}{\delta z} \quad (5)$$

The stability of the ocean forcing (at the boundaries and for the initial condition) is thus ensured by imposing $E^{SCEN} \geq 0$ at all vertical levels. Finally, the sea surface elevation change Δssh,

derived from RCP 4.5 & 8.5 runs is used to adjust the MEDSEA surface layer $\left(ssh^{MEDSEA}\right)$ such as:

$$ssh^{SCEN}\left(t,x,y\right) = ssh^{MEDSEA}\left(t,x,y\right) + \Delta ssh\left(t_{c\lim},x,y\right) \quad (6)$$

2.2.4 AdriSC PGW forcing

The PGW forcing for RCP 4.5 & 8.5 scenarios, used to force the AdriSC PGW simulations, are illustrated below in Figures 3 to 5.

The temperature changes $\left(\Delta T\right)$ imposed at the boundaries of both the ocean and atmosphere models are illustrated in Fig. 3. The vertical variations of the spatially– and time–averaged ΔT presented in Figure 3b clearly show that, near the surface of the earth, the differences in temperature between scenarios RCP 4.5 & 8.5 reach more than 1.5 °C (for both the ocean and the atmosphere). For the ocean, no significant difference between the two scenarios is seen below depth of 1000 m. For the atmosphere, this difference only starts to decrease above 400 hPa and is minimised above 100 hPa. In addition, the time variations of the spatially averaged ΔT for scenario RCP 8.5 (Fig. 2.c) highlights that the temperature change imposed to the atmosphere at 2 m height is, most of the year, at least 0.5 °C higher than the one imposed to the sea surface temperature. Finally, Figs. 3.d and 2.e present the vertical variations of the temporally averaged ΔT along the southern and western boundaries of both the atmosphere and ocean models and illustrate the importance of using spatially varying temperature changes for realistic climate simulations.

In Figure 4, the surface distribution of the temporally–averaged RCP 8.5 changes show that: for the atmosphere, the orography plays a major role in terms of the intensity of the changes (i.e. the strongest increase in temperature, decrease in relative humidity and change in wind speed are generally found at the highest altitudes), and, for the ocean, the changes imposed to the Adriatic and northern Ionian Seas (i.e. strongest increase in temperature and salinity) do not correspond to the changes imposed in the western side of the domain where the strongest changes in current speed occur. Concerning the sea surface elevation, the RCP 8.5 changes are mostly negative and only of the order of a few centimetres (with a maximum of 8 cm). Given that on the one hand, the open boundary of the LMDZ4–NEMOMED8 model (similarly to all the Med–CORDEX simulations, Adloff et al. 2018) does not properly include

the projected Atlantic sea–level changes, but just takes into account the thermosteric effects and, on the other hand, the thermal stretching is balanced by the haline shrinking, these results are in accordance with the estimated –7 cm to 13 cm expected in the Mediterranean Sea (Tsimplis et al. 2008; Jordà & Gomis 2013; Gualdi et al. 2013). Thus, for realistic sea–level projections, mass change–induced sea–level increase — approximated to 50–60 cm in the Mediterranean till 2100 (Jordà & Gomis 2013), should be added to the presented PGW sea–level estimates.

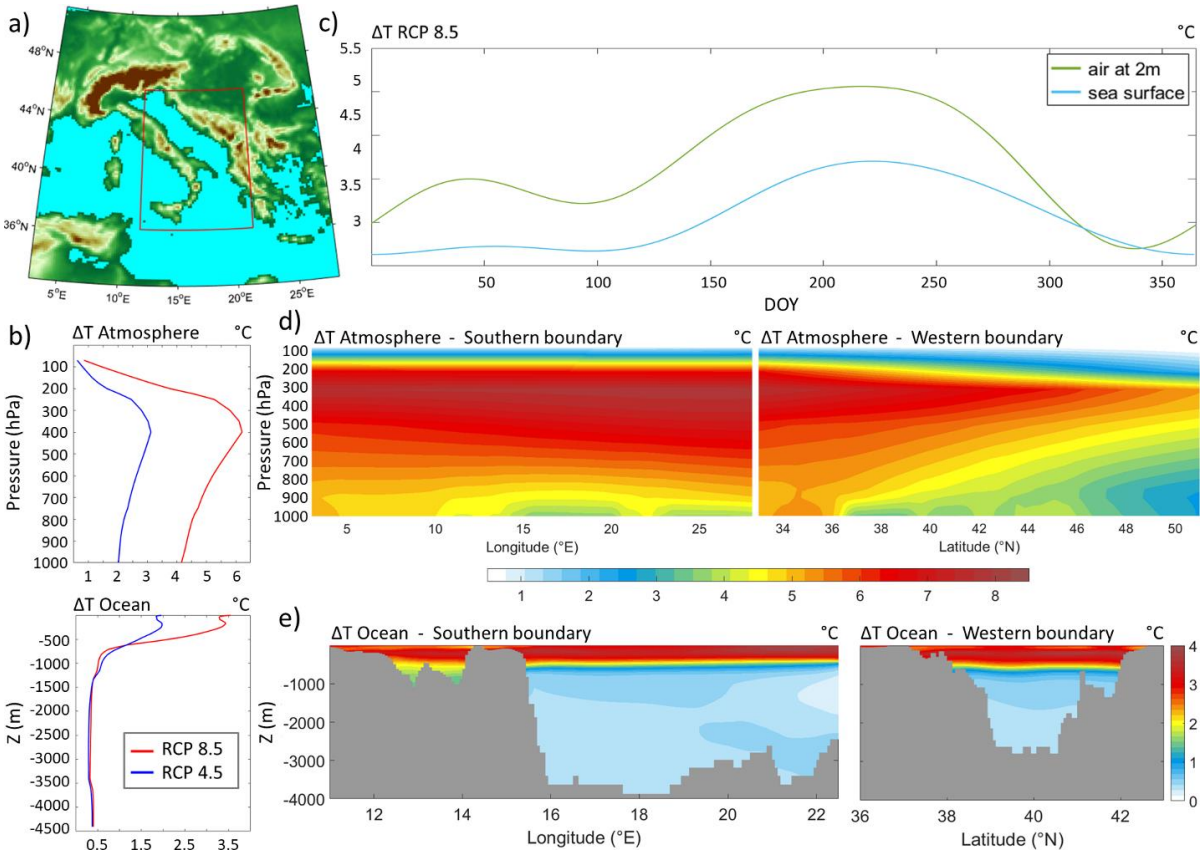

Figure 3. (a) Spatial domain and boundaries of the WRF 15–km model and, within the red box, the ROMS 3–km model. (b) Vertical variations of the spatially– and temporally–averaged temperature changes ΔT for scenarios RCP 4.5 & 8.5 following pressure level in the atmosphere and depth in the ocean. (c) Time evolution depending on the day of a year (DOY) of the spatially– averaged 2–m air (in green) and sea–level (in blue) climatologic temperature changes ΔT for scenario RCP 8.5. Vertical structure of the temporally– averaged temperature changes ΔT (RCP 8.5) imposed at the southern and western boundaries of (d) the AdriSC WRF 15 km model and (e) the AdriSC ROMS 3 km model. From Denamiel et al. (2020a).

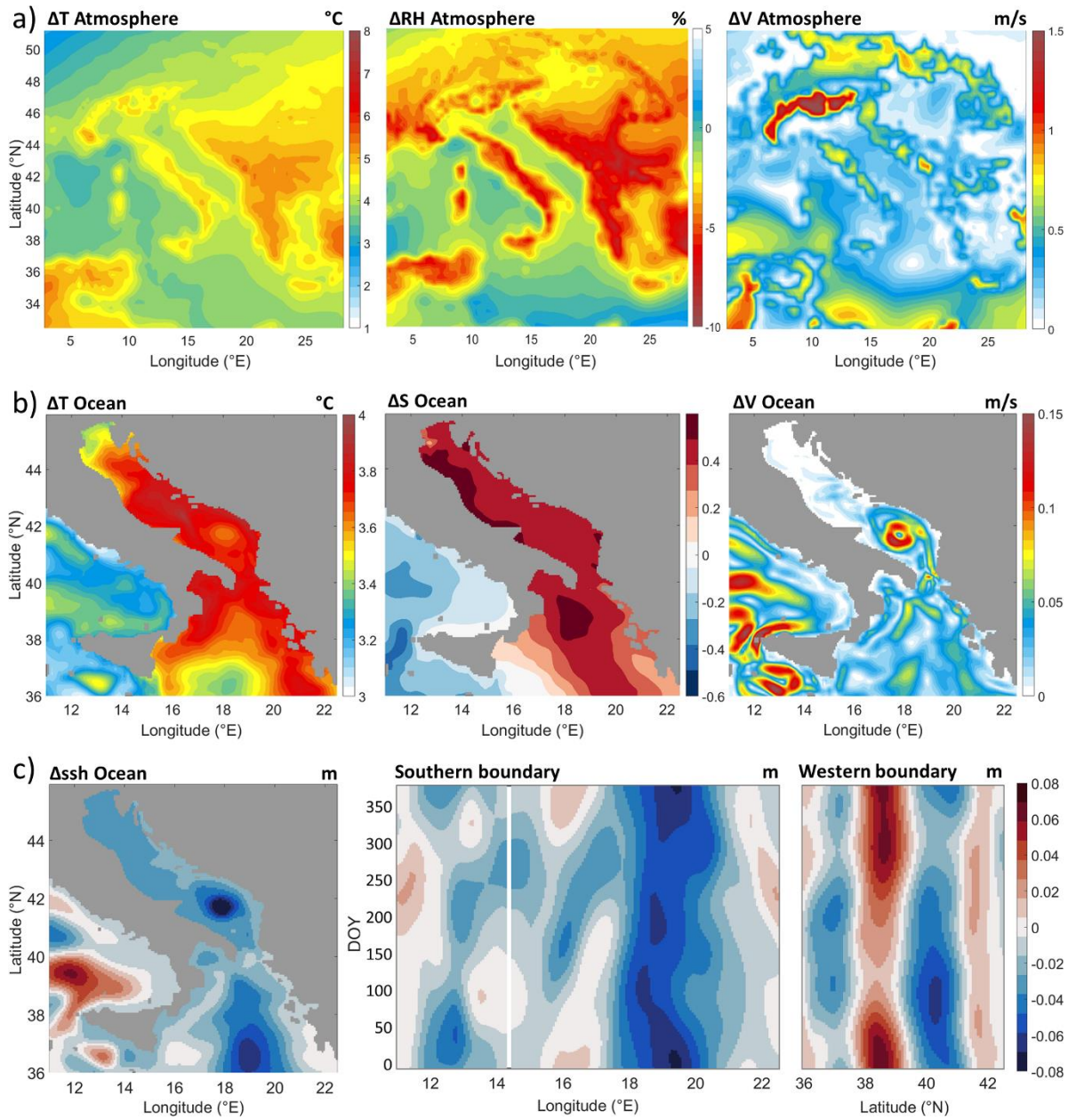

Figure 4. Surface distribution of the temporally–averaged RCP 8.5 changes of (a) temperature (ΔT), relative humidity (ΔRH) and wind speed (ΔV) in the atmosphere for the AdriSC WRF 15 km domain and (b) temperature (ΔT), salinity (ΔS) and current speed (ΔV) in the ocean for the ROMS 3–km domain. The variations of the sea surface elevation (Δssh) RCP 8.5 changes are presented in panel (c) as temporally averaged surface distributions and time–varying open boundary conditions. From Denamiel et al. (2020a).

In addition to the changes imposed to the ERA–I and MEDSEA forcing presented in the previous paragraphs, the volume mixing ratio of five atmospheric gases (carbon dioxide, methane, nitrous oxide, and chlorofluorocarbons 11 and 12) used in the evaluation runs is modified in the scenario runs using projected values (IPCC 2007; Bernstein et al. 2008) averaged between 2070 and 2100 (Table 2). Further, the historical monthly Adriatic Sea's river discharges are climatologically changed for the RCP 4.5 & 8.5 scenarios (Fig. 5) following the

study of Macias et al. (2018). Concerning the waves, the forcing used in the evaluation simulations were kept unchanged for the scenario runs as the required data needed to apply the PGW methodology to the waves was not available. However, since the open boundary of the AdriSC ROMS 3 km grid is located at least 400–km south of the Strait of Otranto, the wave field within the Adriatic basin is not considered to be highly affected by the propagation of this forcing. Finally, as this study aims to estimate the impact of climate change on atmospherically driven extreme events and not to forecast future storms, the tidal forcing imposed for the evaluation runs was also kept unchanged for the scenario runs.

Table 2 Atmospheric gas volume mixing ratios used for the evaluation and scenario runs. From Denamiel et al. (2020a).

	carbon dioxide CO2 (ppmv*)	methane CH4 (ppbv**)	nitrous oxide N2O (ppbv**)	Chlorofluorocarbon	
				CFC–11 (pptv***)	CFC–12 (pptv***)
Evaluation	379	1774	319	251	538
RCP 4.5	528	1680	365	105	242
RCP 8.5	762	3470	408	99	231

* Parts–per–million volume ** parts–per–billion volume *** parts–per–trillion volume

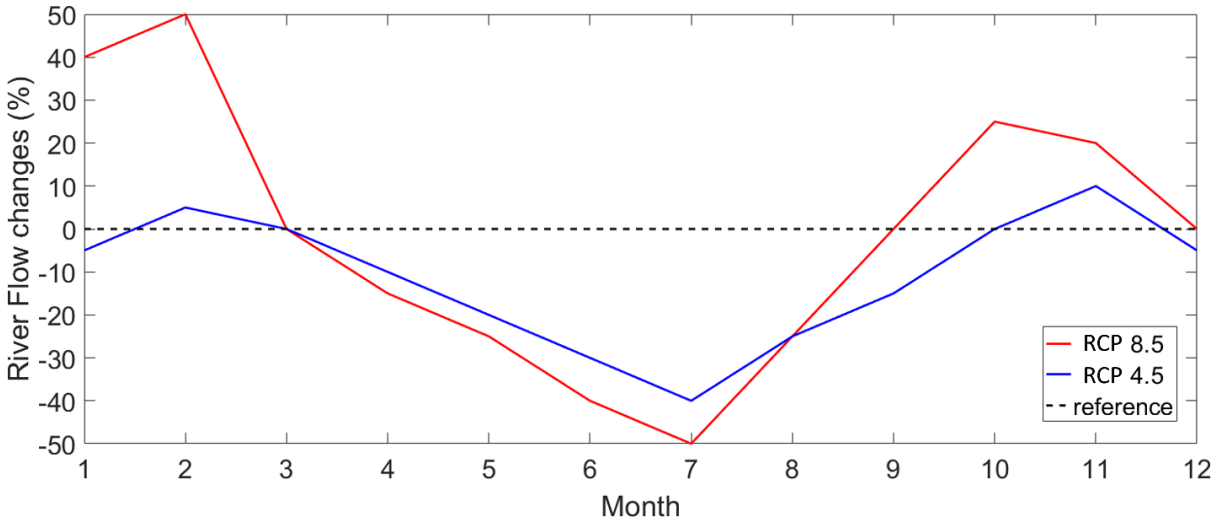

Figure 5. Monthly climatologic changes (in percentage) imposed to the Adriatic Sea river discharges for RCP 4.5 & 8.5 scenarios. From Denamiel et al. (2020a).

2.3 Simulations

2.3.1 Short–term climate simulations

These simulations were set up to reproduce the strongest historical bora windstorms which took place in the Adriatic Sea during the 1991–2018 period. In this thesis, these simulations are primarily used to demonstrate the added value of using kilometre–scale atmospheric models to reproduce extreme bora events (using observations and inter–comparison of the model results) and to assess the impact of climate change under moderate and extreme warming (RCP 4.5 & 8.5 scenarios) with the PGW approach applied to short–term simulations.

2.3.1.1 Selection of the events

The selection process of choosing the extreme events for assessing the impacts of climate change in the northern Adriatic integrates various datasets. The study primarily focuses on the strongest bora storms observed over the past three decades. The 22 representative events, spanning from 1991 to 2018, were carefully chosen from bibliographical research, incorporating meteorological bulletins, local newspapers, photographs, videos, etc. by Denamiel et al. (2020a,b). The events are chosen not only for their severity but also for the increase in available and reliable atmospheric measurements in the late 20th century, ensuring a robust assessment of the added value of the kilometre–scale approach used in the AdriSC model. These 22 bora storms stand as a comprehensive ensemble representing extreme conditions in the northern Adriatic. The references used to select these events can be found in Table 3.

2.3.1.2 AdriSC climate model setup

For each of the selected 22 events, the AdriSC basic module is set–up to run for a short period of three days: 2 days of spin–up before the 25 h of extreme event simulation (Fig. 2 and Table 1). For the evaluation runs, the initial conditions and boundary forcing are provided by the 6–hourly ERA–Interim reanalysis fields (Dee et al. 2011) in the atmosphere, by the daily MEDSEA reanalysis fields (Simoncelli et al. 2019) in the ocean and by either the 6–hourly ERA–Interim wave fields or the hourly MEDSEA–Wave fields (Ravdas et al. 2018), depending on whether the storms took place before or after the 1st January 2006, for the waves. For the far–future runs under RCP 4.5 & 8.5 scenarios, the PGW approach described in section 2.2 is applied. For all the simulations, the AdriSC extreme event module, downscaling both the evaluation and far–future results obtained with the basic module, is run offline for the last

day and half of the basic module simulations: 12 h of spin–up before the 25 h of extreme event simulation. This configuration of the AdriSC modelling suite has proven to provide reliable results (Denamiel et al. 2019, 2020a,b, 2021a).

Table 3 References used to select the date of the 22 representative extreme bora events of the ensemble.

Event	Reference: research articles, meteorological bulletins, news reports and videos
24/11/1991	Brzović and Benković (1994)
28/12/1992	Ivančan–Picek and Tutiš (1996b)
01/02/1994 16/02/1997 09/03/1998	Bilten iz područja meteorologije, hidrologije, primijenjene meteorologije i zaštite čovjekova okoliša, https://meteo.hr/proizvodi.php?section=publikacije&param=publikacije_publikacije_dhmz&el=bilteni
28/03/1995 30/03/1995	Brzović (1999)
21/12/1998	Bajić (1999)
07/11/1999	Klaić et al. (2003)
14/11/2004	Belušić and Klaić (2006)
15/12/2007	https://www.istramet.hr/vijesti/15122006–snijeg–se–zadrzao–i–tokom–dana
10/03/2010	https://www.tportal.hr/vijesti/clanak/orkanska–bura–otkinula–komad–krova–skole–20100310
02/03/2011	https://www.tportal.hr/vijesti/clanak/orkanska–bura–nosi–sve–pred–sobom–20110302
07/02/2012 11/02/2012	Ličer et al. (2016)
11/11/2013	https://rijeka.meteoadriatic.net/vremeplov–orkanska–bura–u–rijeci–i–na–kvarneru–11–11–2013
31/12/2014 01/01/2015	https://www.youtube.com/watch?v=0kNlrL_diFY
05/03/2015	https://www.crometeo.hr/orkanska–bura–na–jadranu–foto–video
17/01/2017	https://www.tportal.hr/vijesti/clanak/snazna–bura–u–istri–stvara–velike–teskoce–20170117
13/11/2017	https://www.tportal.hr/vijesti/clanak/bura–otrgnula–novi–brod–i–zabila–ga–u–mol–u–puli–foto–20171113

24/09/2018	https://www.tportal.hr/vijesti/clanak/orkanska–bura–srucila–se–na–split–kontejneri–setaju–ulicama–problemi–u–pomorskom–prometu–ali–i–na–nebu–foto–20180924

2.3.1.3 Observations

Due to the lack of high–resolution (spatially and temporally) atmospheric gridded products in the northern Adriatic region, the evaluation of the atmospheric models for the ensemble of the 22 selected extreme bora events could only be performed against long–term land–based observations extracted at 9 different stations (Trieste, Ogulin, Rijeka, Senj, Zavižan, Rab, Lošinj, Gospić and Knin; see Table 4) from the databases of the NOAA's National Centers for Environmental Information (Smith et al. 2011; https://www.ncdc.noaa.gov/isd, last visited 15 November 2023) and the Croatian Meteorological and Hydrological Service (DHMZ, http://meteo.hr, last visited 15 November 2023). The coverage of the chosen events by these stations varies from 9 % in Lošinj to 76 % in Trieste with an average of 35 % (Table 4). As all stations but three (Rab, Lošinj and Knin) were in operation before 1991, this relatively low coverage can mostly be explained by the difficulties inherent with obtaining valid measurements during extreme events.

Table 4 Surface data available between 1991 and 2019 from land–based meteorological stations located in the studied area and sorted by decreasing latitude.

Name	Location	Height (m)	Period of measurements	PRC* (%)
Trieste	13.750 °E, 45.650 °N	20	01/01/1991 – 01/01/2019	76
Ogulin	15.233 °E, 45.267 °N	328	01/01/1991 – 01/01/2019	38
Rijeka	14.570 °E, 45.217 °N	85	01/01/1991 – 01/01/2019	16
Senj	14.900 °E, 44.983 °N	26	01/01/1991 – 01/01/2019	43
Zavižan	14.983 °E, 44.817 °N	1597	01/01/1991 – 01/01/2019	44
Rab	14.767 °E, 44.750 °N	20	01/02/1996 – 01/01/2019	30
Lošinj	14.400 °E, 44.567 °N	45	10/05/2004 – 01/01/2019	9
Gospić	15.367 °E, 44.550 °N	564	01/01/1991 – 01/01/2019	44
Knin	16.200 °E, 44.033 °N	255	27/02/1996 – 01/01/2019	11

* Percentage of hourly model results covered by the measurements

2.3.2 Long–term climate simulations

In contrast with the short–term numerical experiments presented in section 2.3.1, the 31–year long AdriSC simulations were set up with the aim to better understand the inter–annual and decadal atmosphere–ocean processes driving the Adriatic basin circulation. However, due to the extreme numerical cost of these simulations, only two runs using the basic module coupling WRF and ROMS (i.e. no wind–wave modelling) have been performed: an evaluation run during the 1987–2017 period forced by reanalysis products and an extreme warming run during the 2070–2100 period for the RCP 8.5 scenario.

2.3.2.1 AdriSC climate model setup

For the evaluation run, the initial conditions and boundary forcing of the AdriSC WRF 15 km grid are provided by the 6–hourly ERA–Interim reanalysis fields at 0.75° resolution (Dee et al. 2011). The SST forcing is provided by the MFS high–resolution (1/16° × 1/16°) MEDSEA re–analysis from the Copernicus Marine Environment Monitoring Service (CMEMS; Simoncelli et al. 2019), which is also used as boundary conditions for the AdriSC ROMS 3 km grid. For the far–future extreme warming run, the PGW approach described in section 2.2 is used.

The long–term AdriSC climate simulations were initialised on 1 November 1986 and 2070 in order to have a short 2–month spin–up period allowing the ocean models to reach a steady state. The short–term climate simulations have indeed shown that rapid equilibrium is reached within the AdriSC ocean models due to (1) the use, before 1 January 1987, of monthly (instead of daily) MEDSEA reanalysis products, which have a relatively fine resolution (about 9 km) and assimilate all available data in the Mediterranean Sea, and (2) the relatively small size of the ROMS ocean domains. Ideally, several long–term simulations should have been run with different spin–up periods in order to better quantify the impact of the initial conditions on the long–term ocean model results. However, due to numerical resource limitations, such systematic tests have not been carried out with the AdriSC climate model.

2.3.2.2 Observations

In–situ temperature and salinity quality checked observations collected along the long–term monitoring Palagruža Sill transect (by the Institute of Oceanography and Fisheries, Croatia; Fig. 1) and the northern Adriatic transect (by the Ruđer Bošković Institute, Croatia; Fig. 1) are used to assess the added value of the AdriSC kilometre–scale approach. These two

datasets present the advantage of having been collected regularly (i.e. nearly every month since 1979 for the northern Adriatic transect and twice a year to seasonally since 1952 for the Palagruža Sill transect) and sampled at predefined stations (i.e. 6 for the northern Adriatic transect and 5 for the Palagruža Sill transect) for standard depths (i.e. 0, 5, 10, 20, 30, 35 m depth for the northern Adriatic transect and 0, 10, 20, 30, 50, 75, 100, 120, 150, 170 m depth for the Palagruža Sill transect). These transects have been established as being the most convenient for maintenance by the monitoring institutions (that are positioned at the transect ends), while covering two important areas for the Adriatic basin–wide dynamics. Namely, the northern Adriatic transect is overlaying the dense water formation site (Bergamasco et al. 1999; Janeković et al. 2014; Vilibić et al. 2019) where the densest Mediterranean waters are being generated (Zore 1963), bringing oxygen to the bottom layers and driving the thermohaline circulation of the Adriatic–Ionian region (Orlić et al. 2007). The Palagruža Sill transect is covering a key region for the exchanges of water masses along the Adriatic Sea and is a passage where quasi–permanent topographically– driven Southern Adriatic Gyre and Middle Adriatic Gyre are exchanging water masses (Artegiani et al. 1997a; Martin et al. 2009). Additionally, dense water outflow from the northern Adriatic can be traced at the deepest and southern parts of the sill (Artegiani et al. 1987), while the across sill transport driven by the Western Adriatic Coastal Current is confined to the western coast (Burrage et al. 2009).

2.4 Methods

2.4.1 Analysis of the short–term simulations

The short–term climate simulations of the AdriSC model were performed with two main aims. The first aim was to bridge the knowledge of the process–oriented atmospheric modelling community (i.e. need for resolutions of the order of 100 m) with the demands of the climate community in terms of model efficiency (i.e. minimization of the computation time and numerical cost drastically increasing with model resolution). As running coupled climate models at 1.5 km resolution in the atmosphere is unrealistic (i.e. within the AdriSC modelling suite, it is 9 times slower to run WRF 1.5 km alone than to run the coupled atmosphere–ocean basic module), the baseline conditions used to assess the added value of the kilometre–scale approach for climate studies are derived from the WRF 3 km results provided by the AdriSC basic module. The impact of the atmospheric models' resolution on the analysis of the baseline bora conditions derived from the AdriSC WRF models as well as from the ERA5 reanalysis (at 0.25° or about 30 km horizontal resolution; Hersbach et al. 2018), for the selected ensemble

of bora events, is thus defined relatively to these conditions. In this context, it is assumed that if the increase in resolution does not strongly affect the dynamics and air–sea interactions during severe bora events (i.e. changes below 1 % of the baseline conditions), this impact is minimised, and lower resolution can be used in climate studies. In addition, distributions of physical quantities in geoscience are generally non–Gaussian during extreme events. Consequently, the median and median absolute deviation (MAD) are used (instead of mean and standard deviation) to represent the most common conditions and their associated variabilities derived from the ensemble of 22 selected extreme bora events. The strategy adopted to perform the statistical analysis of the results is thus:

- to identify and extract the peak of each storm (i.e. maximum wind speed along the lee of the Velebit mountain range) for each model separately. Given the statistical approach used (via the analysis of the ensemble), the precise timing of the events is considered unimportant
- for the description of the basic bora dynamics, to derive meaningful variables such as horizontal wind speed, vertical wind velocity, virtual potential temperature, potential vorticity (PV), turbulence kinetic energy (TKE) for the WRF models (as TKE is not an available product of ERA5 reanalysis), and minimum (in the vertical) static stability over the land, at the peak of each storm
- for the description of the air–sea interactions, to derive the maximum wind stress (τ) which is partially driving the ocean circulation and the minimum sensible (Qs) and latent (Ql) heat fluxes (derived with a constant sea surface temperature averaged from the northern Adriatic ROMS 3 km results for each event)
- to define the baseline conditions and their associated variability, for each of these variables from the WRF 3 km results; and
- to evaluate the impact and variability of the ERA5 reanalysis, WRF 15–km, and WRF 1.5–km horizontal grid resolutions, on each of these variables derived from the distributions of the 22 differences between each model separately and WRF 3 km

For the bora dynamics which overall has a three–dimensional nature, the results are presented as horizontal conditions at 50 m above the ground, vertical cross–sections and probability density functions along the cross–section of four different heights (0.5, 1, 3, and 5 km). The chosen vertical cross–section is extracted for a transect starting near Senj along the strongest

and the most extended offshore jet observed in the baseline conditions for the 10–m maximum wind speed (i.e. median of the ensemble composed of the maximum 10–m wind speed, at each point of the WRF 3 km grid and for each event; Fig. 6a). Additionally, probability density functions of the 10–m wind speed at four heights (0.50, 1, 3, and 5 km) are also derived along the Senj transect. For the air–sea interactions, the results are presented as sea surface plots and probability density functions at three points located at 50, 100, and 150 km along the Senj transect (marked with black dots in Figure 6a) where the formation of dense water is known to occur. It is important to notice that, in the following analyses, these probability density functions are obtained via a kernel smoothing method, which presents the advantage of generating continuous distributions but may overestimate the tails of these distributions. However, all the statistical values of these distributions were extracted directly from the raw model results.

The second aim of the short–term climate simulations was to analyse the impact of climate change on the 22 extreme bora event strength and dynamics by:

- identifying and extracting the peak of each storm for each mode – i.e. evaluation as well as RCP 4.5 & 8.5 scenarios,
- deriving meaningful physical variables such as horizontal wind speed, vertical wind velocity, virtual potential temperature and potential vorticity (PV) at the peak of each storm and for each mode,
- defining the extreme conditions for the evaluation runs (hereafter baseline) and the RCP 4.5 & 8.5 runs, for each of these physical variables, as the median derived from the ensemble of the 22 AdriSC WRF 3 km results,
- evaluating the climate impact on each of these physical variables – called climate adjustment hereafter, as the medians derived from the ensemble of the 22 differences between the peak conditions of RCP 4.5 & 8.5 simulations separately and evaluation results.

In this thesis, these results are presented as horizontal slices from the surface conditions (at 5 m height following the terrain) to 2 km height every 0.5 km and vertical cross–sections (Fig. 6a) extracted for 4 transects (starting near Trieste, Senj, Zavižan and Gospić), chosen where the bora jets were the strongest and the further extended offshore in the evaluation simulations. Additionally, in order to capture the impact of climate change on the sea surface cooling, the spatial variations of the RCP 4.5 & 8.5 baseline and climate adjustment conditions of the

minimum surface heat fluxes (decomposed as total, sensible and latent fluxes) and the minimum sea surface temperature (SST) anomaly (defined as the difference between the hourly SST and the initial SST taken 24–h before each event) are derived from respectively the AdriSC WRF 3 km and AdriSC ROMS 1 km results. The distributions of the hourly surface heat fluxes and SST anomalies in evaluation and scenario (RCP 4.5 & 8.5) modes are also analysed for the ensemble of 22 events at 12 different locations (Fig. 6a, points P1 to P12) where the sea surface cooling was the most intense in evaluation mode.

For all short–term simulations, the physical quantities used for the description of the bora dynamics are as follows:

θ	potential temperature (K)
r	mixing ratio (kg/kg)
$g = 9.81$	gravitational acceleration (m/s^2)
α	specific volume (m^3/kg)
$\mathbf{\Omega}$	angular velocity vector of the earth's rotation (rad/s)
$\mathbf{u}$	three-dimensional wind velocity vector (m/s)
U	horizontal wind speed (m/s)
$\theta_{va} = \theta(1 + 0.61r)$	virtual potential temperature (K)
$N = \left(\frac{g}{\theta_{va}} \frac{\partial \theta_{va}}{\partial z} \right)^{\frac{1}{2}}$	Brunt-Väisälä frequency (1/s or Hz)
$PV = \alpha (2\mathbf{\Omega} + \nabla \times \mathbf{u}).\nabla\theta$	potential vorticity (PVU = 10^{-6} m^2 K s^{-1} kg^{-1})

The physical quantities used for the calculation of the surface heat fluxes are as follows:

U_a	horizontal wind speed at 2 m (m/s)
T_a	air temperature at 2 m (°C)
T_s	sea surface temperature (°C)

r_h	relative humidity at 2 m (%)
ρ_a	density of moist air at 2 m (kg/m^3)
P_a	mean sea level pressure (hPa)
$e_{sat}(T)$	saturation vapor pressure (hPa)
$L(T) = 2501000 - 2370T$	latent heat of vaporization (J/kg)
$C_H, C_E = 0.00115$	turbulent transfer coefficients
$C_p = 1004.67$	specific heat capacity (J K^{-1} kg^{-1})
$q_a \approx \frac{0.62197(0.01\, r_h\, e_{sat}(T_a))}{p_a}$	air saturation specific humidity at 2 m (kg/kg)
$q_s \approx \frac{0.62197(0.98\, e_{sat}(T_s))}{p_a}$	sea surface saturation specific humidity (kg/kg)
$Q_H = \rho_a C_H C_p U_a (T_a - T_s)$	sensible heat flux (W/m^2)
$Q_E = \rho_a C_E U_a L(T_s)(q_a - q_s)$	latent heat flux (W/m^2)

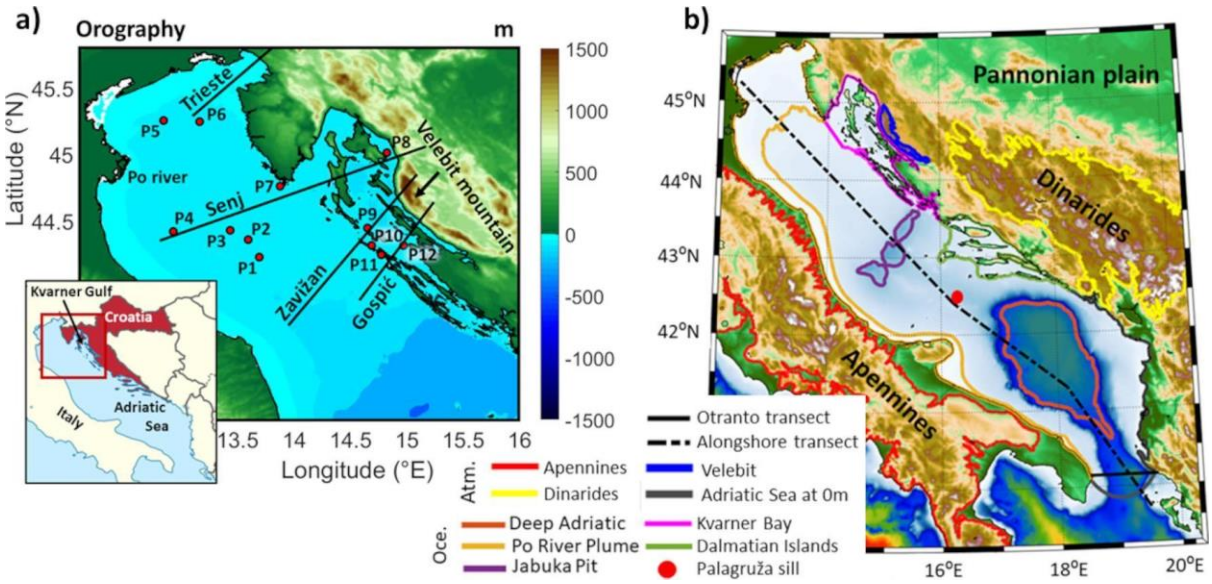

Figure 6. Subdomains, extraction points and transects used for the analysis of (a) the short–term simulations and (b) the long–term simulations.

2.4.2 Analysis of the long–term simulations

In this thesis, the analysis of the evaluation (1987–2017) and extreme warming (2070–2100) long–term climate simulations is twofold. First, the added value of the AdriSC kilometre–scale atmosphere–ocean approach in terms of modelling the Adriatic thermohaline variability linked to the BiOS cycles is discussed. Second, the atmosphere–ocean trends, variability, and number of extreme events from both evaluation (i.e. historical conditions) and extreme warming simulations (i.e. far-future extreme warming conditions) are analysed and compared with the aim to assess the impact of climate change.

2.4.2.1 BiOS–driven thermohaline variability

The added value of the AdriSC kilometre–scale approach is demonstrated by comparing the AdriSC ROMS 1 km salinity and temperature daily results with the long–term observations along the Palagruža Sill and northern Adriatic transects and by connecting the long–term thermohaline variability reproduced by the AdriSC model over the entire Adriatic basin with the well–known BiOS cycles during the 1987–2017 period.

Along the two transects, the AdriSC ROMS 1 km model results are extracted at regular depths (i.e. every metre for the northern Adriatic transect and every 5 m for the Palagruža Sill transect) as linear segments defined by two stations. The results are presented as one single section oriented from west to east for the northern Adriatic transect and from south to north for the Palagruža Sill transect.

The long–term variability is derived from the monthly means of the detrended daily anomalies of sea–level, temperature, salinity, and current speed with Empirical Orthogonal Functions (EOFs). The EOFs are used to compare, in space and time, the most important variability patterns in the Adriatic and northern Ionian seas. Gačić et al. (2010, 2011, 2014) have demonstrated that the BiOS — consisting in the decadal switch from cyclonic to anticyclonic of the circulation in the northern Ionian Sea (and vice versa) — is well described with the change of sign of one of the main EOF components derived from sea–level products in the Ionian Sea. Here, for consistency, the BiOS signal is derived from the sea–surface height field (SSH) of the MEDSEA reanalysis (Simoncelli et al. 2019) distributed by the Copernicus Marine Environment Monitoring Service (CMEMS). All the presented spatial EOFs (also known as Principal Component Analysis or Eigen Analysis) are obtained via a covariance matrix and are normalised (i.e. the sum of squares for each EOF pattern equals one). The time series of the amplitudes (also known as principal components or expansion coefficients) associated with each eigenvalue in the EOF are derived via the dot product of the data and the EOF spatial patterns, and the mean is subtracted from the value of each component time series. Consequently, the BiOS signal derived from one of the MEDSEA sea–level EOFs can be correlated with the long–term variability of temperature, salinity and current speed given by the EOF time series derived from the AdriSC ROMS 1 km model results. All presented correlations are significant with levels below 5 % following the null–hypothesis and the statistical significance of the correlation is conducted by a Monte Carlo simulation using random phase resampling (Ebisuzaki 1997). It should be noted that (1) all correlations and time series comparisons between the BiOS signal and the long–term Adriatic Sea thermohaline variabilities have been made for signals smoothed with a 3–month running mean and (2) for visual purposes, EOF time series have been rescaled in order to have similar amplitudes in the comparison plots.

2.4.2.2 Trends, variability, and extremes

The analysis of the present climate trends and variability extracted from the AdriSC 31–year long evaluation run (i.e. 1987–2017 period) is performed in two distinct ways. First regionally, over the entire Adriatic region and selected ocean transects, and second, monthly, over subdomains of interest. In the regional analysis, anomalies and trends are first derived from the daily data: (1) horizontally, over the entire Adriatic basin (i.e. AdriSC WRF 3 km domain in the atmosphere and AdriSC ROMS 1 km domain in the ocean) at the surface only for the atmosphere but also at the bottom and 100 m depth for the ocean; and (2) vertically, for

two ocean transects (Otranto and Alongshore transects). Daily anomalies are estimated by subtracting the long term mean from each point of the 3D domain (i.e. time, latitude and longitude; hereafter daily seasonal cycles) from the detrended daily data (i.e. calculated trends removed from the model results at each point). Trends are then calculated with the Theil–Sen method (Mondal et al. 2012) and trend significances are calculated with the Mann–Kendall test (Mann 1945; Kendall 1975; Gilbert 1987). Contrary to ordinary least squares regression (Qian et al. 2019), the Theil Sen trend is insensitive to outliers and can be significantly more accurate than simple linear regression for skewed and heteroskedastic data. It also competes well against non-robust least squares even for normally distributed data in terms of statistical power (Mondal et al. 2012). Only trends with significance over 95 % are taken into consideration and presented. Total detrended variances are calculated from the detrended daily data (defined as the sum of the daily seasonal cycles and the anomalies), while percentages of variability caused by anomalies (hereafter percentage anomaly) are computed as the ratio (multiplied by 100) of the variance derived from the anomaly and the total detrended variance. Consequently, the more prominent the seasonal cycle is, the lower the percentage anomaly will be. The subdomains for atmospheric and oceanic variables are presented in Figure 6b and selected due to their importance in terms of physical interpretation (derived either from previous studies or the regional analysis). Subdomains have been selected following well–known dynamical properties of the Adriatic region. For example, the Velebit mountain is a known location for the formation of severe bora winds, the Kvarner Bay is an area where dense water forms, while Jabuka Pit and Deep Adriatic are known collectors of dense water (Denamiel et al. 2022). In addition, some subdomains were selected following the evaluation of the AdriSC model (Pranić et al. 2021). The subdomains are: (1) Adriatic Sea (as a whole), Apennines (with at least 150 m in altitude), Velebit (with at least 800 m in altitude) and Dinarides (with at least 800 m in altitude) for the atmosphere, and (2) Dalmatian Islands (with less than 100 m in depth), Deep Adriatic (deeper than 800 m), Jabuka Pit (deeper than 200 m), Kvarner Bay (deeper than 55 m), and Po River Plume (with less than 40 m in depth) for the ocean. First, for each subdomain, monthly datasets are derived for the mean, maximum, and minimum values extracted from the raw AdriSC daily data only at the surface for each atmospheric variable but also at the bottom and 100 m depth for each ocean variable. Monthly trends and variances are then determined for each variable, depth/height, dataset, and subdomain. Finally, unique mean monthly trend value and mean monthly variance value for each subdomain are derived as the average over all the subdomain points for each variable, depth/height, and dataset. It should also be noted that (1) when less than 50 % of the points of

the subdomain have trends with 95 % of significance, the results are marked with a black diagonal line in the figures, and (2) when the subdomain depths are all lower than 100 m, no data is displayed in the ocean figures for the 100 m depth analysis.

In order to derive the impact of climate change within the Adriatic basin, the far–future trends and variability over the entire Adriatic region as well as the number of extreme events are also extracted from the AdriSC extreme warming run (i.e. 2070−2100 period) and compared with the results of the evaluation run (i.e. 1987–2017 period, hereafter referred as historical conditions). They are derived for the surface AdriSC WRF 3 km daily results (i.e. temperature at 2 m, rain, relative humidity at 2 m and wind speed at 10 m) in the atmosphere, and for the bottom, 100 m depth and surface AdriSC ROMS 1 km daily results (i.e. temperature, salinity, and current speed) in the ocean. Variances and trends are derived over the entire Adriatic region (AdriSC WRF 3 km domain in the atmosphere and AdriSC ROMS 1 km domain in the ocean) similarly to the present climate analysis. The impact of climate change is calculated as percentages of trends/variances, computed as the ratio (multiplied by 100) of the difference between extreme and historical trends/variances and absolute value of historical trends/variances. The results are presented as spatial plots covering the whole studied area. The impact of climate change on the number of extreme events is derived for selected subdomains (Fig. 6b). In the atmosphere, the variables are analysed for the land and sea subdomains in order to reflect the differences in heat capacity and heat transfer mechanisms. Indeed, land surfaces heat up and cool down more rapidly than sea masses, which results in distinct temperature gradients and air pressure variations. Consequently, local wind patterns, cloud formation, and precipitation distribution can significantly differ between land and sea areas. The ocean variables are analysed for the deep and coastal subdomains which cover the Southern Adriatic Pit and the deep areas surrounding it, and the rest of the Adriatic with relatively shallow depths, respectively. These subdomains reflect the differences between the shallow and nearshore areas which may experience more significant temperature and salinity fluctuations in response to extreme weather events, river discharges, tides, etc. and the more stable deep areas less impacted by these processes. For each of the subdomains, monthly means are derived from the extreme warming and historical AdriSC daily results. The monthly analysis is conducted through two distinct approaches applied to each studied variable. First, the difference between extreme warming and historical monthly climatologies is computed, serving as a basic indicator of the monthly changes in average conditions. Second, the 10^{th} and 90^{th} percentiles of the historical monthly data are determined, serving as minimum and

maximum historical thresholds needed to calculate the number of days within a month below or above these thresholds (i.e. the number of extreme low or high events). To quantify the change in occurrences of extreme values under extreme warming conditions, compared to the historical ones, the number of days in the historical run with values below (or above) the minimum (or maximum) historical thresholds are subtracted from the number of days in the far-future climate. This represents approximately 3 days per month. The monthly analysis of the extreme events is not performed both at 100 m depth for the coastal subdomain, as only a few model grid points in this domain fall below 100 m, and for the extreme low rain events as the minimum threshold is 0 mm/day at almost all model domain grid points.

3. ADDED VALUE OF KILOMETRE–SCALE MODELLING

Atmosphere–ocean modelling involves a perpetual trade–off between precision and computational efficiency. This trade–off is particularly pronounced when addressing complex phenomena such as severe bora dynamics and dense water formation in the northern Adriatic. Process–oriented studies have established that achieving an accurate representation of the bora dynamics requires model resolutions on the order of 100 metres, while the first baroclinic mode of the Rossby radius of deformation highlights that less than 500 m resolution is required to properly represent the North Adriatic Dense Water (NAddW) dynamics (Pranić et al. 2023). However, in the context of broader regional climate studies, the challenge is to strike a balance between computational resource constraints and the level of precision required. This often leads to the use of coarser resolutions, typically around 10 kilometres. Unfortunately, this coarser approach fails to capture the intricate details, such as coastal dense water formation or the long–term Adriatic–Ionian thermohaline circulation that emerges from complex events and air–sea interactions. The goal of the work presented in this section is to bridge the knowledge of the process–oriented atmospheric modelling community (i.e. need for resolutions of the order of 100 m) with the demands of the climate community in terms of model efficiency (i.e. minimization of the computation time and numerical cost drastically increasing with model resolution) and prove the added value of the kilometre–scale modelling approach in the Adriatic region with two different cases. The first case deals with the representation of extreme bora events in the northern Adriatic and is presenting the work published by Denamiel et al. (2021a) while the second case examines the capacity of the AdriSC model to reproduce the BiOS-driven Adriatic Sea thermohaline variability and is presenting the work published by Denamiel et al. (2022).

3.1 Case 1: Extreme bora events

In the northeastern Adriatic region, both the physics and the numerical model representation of severe bora events have been intensively studied for over 30 years. These downslope winds strongly influenced by the complex orography can be associated with hurricane–strength gusts up to 50 m/s (Belušić & Klaić 2004). Storms occur most frequently and most intensely along, and downstream of, the lee of the northern Velebit mountain range, where breaking of gravity–waves and jet–like flows develop (e.g. Belušić et al. 2007; Gohm et al. 2008; Grubišić 2004; Klemp & Durran 1987; Kuzmić et al. 2015). Additionally, severe bora events are known to strongly impact a great number of human activities in the coastal Adriatic regions (Biolchi et al. 2019a; Davolio et al. 2015; Kozmar et al. 2012; Lepri et al.

2017; Niziol et al. 1995; Radić et al. 2003; Stocchi & Davolio 2017). The first comprehensive research of the Adriatic bora was performed by Japanese researchers (Yoshino 1976) due to similarities with their own local events.

The representation of extreme bora events is not only a useful tool for evaluating and improving atmosphere–ocean climate models in the Mediterranean Sea (Belušić Vozila et al. 2019) but also a necessity for a chance at meaningful climate projections of the Ionian–Adriatic oceanic system (Soto–Navarro et al. 2020). In regional climate studies, the influence of complex mountain orography on the atmospheric dynamics has been the subject of extensive research over the past few decades. In particular, Vosper et al. (2018) demonstrate that the development of kilometre–scale atmospheric climate models has allowed a better representation of wave–breaking, gap flows, and convection. However, these models are incapable of representing the detailed rotor dynamics for which resolutions of the order of 100 m are needed. In the Adriatic region, some studies have been focusing on the capability of regional climate models to reproduce mesoscale wind phenomena. They found that atmospheric resolution, via a better reproduction of the orography and consequently the enhancement of jet flows on finer grids, is one of the most important model characteristics known to impact wind speed (Belušić et al. 2017). More specifically, for the bora events which are historically studied with (sub)– kilometre–scale models (e.g. Grisogono & Belušić 2009; Kuzmić et al. 2015; Prtenjak et al. 2010; Trošić & Trošić 2010), a brief investigation by Josipović et al. (2018) reveals that regional climate models (with a resolution of 0.11°) are incapable to represent wave–breaking. They thus should not be used to derive the changes in bora wind intensity under climate scenarios. However, this study was only based on 12 moderate events (with observed average wind speed below 15 m/s) selected between December 1999 and November 2000 and not on extreme events during the last 30 years.

The analyses performed here are based on a statistical approach, commonly used in climate studies. The influence of the atmospheric model resolutions (ranging from 30 km in ERA5 reanalysis to 1.5 km in the AdriSC modelling suite) on the representation of the dynamics and air–sea interactions of severe bora storms in the northern Adriatic is thus quantified using the ensemble of 22 extreme events presented in section 2.3.1.1.

3.1.1 Evaluation of the different atmospheric model skills

To assess the skills of ERA5 reanalysis and the AdriSC WRF models during extreme bora events in the northern Adriatic region, the hourly 10–m wind speed and direction, 2–m air

temperature and dew point, as well as the mean sea–level pressure, are extracted from the 22 selected storm simulations at 10 land–based station locations (see section 2.3.1.3). As this analysis is based on a statistical approach using an ensemble of events, the data are analysed as quantile–quantile plots (wind speed, temperature, dew point, and pressure) and rose plot (wind direction). These plots show the capability of the models to overall reproduce the observed distributions of these surface meteorological parameters for the entire set of events (i.e. the capability of the models to represent each event separately is not discussed).

It is also important to notice that the quality of the wind measurements in the northern Adriatic during extreme events can be questioned. In particular, concerning the observations in Senj, study from Klaić et al. (2009) demonstrates that extreme events are substantially stronger than the operationally measured winds due to the sheltered location of the station with respect to bora flow. Similarly, Belušić et al. (2013) and Kuzmić et al. (2015) report that the Rab and Mali Lošinj stations are also located in sheltered areas. As lower–elevation stations are much more likely to be located in sheltered areas, the quantile–quantile distributions of the 10–m wind speed are thus only plotted for higher–elevation stations (Pula, Rijeka, Ogulin, Zavižan, Gospić, and Knin).

On the whole (Fig. 7), for the 22 studied storm events, the models are in good agreement with the available measurements. First, the quantile–quantile distributions are generally following the reference lines, except for the 10–m wind speed which is not well reproduced by any of the models. And, second, the main modelled wind directions are following the observations in the rose plot. Further, at the station locations, no model seems to clearly perform better than the others (except for the wind speed). However, in more detail, some discrepancies between the observation and model distributions are noticeable for all the models, independently of their physics and resolution. First, the observed mean sea–level pressure (Fig. 7b) is underestimated by 2–5 hPa between 1000 and 1030 hPa, with the ERA5 distribution being the closest to the measurements. Second, the observed 2–m air temperature and dew point (Figs. 7c and 7d) are strongly overestimated (by up to 10 °C), particularly by ERA5 and WRF 15 km, between −22 and −7 °C and for the entire distribution (with an average of 2 above −7 °C), respectively. Then, the number of observed occurrences of the 10–m wind direction is overestimated between 30° and 60°, by 100 for WRF 3 km and WRF 1.5 km, by about 150 for WRF 15 km and by 300 for ERA5.

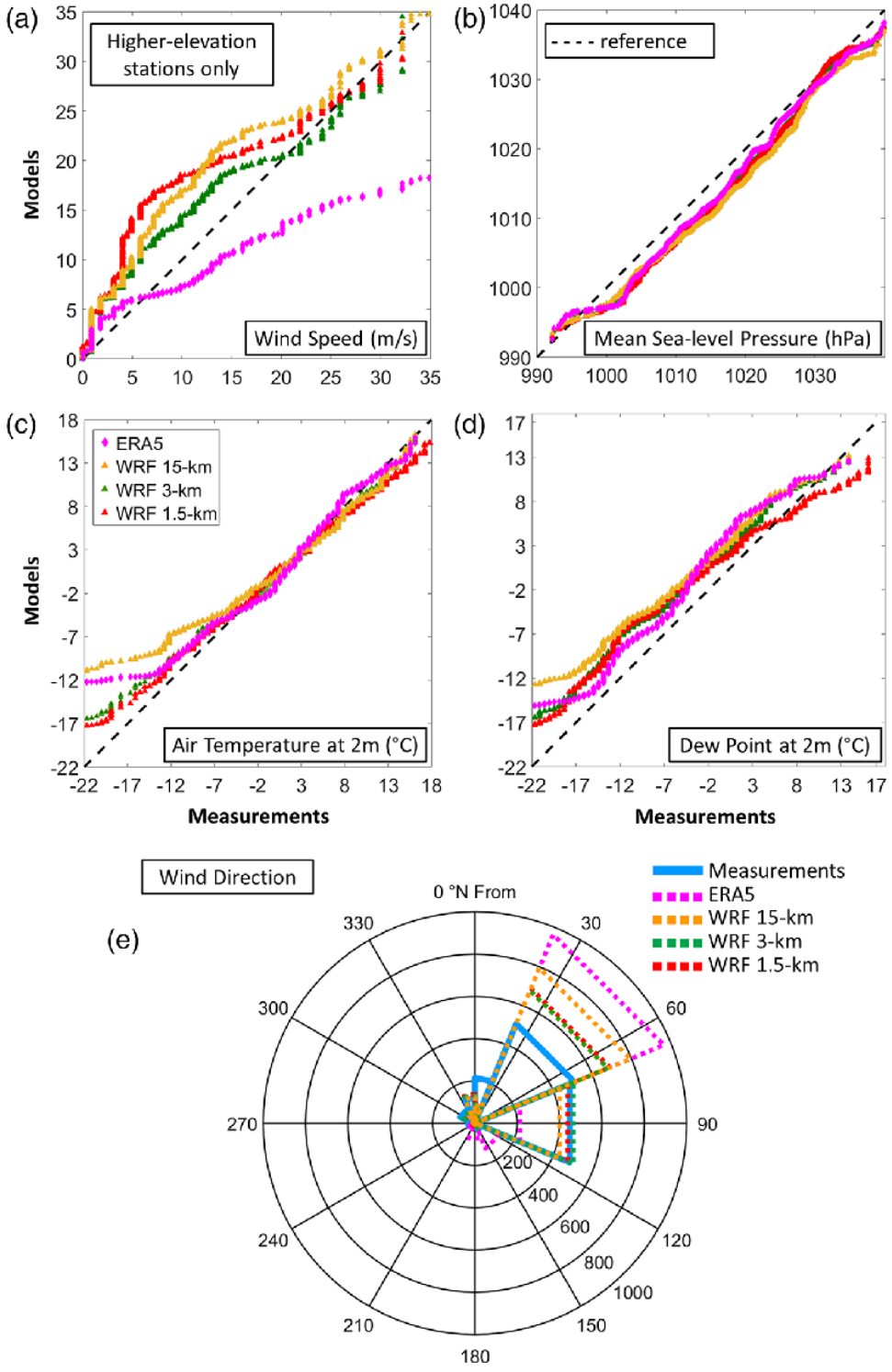

Figure 7. Evaluation of the ERA5 reanalysis and AdriSC WRF 15 km, 3 km, and 1.5 km model results against wind speed (quantile–quantile or q–q plot, only for higher–elevation stations, panel a) and direction (rose plot panel e) at 10 m, mean sea–level pressure (q–q plot panel b) and air temperature and dew point at 2 m (q–q plots panels c and d) measurements at the nine available stations.

Between 60° and 120° the number of observed occurrences of the 10–m wind direction is largely underestimated, by 250 for ERA5, but generally well represented by all the WRF models. For the 10–m wind speed at high–elevation stations, even though the WRF models

capture the extreme values of the storms, they strongly overestimate values between 5 and 20 m/s as previously documented by Belušić et al. (2017) and Obermann–Hellhund & Ahrens (2018). In contrast, ERA5 reanalysis underestimates all the extreme values above 20 m/s by up to 50 % and the values between 5 and 20 m/s by at least 15 %.

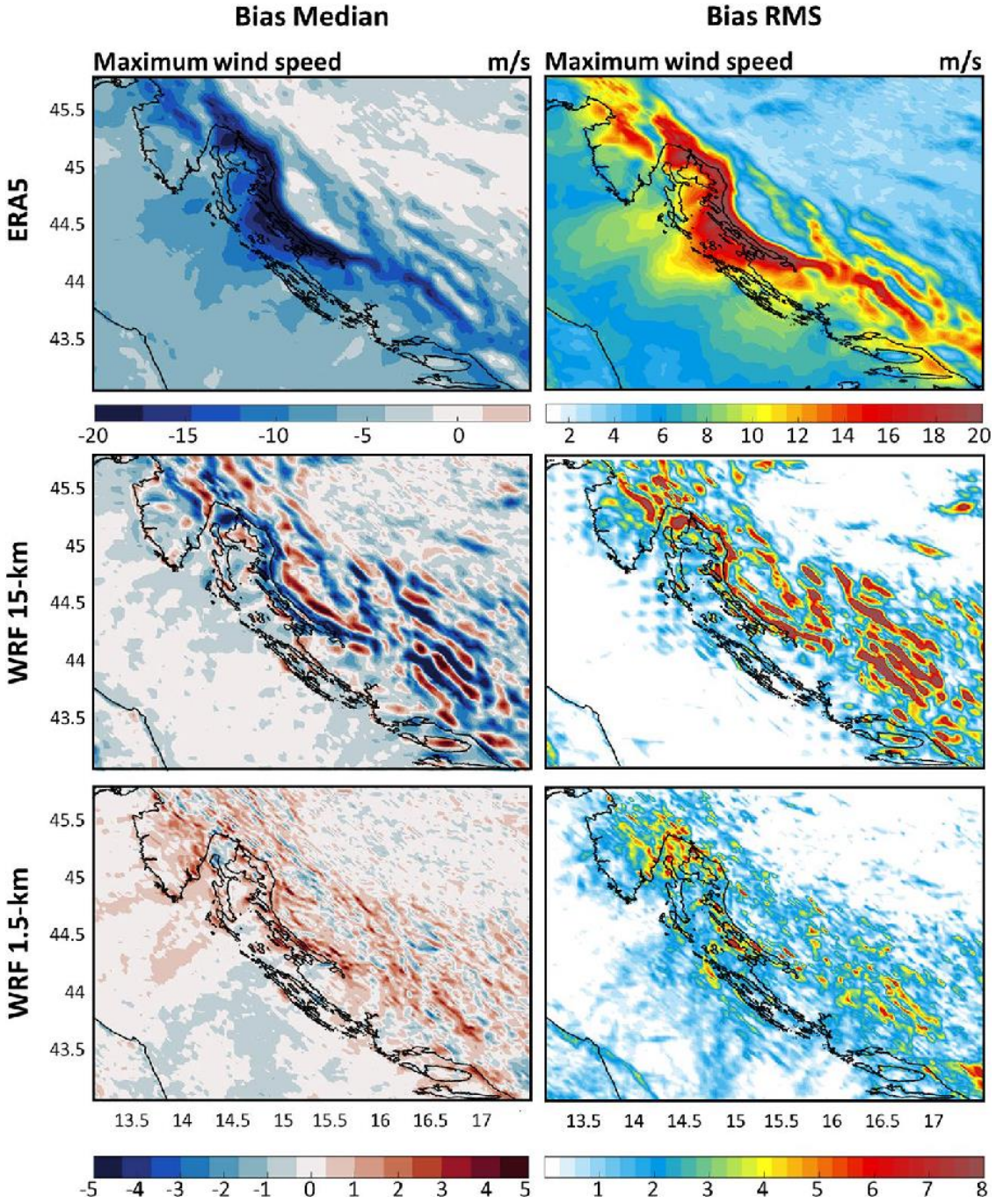

Figure 8. Impact of the model resolution on the 10–m maximum wind speed baseline conditions defined as the median and root–mean–square (RMS), for the ensemble of the 22 bora events of the difference (or bias) between ERA5, AdriSC WRF 15 km, WRF 1.5 km, and AdriSC WRF 3 km model results.

Additionally, for the maximum 10–m wind speed, the baseline conditions are spatially compared with WRF 15 km, WRF 1.5 km, and ERA5 as median biases and variabilities for the ensemble of 22 events (Fig. 8). Although being based on numerical results, this comparison clearly highlights that the ERA5 reanalysis homogeneously underestimates by up to 20 m/s (with a variability of 15 m/s in average) the extreme bora winds along the Velebit mountain range and over the Kvarner Bay. However, biases for the WRF 15 km and WRF 1.5 km models are localised and inhomogeneous (i.e. positive and negative biases are mostly found on opposite sides of the mountain ridges) and only reach up to ±5 m/s (with a maximum variability of 8 m/s) for WRF 15 km and ±1.5 m/s (with a maximum variability of 5 m/s) for WRF 1.5 km. These results, combined with the analysis of the higher–elevation stations (Fig. 7a), confirm that the ERA5 reanalysis is largely underestimating the strength of the extreme bora events in the northern Adriatic region.

The preliminary findings of this evaluation can be summarised as follows. First, all WRF models and ERA5 reanalysis are capable of reproducing, with a certain level of accuracy, the observed 2–m air temperature and dew point as well as the mean sea–level pressure independently of their resolution and physics. Then, the reproduction of the 10–m wind speed and direction highly depends on the model resolution — i.e. the representation of the Velebit mountain complex orography. And, finally, the ERA5 reanalysis seems incapable of reproducing the strength of severe bora surface winds over the whole northern Adriatic region.

3.1.2 Bora dynamics

Here, the capability of the AdriSC WRF 3 km model to reproduce both the basic bora dynamics (excluding the rotor dynamics) in the northern Adriatic region and the impact of atmospheric model resolution on the representation of the severe bora events is assessed. The baseline conditions extracted from WRF 3 km results as well as the ERA5, WRF 15 km, and WRF 1.5 km biases (i.e. differences with WRF 3 km results) defined as the median of the ensemble of 22 events are thus presented in Figures 9, 11 and 13, together with their associated variabilities (represented by the MAD of the ensemble) provided as Figures 10, 12 and 14. It is important to notice that, in these figures, the presented quantities are median (or MAD) values extracted from the ensemble and consequently are not to be compared physically.

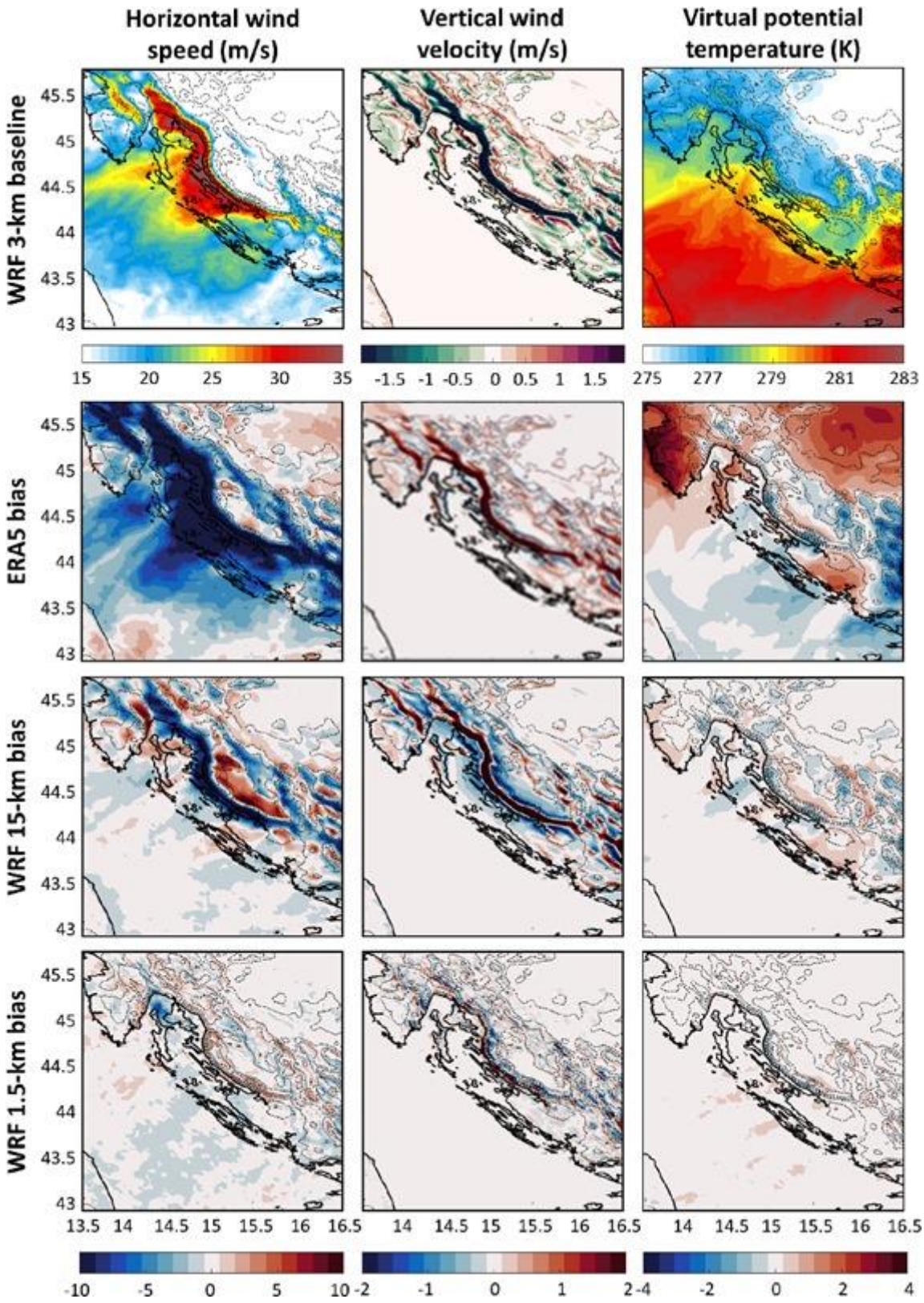

Figure 9. Baseline conditions and biases at 50 m above the surface defined as the median of the distributions of, respectively, the AdriSC WRF 3 km results and the differences between ERA5, AdriSC WRF 15 km, and WRF 1.5 km separately and AdriSC WRF 3 km results for the horizontal wind speed, the vertical wind velocity, and the virtual potential temperature during the peak of each 22 selected extreme bora events. Topographic contours are displayed every 250 m with dashed lines.

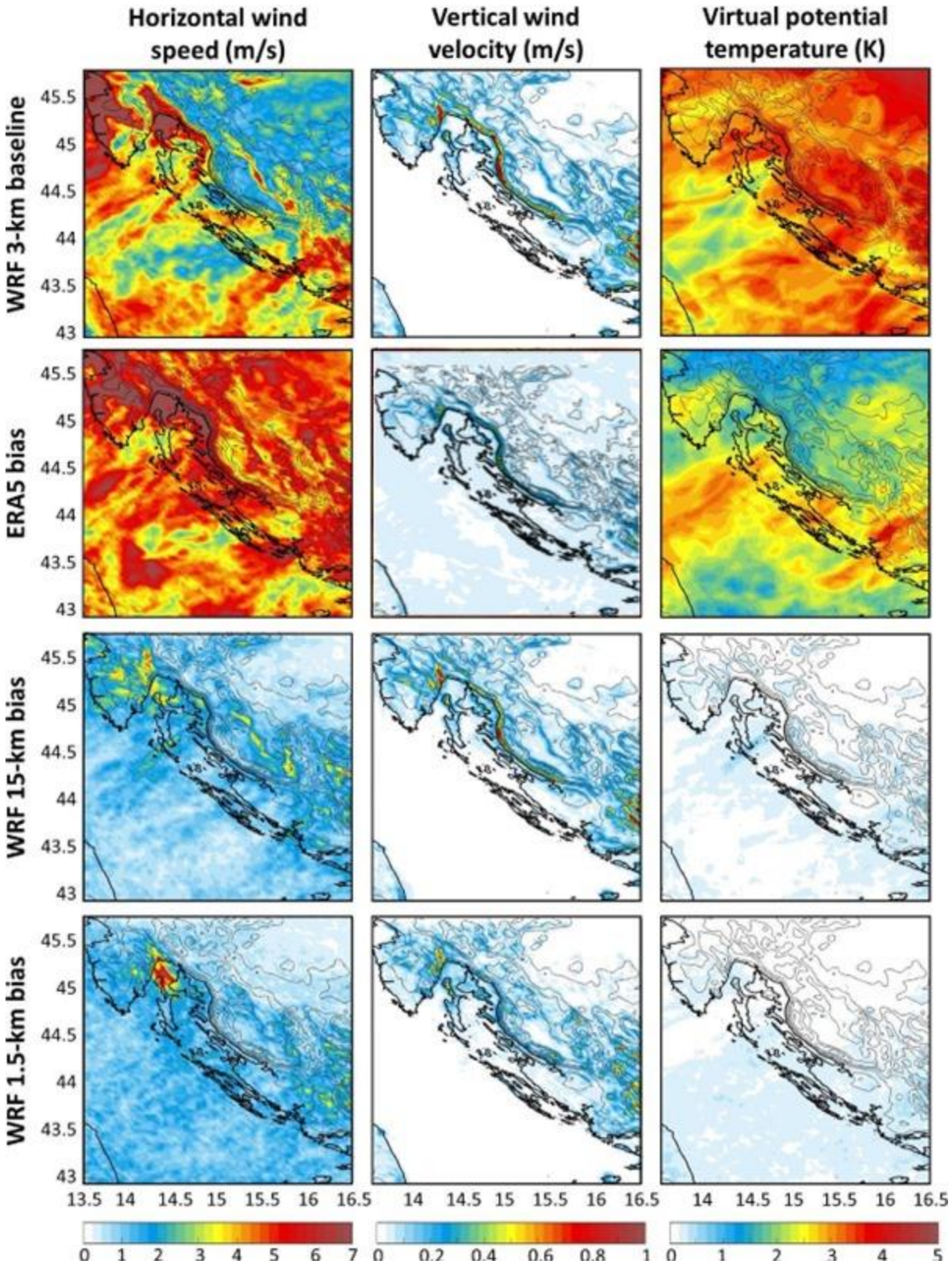

Figure 10. Baseline and bias variability at 50 m above the surface defined as the median absolute deviation (MAD) of the distributions of respectively the AdriSC WRF 3 km results and the differences between ERA5, AdriSC WRF 15 km and WRF 1.5 km separately and AdriSC WRF 3 km results for the horizontal wind speed, the vertical wind velocity and the virtual potential temperature during the peak of each 22 selected extreme bora event. Topographic contours are displayed every 200 m with dashed lines.

Horizontally, at 50 m above the surface (Figs. 9 and 10), the major bora features as well as the impact of model resolution can clearly be seen in the respective baseline conditions and the biases.

The wake and gap jet dynamics along the coast are reproduced with the variations of the horizontal wind speed from north to south — intense jets above 25.5 m/s separated by weaker speeds (Fig. 9). However, this structure is not as clearly defined as in Gohm et al. (2008) or Signell et al. (2010). Indeed, the high variability of the wind speed at the interface between the wakes and the jets up to ±5.6 m/s (Fig. 10) shows that their location may slightly vary from one extreme event to the other. Furthermore, jets are generally associated with TKE values above 2.7 m^2/s^2, which are about 0.5 m^2/s^2 higher than for the wakes (Fig. 11). The exceptions are MAD values above ±1.2 m^2/s^2 (Fig. 12) for which the TKE variability is stronger for the wakes. The PV banners (Fig. 11) are also reproduced with the switch between positive (up to 5.5 PVU) and negative (below −5.5 PVU) potential vorticity bands perpendicular to the Velebit mountain range. It should, however, be noted that at 50 m height the potential vorticity is affected by friction. They are associated with the main jet (negative) and wake (positive) structures along the coast. These results are found to be in good agreement with the PV banners described by Grubišić (2004). As for the wind speed, the highest variability of the potential vorticity ±3.8 PVU (Fig. 12) is mostly located at the interface between the bora wakes and jets. In addition, the lowest virtual potential temperatures at sea (below 278.0 K; Fig. 9) associated with a variability of ±3.5 K (Fig. 10) are simulated along the Senj transect, in areas where extreme bora events are known to drive dense water formation in the northern Adriatic.

The impact of model resolution on the representation of the wake and gap dynamics is quite substantial. First, the horizontal wind speed underestimation along the jets is at least 7.5 ± 4.5 m/s for ERA5 and 2.5 ± 1.5 m/s for WRF 15 km — i.e. about 28 % and 10 % of the baseline conditions, respectively. Second, a relatively low variability is associated with TKE underestimations of at least 0.8 ± 0.4 m^2/s^2 for WRF 15 km along the Senj transect. Third, the absolute PV biases along the coast are above 15.0 ± 12.5 PVU for ERA5 and 7.5 ± 1.8 PVU for WRF 15 km — highlighting that neither ERA5 nor WRF 15 km can reproduce the PV banners simulated in the baseline conditions. And, finally, the overestimation (underestimation) of the virtual potential temperature is up to 2.8 ± 1.7 K for ERA5 and 1.3 ± 0.2 K for WRF 15 km along the main jets (gaps). In terms of the WRF 1.5 km comparison, the absolute biases are always below 1.3 ± 1.7 m/s for the horizontal wind speed, 0.2 ± 0.7 m^2/s^2 for the TKE, 1.5 ± 3.0 PVU for the PV, and 0.3 ± 0.5 K for the virtual potential temperature

— i.e. below 5% of the baseline conditions (except for the PV). However, they are associated with higher variabilities than ERA5 or WRF 15 km showing that some events may be more divergent than others. Consequently, the WRF 3 km results converge toward higher resolution solutions even though the PV banners are not necessarily well characterised for lack of accuracy of the orography representation.

Further, the baseline conditions at 50 m above the surface highlight a minimum static stability below −0.002 K/m (Fig. 11). It is associated with strongly negative vertical velocities below −6.5 m/s (Fig. 9) and TKE above 7.5 m^2/s^2 (Fig. 11) along the lee of the Velebit mountain range, where breaking is known to occur. In consequence, the WRF 3 km model is, most probably (difficult to diagnose at 50 m height), capable of representing mountain waves during extreme bora events when downslope winds along the lee of the Velebit mountain range reach > 35.8 ± 3.5 m/s at 50 m above the surface. Additionally, these variables are associated with high variability along the lee of the Velebit mountain range (Figs. 10 and 12; ±0.0025 K/m for the minimum static stability, ±1.1 m/s for the vertical velocities, and ±1.7 m^2/s^2 for the TKE). Most credibly, the intensity and position of the mountain waves are thus likely to vary from one event to the other.

Concerning the impact of the model resolution, there is a sharp increase of both the minimum static stability by > 0.003 K/m and the vertical velocities by > 5.5 ± 0.8 m/s for ERA5 and WRF 15 km along the Velebit mountain range. There is also a sharp decrease of the TKE by 3.3 ± 1.1 m^2/s^2 for WRF 15 km along the lee of the Velebit mountain range. For WRF 15 km, these changes are also framed by a decrease of minimum static stability and vertical velocities reaching 0.002 ± 0.001 K/m and 2.0 ± 0.2 m/s, respectively, and an increase of TKE by 1.5 ± 1.1 m^2/s^2. Thus, some kind of mountain waves are likely to be represented at this resolution (unlike ERA5 which has a far too smooth orography), but both their intensity and location cannot be captured properly. Additionally, near the coastline, along the Velebit mountain range, the horizontal wind speed is decreased by at least 21.5 ± 6.4 m/s for ERA5 and 12.5 ± 1.8 m/s for WRF 15 km — i.e. > 35 % of the baseline conditions.

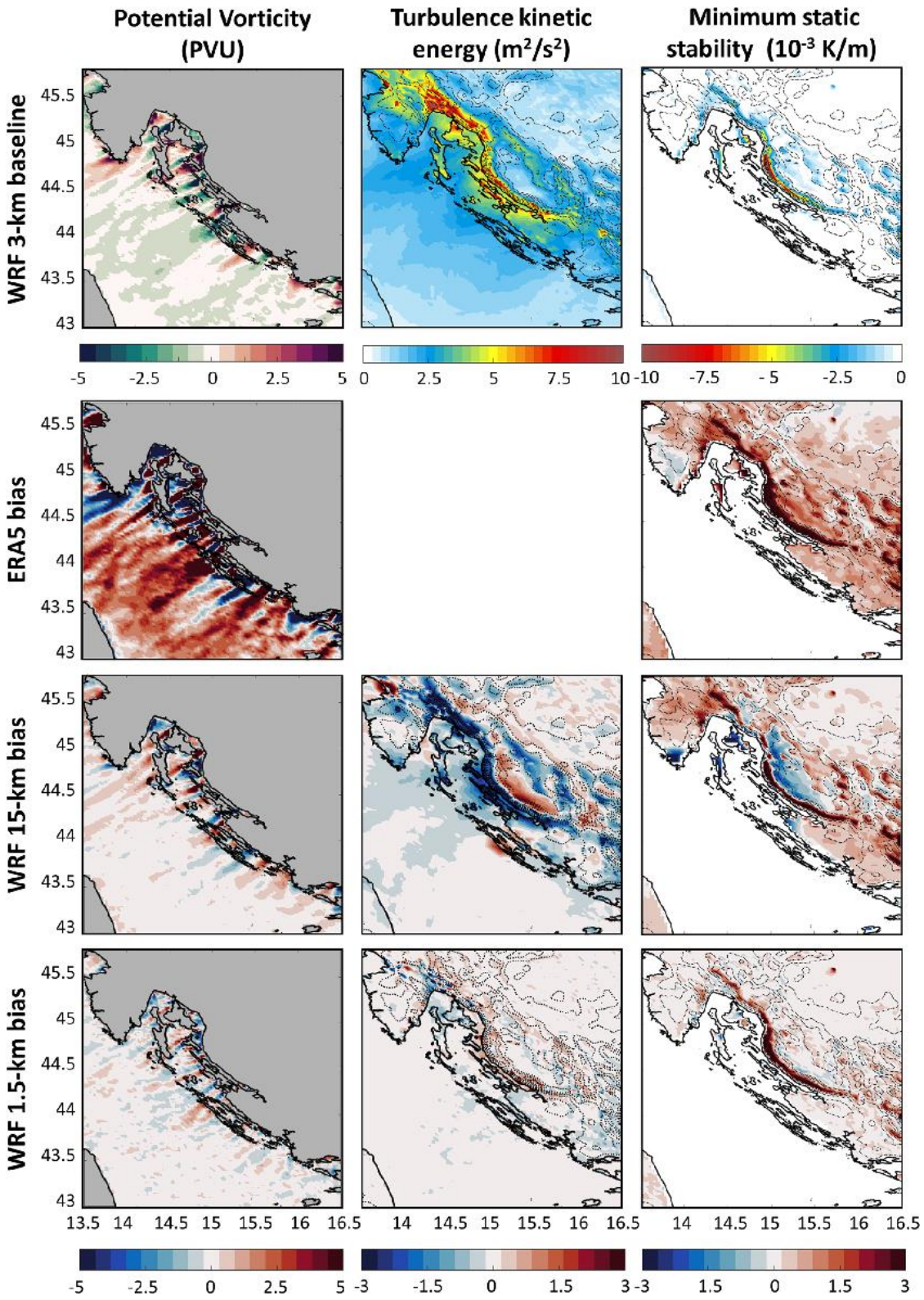

Figure 11. Baseline conditions and biases at 50 m above the surface defined as the median of the distributions of, respectively, the AdriSC WRF 3 km results and the differences between ERA5, AdriSC WRF 15 km, and WRF 1.5 km separately and AdriSC WRF 3 km results for the potential vorticity, the turbulence kinetic energy, and the minimum static stability during the peak of each 22 selected extreme bora events. Topographic contours are displayed every 250 m with dashed lines.

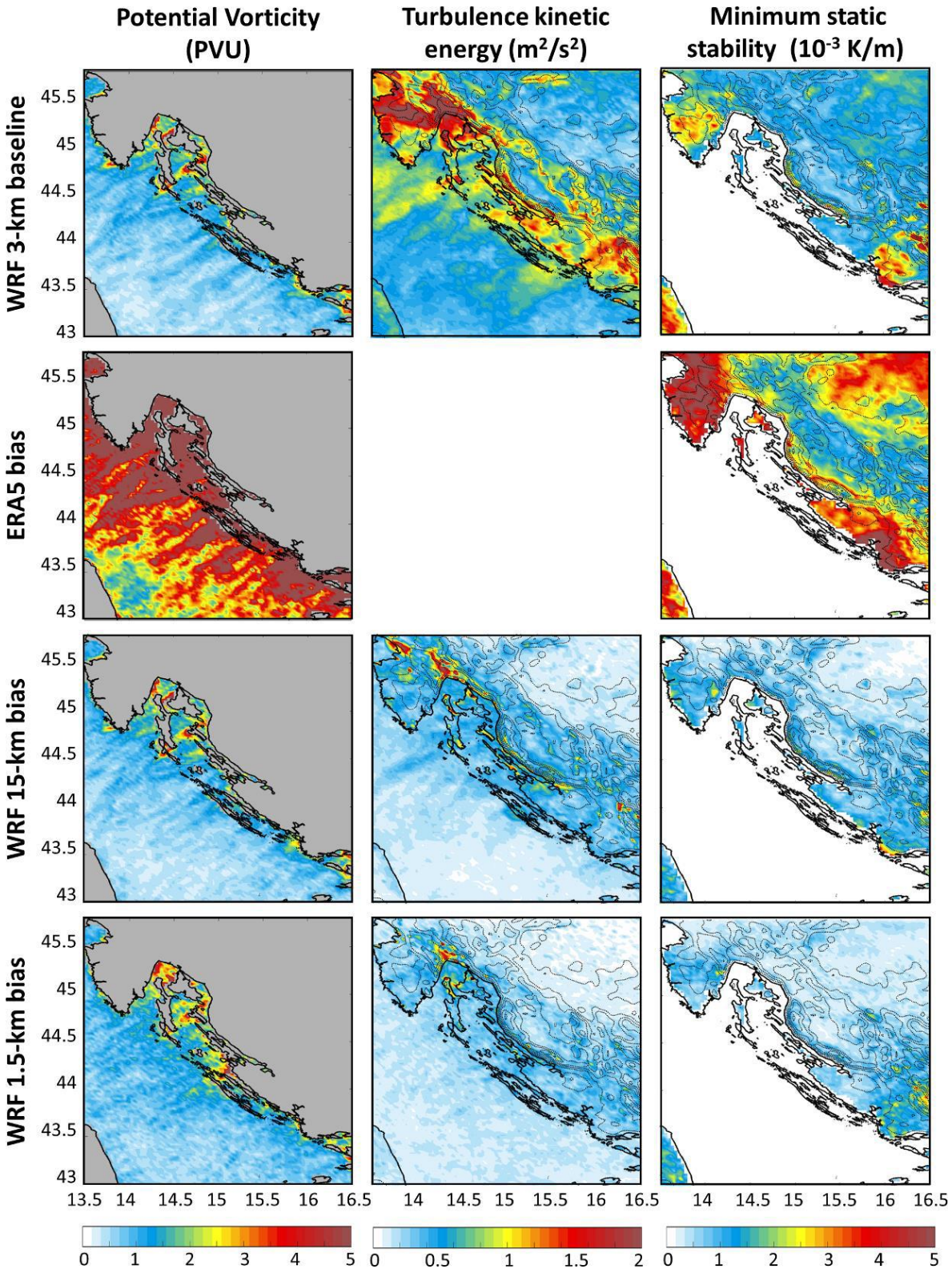

Figure 12. Baseline and bias variability at 50 m above the surface defined as the median absolute deviation (MAD) of the distributions of respectively the AdriSC WRF 3 km results and the differences between ERA5, AdriSC WRF 15 km and WRF 1.5 km separately and AdriSC WRF 3 km results for the potential vorticity, the turbulence kinetic energy and the minimum static stability during the peak of each 22 selected extreme bora event. Topographic contours are displayed every 200 m with dashed lines.

In terms of the WRF 1.5 km model comparison, along the Velebit mountain range the biases are still high — with 1.8 ± 0.2 m/s for the vertical wind velocities, 1.2 ± 0.5 m^2/s^2 for the TKE, and 0.003 ± 0.005 K/m for the static stability. However, the horizontal wind speed increase of about 1.6 ± 1.1 m/s only represents 4 % of the baseline conditions even though some events may be more divergent than others due to the high variability. Consequently, the potential mountain waves might occur in a slightly different location than seen in the baseline conditions, but their intensity is most probably not strongly impacted by the higher resolution of the model.

The analysis of the bora vertical structure with the Senj cross–shore transect (Figs. 13 and 14) provides a better description of the three–dimensional dynamics reproduced by the WRF 3 km simulations (i.e. baseline conditions) and how model resolution impacts it. It should be noticed that, in order to compare the different models, all the results have been interpolated (without extrapolation) into the vertical profile extracted for the WRF 3 km results. Additionally, the lowest level of extraction for the ERA5 results on the pressure levels is 1000 hPa and the WRF 15 km is too coarse to accurately represent the orography. Consequently, after interpolation, the first layers of the cross–sections (at the surface) with data depend on how the orography is represented in the different models and hence, their horizontal resolution. Therefore, the space left without results for both ERA5 and WRF 15 km (i.e. blank layer near the surface in Fig. 13 and 14) is bigger than for WRF 3 and 1.5 km.

Even though the Senj city is located at the edge of the lowest mountain pass of the Velebit mountains with a west–northwestward orientation, the extracted Senj transect is located along a relatively small mountain peak (< 1 km of height; Figs. 13 and 14) due to its west–southwestward orientation. The dynamics captured by the baseline conditions along this transect is relatively complex and probably not well represented at 3–km resolution. First, mountain waves and potentially wave–breaking are characterised by a sharp descent– and–reascent of the isentropes (despite the unavoidable smoothing of the statistical approach) as well as by strongly positive and negative vertical velocities. The latter have values above -1.8 ± 0.6 m/s, occurring on the lee of the mountain between 2 and 5 km of height. The associated TKE values are about 0.5 ± 0.5 m^2/s^2 between 2 and 3 km of height. Second, mountain wave–like patterns are found between 1.5 and 2 km of height in the lee of the Cres Island located at about 60 km along the transect and are characterised by a descent–and–reascent of the isentropes associated with negative vertical velocities of −1.0 ± 0.8 m/s and TKE values of about 0.5 ± 0.5 m^2/s^2. Third, a fast and deep boundary layer flow is extending up to 140 km

across the transect, with horizontal wind speeds of 32.5 ± 3.0 m/s up to 2 km of height (1.5 km in average). Such a flow is formed with the downslope bora winds along the lee of the mountain, then propagates toward the sea and finally sustains/reinforces its speed in the presence of the Cres Island. Fourth, between the lee of the mountain and the Cres Island, mountain wave–like patterns are produced but seem to be influenced by the island, probably due the use of relatively low resolution to derive the baseline conditions and/or the smoothing by the statistical approach.

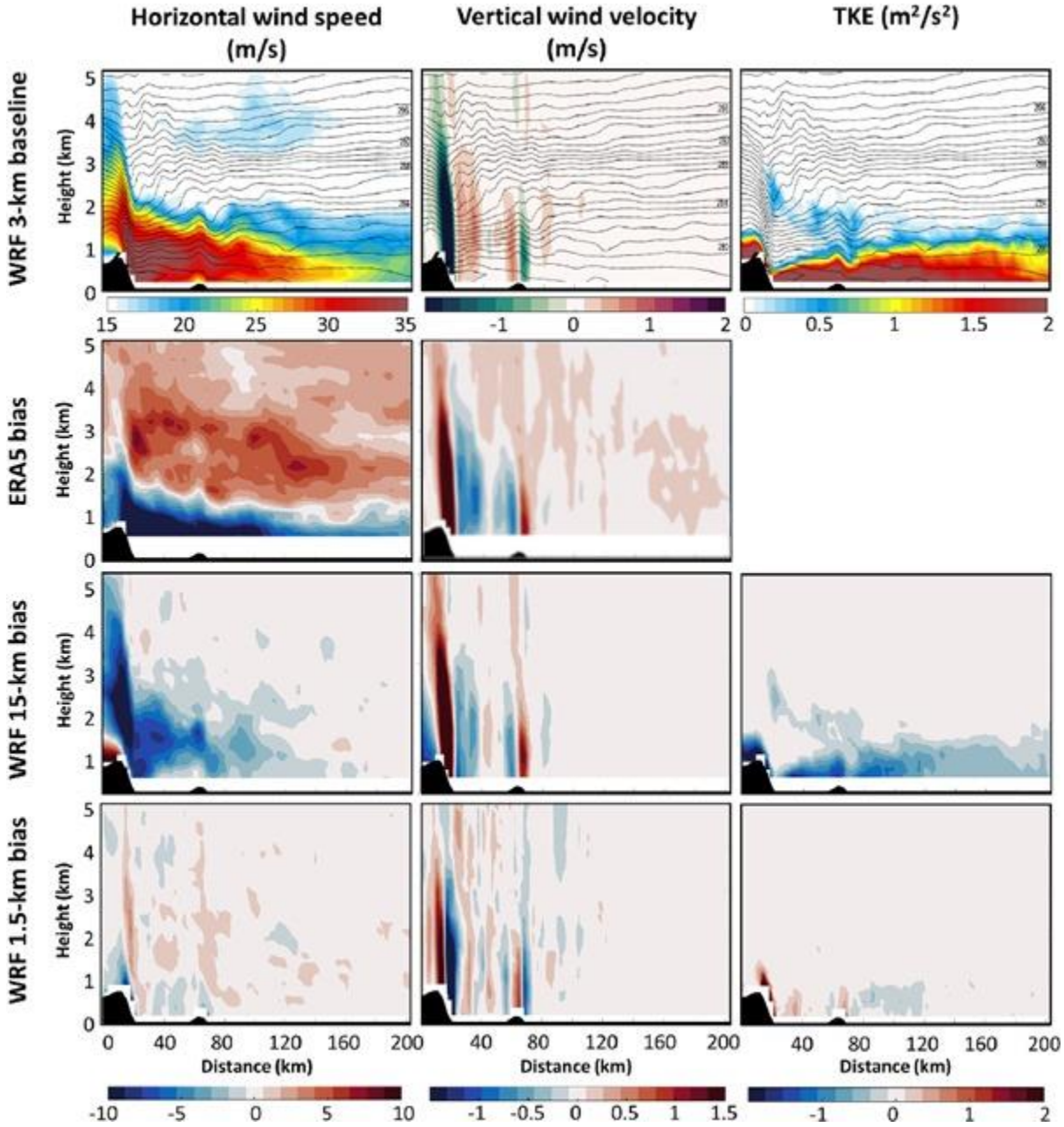

Figure 13. Senj cross–shore transect of baseline conditions and biases defined as the median of respectively the AdriSC WRF 3 km results and the differences between ERA5, AdriSC WRF 15 km, and WRF 1.5 km separately and AdriSC WRF 3 km results for the horizontal

wind speed, the vertical wind velocity, the turbulence kinetic energy, and the virtual potential temperature (black isentropes) during the peak of each 22 selected extreme bora events.

The impacts of the atmospheric model resolution can clearly be seen along the Senj transect. The ERA5 reanalysis is incapable of capturing the expected dynamics. The horizontal wind speed is decreased by at least 11.5 ± 9.0 m/s (i.e. about 35 % of the baseline conditions) and the vertical wind velocities are increased by > 1.5 ± 1.5 m/s along the lee of the mountain.

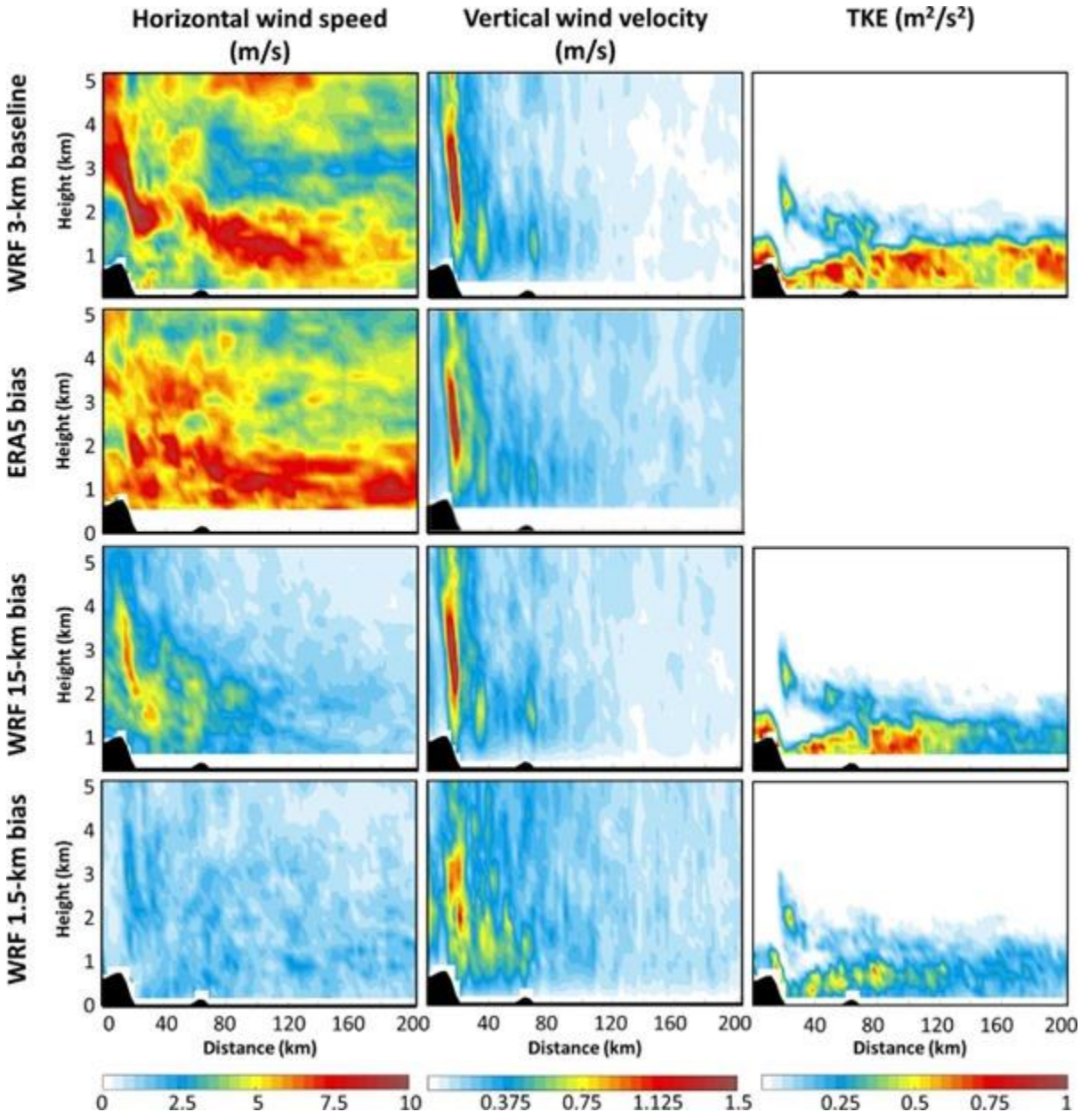

Figure 14. Baseline and bias variability along the Senj transect defined as the median absolute deviation (MAD) of the distributions of respectively the WRF 3 km results and the differences between ERA5, AdriSC WRF 15 km, and WRF 1.5 km separately and AdriSC WRF 3 km results for the horizontal wind speed, the vertical wind velocity and the turbulence kinetic energy during the peak of each 22 selected extreme bora events.

Further, the WRF 15–km model cannot properly capture the intensity of the mountain wave (and wave–breaking) dynamics. First, it strongly overestimates the vertical wind velocities by > 1.5 ± 1.5 m/s in the lee of the mountain up to 4 km of height. Second, it generally underestimates the TKE by at least 2.0 ± 0.8 m^2/s^2, up to 1 km of height and by 1.0 ± 0.5 m2/s2 at the locations of the identified mountain wave–like patterns in the baseline conditions. Finally, it strongly underestimates the horizontal wind speed by (1) down to 15.0 ± 7.5 and 10.0 ± 7.5 m/s in average (i.e. 46 % and 30 % of the baseline conditions, respectively) up to 4 km of height (2 km in average) between the lee of the mountain and the Cres island, and by (2) 2 to 4 ± 1.5 m/s, up to 2 km of height, past the island of Cres. Along the Senj transect (Figs 13 and 14), the baseline conditions seem to converge toward the highest resolution dynamics as the WRF 1.5 km biases are generally minimised. This is particularly true for the horizontal wind speed with an absolute bias below 2.5 ± 1.0 m/s, representing 7 % of the baseline conditions. However, the WRF 3–km model cannot accurately capture the mountain wave and/or wave–breaking dynamics as can be seen with the WRF 1.5–km vertical wind velocity bias results. First, they reach a minimum of −1.5 ± 1.2 m/s along the lee of the mountain, showing that the amplitude of the waves (potentially the intensity of the wave–breaking) is not well represented at 3 km. Second, they switch between positive and negative values of about 0.5 ± 0.7 m/s of intensity between the lee of the mountain and Cres Island, probably revealing the presence of mountain waves not properly captured by the baseline conditions.

To better quantify the impact of atmospheric model resolution on the bora dynamics which is well summarised with the intensity of the horizontal wind speeds, the distributions of the hourly results for ERA5 reanalysis as well as AdriSC WRF 15 km, WRF 3 km, and WRF 1.5 km models are compared. They are presented as probability density functions (Fig. 15) and as median, normalised absolute median (i.e. NAM defined as the absolute value of the division of the bias median by the median of the WRF 3 km baseline results), and variability (i.e. MAD) of the ERA5, WRF 15 km, and WRF 1.5 km biases (Table 5) along the Senj transect at four different heights (0.5, 1, 3, and 5 km). First, for all the heights, Figure 15 and Table 5 clearly highlight that ERA5 reanalysis is strongly underestimating or overestimating the horizontal wind speeds compared to the WRF 3 km results — i.e. biases varying between −8.5 ± 6.9 and 3.0 ± 4.9 m/s, representing between 14 % and 30 % of the WRF 3 km baseline conditions. Thus, ERA5 surely cannot be used to directly drive the ocean circulation nor to evaluate climate atmospheric models during severe bora events in the northern Adriatic. Second, the horizontal wind speed distributions from WRF 3 km and WRF 1.5 km are extremely close for

all the heights — i.e. biases varying between 0.0 ± 1.6 and 0.2 ± 0.9 m/s, representing 0–1 % of the baseline conditions. Finally, the horizontal wind speed distributions from WRF 3 km and WRF 15 km are overall not so divergent — i.e. biases varying between −1.3 ± 2.1 and 0.1 ± 0.8 m/s, representing 0–5 % of the baseline conditions depending on the height. For the less intense events, all WRF models thus seem to converge toward a similar solution, particularly at 5 km of height. However, the most important differences between WRF 15 km and WRF 3 km results are found, at all heights (except 5 km), for the tail of the distributions and thus for the most extreme bora conditions — i.e. underestimation by 4.6–7.6 m/s of the 99th percentiles of the WRF 3 km distributions. This means that the WRF 15–km model is likely to not be able to drive the most intense sea surface cooling and potentially the dense water formation in the northern Adriatic Sea.

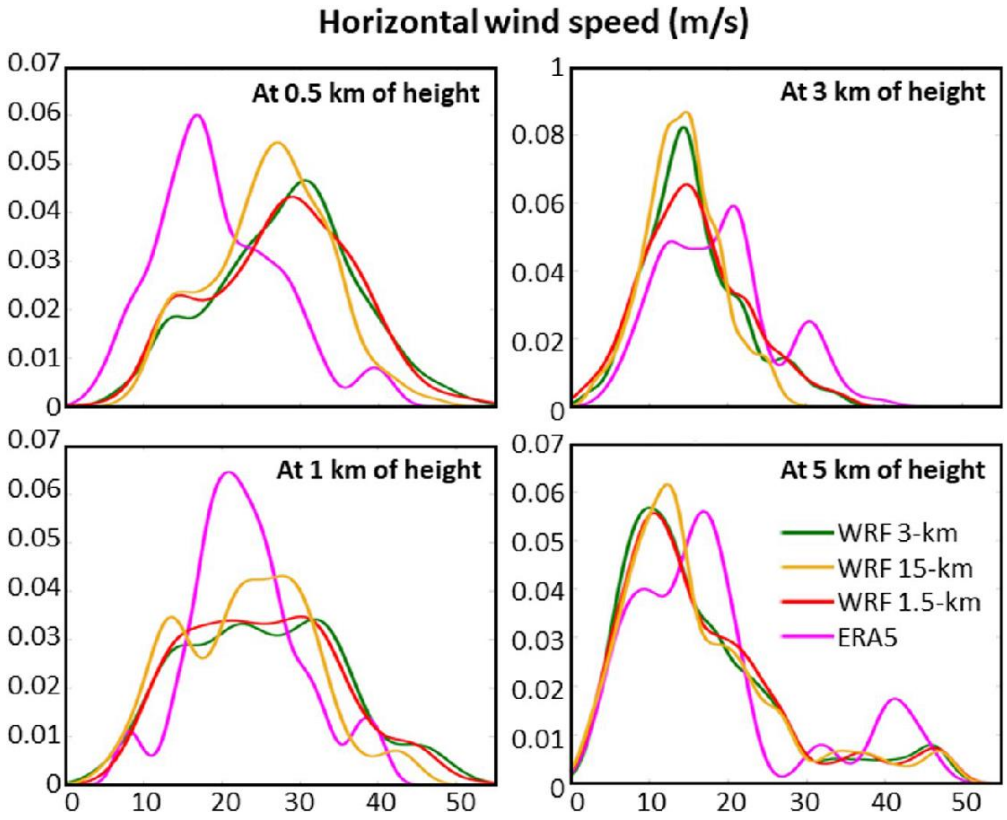

Figure 15. Probability density functions of the hourly horizontal wind speed extracted from AdriSC WRF 3 km, WRF 15 km, and WRF 1.5 km models as well as ERA5 reanalysis at four different heights (0.5, 1, 3, and 5 km) along the full Senj transect.

Table 5 The median, normalised absolute median (NAM), and variability (MAD) of the horizontal wind speed biases over the ensemble of 22 selected extreme bora events along the Senj transect at four different heights (0.5, 1, 3, and 5 km). The biases are defined as the differences between ERA5, AdriSC WRF 15 km, and WRF 1.5 km separately and AdriSC WRF 3 km results. The NAM is defined as the absolute value of the division of the bias median by the median of the AdriSC WRF 3 km baseline results.

	Height (km)	Median (m/s)	NAM (%)	MAD (m/s)
ERA5 bias	0.5	−8.5	30	6.9
	1	−3.3	14	8.0
	3	3.0	21	4.9
	5	1.9	14	4.2
WRF 15 km bias	0.5	−1.3	5	2.1
	1	−1.1	4	2.6
	3	−0.4	3	1.3
	5	0.1	0	0.8
WRF 1.5 km bias	0.5	0.1	0	1.5
	1	0.0	0	1.6
	3	0.1	0	1.2
	5	0.2	1	0.9

In brief, the known basic bora features are overall reproduced in the baseline conditions defined, during the peak of the storms, as the median of the WRF 3 km simulations over the ensemble of 22 selected representative events. However, due to the use of the relatively coarse (i.e. 3 km) resolution and thus of the imprecise representation of the Velebit mountain range orography in the atmospheric grid, the baseline conditions lack of accuracy particularly in terms of the proper location and intensity of the PV banners and the mountain waves (and potentially the wave–breaking). Finally, neither ERA5 reanalysis nor WRF 15 km results seem capable to represent the basic dynamics or even the strength of the extreme bora events — i.e. horizontal wind speed biases of > 28 % of the baseline conditions near the lee of the mountains and up to 30 % for ERA5 and 5 % for WRF 15 km at 0.5 km of height along the Senj transect. Additionally, the WRF 15 km distributions underestimate by up to 7.6 m/s the 99th percentiles of the WRF 3 km distributions. The baseline conditions, however, tend toward the results obtained with the WRF 1.5 km model, particularly concerning the strength of the bora events — i.e. horizontal wind speed biases about 4–7 % of the baseline conditions near the lee of the mountains and of 0–1 % along the Senj transect.

3.1.3 Air–sea interactions

In the context of ocean studies, the accurate representation of basic bora dynamics by atmospheric models is not as crucial as the proper simulation of the intensity of the wind stress partially driving the ocean circulation. Even more important is proper simulation of the air–sea fluxes driving the sea surface cooling and preconditioning the dense water formation in the northern Adriatic region during severe bora events. Here, the capability of the AdriSC WRF 3 km model to appropriately force the ocean circulation in the northern Adriatic region during severe bora events is thus quantified. First, the baseline conditions extracted from WRF 3 km results are analysed. Then, the impact of model resolution with the ERA5, WRF 15 km, and WRF 1.5 km biases (i.e. differences with WRF 3 km results) is assessed.

The maximum total wind stress as well as the minimum latent and sensible heat fluxes are thus presented as the median (Fig. 16) and associated variability (represented by the MAD of the ensemble; Fig. 17) of the ensemble of 22 events. The chequered patterns seen in the WRF 15 km results (Figs. 16 and 17) are mostly linked to the choice of the colour scale of the baseline plots, but they are also a common feature when WRF is used at the regional scale. The known bora air–sea interactions can clearly be seen in the baseline conditions (Figs. 16 and 17).

The most intense maximum wind stresses (i.e. above 0.60 ± 0.30 N/m^2) as well as negative minimum fluxes of latent heat (i.e. below -350 ± 80 W/m^2) and sensible heat (i.e. below -150 ± 60 W/m^2) are found both within the Kvarner Bay and along the bora jets. In terms of the impact of atmospheric model resolution, the ERA5 reanalysis is underestimating the maximum wind stresses by at least -0.30 ± 0.10 N/m^2 over the entire northern Adriatic domain (i.e. 50 % of the baseline conditions) and by $> -0.50 \pm 0.30$ N/m^2 within the Kvarner Bay and along the Senj transect (i.e. > 75 % of the baseline conditions). Consequently, ERA5 is overestimating the minimum fluxes of latent heat by $> 50 \pm 60$ W/m^2 over the entire domain and of sensible heat by $>50 \pm 50$ W/m^2 within the Kvarner Bay and along the Senj transect. Concerning the WRF 15 km model, it also underestimates the maximum wind stresses by at least -0.15 ± 0.05 N/m^2 within the Kvarner Bay and along the Senj jet (i.e. 25 % of the baseline conditions). Consequently, WRF 15 km model overestimates, for the entire domain, the negative minimum latent and sensible heat fluxes by at least 10 ± 10 W/m^2 and up to 25 ± 20 W/m^2 for the latent heat fluxes along the bora jets. Finally, in accordance with the previous results, the baseline air–sea conditions tend toward the higher resolution results.

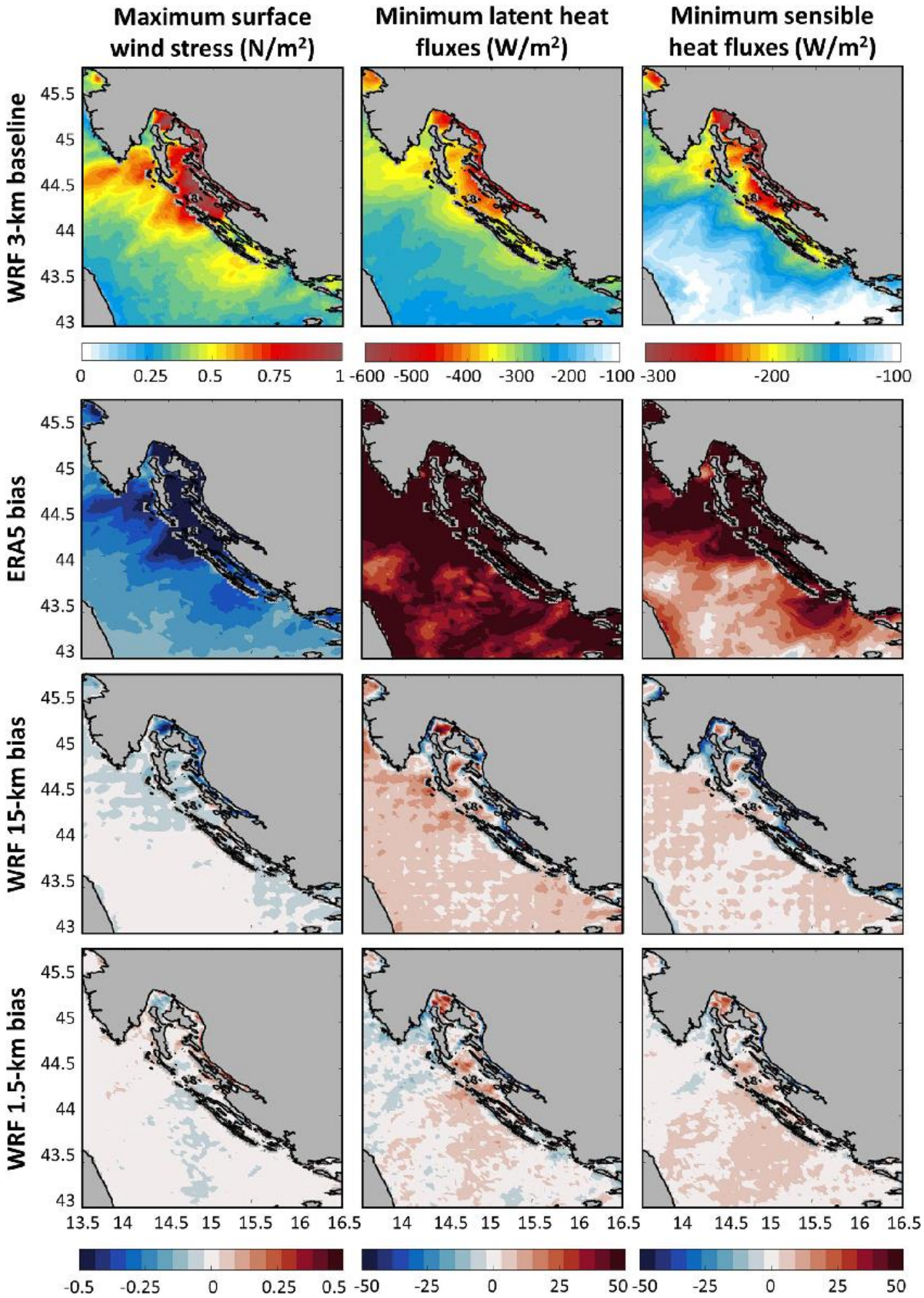

Figure 16. Baseline conditions and biases at sea surface defined as the median of the distributions of respectively the WRF 3 km results and the differences between ERA5, WRF 15 km, and WRF 1.5 km separately and WRF 3 km results for the maximum wind stress as well as the minimum sensible and latent heat fluxes for each 22 selected extreme bora events.

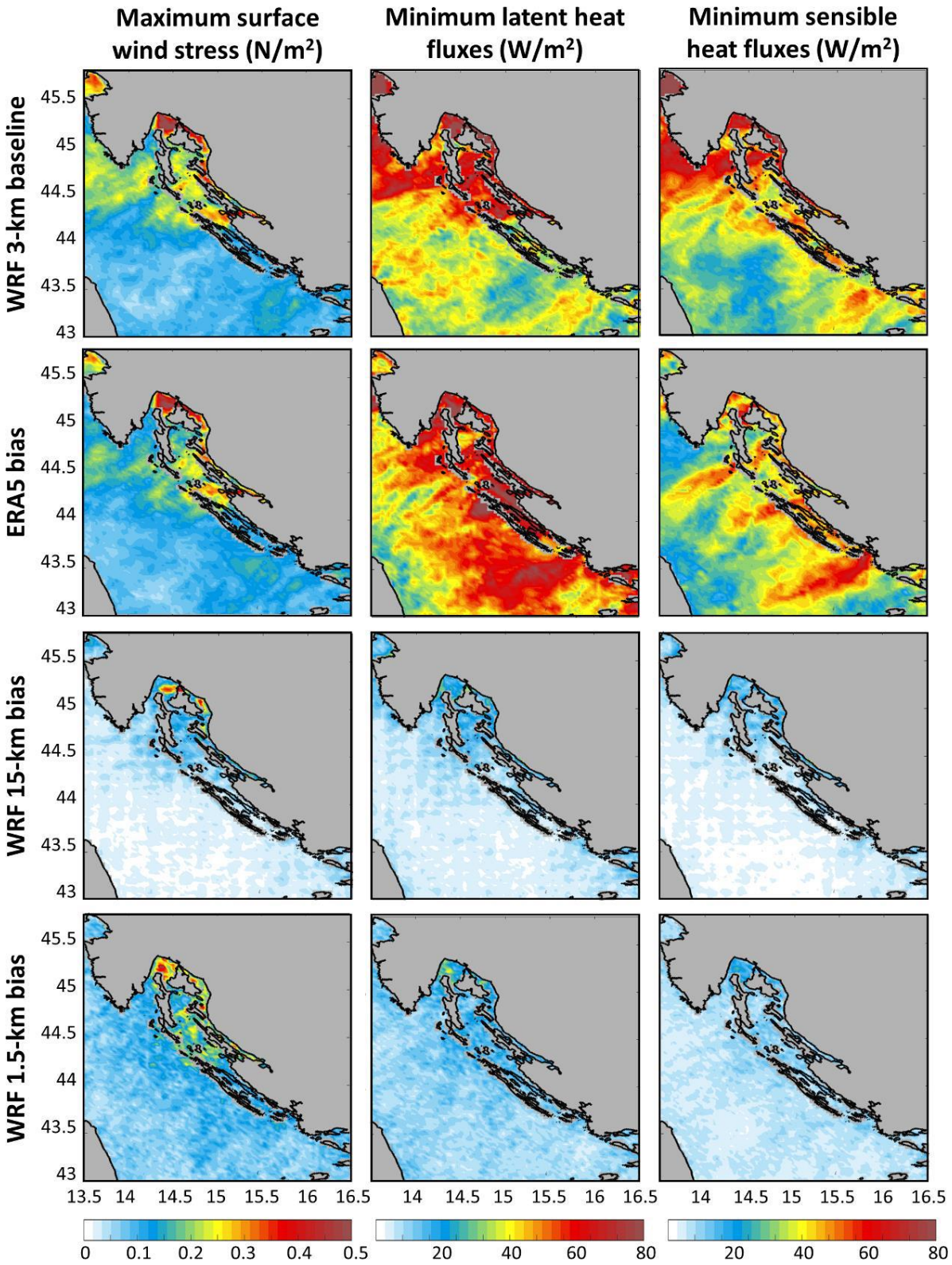

Figure 17. Baseline and bias variability at sea surface defined as the median absolute deviation (MAD) of the distributions of respectively the WRF 3 km results and the differences between ERA5, AdriSC WRF 15 km, and WRF 1.5 km separately and AdriSC WRF 3 km results for the maximum wind stress as well as the minimum sensible and latent heat fluxes for each 22 selected extreme bora events.

The WRF 1.5 km biases are minimised with absolute wind stress biases on average below 0.05 ± 0.10 N/m^2 (i.e. about 8 % of the baseline conditions) and absolute latent and sensible heat flux biases on average below 7 ± 10 W/m^2 over the entire domain (i.e. seven time less than ERA5 and 3.5 time less than WRF 15 km). Concerning the heat fluxes, the WRF 3 km model seems, however, to slightly overestimate their intensity in the vicinity of the Senj jet with negative WRF 1.5 km biases of the order of −10 ± 10 W/m^2.

To better quantify the impact of atmospheric model resolution on the heat fluxes, the distributions of the minimum latent and sensible heat fluxes for ERA5 reanalysis as well as AdriSC WRF 15 km, WRF 3 km, and WRF 1.5 km models are compared. They are presented as probability density functions (Fig. 18) and as median, normalised absolute median (i.e. NAM defined as the absolute value of the division of the bias median by the median of the WRF 3–km baseline results), and variability (i.e. MAD) of the ERA5, WRF 15 km, and WRF 1.5 km biases (Table 6) for three points along the Senj transect (at 50 km, within the Kvarner Bay, at 100 km, after the Cres island, and at 150 km, in the middle of the northern Adriatic shelf; black dots in Fig. 6a). First, for all the locations and for both minimum latent and sensible heat fluxes, Figure 18 and Table 6 clearly highlight that ERA5 reanalysis is strongly overestimating the heat fluxes compared to the WRF 3 km results — i.e. biases varying between 71 ± 46 to 143 ± 42 W/m^2 for the minimum latent heat and 37 ± 25 to 100 ± 28 W/m^2 for the minimum sensible heat, representing 23–36 % and 22–46 % of the baseline conditions, respectively. Thus, ERA5 surely cannot be used to drive the sea surface cooling during severe bora events and the formation of coastal dense waters in the northern Adriatic. Second, the distributions of minimum heat fluxes from WRF 3 km and WRF 1.5 km are extremely close for all the locations — i.e. biases varying between 0 ± 5 to 6 ± 3 W/m^2 for the minimum latent heat and 2 ± 4 to 5 ± 7 W/m^2 for the minimum sensible heat, representing 0–1 % and 1–2 % of the baseline conditions, respectively. For moderate events, the WRF 3 km minimum latent heat fluxes between −500 and −300 W/m^2 tend to be overestimated by up to 7 W/m^2 within the Kvarner Bay (at 50 km) and underestimated by down to −7 W/m^2 after the Cres island (at 100 km) compared to the WRF 1.5 km results. Finally, the most important differences between WRF 15 km and WRF 3 km results are found within the Kvarner Bay, for the location at 50 km along the Senj transect — i.e. biases of 15 ± 14 W/m^2 for the minimum latent heat and 14 ± 14 W/m^2 for the minimum sensible heat representing 4 % and 6 % of the baseline conditions, respectively (i.e. about 3 and 5 times bigger than for the WRF 1.5 km biases).

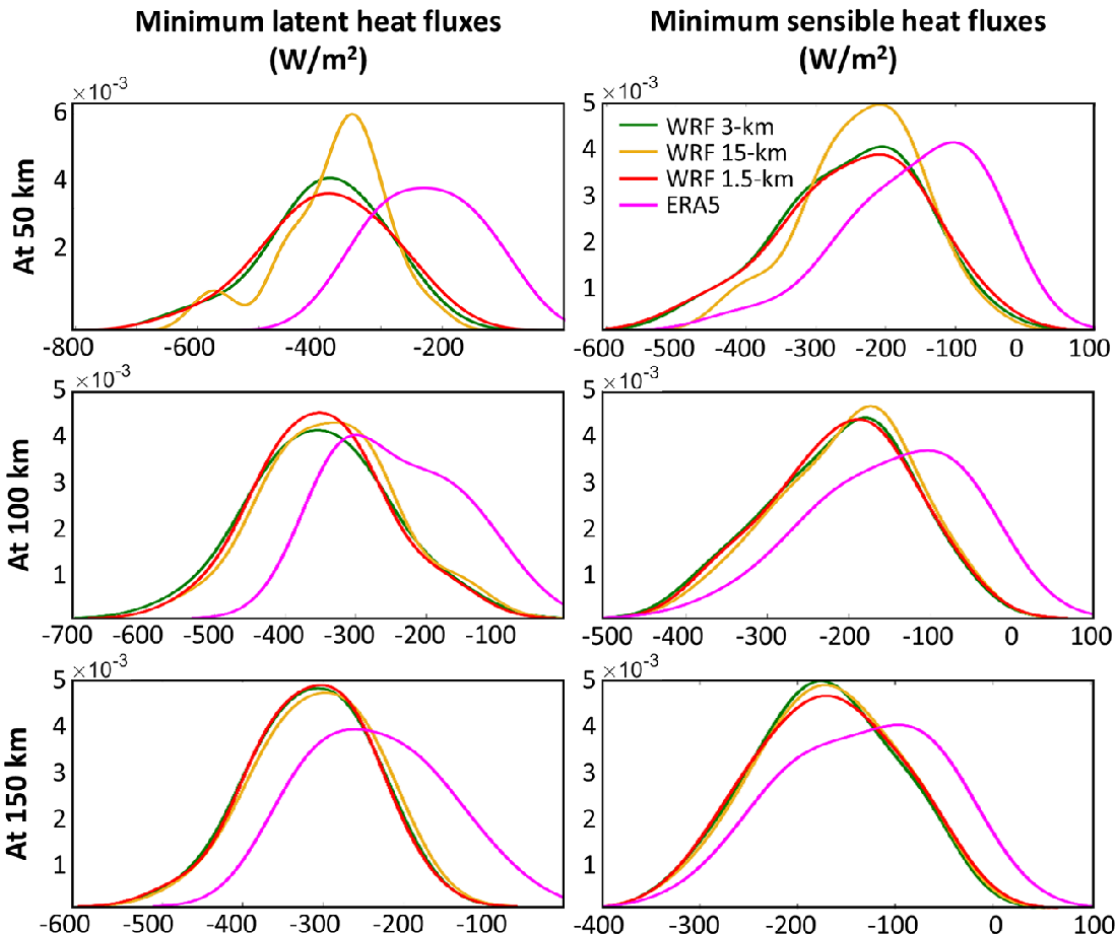

Figure 18. Probability density functions of the minimum latent and sensible heat fluxes extracted from AdriSC WRF 3 km, WRF 15 km, and WRF 1.5 km models as well as ERA5 reanalysis at three points located 50, 100, and 150 km along the Senj transect.

At this location, where dense waters are known to be formed (Vilibić et al. 2018), both the most intense negative minimum latent and sensible heat fluxes (below −400 and −300 W/m^2, respectively) are likely to be underestimated in the WRF 15 km model by at least −40 W/m^2, and down to −100 W/m^2 for the strongest events. On the contrary, for moderate events, the minimum heat fluxes tend to be overestimated by the WRF 15 km model and, for the less intense events, all WRF models seem to converge toward a similar solution.

In a nutshell, despite using a constant and homogeneous sea surface temperature to calculate the minimum heat fluxes during each of the 22 selected bora events and thus neglecting the nonlinear interactions between sea surface cooling and atmospheric forcing (which are likely to increase/reinforce the differences found in this study), the ERA5 reanalysis and the WRF 15 km model have been found incapable to capture the intensity of the air–sea interactions in the northern Adriatic (i.e. underestimation of the maximum wind stress and overestimation of the negative minimum heat fluxes). In more detail, along the Senj transect,

the ERA5 and WRF 15 km minimum heat flux biases are found to be 22–46 % and 2–6 % bigger than the baseline conditions, respectively. Additionally, the WRF 15 km model underestimates the heat fluxes by up to 100 W/m^2 for the strongest bora conditions likely to contribute to the dense water formation. For the WRF 1.5 km model, the biases tend toward 0 % and 1 % of the baseline conditions for the latent and sensible heat fluxes, respectively. The baseline air–sea interactions thus seem to converge toward higher resolution solutions and should be able to properly drive the sea surface cooling during severe bora events in the northern Adriatic.

Table 6. The median, normalised absolute median (NAM) and variability (MAD) of the minimum sensible and latent heat flux biases over the ensemble of 22 selected extreme bora events for three locations at 50 km, 100 km and 150 km along the Senj transect. The biases are defined as the difference between ERA5, AdriSC WRF 15 km and WRF 1.5 km separately and AdriSC WRF 3 km results. The NAM is defined as the absolute value of the division of the bias median by the median of the AdriSC WRF 3 km baseline results.

		Minimum latent heat fluxes			Minimum sensible heat fluxes		
	Location (km)	Median (W/m²)	NAM (%)	MAD (W/m²)	Median (W/m²)	NAM (%)	MAD (W/m²)
ERA5 bias	50	143	36	42	100	46	28
	100	91	26	54	62	33	29
	150	71	23	46	37	22	25
WRF 15–km bias	50	15	4	14	12	6	12
	100	11	3	4	8	4	3
	150	6	2	3	3	2	2
WRF 1.5–km bias	50	3	0	11	5	2	7
	100	3	1	7	2	1	4
	150	0	0	5	2	1	4

3.2 Case 2: BiOS–driven thermohaline variability

On the one hand, the BiOS phases in the northern Ionian have been widely studied based on *in–situ* and remote sensing observations (e.g. Malanotte–Rizzoli et al. 1997; Larnicol et al. 2002; Pujol and Larnicol 2005; Borzelli et al. 2009; Bessières et al. 2013; Gačić et al. 2010, 2014). However, due to the well–documented difficulties that RCMs have to capture the hurricane–strength bora events driving the dense water formation in the northern Adriatic (Theocharis et al. 2014; Dunić et al. 2018; Denamiel et al. 2021a), the BiOS reversal mechanism, as defined by Gačić et al. (2010), remained partially unproven till recently. With a rotating tank experiment, Rubino et al. (2020) and Gačić et al. (2021) demonstrated that the

injection of dense water on a sloping bottom could trigger the reversal of their near–surface gyre circulation. Further, the 100–year long realistic numerical simulation of Liu et al. (2021) reproduced the known BiOS phases between 1985 and 2010, despite not properly capturing the highest salinities and densities measured in the northern Ionian. By using an artificial cooling over the entire Adriatic Sea, Liu et al. (2021) also confirmed the results obtained by Rubino et al. (2020), and provided evidences that the NIG reversal from a cyclonic to an anticyclonic phase occurs 1–2 years after a major cooling event driving the Adriatic dense water formation.

On the other hand, many of the processes observed in the Adriatic Sea have been connected and even correlated to the decadal variability of the BiOS. For example, Civitarese et al. (2010) demonstrated the impact of the BiOS on the nutrient content in the Adriatic Sea (i.e. decrease/increase of the nitracline depending on the cyclonic/anticyclonic circulation of the NIG); Lavigne et al. (2018) explained the phytoplankton phenology in terms of the decadal reversals of the Ionian circulation and Mihanović et al. (2015) extracted BiOS–driven phases from long–term measurements of salinity, temperature and dissolved oxygen in the middle Adriatic. The abundance and species within the Adriatic zooplankton communities have also been connected to the BiOS by Batistić et al. (2014). More recently, Peharda et al. (2018) found a consistent anti–correlation between the bivalve chronology in the northern Adriatic Sea and the BiOS regimes while Vilibić et al. (2020) and Ciglenečki et al. (2020) strongly correlated bottom salinity and the surface active substances fraction of the dissolved organic carbon in the northern Adriatic to the delayed BiOS index. However, no numerical study has ever quantified the impact of the BiOS regimes on the decadal variability of the Adriatic Sea as the available long–term ocean runs were not properly simulating the dense water formation, spreading and storage within the Adriatic basin (Dunić et al. 2018). Here, the added value of the kilometre–scale AdriSC climate model is demonstrated by connecting the BiOS phases to the long–term variability of the Adriatic Sea during the 1987–2017 period.

3.2.1 Evaluation along the long-term monitoring Adriatic transects

First, the performances of the AdriSC ROMS 1 km model along the long–term monitoring northern Adriatic and Palagruža Sill transects are investigated with scatter plots (Fig. 19). Overall, they show that the hexagons with the largest number of points are following the reference line for both temperature and salinity, which indicates that the vast majority of the AdriSC ROMS 1 km results correspond well to the observations in both intensity and timing.

However, for the northern Adriatic transect, the model systematically overestimates the salinity observations below 37.

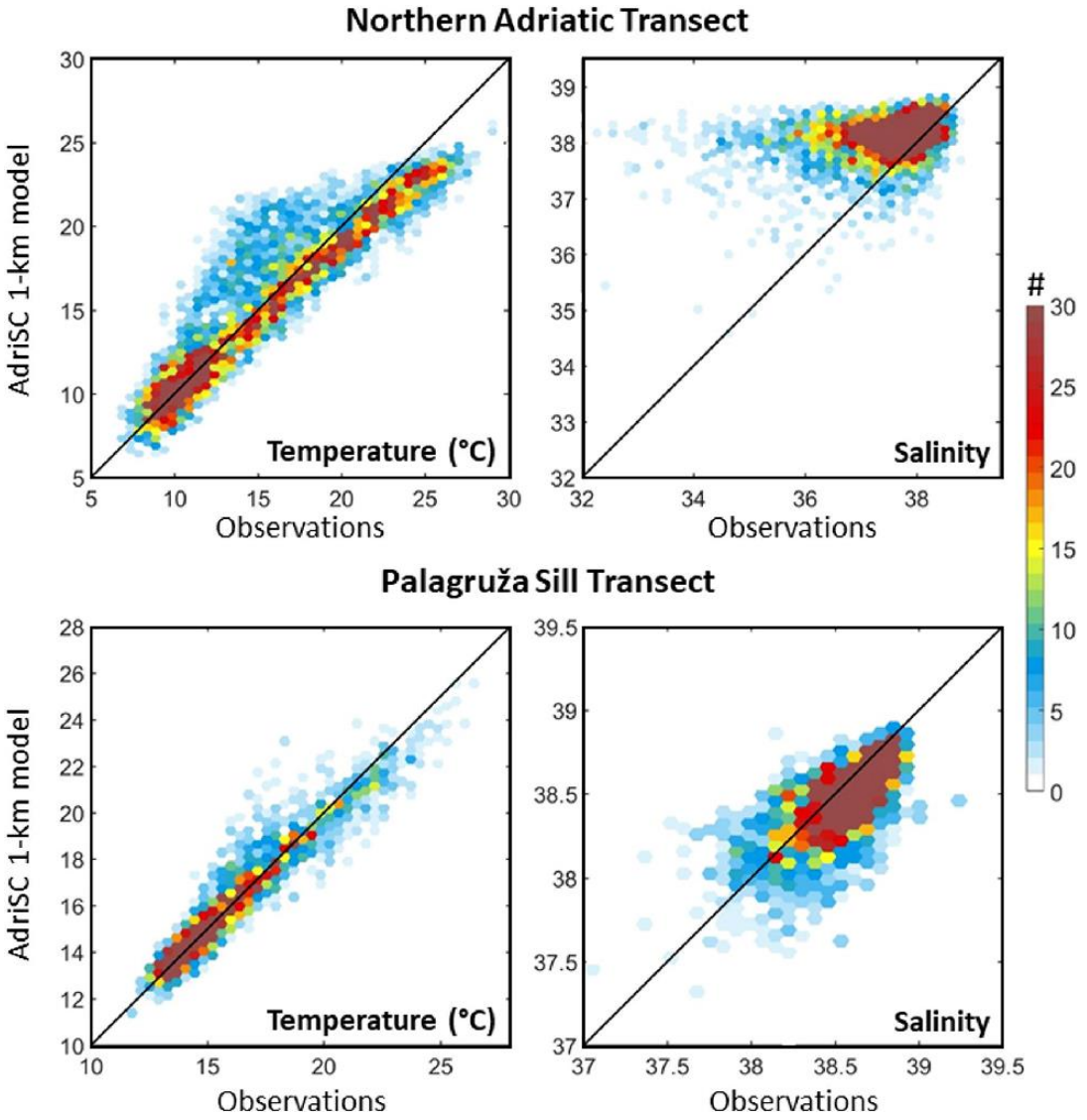

Figure 19. Evaluation of the AdriSC ROMS 1 km temperature (left panels) and salinity (right panels) results for the 1987–2017 period against observations between the surface and 35 m depth for the northern Adriatic transect (top panels) as well as the surface and 170 m depth for the Palagruža Sill transect (bottom panels) with scatter plots showing the density (number of occurrences #) with hexagonal bins.

This highlights that the AdriSC ROMS 1 km model is not accurately reproducing the intensity, the complex variability, and the extent of the Po River freshwater plume known to strongly influence the thermohaline circulation in the northern Adriatic Sea (Kourafalou 1999; Manzo et al. 2018). It should also be highlighted that, along the northern Adriatic transect, the temperatures above 20 °C (i.e. temperatures in the surface layer modelled during summer) are also systematically underestimated by up to 2.5 °C while they can be overestimated by up to 5

°C between 10 and 20 °C. The AdriSC ROMS 1 km has been demonstrated to present a cold summer temperature bias linked to various factors such as a deficit of solar radiation by the AdriSC atmospheric model during the summer, or the fact that the river temperatures are imposed by taking the ERA–Interim skin temperatures the closest to the river estuaries (Pranić et al. 2021). Additionally, the northern Adriatic transect is located in shallow waters (below 40 m depth) where the optical properties of the water, not well parameterized in the Adriatic Sea, are playing a crucial role in modelling the turbidity and hence vertical mixing. The turbidity is responsible for most of the downward shortwave radiation absorption in the upper layer and hence highly influences all the temperatures along the transect. By contrast, for the Palagruža Sill transect, despite some minor scattering for few occurrences up to ± 0.25 for the salinity and ± 2 °C for the temperature, the AdriSC ROMS 1 km model is in good agreement with the observations and thus provides reliable results concerning the thermohaline circulation.

Second, as the AdriSC ROMS 1 km model is showing some skill in representing the thermohaline properties along the two long–term monitoring Adriatic transects, an Empirical Orthogonal Functions (EOF) analysis is performed in order to find potential long–term variabilities. For this section, the five main EOF components (representing the highest percentages of the signal) of salinity and temperature monthly detrended anomalies are extracted and presented along both transects in Fig. 20 for the first component (hereafter referred as EOF 1) while the remaining components (EOFs 2 to 5) are not shown in this study.

Along the northern Adriatic transect, for both temperature and salinity, none of the EOF components captures interannual to decadal variabilities. This predominant lack of long–term variability can be probably explained by the influence of the Po River plume, which affects the full transect, even the eastern stations (Vilibić et al. 2019). For example, dissolved oxygen and organic carbon measured at the easternmost station have been strongly correlated to the long–term variability of the Po River discharge (Vilibić et al. 2020; Ciglenečki et al. 2020). The impact of the Po River plume is also seen on the spatial patterns of the salinity EOF 1 (66.2 % of the signal) which highlight a difference in the strength of EOF signals between the upper layer up to 10 m depth and the rest of the profile (i.e. presence in the upper layer of a stronger signal for salinity along almost entire northern Adriatic transect). For the temperature, EOF 1 (79.5 % of the signal) contains no decadal variability, reflecting the fact that the northern Adriatic transect is located along a shallow shelf (at less than 40 m depth), highly affected by and rapidly responding to local atmospheric processes and tides and the respective heat distribution within the water column.

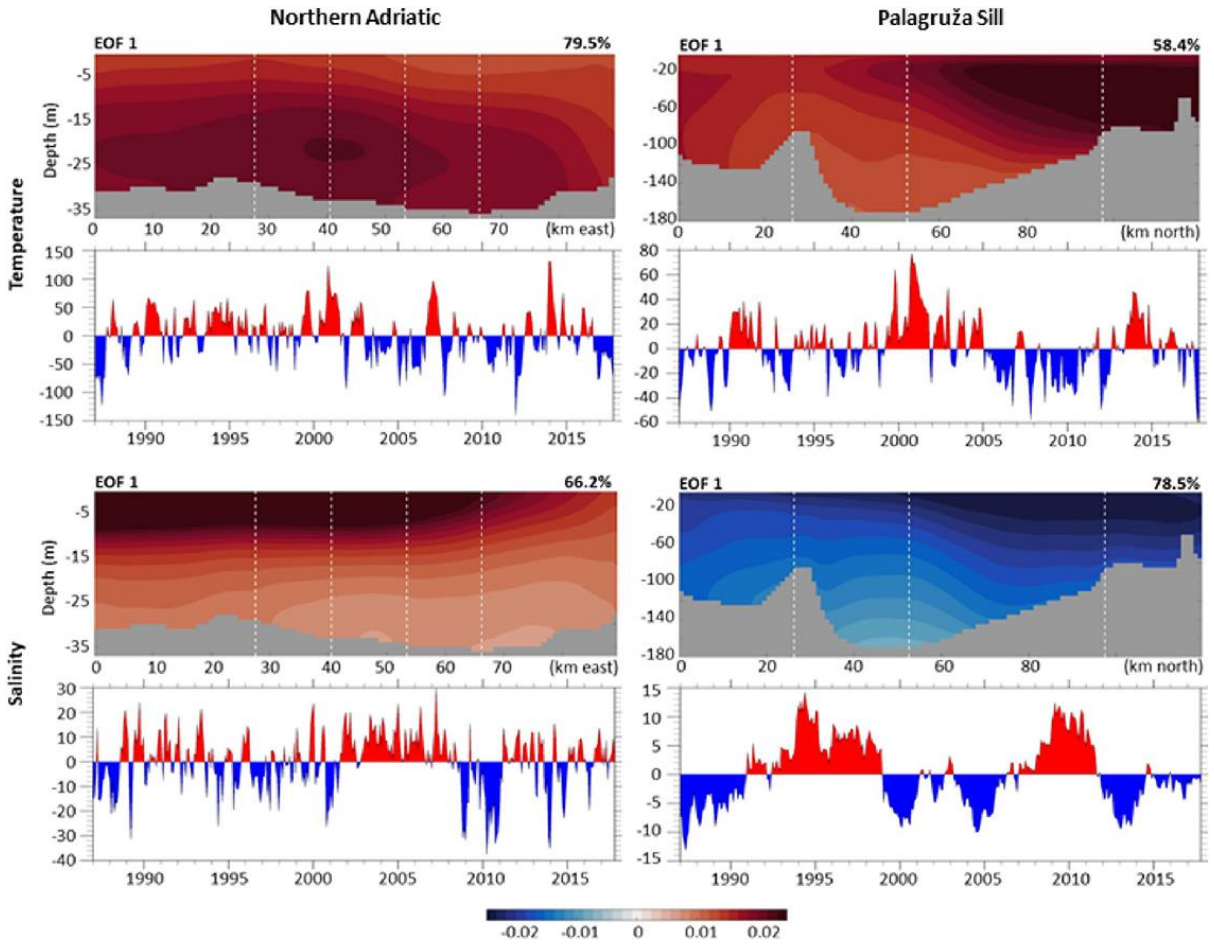

Figure 20. First normalised spatial EOF components and associated time series of amplitude derived along the northern Adriatic (left panels) and the Palagruža Sill (right panels) transects during the 1987–2017 period from the AdriSC ROMS 1–km temperature (top panels) and salinity (bottom panels) monthly anomalies. The dotted white lines represent the locations of the sampling stations along the long–term monitoring transects.

By contrast, the Palagruža Sill transect located in the middle of the Adriatic Sea in deeper waters less influenced by river discharges, tides and atmospheric conditions, is more likely to capture long–term variabilities. Still, for the AdriSC ROMS 1 km temperature results, none of the EOF components displays any decadal variability even though EOF 1 (representing 58.4 % of the signal) presents some interannual variabilities, particularly strong in the northern shallower part of the transect. However, for the AdriSC ROMS 1–km salinity results, the time series of amplitude associated with the EOF 1 (representing 78.5 % of the signal) clearly shows some well–defined interannual to decadal oscillations. Additionally, the EOF 1 spatial patterns highlight some differences: the weakest signal can be seen in the deepest part of the transect while the strongest signal is present in the northern shallower part. More importantly, the oscillations obtained with the AdriSC ROMS 1 km salinity results are in good agreement with the BiOS driven phases defined by Mihanović et al. (2015) with a Self–Organizing Maps

(SOM) method applied to temperature, salinity and dissolved oxygen observations along the Palagruža Sill transect during the 1952–2010 period. Indeed, the mostly negative amplitudes are obtained for the 1987–1990, 1999–2006 and 2012–2017 periods instead of the 1987–1990 and 1999–2005 periods found in Mihanović et al. (2015). And, the mostly positive amplitudes are occurring for the 1991–1998 and 2007–2011 periods instead of 1991–1996 and 2009–2010 periods described in Mihanović et al. (2015). The fact that certain phases are shifted by a year or two compared to Mihanović et al. (2015) can be largely attributed to their definition of intermittent phases for the 1997–1998 and 2006–2008 periods. This definition is directly linked to their interpretation of the results derived with the SOM method and does not apply to the EOF method presented in this study nor, more generally, to the BiOS indices (Gačić et al. 2010, 2014; Civitarese et al. 2010; Liu et al. 2021). Further, Mihanović et al. (2015) used an observational dataset stopping in 2010 and the phases obtained with the SOM method may have been slightly shifted if the records extended till 2018 (as seen in the sensitivity experiments provided in Fig. 5 of their study). In brief, while the AdriSC ROMS 1 km model struggles to reproduce the complex variability of the Po River plume influencing the thermohaline properties of the entire long–term monitoring northern Adriatic transect, it performs well along the Palagruža Sill transect where salinity and temperature scatter has been shown to be minimal. Additionally, despite not seeing substantial long–term variability along the northern Adriatic transect due to the dominance of local processes such as Po River plume spreading, the EOF analysis of the AdriSC ROMS 1 km salinity results along the Palagruža Sill transect does reproduce the phases previously extracted from the observations by Mihanović et al. (2015). Further, as both Modified Atlantic Water and Levantine/Eastern Mediterranean waters are mainly characterised by their salt content, the BiOS signal is thus expected to be principally seen in the salinity EOFs. Consequently, both the AdriSC ROMS 1 km results and the EOF methodology presented in this study are reliable enough to be applied over the entire Adriatic Sea.

3.2.2 Interannual to decadal variability of the Adriatic Sea thermohaline circulation

Here, the AdriSC ROMS 1 km salinity, temperature and current speed monthly detrended anomalies are extracted over the entire Adriatic Sea at the sea–surface, the sea–bottom and at 100 m depth.

First, the five main EOF components (representing the highest percentages of the signal) derived from these results are analysed by correlating the Ionian BiOS signal (hereafter simply referred as BiOS signal) with the time series of EOF amplitude (Fig. 21 and Table 7).

The temporal variability of the BiOS signal is defined as the second normalised spatial EOF component and associated time series of amplitude derived from the MEDSEA SSH fields in the Ionian Sea during the 1987–2017 period (top panels, Fig. 21). The spatial extent as well as the interannual to decadal variabilities of the obtained signal are in good agreement with indices calculated from altimetry data (Gačić et al. 2010, 2014), cruise observations (Civitarese et al. 2010), and model results (Liu et al. 2021). More precisely, the anticyclonic phases (positive sign of the EOF amplitude) are clearly seen for the 1987–1997 and 2006–2009 periods, while the cyclonic phases (negative sign of the EOF amplitude) are present for the 1998–2005 and 2010–2017 periods. However, small discrepancies concerning the timing of the reversals exist between the different BiOS indices. For example, the obtained 2006–2009 anticyclonic phase is 1 year shorter compared than the one derived by Gačić et al. (2010) and Bessières et al. (2013). In fact, uncertainties concerning the precise timing of the reversals are known to be introduced by the presence of mesoscale eddies during the transition periods of the BiOS (Gačić et al. 2014; Liu et al. 2021) and different methods can give slightly shifted phases. Consequently, it can be safely concluded that the BiOS regimes are appropriately reproduced by the second normalised EOF of the MEDSEA SSH fields in the Ionian Sea.

The correlation coefficients obtained between the BiOS signal and the time series of temperature, salinity and current speed EOF amplitudes at the surface, 100 m depth, and the bottom of the Adriatic Sea are presented in Table 7 for the BiOS signal with 0–year to 3–year lags. The re–scaled time series of the BiOS signal on top of the re–scaled EOF amplitudes with the highest correlation coefficients and representing the highest percentages of the signal are also plotted in Figure 21 (bottom panels).

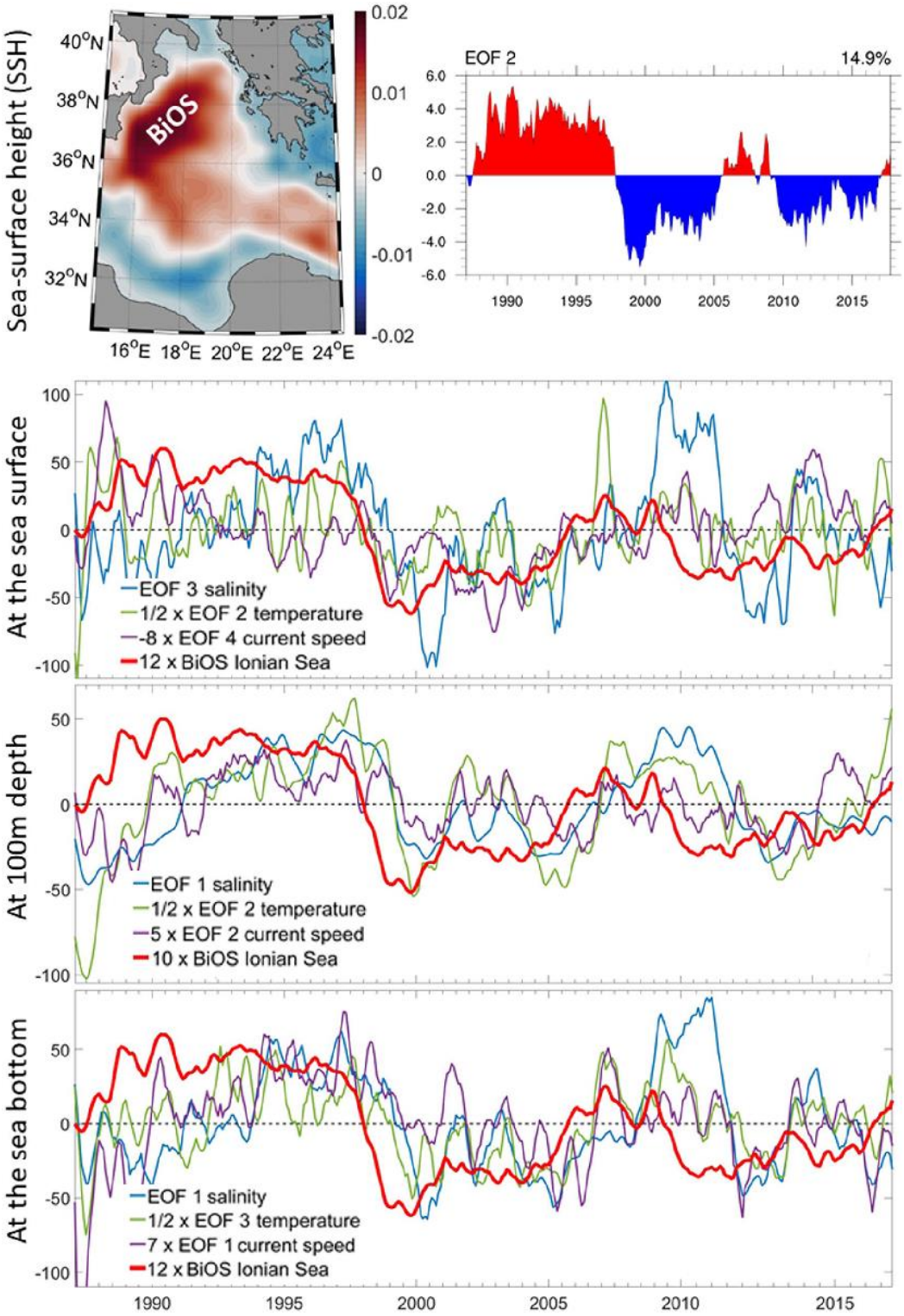

Figure 21. Second normalised spatial EOF component (top left panel) and associated time series of amplitude (top right panel), characteristic of the BiOS signal, derived in the Ionian Sea during the 1987–2017 period from the MEDSEA reanalysis sea–surface height results. Comparison of the re–scaled BiOS signal with the time series of rescaled normalised EOF amplitudes—with the highest correlations to the BiOS signal including a 1–year or 2–year lag—derived during the 1987–2017 period from the AdriSC ROMS 1–km temperature, salinity and current speed monthly anomalies at the surface, the bottom and 100 m of depth (3 bottom panels).

For the temperature, the highest correlations are obtained between the BiOS signal with 1–year lag and EOF 2 amplitudes at the sea–surface (0.30) and at 100 m depth (0.58) as well as EOF 3 amplitudes at the bottom (0.57). For the salinity, the highest correlations are obtained between the BiOS signal with 2–year lag and EOF 3 amplitude at the sea–surface (0.55) as well as EOF 1 amplitudes at 100 m depth (0.66) and the sea–bottom (0.53). For the current speed, the highest correlations are also obtained between the BiOS signal with 2–year lag and EOF 2 amplitude at 100 m depth (0.44) as well as EOF 1 amplitude at the sea–bottom (0.51). As expected, surface current speeds that are mainly driven by the atmospheric processes only present anti–correlations with the BiOS signal and EOF 4 that has the strongest anti–correlation with the BiOS signal including a 0–year, 1–year or 2–year lag is used hereafter. Further, except for the sea–surface, the temperature EOF amplitudes are still well–correlated with the BiOS signal, including 2–year lag with 0.55 for EOF 2 at 100 m depth and 0.50 for EOF 3 at the sea–bottom.

Correlation analyses are also performed between the time series of temperature and salinity EOF amplitudes extracted along the long–term monitoring northern Adriatic and Palagruža Sill transects and the BiOS signal with 0–year to 3–year lags and are presented in Table 8. As before, the only meaningful correlation is found between the BiOS signal with a 2–year lag and the salinity EOF 1 amplitude time series along the Palagruža Sill transect (i.e. correlation coefficient of 0.62). The fact that the Adriatic Sea haline response is delayed by approximately 2 years compared to the BiOS reversals sheds some light on the previously presented results. For example, the salinity EOF 1 amplitude sudden and short reversal from negative to positive seen in 2014–2015 along the Palagruža Sill (bottom right panel, Fig. 20) can be associated to the observed premature inversion of the BiOS signal in late 2012 caused by substantial generation of dense waters (Gačić et al. 2014). Other sudden and short reversals from negative to positive or variability of the salinity EOF 1 amplitude along the Palagruža Sill transect could also be the 2–year delayed response to BiOS signal variability driven by extreme bora events, like the ones documented between 1998 and 2017 in Denamiel et al. (2021a). However, it should be noted that these reversals are not present in the obtained BiOS signal (top right panel, Fig. 4). Yet the 2000–2001 and 2013–2014 periods are marked with a pronounced increase of the SSH EOF amplitude, from approximately −6.0 to −1.5 and −4.0 to −0.25. This is probably linked to the lack of accuracy of the atmospheric forcing used to produce the MEDSEA fields. Indeed, the change of vorticity in the northern Ionian Sea leading to the change of sign of the

SSH EOF highly depends on the dense water travelling through the strait of Otranto and resulting from the intensity of the bora–induced cooling over the Adriatic Sea.

Table 7. Correlation coefficients between the time series of normalised EOF amplitudes of the BiOS signal extracted from MEDSEA (EOF 2 of SSH) with 0–year to 3–year lags and the temperature, salinity, current speed signals at the surface (Surf.), the bottom (Bot.) and 100 m depth (100m) extracted from the AdriSC ROMS 1–km model (EOFs 1 to 5). Non–significant correlations following the null hypothesis are marked with the "/" symbol. The highest correlations are highlighted in bold.

		Temperature			Salinity			Current Speed		
Lag	EOF	Surf.	100m	Bot.	Surf.	100m	Bot.	Surf.	100m	Bot.
0–year	1	/	–0.16	/	0.11	0.24	0.15	–0.21	–0.43	0.19
	2	**0.38**	**0.31**	/	0.23	0.20	**0.20**	/	**0.19**	–0.19
	3	0.24	/	**0.45**	**0.27**	**0.47**	/	/	/	**0.41**
	4	/	–0.38	–0.16	–0.12	–0.20	/	–0.34	/	–0.17
	5	0.17	–0.34	/	0.26	0.15	0.14	–0.16	–0.13	–0.22
1–year	1	/	–0.19	/	/	**0.55**	**0.41**	–0.13	–0.33	**0.41**
	2	**0.30**	**0.58**	/	0.34	/	0.40	/	**0.35**	/
	3	0.19	/	**0.57**	**0.50**	0.27	0.19	/	/	0.37
	4	/	–0.17	/	–0.26	–0.15	/	–0.27	/	/
	5	0.18	–0.22	0.21	0.43	0.14	/	–0.13	–0.22	–0.18
2–year	1	/	–0.21	/	/	**0.66**	**0.53**	/	–0.24	**0.51**
	2	**0.14**	**0.55**	/	0.28	–0.13	0.48	/	**0.44**	0.17
	3	/	0.12	**0.50**	**0.55**	/	0.12	–0.13	0.11	0.27
	4	/	/	/	–0.37	/	/	–0.19	/	0.14
	5	/	/	0.43	0.41	/	/	/	–0.12	–0.15
3–year	1	**0.13**	–0.21	/	/	**0.60**	0.43	/	–0.16	**0.48**
	2	0.13	**0.38**	/	0.20	–0.22	**0.50**	/	**0.36**	0.21
	3	/	0.29	0.37	**0.39**	/	/	/	0.21	/
	4	0.18	/	/	–0.39	0.18	/	–0.13	/	0.15
	5	/	/	**0.44**	0.33	/	/	/	/	–0.16

At this point it must also be mentioned that correlations should be interpreted with some caution. As seen in the previous section, the temperature EOFs did not show any decadal variability along the long–term monitoring transects and thus may not be such a strong indicator of the Adriatic Sea response to the BiOS signal, contrarily to the salinity EOFs. Further, as mentioned before, both Modified Atlantic Water and Levantine/Eastern Mediterranean waters — which are the main tracers of the BiOS signal phases in the Adriatic Sea — are mainly characterised by their salt content. That can be assessed also from much lower percentages of explained variance in temperature vs. salinity for different EOFs

correlated with the BiOS signal: EOF 2 in temperature (18.3 %) vs. EOF 1 in salinity (60.8 %) at 100 m and EOF 3 in temperature (6.5 %) vs. EOF 1 in salinity (37.1 %) at the bottom. Indeed, the wintertime cooling, in particular during severe bora events (Janeković et al. 2014; Denamiel et al. 2021a), may substantially uptake the heat from the deep Adriatic (i.e. up to 900 m) to the atmosphere (e.g. Gačić et al. 2002; Cardin et al. 2020). Consequently, temperature might not be as a conservative tracer in the deep Adriatic as salinity. Coming from correlations with salinity EOFs, the response time of the Adriatic thermohaline circulation to the BiOS phases is thus likely to be of approximately 2 years.

Table 8. Correlation coefficients between the time series of normalised EOF amplitudes of the BiOS signal extracted from MEDSEA (EOF 2 of SSH) with 0–year to 3–year lags and the temperature, salinity, current speed signals along the northern Adriatic and Palagruža Sill long–term monitoring transects extracted from the AdriSC ROMS 1–km model (EOFs 1 to 5). Non–significant correlations following the null hypothesis are marked with the "/" symbol. The highest correlations are highlighted in bold.

		Northern Adriatic		Palagruža Sill	
Lag	EOF	Temperature	Salinity	Temperature	Salinity
0–year	1	**0.12**	/	–0.23	**0.27**
	2	/	–0.20	/	0.20
	3	–0.15	/	0.22	–0.29
	4	/	/	–0.14	/
	5	/	/	**0.42**	/
1–year	1	/	/	–0.29	**0.55**
	2	/	–0.36	/	/
	3	/	0.11	0.31	–0.14
	4	/	**0.26**	–0.28	/
	5	/	–0.25	**0.41**	/
2–year	1	**0.11**	–0.22	–0.22	**0.62**
	2	/	–0.48	–0.11	–0.12
	3	/	0.16	**0.27**	/
	4	/	**0.32**	–0.35	/
	5	/	–0.23	0.17	0.11
3–year	1	/	–0.26	–0.14	**0.52**
	2	/	–0.38	–0.16	–0.27
	3	/	/	**0.30**	0.14
	4	/	**0.24**	–0.19	/
	5	/	–0.12	/	/

As one of the major drawbacks of any EOF analysis is the potential lack of physical meaning of the obtained components, the spatial patterns of the temperature, salinity and

current speed EOF components with the highest correlation to the BiOS signal (including a 2–year lag) are now analysed with the aim to connect them to the known dynamical properties of the Adriatic Sea (Figs. 22, 23, 24).

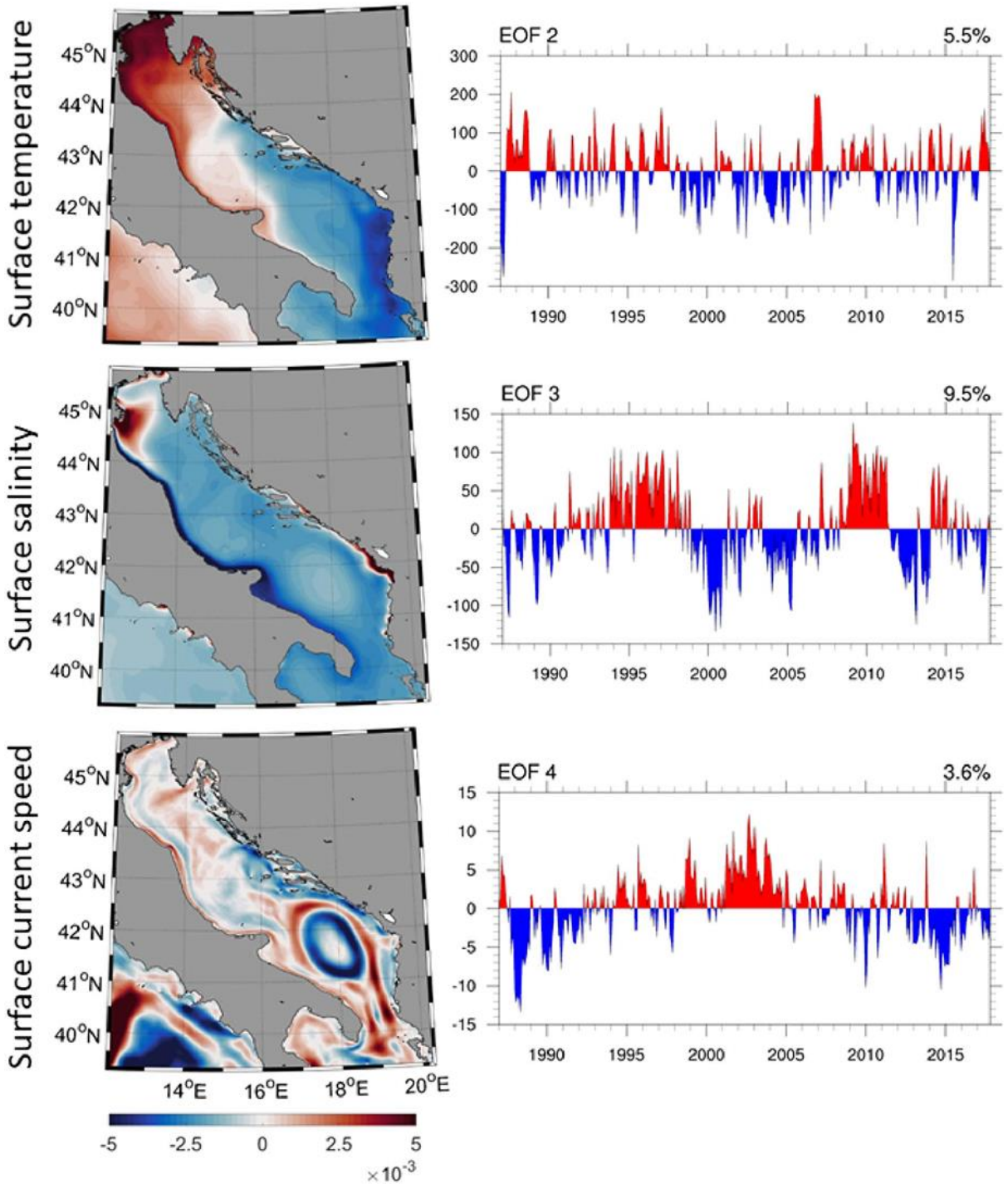

Figure 22. AdriSC ROMS 1 km sea–surface temperature (top panels), salinity (middle panels) and current speed (bottom panels) normalised spatial EOF components (left panels) and associated time series of amplitude (right panels) with the highest (anti) correlation to the BiOS signal (including a 1–year or 2–year lag) during the 1987–2017 period.

At the sea–surface where the influence of the atmospheric forcing and the river fresh water discharges are the highest (Fig. 22) and masking the BiOS signal, the time series of the EOF amplitudes tend to display important interannual variabilities for temperature, salinity and current speed. Additionally, the associated spatial patterns highlight some major differences. First, the spatial patterns of the temperature EOF 2 (representing only 5.5 % of the signal) is strongly negative in the south and strongly positive in the north and associated with time series where the delayed BiOS reversals cannot be easily distinguished. Second, the spatial patterns of the salinity EOF 3 (representing only 9.5 % of the signal) are homogeneously negative over the entire Adriatic Sea, except along the coast where the influences of the river discharges are the strongest (the Po River plume, other northern Adriatic rivers, Neretva river, Albanian rivers). Such a multipolar structure might resemble river plumes being more confined towards river mouths and coastlines during high salinity conditions in the Adriatic and vice versa. Third, the spatial patterns of the current speed EOF 4 (representing only 3.6% of the signal) are extremely complex and the associated time series disconnected to the BiOS signal. Still, it seems that the BiOS sporadically influences the size of the South Adriatic Gyre, which can be confined either closer to the coastlines or to the centre of the pit as the result of different BiOS regimes, while also affecting the transport rates in the Strait of Otranto.

At 100 m depth (Fig. 23) where, in contrast with the sea surface, the thermohaline circulation is dominant, (1) the obtained EOFs all represent a large or major part of the signal (18.3 % for the temperature, 60.8 % for the salinity and 9.0 % for the current speed), (2) the associated time series all display the 1 year (for temperature) or 2 year (for salinity and current speed) delayed response in reaching maximum correlations to the BiOS signal and (3) the spatial patterns with a mostly negative signal are all nearly homogeneous over the entire Adriatic Sea, in particular for the salinity. Additionally, for all the variables, the weakest signal is found in the middle of the South Adriatic Pit which seems less influenced by the BiOS signal than the rest of the domain. Indeed, the centre of the South Adriatic Pit is the centre of the cyclonic gyre, where upwelling and deep convection take place (i.e. vertical processes are bringing more water masses from the deep and surface Adriatic than at the perimeter of the gyre) while being somehow separated from the advected waters. In contrast, the perimeter of the South Adriatic Pit is characterised by a persistent and strong current, bringing waters from the Ionian Sea and keeping about 90 % of them in the loop (Gačić et al. 2014).

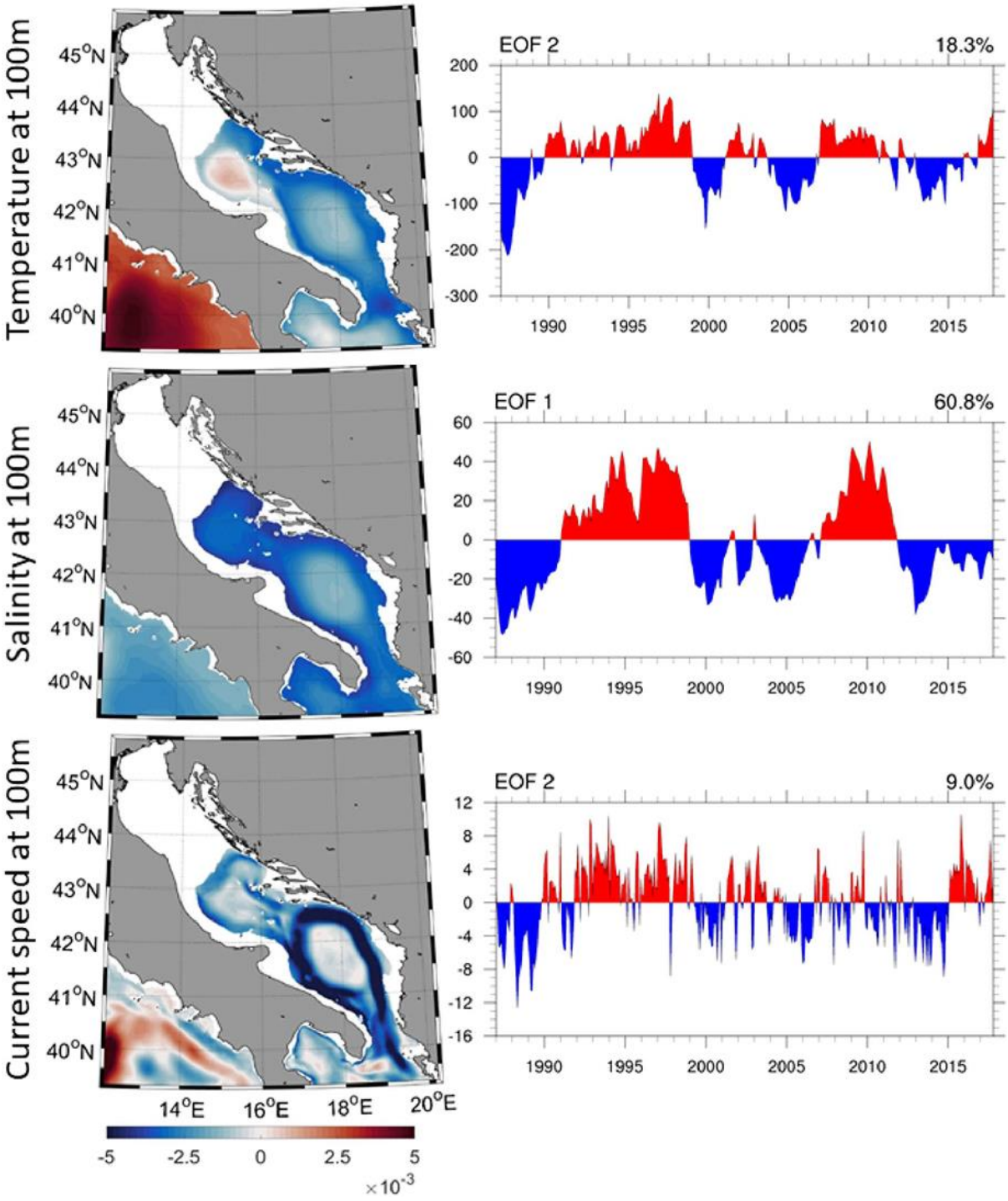

Figure 23. Same as Figure 22 but for AdriSC ROMS 1 km temperature (top panels), salinity (middle panels) and current speed (bottom panels) at 100 m depth.

This can be seen in the spatial patterns of the current speed EOF 2 where the South Adriatic Gyre is highly sensitive to the BiOS signal despite the associated time series of amplitudes displaying a BiOS related signal strongly embedded in the interannual variabilities. Further, the spatial EOF of the temperature at 100 m clearly shows a distinct area with positive signal in the western part of the Jabuka Pit and southern Palagruža Sill which are known collectors

of the dense waters formed during extreme bora events. It should also be noted that the brief inversions of the BiOS signal, already mentioned for the salinity EOF analysis along the Palagruža Sill transect, can clearly be seen in the time series of both temperature and salinity EOF amplitudes. At 100 m depth, it even seems that the temperature inversions are stronger than the ones of the salinity.

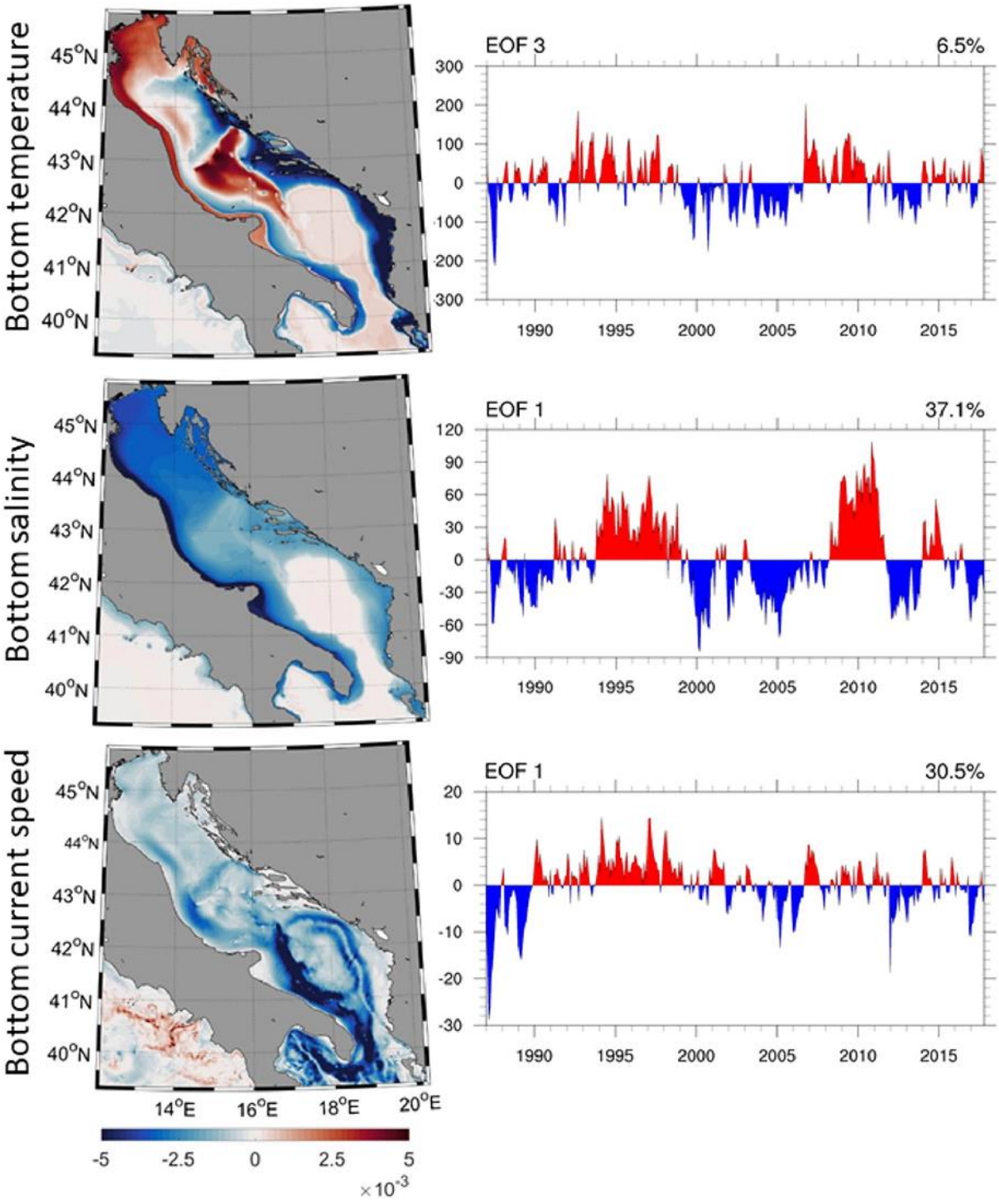

Figure 24. Same as Figure 22 but for AdriSC ROMS 1 km temperature (top panels), salinity (middle panels) and current speed (bottom panels) at the sea–bottom.

Finally, at the sea–bottom (Fig. 24), the obtained EOFs most correlated to the BiOS signal are spatially homogeneous (negative over the entire Adriatic Sea) and represent a large part of the signal (more than 30 %) for the salinity and the current speed. Precisely, salinity EOF 1 spatial amplitude (accounting for 37.1 % of the signal) is the largest in the northern Adriatic and along the Western Adriatic Coastal Current. Such a strong effect of the delayed BiOS signal to the northern Adriatic bottom salinity indicates that wintertime cooling and dense water production are preconditioned by the salinity content driven by the BiOS. Interestingly, this even affects the shallow northern Adriatic somehow contrasting with the findings along the northern Adriatic transect indicating no BiOS driven salinity variability (Fig. 20). Yet, the transect analyses included the surface layer strongly shaped by local processes and masking the effects of the basin wide processes like the BiOS. Regarding the bottom temperature (Fig. 24), EOF 3 is correlated to the delayed BiOS phases. But it represents only 6.5 % of the temperature signal and, consequently, the local cooling due to extreme bora events probably affects the bottom temperature changes much more than the advection of waters driven by BiOS. Still, the EOF 3 spatial patterns present an interesting distribution. They are strongly negative along the south– and middle– eastern Adriatic coast till the Kvarner Bay and along the south–western Adriatic. But they are positive in areas where the northern Adriatic dense waters are known to be either (1) formed during extreme bora events like the northern Adriatic shelf (Bergamasco et al. 1999) or the Kvarner Bay (Janeković et al. 2014; Vilibić et al. 2018), (2) travelling towards the northern Ionian Sea—i.e. along the Italian coast (Artegiani et al. 1987; Vilibić et al. 2013) or (3) collected within the Adriatic Sea — i.e. the Jabuka Pit (Marini et al. 2006) and the South Adriatic Pit (Querin et al. 2016). Therefore, this EOF is describing the connection between the BiOS signal and the Adriatic dense water formation and spreading, which is not as intuitive for temperature as for salinity. Precisely, the cyclonic BiOS signal is resulting in an advection of warmer waters, reaching maximum correlations after 2 years, while simultaneously connected with colder–than–usual winters that produce dense waters with lower temperatures. In fact, such a coincidence between these two unrelated processes is not frequent in the Adriatic — for that reason accounts just for a small percentage of EOF solutions — but still recognized as the third most frequent EOF driving the bottom temperature. For the current speed, the EOF 1 spatial patterns (consisting in 30.5 % of the signal) are similar to the one described at 100 m depth which highlights that the South Adriatic Gyre is mostly affected by the 2–year delayed BiOS signal below 100 m depth.

In summary, except at the sea–surface where the atmospheric–and river– driven processes are dominant, the Adriatic Sea thermohaline circulation is well correlated with the 2–year delayed BiOS phases derived from the sea–surface height variability in the Ionian Sea. Overall, salinity is found to be the best indicator of the response of the Adriatic Sea to the BiOS phases. Indeed, salinity EOFs always (1) have correlations above 0.5 with the 2–year delayed BiOS signal, (2) represent a large part of the signal (from 9.5 % in surface to 60.8 % at 100 m depth) and (3) are mostly homogeneous spatially. Temperature variability, however, is too much influenced by the atmospheric–driven extreme bora events in the northern Adriatic to be a reliable tracer of the impact of the BiOS in the Adriatic Sea.

3.3 Discussion

Hereafter, a discussion on the added value of the kilometre–scale modelling approach in the Adriatic basin is presented. In particular, the results obtained with the AdriSC model for both short–term extreme bora events and long–term BiOS–driven thermohaline variability are put in the context of demonstrating the need for such an approach.

3.3.1 Extreme bora events

The severe bora windstorms present an interesting multidisciplinary research topic as being strongly influenced by the complex coastal orography and impacting the Adriatic Sea long–term thermohaline circulation. The AdriSC modelling suite has thus been specifically developed to represent, with high–resolution limited–area models, the complex atmosphere–ocean interactions over the elongated semi enclosed Adriatic basin. In this thesis, the capability of the AdriSC WRF 3 km atmospheric numerical model to balance accuracy, in the representation of basic bora features and associated air–sea interactions, and numerical efficiency, in terms of cost and computational time increasing with higher resolutions, has been leveraged via a statistical approach. This approach is based on the comparison of the baseline conditions with the AdriSC WRF 15 km and WRF 1.5 km results and the ERA5 reanalysis (at 30–km resolution), for an ensemble of 22 extreme bora events. Such a method has some intrinsic limitations. First, the use of a relatively small ensemble of 22 storms may not be fully representative of the historical Adriatic extreme bora events. Second, the shortness of the simulations carried over a 3–day period increases the influence of the imposed initial conditions on the analysed results compared to long–term simulations. However, this statistical approach presents the advantage of covering historical bora storms from 1991 to 2018 using far less computational resources than running a climate model for a classical 30–years

evaluation period. Consequently, it allows quantifying the performance of a climate model prior to the long–term runs. The main findings of this study are thus as follows:

1) ERA5 reanalysis strongly underestimates the extreme bora speeds due to its incapacity to reproduce the basic bora dynamics; as a consequence, during bora events in the northern Adriatic, ERA5 cannot be used either as a reference for climate model evaluation nor as a forcing for ocean models
2) the baseline conditions derived from the WRF 3 km results for a unique ensemble of 22 extreme events are found to reproduce the known basic bora dynamics to some extent (i.e. lack of accuracy particularly in terms of the proper location and intensity of the PV banners and the mountain waves but generally good representation of the intensity of the horizontal wind speeds) and thus to put in perspective the previously published results by deriving permanent bora features during extreme events
3) WRF 15 km model is found to highly diverge from the baseline conditions (e.g. horizontal wind speed biases above 28 % near the lee of the mountains and of 5 % at 0.5 km along the Senj transect associated with a 7.6 m/s underestimation of the 99^{th} percentile).
4) the baseline condition biases with the WRF 1.5 km model are minimised for both bora dynamics (e.g. below 6 % near the lee of the mountains, and of 0–1 % along the Senj transect, for the horizontal wind speed) and air–sea interactions (e.g. heat fluxes up to 46 % for ERA5, 6 % for WRF 15 km (with underestimations reaching 100 W/m^2 during the most extreme events), and only 2 % for WRF 1.5 km, along the Senj transect). The baseline conditions are thus found to converge toward higher resolution solutions

In light of these results, particularly the divergence from the baseline conditions of the WRF 15 km model in most of the coastal areas, one important question remains unanswered. With the ultimate aim to reproduce dense water formation in the northern Adriatic Sea during extreme events, how important is it for the atmospheric models to properly capture the bora–driven dynamics and air–sea interactions in the coastal areas of the Kvarner Bay? Given the present knowledge of the Adriatic Sea scientific community, no definitive answer can be provided. However, several facts have been recently proven. First, dense water is formed within the Kvarner Bay (Vilibić et al. 2018). Second, due to the ocean circulation, the correlations between bora–driven heat fluxes and sea surface cooling are generally weak in the northern Adriatic during extreme bora storms (Denamiel et al. 2020b). They are even totally

insignificant around the Cres Island due to the transport of waters from the Kvarner Bay to the northern Adriatic shelf. However, these correlations are the highest within the coastal areas of the Kvarner Bay. Finally, dense water is also formed in the middle of the northern Adriatic shelf where some correlations between heat fluxes and sea surface cooling exist (Denamiel et al. 2020b). The above question can thus be reformulated as: how much of the dense water formed in the northern Adriatic shelf is coming from direct sea surface cooling at the shelf, and how much is coming from the transport of waters from the Kvarner Bay (of limited size, but far more affected by bora–driven cooling)? The only available interannual study of the northern Adriatic dense water formation is based on uncoupled atmosphere and ocean model results for an 8–years long period (Mihanović et al. 2018). It highlights that bora–driven dense water formation rates can reach up to 40 % within the Kvarner Bay during extreme winters preconditioned by high salinity conditions. Additionally, Dunić et al. (2019) have demonstrated that coupled atmosphere–ocean RCMs over the entire Mediterranean Sea have no capacity to reproduce dense water formation rates in the Adriatic Sea. It is however unknown whether this is linked to the atmospheric model or the ocean model resolutions. Following these studies and the presented results, it is reasonable to hypothesise that the proper representation of the bora–driven sea surface cooling within the Kvarner Bay may be critical to the accurate modelling of the sea surface cooling in the northern Adriatic shelf and, hence, of the dense water formation.

Consequently, even though ensembles of atmospheric RCMs can robustly represent the climate trends of the bora strength (Belušić Vozila et al. 2019), coupled atmosphere–ocean RCMs (usually having resolutions of the order of 10 km in the Mediterranean, Soto–Navarro et al. 2020) cannot be used in oceanographic climate studies dealing with thermohaline circulation and dense water formation driven by extreme bora events. As proven in this thesis, these processes require a better reproduction of the orographically driven atmospheric dynamics and particularly of the bora strength which can be partially achieved with the kilometre–scale approach used in the basic module of the AdriSC modelling suite.

3.3.2 BiOS–driven thermohaline variability

The principal novelty of this study consists in using, for the very first time, a kilometre–scale climate model to investigate, via an EOF and correlation approach, the impact of the BiOS on the Adriatic Sea thermohaline circulation at different depths over the entire basin. The main findings are twofold. On the one hand, the AdriSC ROMS 1 km model is proven to

be, to this date, the only numerical model capable to reproduce the BiOS–driven phases observed along the Palagruža Sill long–term monitoring transect on a climate scale. On the other hand, over the entire Adriatic basin, the BiOS signal is demonstrated to be only weakly correlated to the sea–surface circulation and the two main temperature EOF time series (except at 100 m depth with a 1– or 2–year lag), but better correlated with a 2–year lag to the salinity and current speed two main EOF time series at 100 m depth and the sea–bottom. However, due to the uncertainties associated with the numerical results and the methods used in this work, the validity of this approach is further discussed hereafter.

First, EOF methods have been widely used within the climate community in order to identify the modes of variability and the predictability of the Earth system (Navarra and Simoncini 2010). Some known examples are the extraction of the El Niño Southern Oscillation (ENSO) interdecadal variabilities by Zhang et al. (1997) and Newman et al. (2003) or the study of the Atlantic thermohaline circulation variability by Hawkins and Sutton (2007). However, EOF analyses suffer from major drawbacks such as the orthogonality of the EOF patterns and the uncorrelatedness of the associated time series (e.g. Jolliffe 2002; Hannachi 2007; Monahan et al. 2009). Consequently, the interpretation of EOF results in physical terms is not necessarily straightforward, except when an outstanding mode is present (e.g. ENSO in global sea–surface temperature or North Atlantic Oscillation in mean sea–level pressure). In the presented results of the Adriatic thermohaline circulation response to the BiOS regimes, such a predominant mode exists particularly for the salinity and current speed results at 100 m depth and the sea–bottom. Consequently, the correlation between the EOF time series obtained in the Adriatic Sea and the BiOS signal extracted in the northern Ionian Sea provides relevant information concerning the BiOS mechanisms, with relatively high values obtained for the correlation coefficients (i.e. maximum value of 0.66).

Second, during the studied 1987–2017 period, the BiOS reversals are found to impact the Adriatic thermohaline circulation with approximately 2–year delay. Mihanović et al. (2015) observed similar response time during 1993–2014 period, based on the long–term monitoring Palagruža Sill transect measurements and satellite altimetry data. Additionally, the 2–year delay corresponds to the decay time of 26 months of the Adriatic Deep Water estimated by Vilibić and Orlić (2002) with a simple box model. Thus, it may be the natural response time of the southern Adriatic basin to a change in water masses, which was proven to be driven by the BiOS in this study. However, Mihanović et al. (2015) also highlighted that during exceptional conditions such as the Eastern Mediterranean Transient (EMT; Roether et al. 2007)

in the 1990s, the delay may be reduced to 1 year, while prolonged to more than 2 years during slow BiOS reversals. It should be noted that EMT conditions were extraordinary during this period as the dense water flow of Aegean origin was almost an order of magnitude larger than the dense water flow of Adriatic origin. Consequently, these conditions resulted in the strongest anticyclonic phase of the BiOS ever recorded.

Finally, spatial results of the EOFs obtained for the AdriSC ROMS 1 km salinity, temperature and current speed, clearly display three different types of circulation. At the surface, the circulation is nearly totally disconnected from the BiOS signal. This can be explained by the known influence of the temporal changes of both the atmospheric forcing (Béranger et al. 2010; Janeković et al. 2014) and the river freshwater discharges (Orlić et al. 1992; Lazar et al. 2007) on the Adriatic surface thermohaline circulation. In intermediate and deep layers (here represented by EOFs at 100 m and the bottom layer) the haline circulation displaying strong interannual and decadal oscillations associated with nearly homogeneous spatial patterns is known to be driven mostly by the BiOS and the EMT (Roether et al. 2007; Gačić et al. 2010, 2014). Further, the bottom temperature EOF 3 spatial patterns (interpreted as representing the dense water formation, spreading and storage locations) were connected with a delayed BiOS signal. In the Adriatic basin, dense waters were observed at the exact locations (Vilibić et al. 2004; Wang et al. 2006) and are known to drive the deep Adriatic thermohaline circulation (Orlić et al. 2007; Vilibić et al. 2013). However, this signal is an order of magnitude less pronounced than the BiOS–induced intermediate and deep salinity signal, nominating the salinity as the major tracer of the incoming Adriatic water masses.

To sum up, the analysis of the AdriSC ROMS 1 km salinity, temperature, and current speed EOF modes has numerically confirmed and generalised, for the very first time, the known influence of the BiOS on the Adriatic Sea thermohaline circulation till now only derived from *in–situ* observations. Consequently, this thesis has demonstrated the added value of the kilometre–scale approach used within the AdriSC climate model and further analysis of the AdriSC results can now be performed in order to study the BiOS–driven physical processes within the Adriatic Sea as well as the effect of the Adriatic dense water on the NIG reversals.

4. FAR–FUTURE OF EXTREME BORA EVENTS

So far, the future climate of the bora winds has been documented through an assessment of EURO–CORDEX climate models of 0.11° horizontal resolution (i.e. at a resolution an order of magnitude coarser than recommended) by Belušić Vozila et al. (2019). This analysis underpins a decrease of both intensity and frequency of the bora wind in the future climate, except in the northern Adriatic, however the wind regimes over such a complex mountainous region were found to be extremely sensitive to the representation of the orography in the regional models.

Consequently, understanding the impact of climate change on the severe bora dynamics, and the associated northern Adriatic air–sea exchanges, requires the use of kilometre–scale coupled atmosphere–ocean climate models such as the AdriSC modelling suite, with resolutions varying from 15 km to 1.5 km in the atmosphere and from 3 km to 10 m in the ocean. The same ensemble of extreme bora events previously presented in sections 2.3.1.1 and 3.1 was thus used to produce short-term AdriSC climate projections based on the PGW approach for the far-future 2070-2100 period (section 2.2). In this chapter, the impact of moderate and extreme warming (RCP 4.5 & 8.5 scenarios, respectively) on both the bora strength and dynamics, and the associated air–sea surface heat transfer, is thus quantified. The work presented in this chapter is published in the study by Denamiel et al. (2020b).

4.1 Bora dynamics

To better understand the impact of climate change on the extreme bora simulations in the northern Adriatic for the 2070–2100 period, the AdriSC WRF 3 km model RCP 4.5 & 8.5 conditions (i.e. median of peak conditions — hereafter referred as RCP 4.5 & 8.5 baseline conditions) and climate adjustments (i.e. median of the difference between RCP 4.5 & 8.5 separately and evaluation peak conditions) are presented as horizontal slices between the surface and 2 km of height (Figs. 25 and 26) and as vertical profiles for the four cross–shore transects (Figs. 27 to 31).

Horizontally, the major known bora features can clearly be seen in the RCP 4.5 & 8.5 baseline conditions derived from the AdriSC WRF 3 km simulations. The wake and jet dynamics along the coast (Jiang & Doyle, 2005; Belušić & Klaić, 2006; Gohm et al. 2008; Signell et al. 2010) still exists in the climate projections with variations of the horizontal wind speed magnitude from north to south — i.e. intense jets above 20 m/s between the surface and 1 km height separated by lower speeds (Figs. 25 and 26).

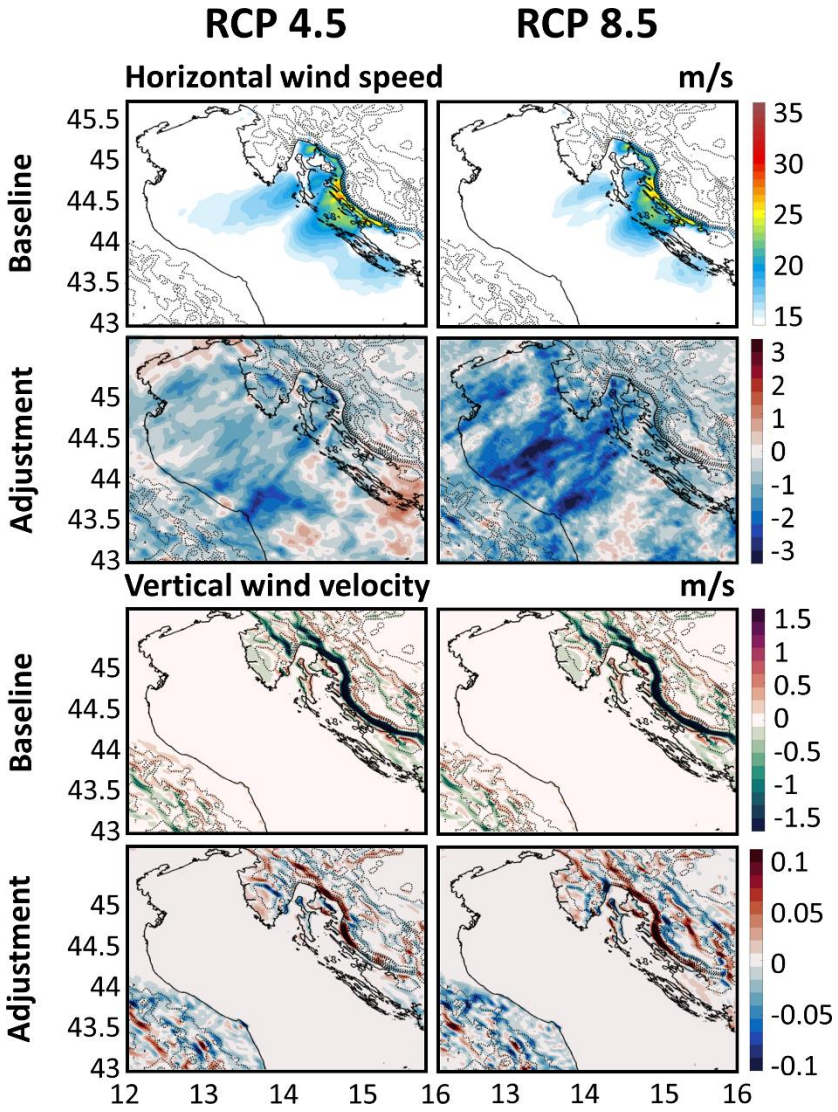

Figure 25. Baseline RCP 4.5 & 8.5 conditions (median of the scenario results) and climate adjustment (median of difference between scenario and evaluation results) for horizontal wind speed and vertical wind velocity at the surface (about 5 m height) during the peak of 22 selected extreme bora events. Topographic contours are displayed every 250 m with dashed lines.

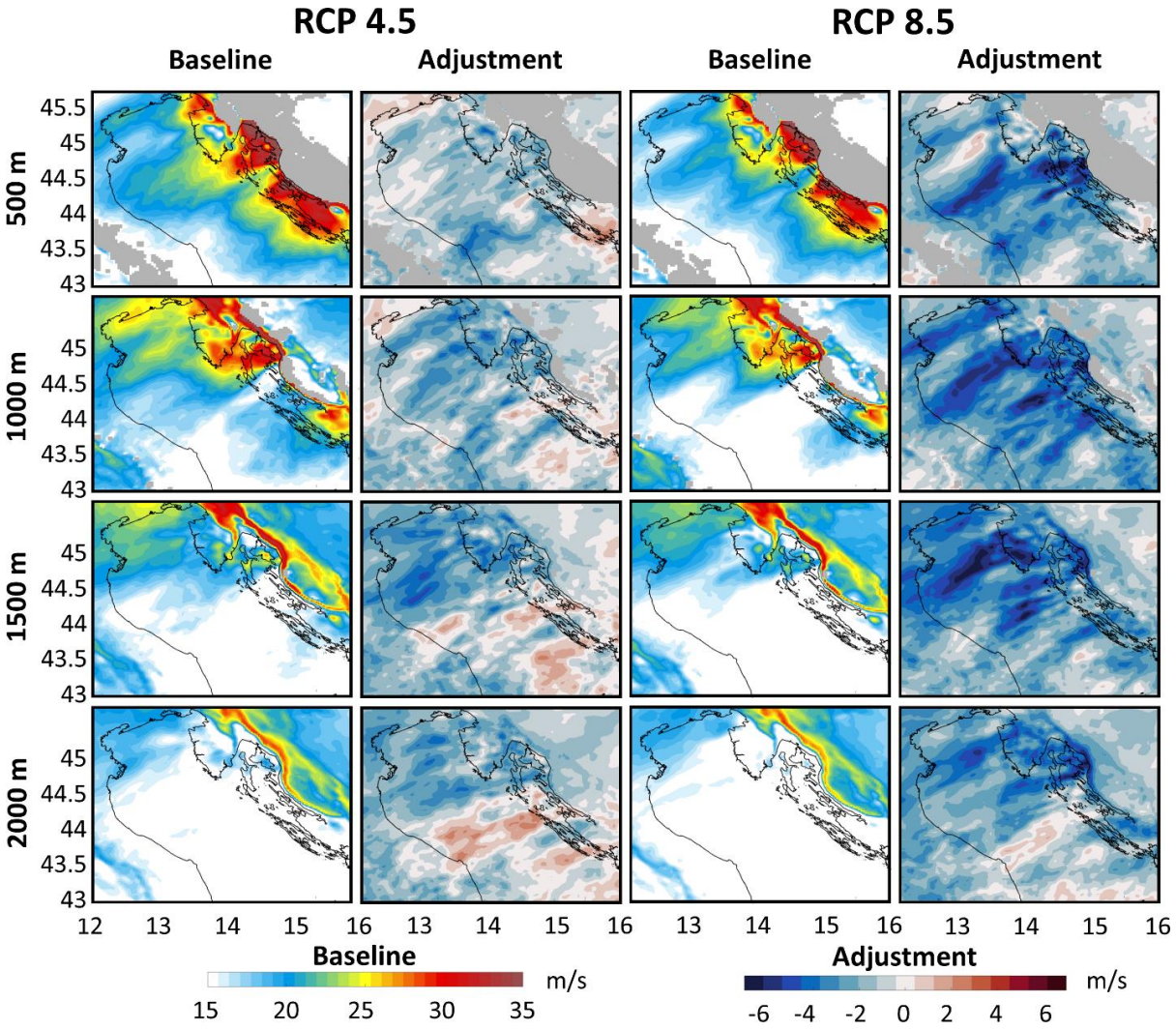

Figure 26. Baseline RCP 4.5 & 8.5 conditions (median of the scenario results) and climate adjustment (median of difference between scenario and evaluation results) for horizontal wind speed at heights of 500 m, 1000 m, 1500 m and 2000 m during the peak of 22 selected extreme bora events.

However, the intensity of these bora jets largely decreases between the surface and 2 km height (Figs. 25 and 26), with climate adjustments up to –3.5 m/s and –6 m/s for RCP 4.5 & 8.5 scenarios, respectively. As this decrease in intensity is not homogeneous, the location of the wakes and jets may also slightly vary between the future scenario (RCP 4.5 & 8.5) and the evaluation conditions. To be noted, the Trieste jet — known to be overall less intense than the other jets along the Velebit mountain range, is projected to decrease down to 15 m/s near the surface in the climate projections and is thus not represented in Figure 25. Finally, the vertical velocities are strongly negative along the lee of the Velebit mountain range (up to –1.5 m/s at surface) and positive along the coastline (about 0.5 m/s at surface). The associated climate adjustments are above 0.1 m/s along the lee of the Velebit mountain range. Consequently,

mountain waves might be less intense under climate change which could explain the decrease of the wind speed intensity during bora events in future climate.

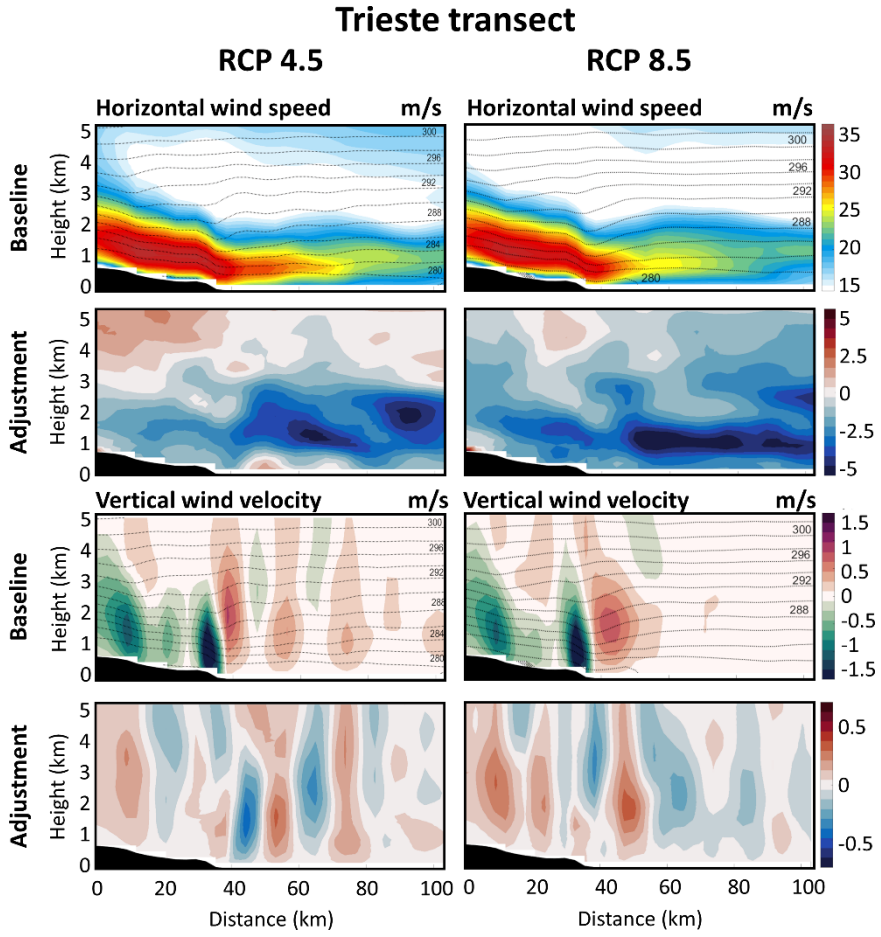

Figure 27. Trieste cross–shore transect of baseline RCP 4.5 & 8.5 conditions (median of the scenario results) and climate adjustment (median of difference between scenario and evaluation results) for the horizontal wind speed, vertical wind velocity and virtual potential temperature (black isolines) during the peak of 22 selected extreme bora events.

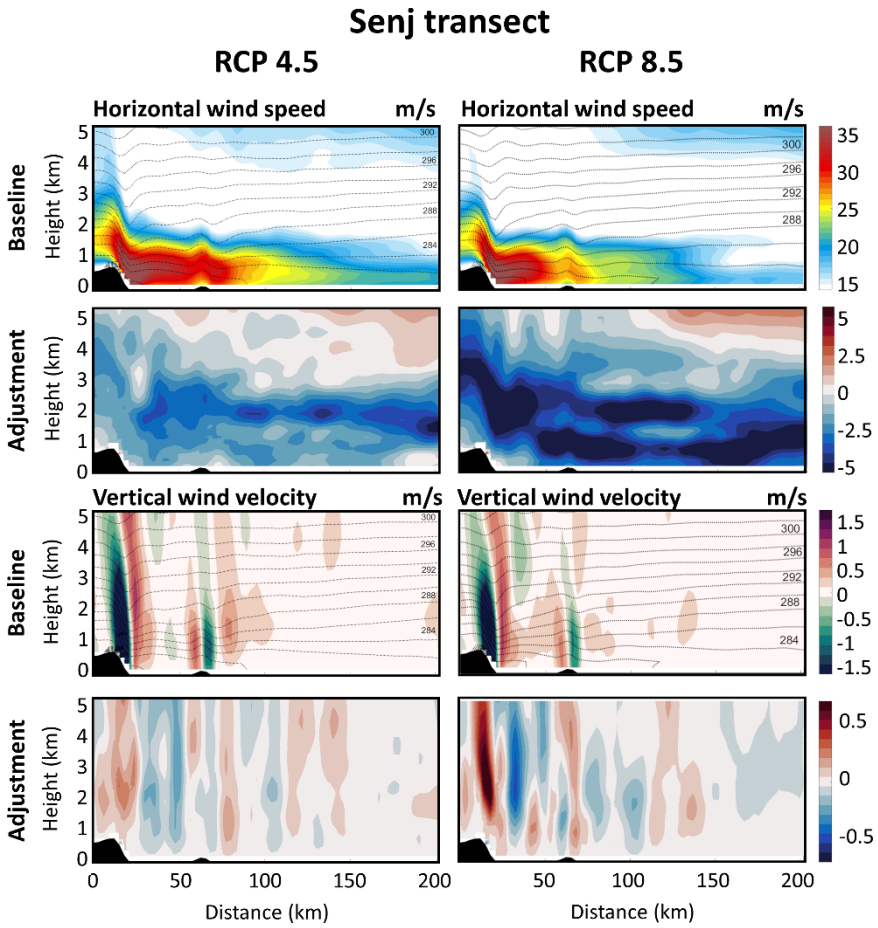

Figure 28. Same as Figure 27 but for the Senj cross–shore transect.

The vertical structures along the cross–shore transects (Figs. 27 to 30) also present for both RCP 4.5 & 8.5 scenarios the major known features of bora flows, even though, the WRF 3 km model can only capture the hydraulic jump–like flow features (Grisogono & Belušić, 2009; Prtenjak & Belušić, 2009; Prtenjak et al. 2010). For all transects (Figs. 27 to 30), strong atmospheric wave dynamics in the lee of the mountains — i.e. positive and negative vertical velocities with a magnitude above 1.5 m/s and sharp descent and re–ascent of the isentropes extending till 5 km of height — are present in both RCP 4.5 & 8.5 scenarios. Yet, the associated climate adjustments — strongly positive (above 0.3 m/s and 0.5 m/s for respectively RCP 4.5 & 8.5 scenarios) where the vertical velocities are negative and vice versa — might suggest that the atmospheric waves will be less intense in future climate projections than in evaluation mode as already seen in the surface plots (Fig. 25).

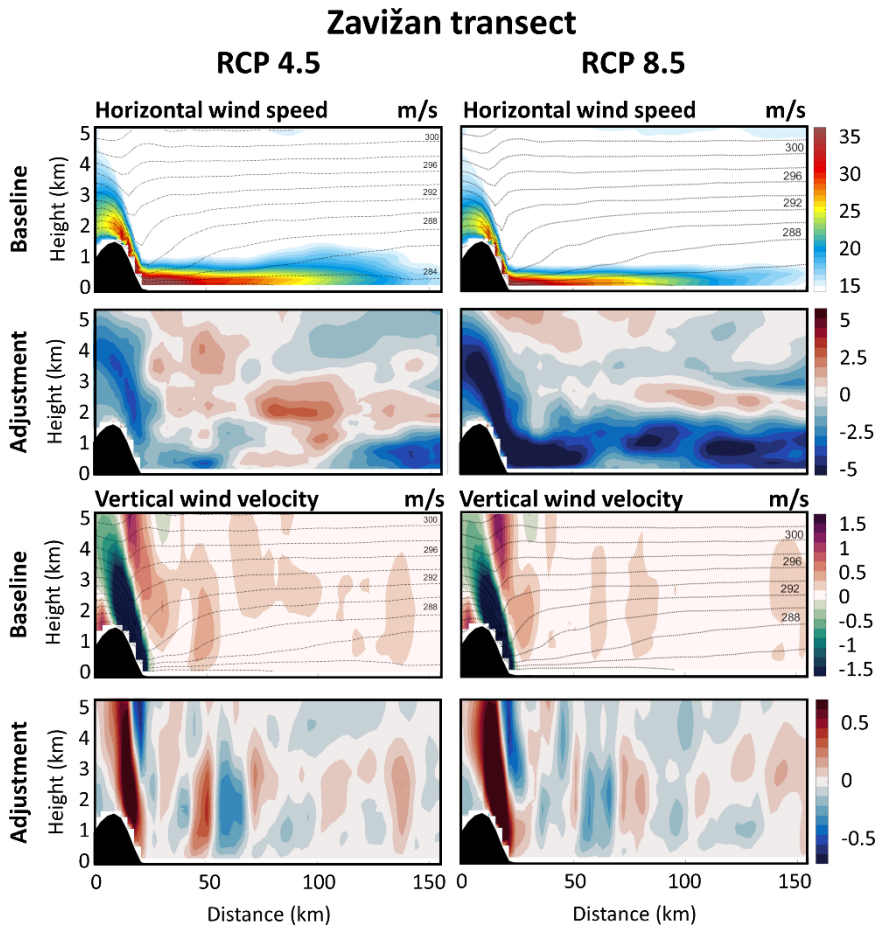

Figure 29. Same as Figure 27 but for the Zavižan cross–shore transect.

For the Trieste and Senj transects – located in mountain passes below 900 m, the RCP 4.5 & 8.5 baseline conditions (Figs. 27 and 28) show a deep boundary layer flow with horizontal wind speed of 30 m/s. The bora jets along the Trieste and Senj transects are strongly decelerated with climate adjustments below –2.5 m/s and –5 m/s for RCP 4.5 & 8.5 scenarios, respectively, up to 3 km above the surface.

For the Zavižan and Gospić transects – crossing high mountain peaks (1100 to 1500 m), the RCP 4.5 & 8.5 baseline conditions (Figs. 29 and 30) show a fast and thin boundary layer flow (horizontal velocities above 30 m/s near the surface and 0.5 km of height). As for the Trieste and Senj transects, the bora jets are also strongly decelerated with climate adjustments up to –2.5 m/s and –5 m/s for RCP 4.5 & 8.5 scenarios, respectively, but up to only 1.5 km above the surface. Furthermore, for both the Zavižan and the Gospić transects, horizontal wind speeds between 1.5 km and 3 km height are accelerated up to 2.5 m/s, mostly in the RCP 4.5 climate projections.

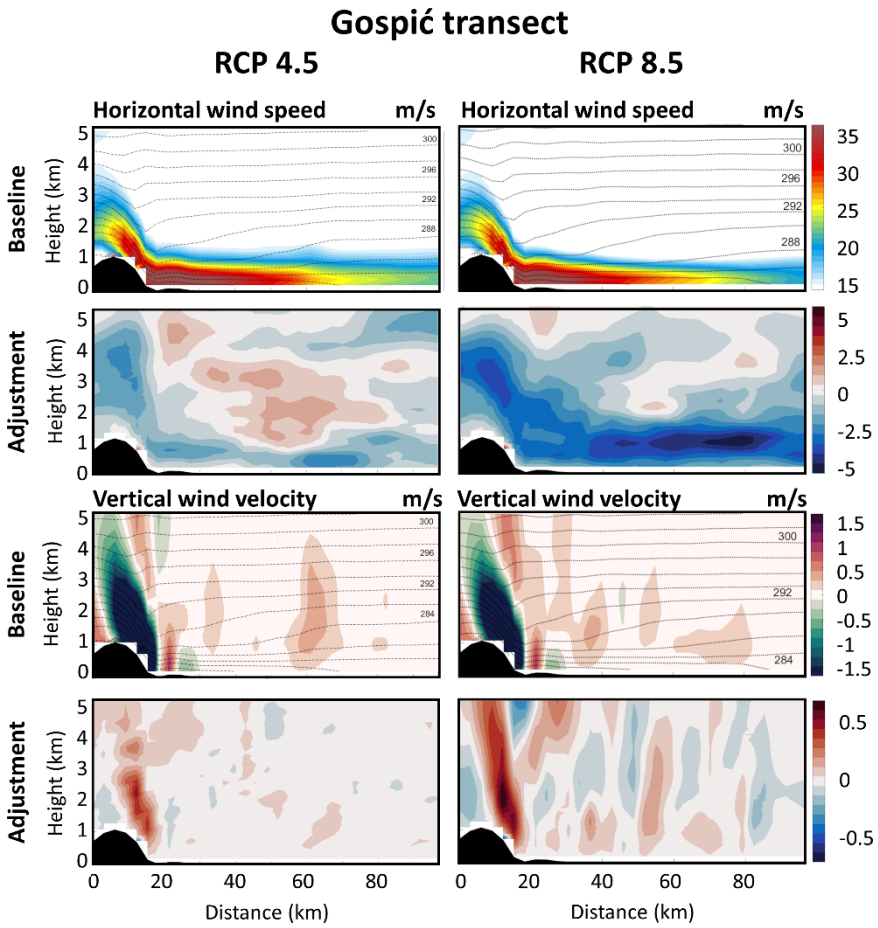

Figure 30. Same as Figure 27 but for the Gospić cross–shore transect.

To summarise, the PGW climate projections for the 2070–2100 period (under RCP 4.5 & 8.5 scenarios) of the ensemble of extreme bora events reveal that, despite a strong decrease in intensity of both the horizontal wind speeds as previously found in Belušić Vozila et al. (2019) and the atmospheric waves along the lee of the Velebit mountain range (Fig. 27), the main bora features – including jet and gap dynamics (Figs. 25 and 26) – are expected to remain similar to the known bora dynamics as described in details by Grisogono and Belušić (2009), even though far less energetic.

4.2 Air–sea interactions

Over the northern Adriatic Sea where the densest water in the Mediterranean Sea are formed, the bora jets not only drive the westward offshore circulation leading to coastal downwelling along the Italian coastline (Kourafalou, 1999), but also generate intense air–sea interactions increasing the net upward sea surface heat fluxes and thus inducing negative buoyancy fluxes associated with sea surface cooling (e.g. Zore–Armanda & Gačić, 1987; Beg Paklar et al. 2001; Raicich et al. 2013; Janeković et al. 2014; Ličer et al. 2016; Vilibić et al.

2016, 2018). To better understand the impact of climate change on sea surface cooling during extreme bora events projected for the 2070–2100 period, the total heat flux (positive downward and negative for heat loss) — including long–wave and short–wave radiations as well as sensible and latent heat flux — and the sea surface temperature (SST) anomaly (negative for sea surface cooling) are presented for RCP 4.5 & 8.5 scenarios as: (1) minimum (Fig. 31) baseline conditions (i.e. median over the ensemble of minimum values for each event) and climate adjustments (i.e. median of the difference between scenario and evaluation minimum conditions), and (2) probability distribution functions (PDFs) for the ensemble of hourly results (Fig. 32) at 12 locations (Fig. 6a, points P1 to P12) where the most intense sea surface cooling is occurring.

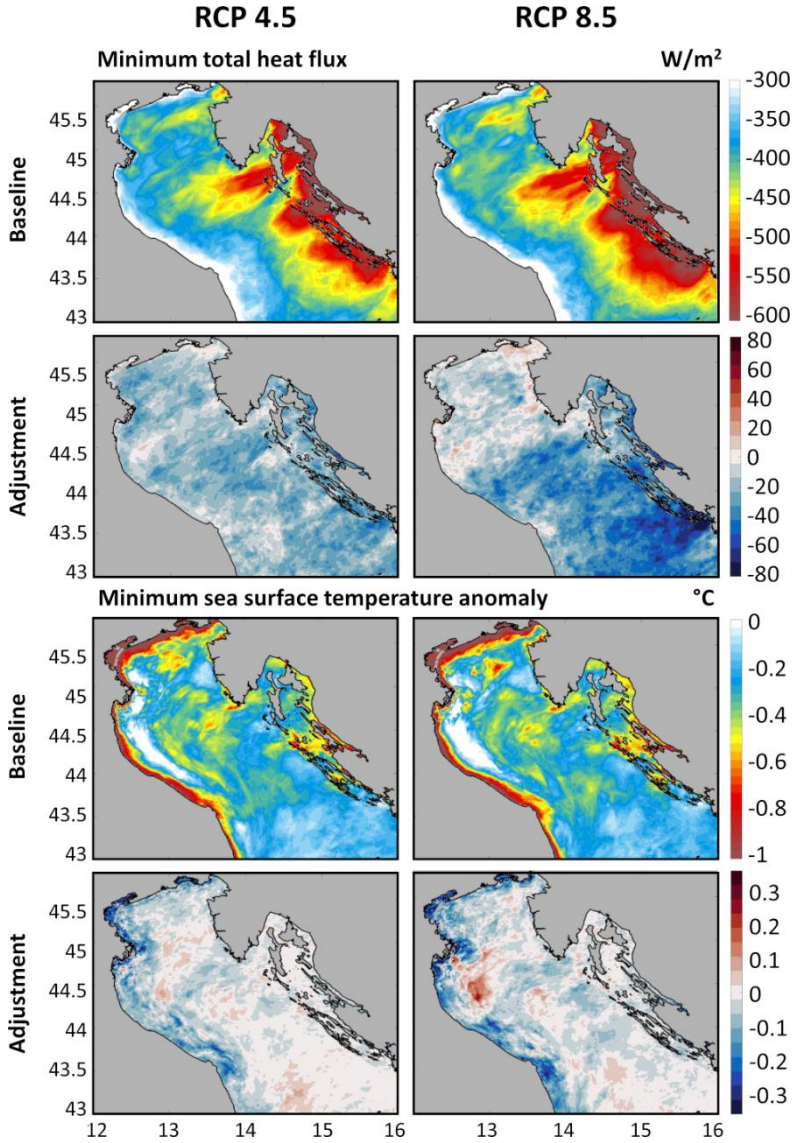

Figure 31. Baseline RCP 4.5 & 8.5 conditions (median of the scenario results) and climate adjustment (median of difference between scenario and evaluation results) for the minimum

of both the total heat flux and the sea surface temperature anomaly during each of the 22 selected events.

Spatially, the known bora air–sea interactions can still clearly be seen in the RCP 4.5 & 8.5 baseline conditions derived from the AdriSC WRF 3 km and ROMS 1 km simulations (Fig. 31). The largest total heat losses (i.e. the most negative total heat fluxes) are still found along the bora jets – in particular following the Trieste, Senj, Zavižan and Gospić transects with median values above 550 W/m^2. The largest sea surface cooling areas (i.e. negative SST anomalies) are found (1) along the Italian coastline where the sea is quite shallow, thus prone to intense cooling, and strongly influenced by rivers (more than 1 °C for both scenarios), (2) within the Kvarner Bay coastal area (above 0.5 °C and 0.6 °C for RCP 4.5 & 8.5 scenarios, respectively) and (3) within the open northern Adriatic shallow shelf (above 0.6 °C and 0.7 °C for RCP 4.5 & 8.5 scenarios, respectively). Additionally, for both future climate projections, the total heat losses increase along the bora jets — climate adjustments of the total heat flux reaching –40 W/m^2 and –60 W/m^2 for RCP 4.5 & 8.5 scenarios respectively — except along the Trieste transect where the climate adjustments reach 10 W/m^2 for the RCP 8.5 scenario. Surprisingly, this spatial analysis of the climate adjustments during extreme bora events, showing an increase in total heat losses, might look in contradiction with the substantial decrease in intensity of the bora winds forecasted in future climates (Fig. 26). These results are thus further analysed in this study. Additionally, concerning the sea surface cooling (Fig. 31), the impact of climate change seems inconclusive for both RCP 4.5 & 8.5 projections, with SST climate adjustments varying between –0.2 °C and 0.2 °C, over the entire domain.

In line with the spatial analysis, PDFs of hourly total heat fluxes and SST anomalies at locations P1 to P12 (Fig. 32) confirm that, under both RCP 4.5 & 8.5 scenarios, the total heat losses are likely to increase. Further, the distributions of the future sea surface cooling are overall likely to be similar to the evaluation mode. In more detail, the sea surface cooling is clearly likely to decrease at points P1, P2 and P4 and to increase at points P6, P7 and P12, while for the other points the impact of climate change is most likely to vary from event to event. The change in SST anomaly PDFs between RCP 4.5 & 8.5 scenario and evaluation modes, as may be notably noticed at points P1 and P4, identify the ocean regions where hourly SST changes are not only driven by the bora–driven cooling, but also by other bora–driven ocean processes acting on hourly timescale such as the fluctuations of the thermohaline front normally present in the northern Adriatic (Jeffries and Lee, 2007; Kokkini et al. 2017) and the local upwelling and downwelling due to horizontal shear in regions with strong bora–driven

currents — e.g. along the Senj jet (Kuzmić et al. 2007). The PDF analysis (Fig. 32) thus confirms the findings of the spatial analysis (Fig. 31) and raised two important questions: (1) how well the sea surface cooling is correlated to the heat losses, and (2) how these heat losses can increase under climate change while the intensity of the wind decreases?

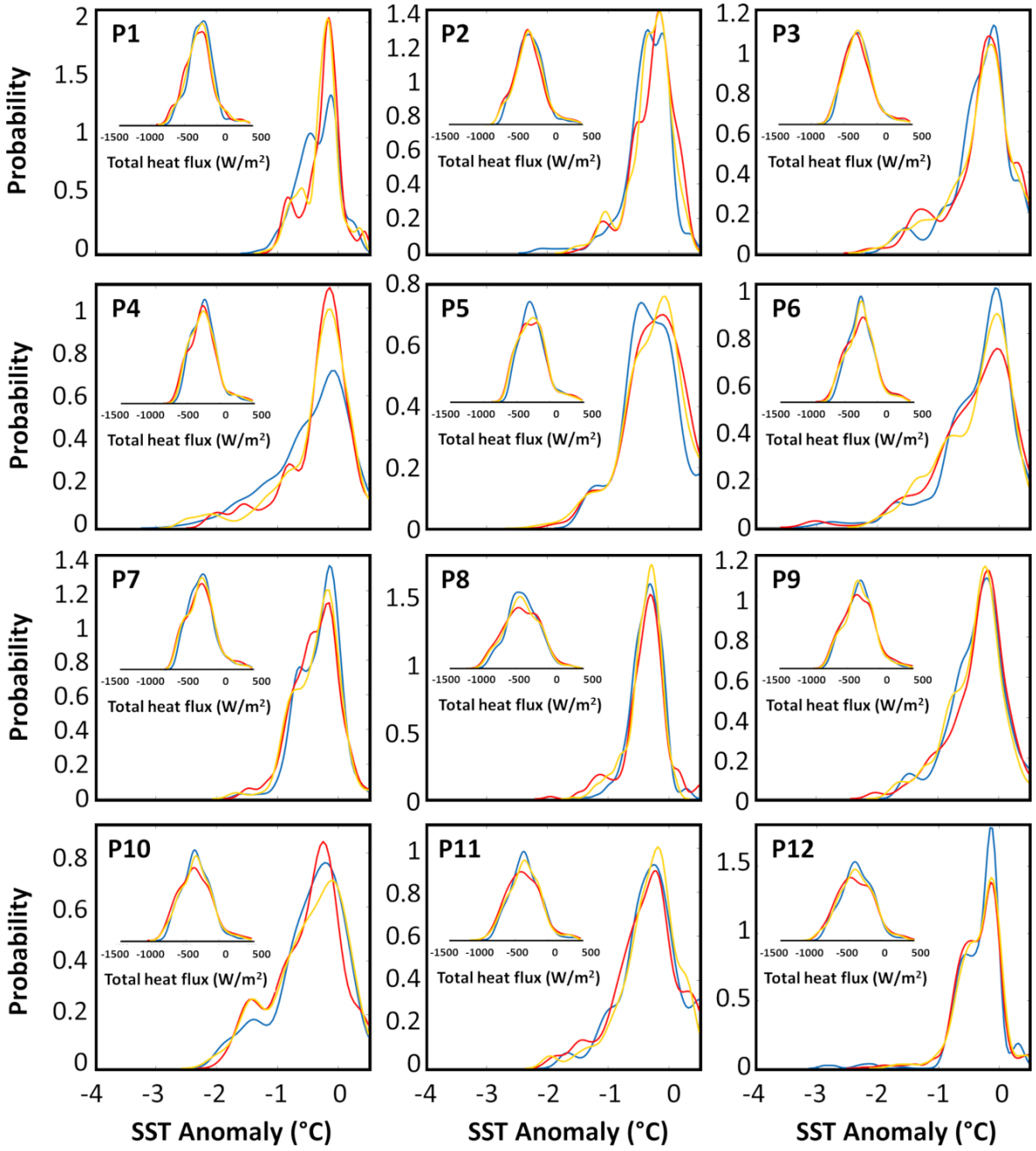

Figure 32. Probability density functions of the hourly evaluation (in blue), RCP 4.5 (in orange) and RCP 8.5 (in red) total heat fluxes and the sea surface temperature (SST) anomalies for the ensemble of the 22 selected event results at locations P1 to P12.

To answer the first question, the total heat flux is first decomposed into radiation (including long– and short– waves), latent heat flux and sensible heat flux. As the impact of radiation on

sea surface cooling is known to be negligible during extreme bora events, only the RCP 4.5 & 8.5 baseline conditions and climate adjustments of the sensible and latent heat fluxes are analysed hereafter (Fig. 33).

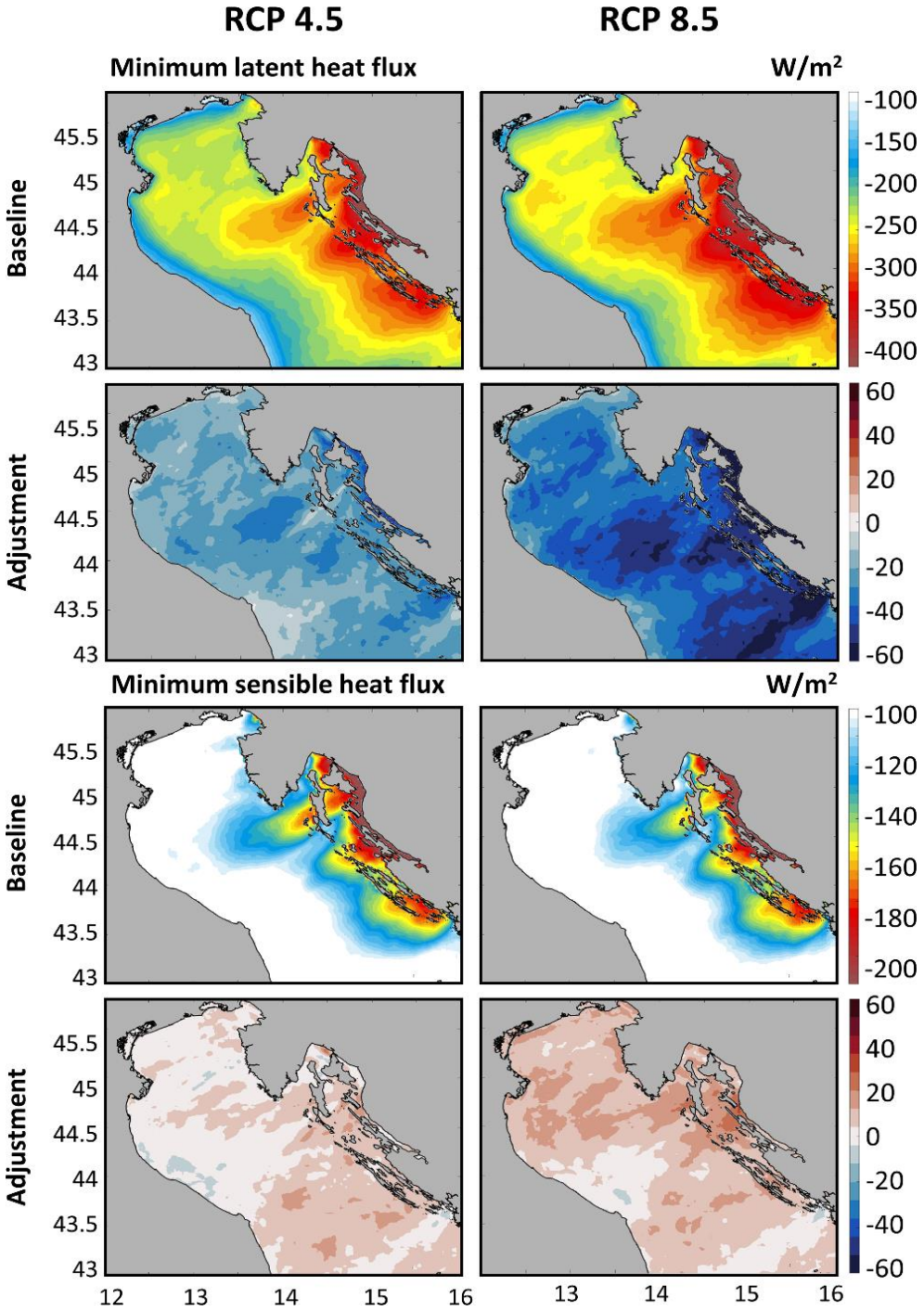

Figure 33. Baseline RCP 4.5 & 8.5 conditions (median of the scenario results) and climate adjustment (median of difference between scenario and evaluation results) for the minimum of both the latent heat flux and the sensible heat flux during each of the 22 selected events.

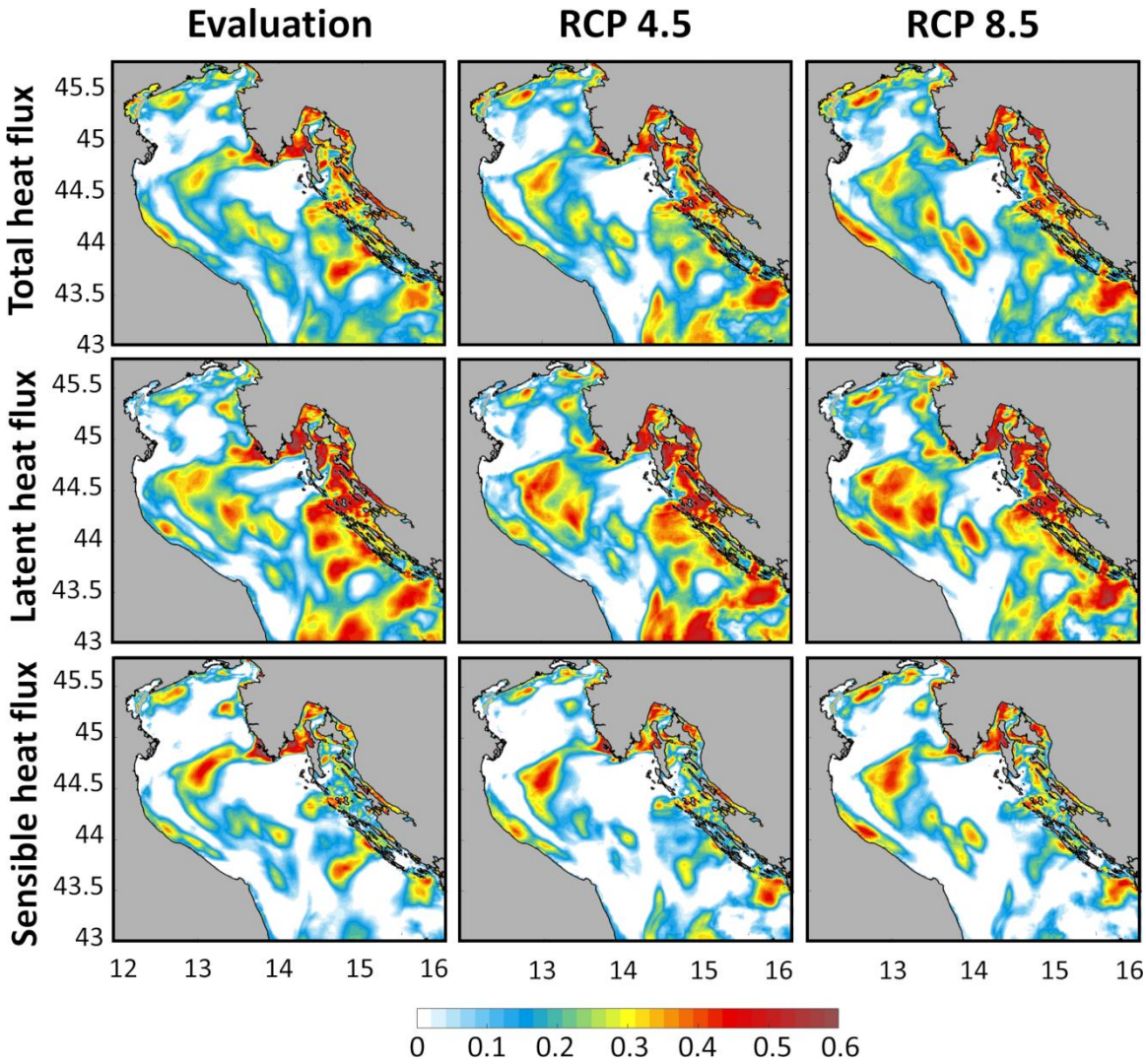

Figure 34. Spatial variations of the Pearson's correlation coefficients calculated between the hourly sea surface temperature and the hourly total, sensible and latent heat fluxes for the evaluation, RCP 4.5 & 8.5 results of the 22 selected extreme bora events. The areas where the correlation is insignificant (following the null hypothesis of the t–test) are represented in white.

The RCP 4.5 & 8.5 baseline conditions reveal that latent heat losses (with respective values reaching up to 350 W/m^2 and 400 W/m^2 respectively) are twice as strong as sensible heat losses (reaching up to 200 W/m^2) along the main bora jets. Furthermore, and even more interestingly, the RCP 4.5 & 8.5 climate adjustments show a homogeneous increase of the latent heat losses reaching up to 35 W/m^2 and 60 W/m^2 respectively, and a nearly homogeneous decrease of the sensible heat losses reaching –15 W/m^2 and –20 W/m^2 respectively (as expected with the decrease of the bora wind speeds). Additionally, the spatial correlations of the SST anomalies with the total, sensible and latent heat fluxes in both evaluation and climate projection (for RCP 4.5 & 8.5 scenarios) modes are presented in Figure 34. To be noted, the white areas representing insignificant correlations are located where the bora–driven ocean dynamics is

expected to be the strongest: (1) in the vicinity of the Po river delta, where the freshened coastal waters of different temperature are advected off the coast through a cyclonic gyre (Zore–Armanda and Gačić, 1987; Beg Paklar et al. 2001; Kuzmić et al. 2007), (2) along the western Adriatic coast influenced by the Po river waters, where the western coastal current of waters with lower salinity and different temperature is normally intensified and becomes laminar during bora events (Vilibić et al. 2009), and (3) along the Senj transect where the Kvarner Bay waters are transported towards the northern Adriatic shelf and generate a thermohaline front that may fluctuate (Kokkini et al. 2017). However, the analysis clearly shows that the highest correlations over the entire northern Adriatic domain are found for the latent heat fluxes and tend to slightly increase in the middle of the shelf under RCP 4.5 & 8.5 scenarios. Consequently, the increase in latent heat losses under climate change projections is driving the sea surface cooling during extreme bora events, and therefore may influence the dense water formation and the thermohaline circulation in the area. A thorough analysis of the latent heat flux is thus performed further in this study.

To answer the second question and understand the increase in latent heat losses despite the decrease of the bora wind speeds under climate projections, a full diagnosis of the different physical quantities (i.e. relative humidity and air–sea saturation specific humidity) used to derive these fluxes is performed for the RCP 8.5 scenario only (Fig. 35). Along the bora jets in the northern Adriatic Sea, the baseline relative humidity (between 85 and 90 %) is expected to decrease under RCP 8.5 climate projections as it is associated with nearly homogeneous negative climate adjustments reaching –3 % (except along the Trieste transect where values are positive and reach up to 2 %). The increase of the saturation specific humidity (SAT) – associated with positive climate adjustments due to the projected increase in temperatures – is consequently lower in the air (1.5 g/kg), as compensated by the decrease in relative humidity, than over the sea (2.5 g/kg on average). As a final result, the air–sea SAT differences driving the latent heat losses is much lower (below –4.5 g/kg) for the RCP 8.5 scenario than for the evaluation conditions (–3.5 g/kg on average). Under the RCP 4.5 & 8.5 climate changes used in this study, the decrease of relative humidity during extreme bora events is thus key to the increase in latent heat losses driving the future sea surface cooling in the northern Adriatic Sea, which is likely to be as strong as in the evaluation mode, despite the projected sharp decrease in wind speeds.

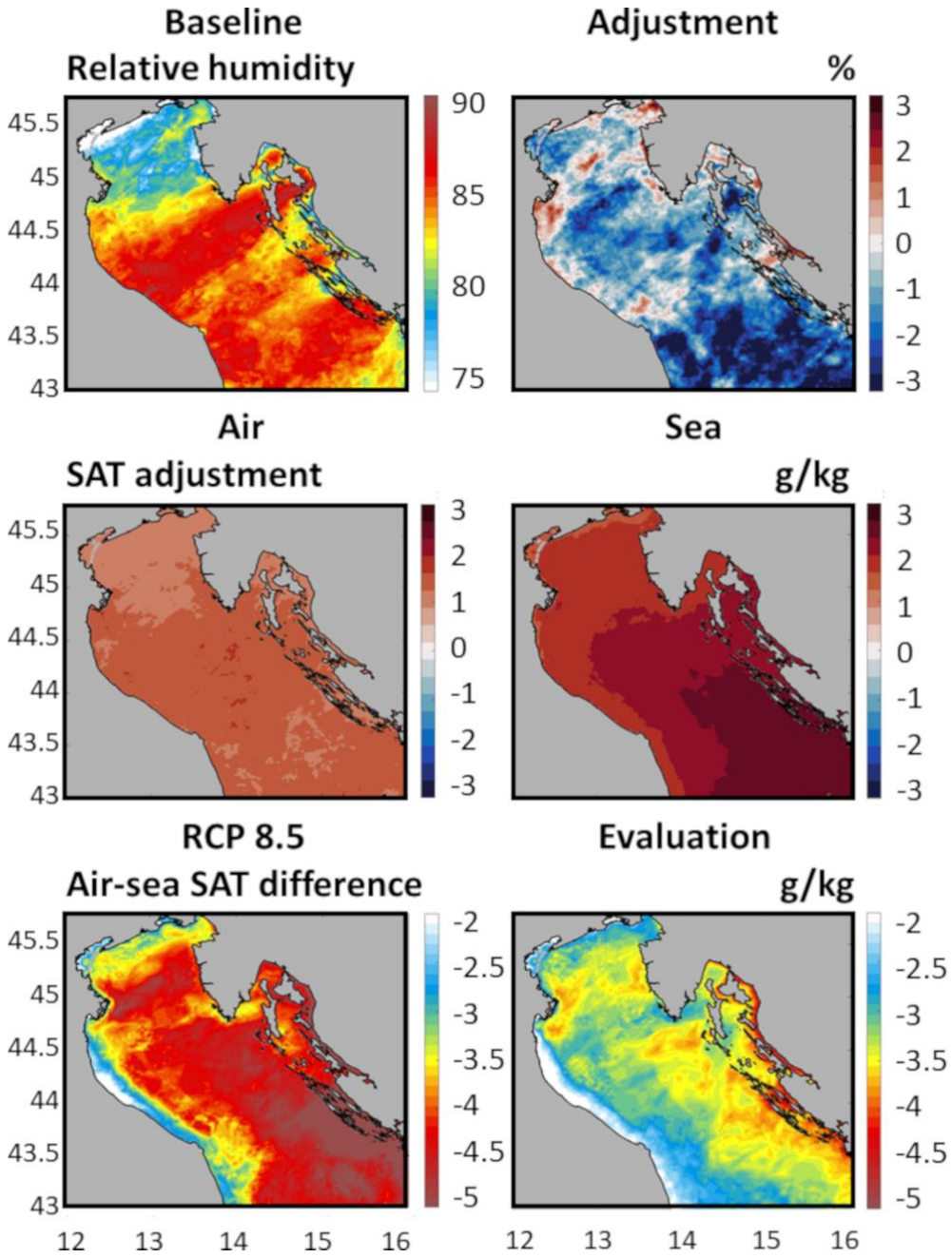

Figure 35. RCP 8.5 baseline and climate adjustment conditions of the relative humidity at 2 m (top panels), RCP 8.5 climate adjustment conditions of 2 m air and sea surface saturation specific humidity (SAT) (middle panels) and median, over the ensemble of 22 selected events, of the air–sea saturation specific humidity (SAT) difference for both RCP 8.5 and evaluation modes (bottom panels).

Lastly, in order to better understand the interconnections between latent heat losses and sea surface cooling, the joint probability distributions of latent heat fluxes and SST anomalies, in evaluation and scenario (RCP 4.5 & 8.5) modes, are analysed for points P1 to P12 (Figs. 36 and 37).

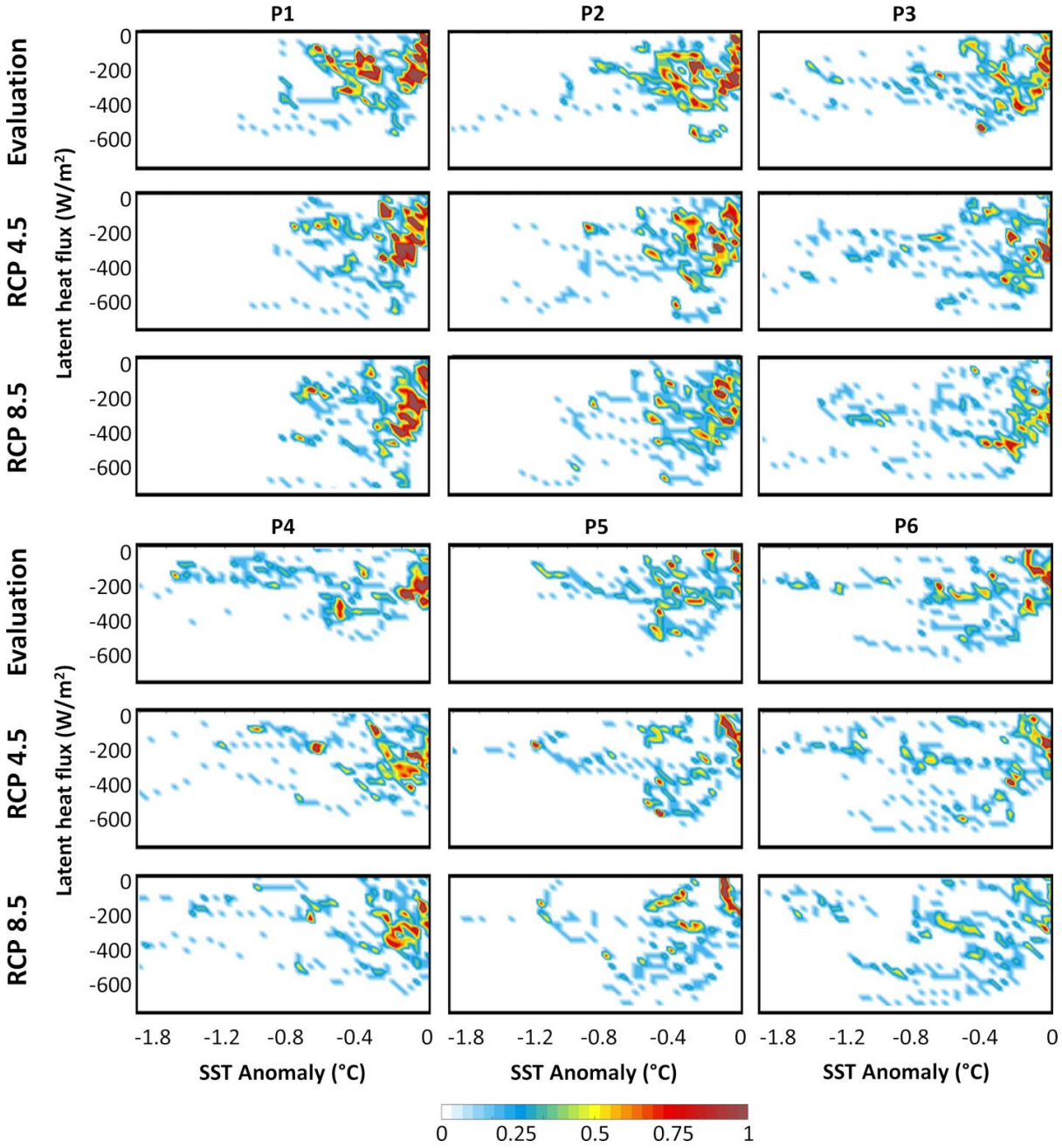

Figure 36. Joint probability distributions (in percent) derived at points P1 to P6 from the hourly surface latent heat fluxes (between –800 W/m^2 and 0 W/m^2) and the SST anomalies (between –2 °C and 0 °C) defined for the ensemble of 22 events in both evaluation and scenario (RCP 4.5 and RCP 8.5) modes.

Overall, as expected due to the somewhat weak correlation between the two physical quantities (Fig. 34), no linear behaviour can be derived from the joint probabilities even though, along the northern Croatian coastline for points P7 to P12 (Fig. 37) — at locations where the Pearson's correlation coefficient reaches up to 0.6 — the linear relationship seems stronger than in the middle of the northern Adriatic shelf (P1 to P6). However, for all the points compared to the evaluation results, the higher probabilities are shifted towards the largest latent

heat losses by about 40 W/m^2 in RCP 4.5 scenario and 70 W/m^2 in RCP 8.5 scenario for mild sea surface cooling (below 1 °C), and by 100 W/m^2 in RCP 4.5 scenario and 150 W/m^2 in RCP 8.5 scenario for intense sea surface cooling (above 1.75 °C). In other words, the latent heat losses needed to cool by 1 °C the sea surface water under global warming are increased by 40 to 100 W/m^2 for RCP 4.5 scenario and by 70 to 150 W/m^2 for RCP 8.5 scenario compared to the evaluation mode.

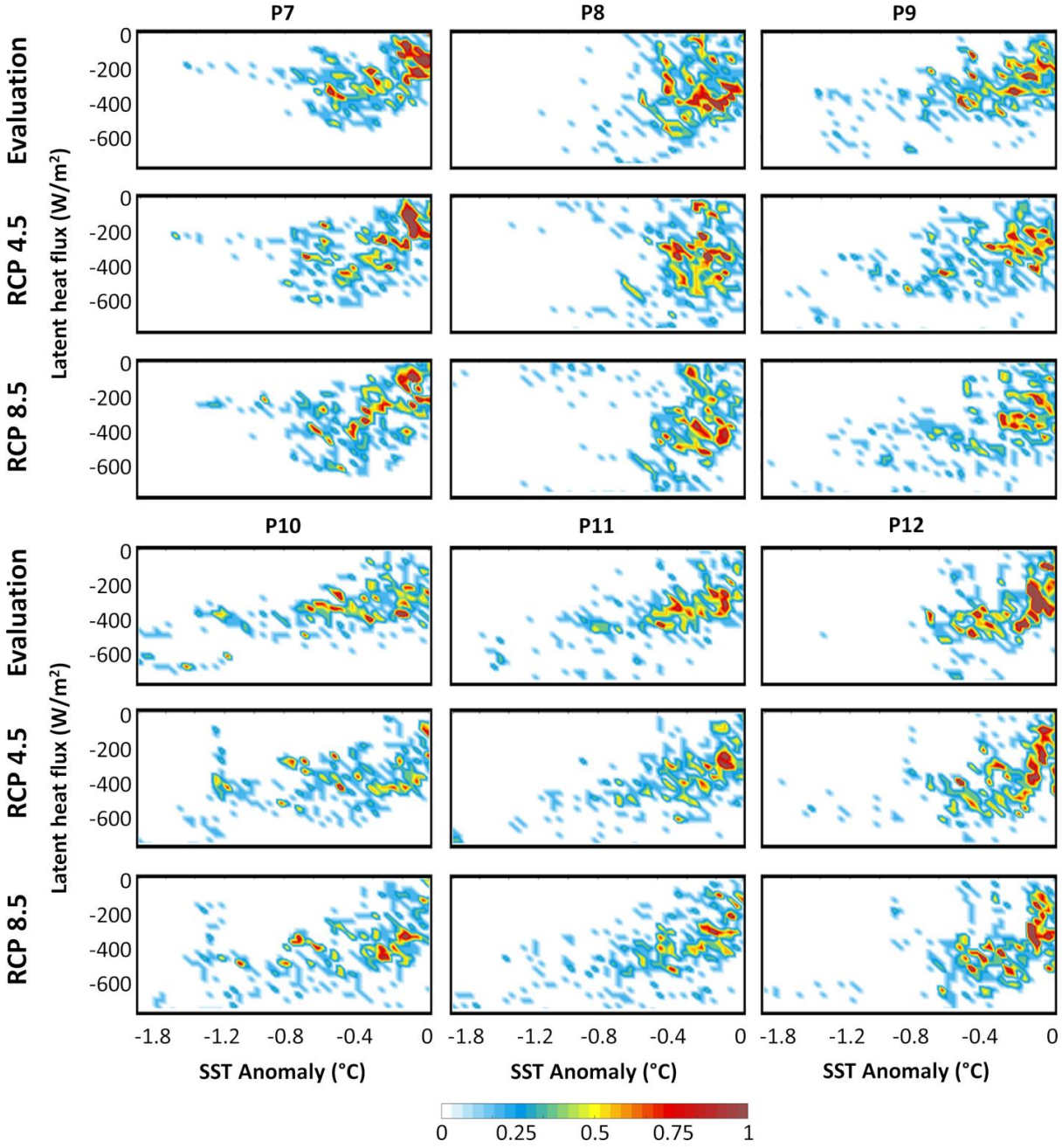

Figure 37. Joint probability distributions (in percent) derived at points P7 to P12 from the hourly surface latent heat fluxes (between –800 W/m^2 and 0 W/m^2) and the SST anomalies (between –2 °C and 0 °C) defined for the ensemble of 22 events in both evaluation and scenario (RCP 4.5 & 8.5) modes.

Table 9. Probabilities (in percent) derived from the joint probability distributions at points P1 to P12 of the hourly surface latent heat fluxes and the SST anomalies defined for the ensemble of 22 events in both evaluation and scenario (RCP 4.5 & 8.5) modes.

	Probability (%) of latent heat flux below –400 W/m² and negative SST anomaly			Probability (%) of latent heat flux below –400 W/m² and SST anomaly below –1 °C			Probability (%) of negative latent heat flux and SST anomaly below –1 °C		
	Evaluation	RCP 4.5	RCP 8.5	Evaluation	RCP 4.5	RCP 8.5	Evaluation	RCP 4.5	RCP 8.5
P1	0.0	3.3	4.2	0.0	2.9	3.9	2.1	0.8	0.6
P2	1.1	4.7	5.3	1.1	3.6	3.6	3.5	5.5	4.4
P3	0.0	2.3	2.7	0.0	2.3	2.0	6.4	9.2	10.0
P4	0.0	0.0	1.2	0.0	0.0	1.2	12.0	6.2	7.1
P5	0.2	0.3	3.0	0.2	0.3	3.0	5.2	5.8	5.5
P6	0.5	4.4	4.7	0.5	3.5	3.8	7.4	11.2	9.2
P7	0.0	0.8	2.6	0.0	0.8	2.6	1.8	2.4	3.5
P8	4.4	10.5	12.7	4.1	8.5	10.3	1.1	3.5	5.9
P9	2.4	3.3	5.0	0.9	0.9	2.7	6.2	7.6	7.6
P10	3.6	4.8	8.6	0.0	1.2	3.2	11.7	13.2	13.5
P11	3.5	7.0	9.4	1.7	3.5	5.2	7.1	6.2	8.0
P12	3.9	6.5	11.1	3.9	5.9	9.5	0.2	2.6	2.7

To better quantify this shift in intensity of the latent heat losses needed to cool the sea surface, three probabilities are extracted from the joint probability distributions at locations P1 to P12 and presented in Table 9: probability in percent of latent heat flux below –400 W/m2 for negative SST anomalies $\Pr(Q_E \le -400\ \mathrm{W/m^2} \cap \Delta SST \le 0\ ^\circ C)$, probability in percent of negative latent heat flux for SST anomaly below –1 °C $\Pr(Q_E \le 0\ \mathrm{W/m^2} \cap \Delta SST \le -1\ ^\circ\mathrm{C})$, as well as probability in percent of latent heat flux below –400 W/m^2 for SST anomaly below –1 °C $\Pr(Q_E \le -400\ \mathrm{W/m^2} \cap \Delta SST \le -1\ ^\circ\mathrm{C})$. In average and for all the locations, the probabilities in scenario modes are always higher than in evaluation mode:

1) by 2.4 % and 4.2 % for RCP 4.5 & 8.5 scenarios, respectively, concerning $\Pr(Q_E \le -400\ \mathrm{W/m^2} \cap \Delta SST \le 0\ ^\circ\mathrm{C})$ — all sea surface cooling are thus more likely

to require latent heat losses above 400 W/m^2 in scenario modes (particularly in RCP 8.5 scenario) than in evaluation mode;

2) by 0.8 % and 1.1 % for RCP 4.5 & 8.5 scenarios, respectively, concerning $\Pr(Q_E \le 0\ \mathrm{W/m^2} \cap \Delta SST \le -1\ \mathrm{°C})$ — sea surface cooling above 1 °C is thus, in average, slightly more likely to occur in scenario modes than in evaluation mode;

3) and by 1.8 % and 3.2 % for RCP 4.5 & 8.5 scenarios, respectively, concerning $\Pr(Q_E \le -400\ \mathrm{W/m^2} \cap \Delta SST \le -1\ \mathrm{°C})$ — following the two previous results, sea surface cooling above 1 °C associated with latent heat losses above 400 W/m^2 are thus more likely to happen in scenario modes (particularly in RCP 8.5 scenario) than in evaluation mode.

Additionally, for all three probabilities, the minimum and maximum changes between scenario and evaluation modes are found for locations P4 and P8 at the end and the beginning of the Senj transect respectively, with values of:

1) 0 % at P4, 6.1 % at P8 for RCP 4.5 scenario and 1.2 % at P4, 8.3 % at P8 for RCP 8.5 scenario concerning $\Pr(Q_E \le -400\ \mathrm{W/m^2} \cap \Delta SST \le 0\ \mathrm{°C})$ — along the Senj transect, sea surface cooling is thus likely to require much higher latent heat losses (above 400 W/m^2) at the beginning of the transect, within the Kvarner Bay, in scenario modes than in evaluation modes but nearly no latent heat losses above 400 W/m^2 at the end of the transect for all the modes (0 % in both evaluation and RCP 4.5 modes and 1.2 % in RCP 8.5 mode);

2) –5.8 % at P4, 2.4 % at P8 for RCP 4.5 and –4.9 % at P4, 4.8 % at P8 for RCP 8.5 scenario concerning $\Pr(Q_E \le 0\ \mathrm{W/m^2} \cap \Delta SST \le -1\ \mathrm{°C})$ — in a warmer future, sea surface cooling above 1 °C is likely to increase at the beginning of the Senj transect (by 2.4 % and 4.8 % in RCP 4.5 & 8.5 modes respectively) but largely decrease at the end of the transect (by about –5 % for both scenario modes) in the middle of the northern Adriatic shelf;

3) 0 % at P4, 4.4 % at P8 for RCP 4.5 scenario and 1.2 % at P4, 6.2 % at P8 for RCP 8.5 scenario concerning $\Pr(Q_E \le -400\ \mathrm{W/m^2} \cap \Delta SST \le -1\ \mathrm{°C})$ — following the two previous results, sea surface cooling above 1 °C associated with latent heat losses above 400 W/m^2 is thus likely to strongly increase at the beginning of the Senj transect (up to

6.2 % for RCP 8.5 scenario) but remain identical at the end of the transect in a warmer climate.

Finally, the highest probabilities of extreme sea surface cooling $\Pr(Q_E \leq 0 \text{ W/m}^2 \cap \Delta SST \leq -1 \text{ °C})$, are found for locations P10 in the Kvarner Bay near the Zavižan transect (11.7 % in evaluation mode, 13.2 % and 13.5 % in RCP 4.5 & 8.5 scenario modes), P4 at the end of the Senj transect (12 % in evaluation mode), P6 at the end of the Trieste transect (11.2 % in RCP 4.5 mode) and P3 in the middle of the northern Adriatic shelf near the Senj transect (10 % in RCP 8.5 mode).

In a nutshell, despite the expected sharp decrease in intensity of the severe bora wind speeds in a warmer climate under RCP 4.5 or RCP 8.5 scenarios for the 2070–2100 period, the sea surface cooling in the northern Adriatic Sea — preconditioning the formation of the densest waters in the Mediterranean Sea and mostly impacted by the latent heat losses, is expected to remain identical or even to slightly increase for values above 1 °C. This can be explained by the increase of the latent heat losses resulting from the forecasted decrease in relative humidity in the PGW climate simulations. Additionally, the maximum changes (between scenario and evaluation modes) in both sea surface cooling and latent heat losses are expected to occur along the Senj transect, where historically the strongest bora winds are blowing. Finally, the locations of the extreme sea surface cooling is likely to change in the future, except maybe in the vicinity of point P10 in the Kvarner Bay near the Zavižan transect.

4.3 Discussion

Due to the extremely high computational cost of coupled kilometre–scale models, climate studies in the Mediterranean and Adriatic Seas have been carried out with regional climate models with resolutions of the order of 10 km. However, although many important features of the general atmosphere–ocean circulation are captured with such models, they often reach their limits during extreme events in coastal areas where both the orography and the geomorphology strongly influence the intensity of the storms (Vosper et al. 2018). This is particularly true in the Adriatic Sea during severe bora events, where several studies have demonstrated that bora dynamics can only be captured with limited area atmospheric models (Grisogono & Belušić, 2009; Trošić & Trošić, 2010; Prtenjak et al. 2010; Kuzmić et al. 2015; Josipović et al. 2018; Belušić Vozila et al. 2019; Denamiel et al. 2020a, 2021a).

Despite the known numerical cost and slowness of the AdriSC climate model with resolutions of 3–km in the atmosphere and 1–km in the ocean (Denamiel et al. 2019, 2020a), the conjoint use of an ensemble approach and the PGW methodology for short–term simulations (i.e. 3 days) allowed to both accurately represent historical bora storms and, in this analysis, better understand the impact of global warming on extreme bora dynamics and sea surface cooling in the northern Adriatic region (under both RCP 4.5 & 8.5 scenarios). This has been achieved using far less computational resources than a traditional regional climate model running 30 years in evaluation mode, 50 years in historical mode and 100 years in scenario mode. Such a method has nevertheless some intrinsic limitations, including:

1) the use of a relatively small ensemble of 22 storms which may not be fully representative of neither the historical Adriatic extreme bora events nor their future projections for the 2070–2100 period;
2) the shortness of the simulations carried over a three–day period which increases the influence of the imposed initial conditions on the analysed results compared to long–term simulations;
3) the use of the same ensemble of storms in evaluation and climate projection modes which prevents the forecast of the extreme event frequency under climate change;
4) the derivation of the PGW forcing from a single model instead of an ensemble of regional climate models which would have provided more robust climate change projections.

Notwithstanding these limitations, the statistical approach presented in this study – consisting in running ensembles of short simulations for extreme events, has provided some new insights in terms of the future of the bora dynamics and sea surface cooling for the 2070–2100 period under both RCP 4.5 & 8.5 scenarios:

1) the sharp decrease in intensity of the bora horizontal wind speeds between the surface and 2 km of height — also seen, to some extent, by the EURO–CORDEX ensemble (Belušić Vozila et al. 2019) — is mostly due to the strong decrease in intensity of the atmospheric waves along the lee of the Velebit mountain range which is generally not well captured by regional climate models (Josipović et al. 2018);
2) the other known bora features — only seen with kilometre–scale atmospheric models as driven by the complex orography and consisting in jet and gap dynamics — are expected to remain preserved in a warmer climate;

3) due to the decrease in relative humidity, the latent heat losses, driving the sea surface cooling in the northern Adriatic Sea, are expected to increase under global warming despite the decrease of the bora wind speeds;
4) the extreme sea surface cooling (above 1 °C) is expected, on the one hand, to require larger latent heat losses (due to the presence of warmer waters) and, on the other hand, to remain identical or even to slightly increase in the future, even though not necessarily at the same locations than in evaluation mode.

Following the results presented here, for a far–future warmer climate, due to an increase in latent heat losses driven mostly by a decrease in relative humidity, the rates of dense water formation might remain untouched which might have important consequences concerning the thermohaline circulation in the Adriatic–Ionian region. In particular it may influence the future of the decadal oscillations of the Adriatic thermohaline and biogeochemical properties driven by the BiOS (Gačić et al. 2010; Civitarese et al. 2010; Vilibić et al. 2012; Batistić et al. 2014), the ventilation of deep Adriatic and Eastern Mediterranean waters (Powley et al. 2016; de Ruggiero et al. 2018), the open–ocean convection in the southern Adriatic (Gačić et al. 2002) and the anoxic conditions in the northern and middle Adriatic as well as the associated impact to the benthic organisms (Krasakopoulou et al. 2005; Blasnig et al. 2013). The findings of this study may also be relevant to other dense water formation areas (e.g. Ivanov et al. 2004) and other coastal areas substantially influenced by the orography, for which climate change assessment requires kilometre–scale simulations.

As the increase of both air–sea flux intensity and sea surface cooling during future extreme bora events is not aligned with previous findings from Soto–Navarro et al. (2020) who analysed the results of the Med–CORDEX ensemble, more research is needed to confirm the validity of these findings. In particular, the analysis of the 31–year long AdriSC climate simulations for both evaluation and RCP 8.5 simulations will provide, in a near future, more robust results concerning the sea surface cooling but also the dense water formation in the northern Adriatic shelf. In addition, the sensitivity of the AdriSC model RCP 4.5 & 8.5 projections to the PGW forcing should also be investigated in order to increase the confidence in the results presented in this thesis.

5. TRENDS, VARIABILITY AND EXTREMES

In this chapter, the atmosphere-ocean trends, variability, and extremes are quantified for both the AdriSC evaluation simulation during the 1987–2017 period and the AdriSC far–future extreme warming simulation during the 2070–2100 period. The potential implications of the far–future changes projected with the AdriSC model for the atmosphere–ocean dynamics, as well as the limitations of the AdriSC results and their similarities and differences with the EURO– and Med–CORDEX RCMs, are also thoroughly discussed. The presented work is published in the studies by Tojčić et al. (2023, 2024).

5.1 Historical conditions (1987–2017)

The AdriSC climate model is used to analyse, for the very first time, the atmosphere–ocean trends and variability of the Adriatic present climate during the 1987–2017 period which remained, till this day, partially unknown, particularly in the ocean. The obtained trends and variability over different time and spatial scales in the Adriatic region are derived from the 3–km WRF daily results in the atmosphere and the 1–km ROMS daily results in the ocean extracted from the AdriSC evaluation run during the 1987–2017 period.

5.1.1 Regional analysis

5.1.1.1 Atmosphere

In the atmosphere, decadal trends and variability over the Adriatic basin (Fig. 38; left panels) reflect the impact of the significant warming that took place during the 1987−2017 period. Consequently, trends of temperature at 2 m are all significant but interestingly higher over the sea (up to 0.5−0.6 ºC per decade) than over the land (only up to 0.4 ºC per decade). Rain decadal trends are generally positive over the sea and along the coast, with (1) the highest values of up to 0.5 mm/day per decade over central and southern Adriatic and southern parts of the eastern coast, and (2) negative values over the Dinarides and Velebit mountains as well as further inland on the Croatian side, where values drop to –0.4 mm/day per decade. However, for the relative humidity at 2 m and the wind speed at 10 m, large areas of the trend plots appear in light–grey, meaning that trends are insignificant (i.e. significance lower than 95 %). Nevertheless, significant trends show some interesting features.

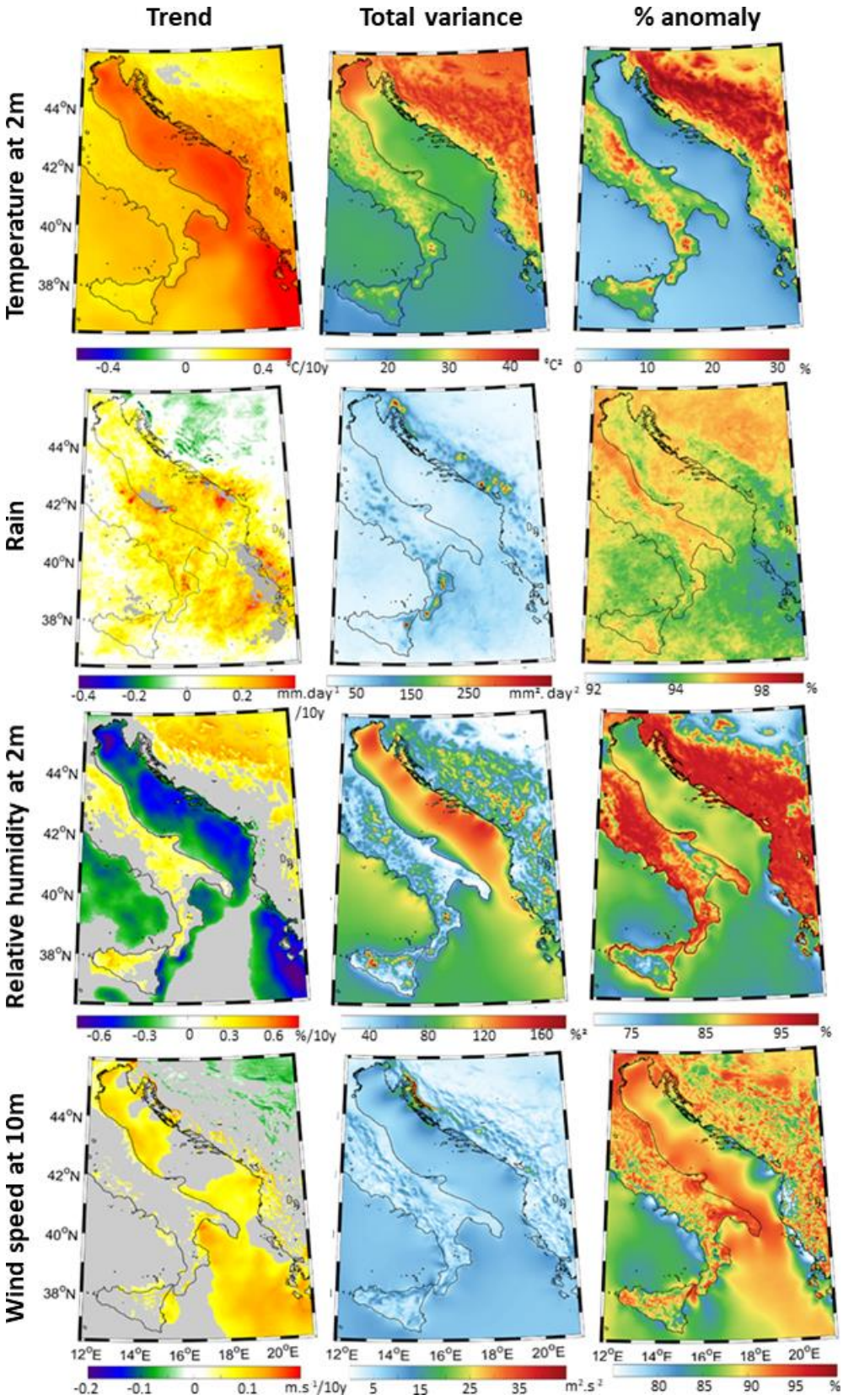

Figure 38. Trends (left panels), total variances (middle panels) and percentage anomalies (right panels) for temperature at 2m, rain, relative humidity at 2m and wind speed at 10m over the entire Adriatic region. Insignificant trends (significance < 0.95) are shown in light–grey in the left panels.

For the relative humidity at 2 m, they are strongly negative over the sea — about –0.3 % per decade along the Italian coast and the Po River plume and down to –0.6 % per decade in the northern Adriatic and areas in the middle and southern Adriatic far from the shore — but strongly positive over the land, varying between 0.3 % and 0.5 % per decade. For the wind speed at 10 m, significant trends are positive over the sea and along the Adriatic coasts (between 0.1 m/s and 0.2 m/s per decade), but negative further inland in the Pannonian plain (about –0.1 m/s per decade). Concerning the total variance (Fig. 38; middle panels), the variability of the temperature at 2 m is (1) the highest over the land particularly in the Dinarides (up to 40 $^{o}C^{2}$), (2) a bit lower over the Apennines, the northern Adriatic shallow sea and the Po River plume (up to 30 $^{o}C^{2}$), and (3) the lowest over the rest of the Adriatic Sea (around 25 $^{o}C^{2}$). In contrast, rain total variance is nearly homogeneous over the whole studied region (below 100 mm^{2}/day^{2}), except for several areas of higher values (above 400 mm^{2}/day^{2}) in the south of Italy, around Rijeka and the Kotor Bay where strong precipitations are known to occur (Marjanović et al. 2017). Further, the total variance of relative humidity at 2 m is (1) the strongest over the Adriatic Sea (above 140 $\%^{2}$), except along the Italian coast, which agrees with the trend patterns, and (2) the lowest over the land (below 80 $\%^{2}$), except on higher altitude mountain peaks in the Apennines and the Dinarides (above 120 $\%^{2}$). Finally, the highest total variances in wind speed at 10 m are found along the Velebit mountains (up to 40 m^{2}/s^{2}) where the strongest Bora wind events occur (Alpers et al. 2007), but is generally below 10 m^{2}/s^{2} in the rest of the Adriatic basin. Percentage anomalies (i.e. percentage of non–seasonal variance in the total variance) are high for all variables except for temperature. Namely, over 92 % of rain variability and 95 % of wind speed variability are not related to seasonality over the entire domain, except for the coastal areas where these percentages vary between 75 % and 80 %. For the relative humidity at 2 m, a strong contrast in percentage anomaly exists between land and sea: non–seasonal variability is over 95 % in most land areas but below 80 % over the sea. Temperatures are, as expected, seasonally driven with low percentages of barely 10 % over the sea, and an average of 25 % over the land, with lower values along the coast and higher values in the mountainous areas.

5.1.1.2 Ocean

Decadal trends and variability in the ocean are analysed horizontally at different depths (surface, 100 m, and bottom) in Figs. 39 to 41 and vertically along the Otranto and Alongshore transects in Figs. 42 and 43.

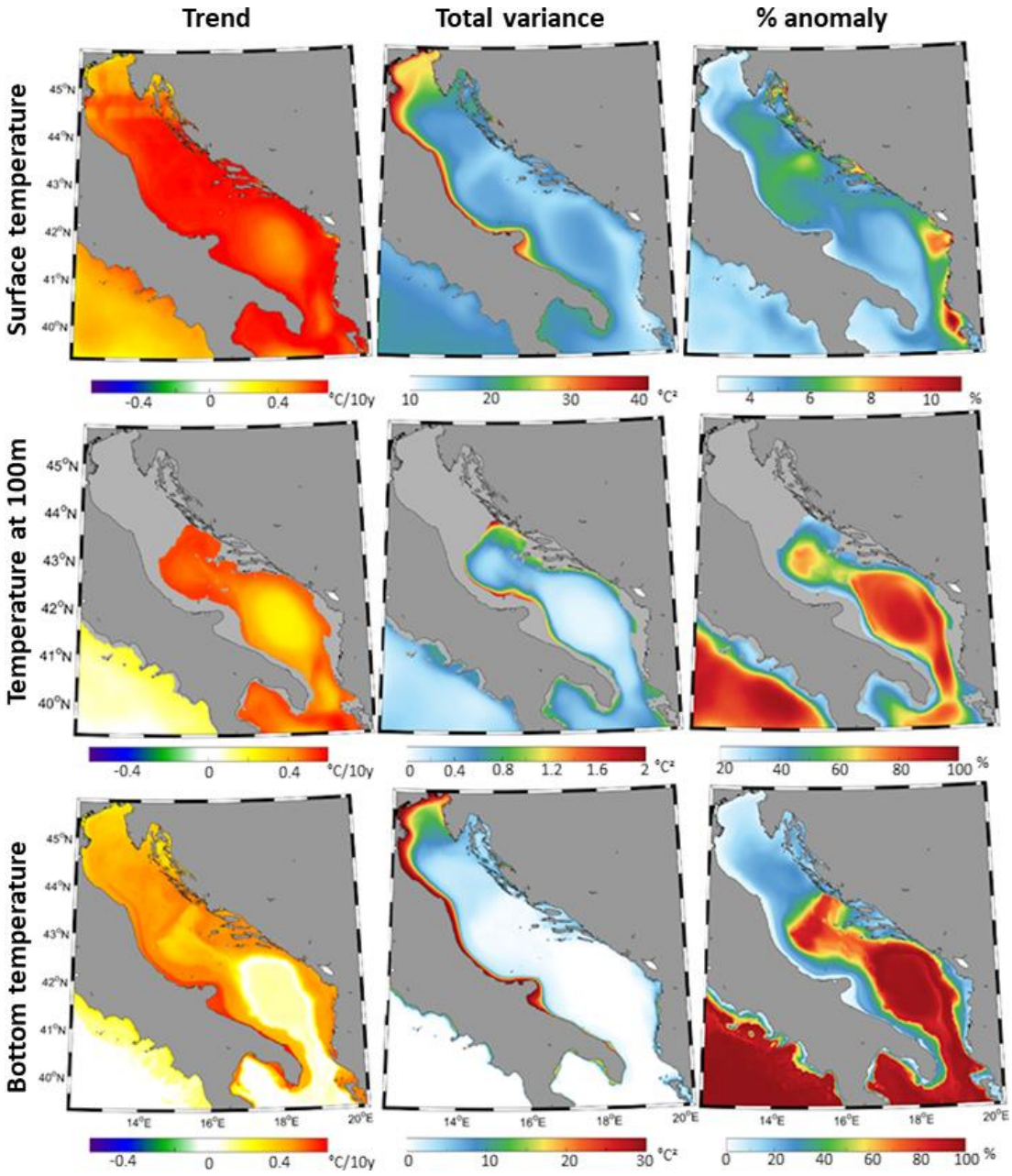

Figure 39. Trends (left panels), total variances (middle panels) and percentage anomalies (right panels) for temperature at the surface, 100m depth and the bottom of the sea. Insignificant trends (significance < 0.95) are shown in light–grey in the left panels.

It should be noted that, in the ocean, trends are nearly always significant for temperature and salinity, but not for current speed which can display areas of insignificant trends (highlighted in light–grey in the plots).

Following the results presented in the atmosphere, sea surface temperature trends (Fig. 39; left panels) vary between 0.4 ºC and 0.6 ºC per decade, with lowest trends over the deepest Southern Adriatic Pit, where quasi–permanent cyclonic gyre is generating an upwelling (Gačić et al. 2002), and northernmost areas of the Adriatic Sea strongly affected by freshwater load

(Franco & Michelato 1992). At 100 m depth, which is roughly the maximum depth of the seasonal thermocline (Buljan & Zore–Armanda 1976; Artegiani et al. 1997), and the bottom, the differences between temperature trends above the deepest part of the Adriatic Sea and the rest of the domain are even more pronounced: 0.2 ºC per decade vs. 0.4 ºC per decade at 100 m depth and 0.1 ºC per decade vs. up to 0.4 ºC per decade at the bottom. Convincingly, the heating of the Adriatic deep waters is much lower than of the surface waters, like observed for the Mediterranean (Vargas–Yanez et al. 2017), while the transport of deep cold waters is lowering the heating in upper layers within cyclonic gyres. Further, the temperature total variance (Fig. 39; middle panels) is (1) the highest (over 35 $ºC^2$) along the Po River plume but generally low over the entire Adriatic Sea (below 15 $ºC^2$) in surface, (2) mostly close to 0.1 $ºC^2$ in the deepest areas of the Adriatic Sea at 100 m depth and the bottom, and (3) reaching up to 30 $ºC^2$ along the Po River plume and 10 $ºC^2$ in the shallowest part of the northern Adriatic at the bottom. Additionally, the temperature percentage anomalies (Fig. 39; right panels) mirror the patterns of the total variance at all depths. The variability is, as expected, mostly seasonally driven at depths above the seasonal thermocline, with non–seasonal values: (1) up to 10 % at the surface, and particularly low in the shallow northern Adriatic and Po River plume, while (2) reaching 80–100 % in the deep Adriatic region, being the largest at the very bottom of the Southern Adriatic Pit. This implies that the Po River plume is keeping the heat near the surface due to a strong haline–driven stratification and therefore exhibiting much stronger seasonal variability in temperature than the rest of the Adriatic. By contrast, the deepest parts of the Adriatic, which are known to be collectors of dense waters generated on the northern Adriatic shelf during wintertime (Vilibić & Supić 2005), are exhibiting the lowest seasonal changes, in particular, in the 1200–m deep Southern Adriatic Pit where these waters are advected every few years to the very bottom (Querin et al. 2016).

Salinity trends and variability are, however, quite different (Fig. 40). On the surface, salinity percentage anomalies are the lowest along the shore, below 65 %, while increasing to 90 % and above when moving away from the shore and going above the deeper sea areas. Indeed, low seasonal surface salinity variability is resembling stable structures, not affected by seasonality in coastal dynamics, like the inflow of surface waters from the Ionian Sea and their recirculation within the cyclonic gyre in the Southern Adriatic Pit. Non–seasonal salinity variability is much higher at 100 m and on the bottom, with values between 80 and 100 % in most areas, with the highest values at the deepest parts.

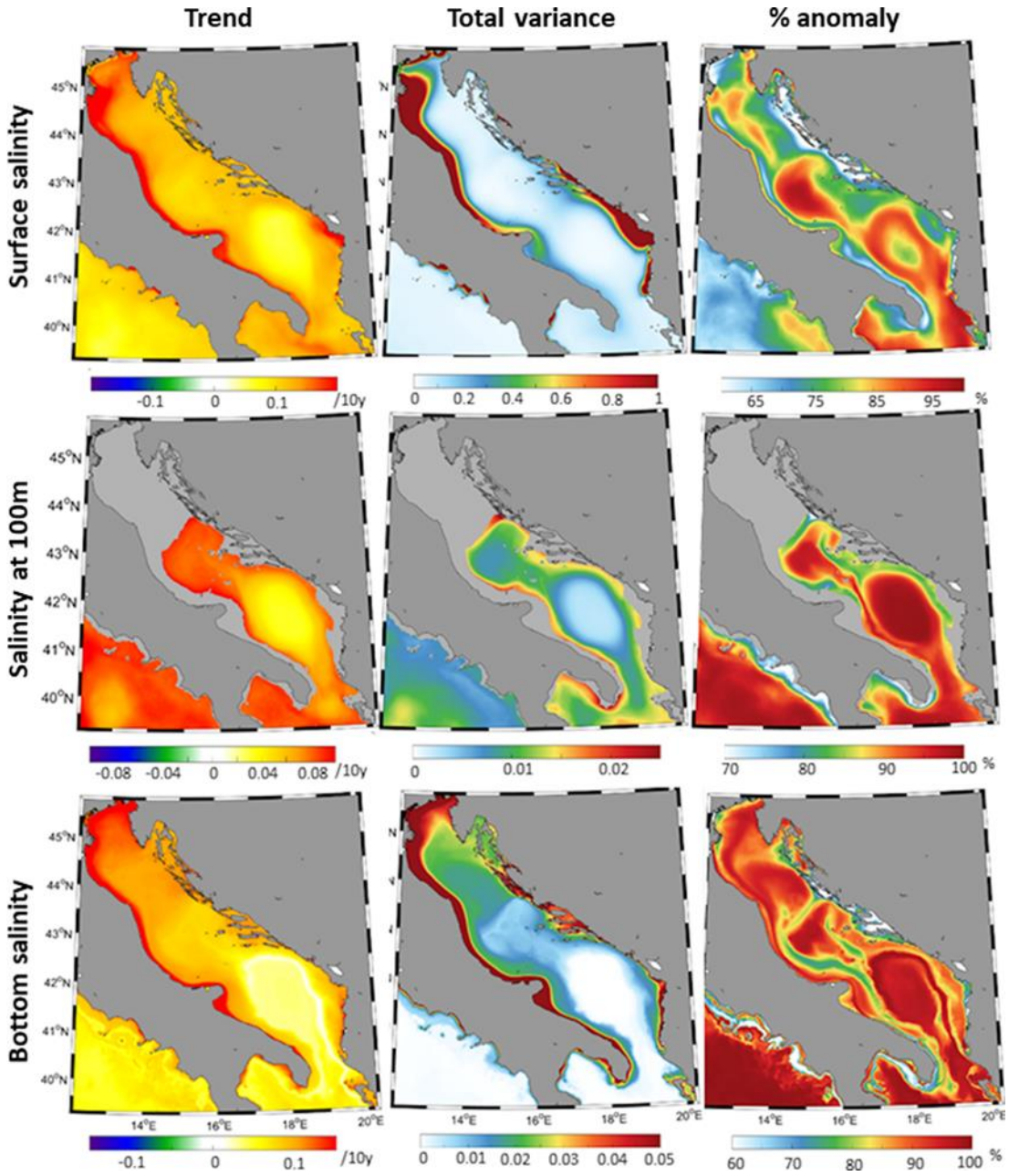

Figure 40. Trends (left panels), total variances (middle panels) and percentage anomalies (right panels) for salinity at the surface, 100m depth and the bottom of the sea. Insignificant trends (significance < 0.95) are shown in light–grey in the left panels.

Interestingly, seasonal variations have banners of lower percentage anomaly following the bathymetry, indicating the areas where near–bottom structures are seasonally modulated (e.g. depth of the Po River plume or outflow from Kvarner Bay). Further, surface salinity trends are positive, with the lowest values, down to 0.03 per decade, in the deep Adriatic area, and the highest values up to 0.2 per decade, along the Po River plume. This agrees with Vilibić et al. (2013), who found positive trends along the whole Palagruža Sill transect in the middle Adriatic Sea, but much higher in the coastal regions occupied by freshened waters. Further,

positive trends in salinity are resembling reduced inflow by rivers, also in nutrients as the northern Adriatic is resembling much lower productivity in the last 10 years (Djakovac et al. 2012; Totti et al. 2019). Similar patterns are found on the bottom, with slightly higher trends in the northern Adriatic, and slightly lower ones in the deepest parts, down to 0.015 per decade.

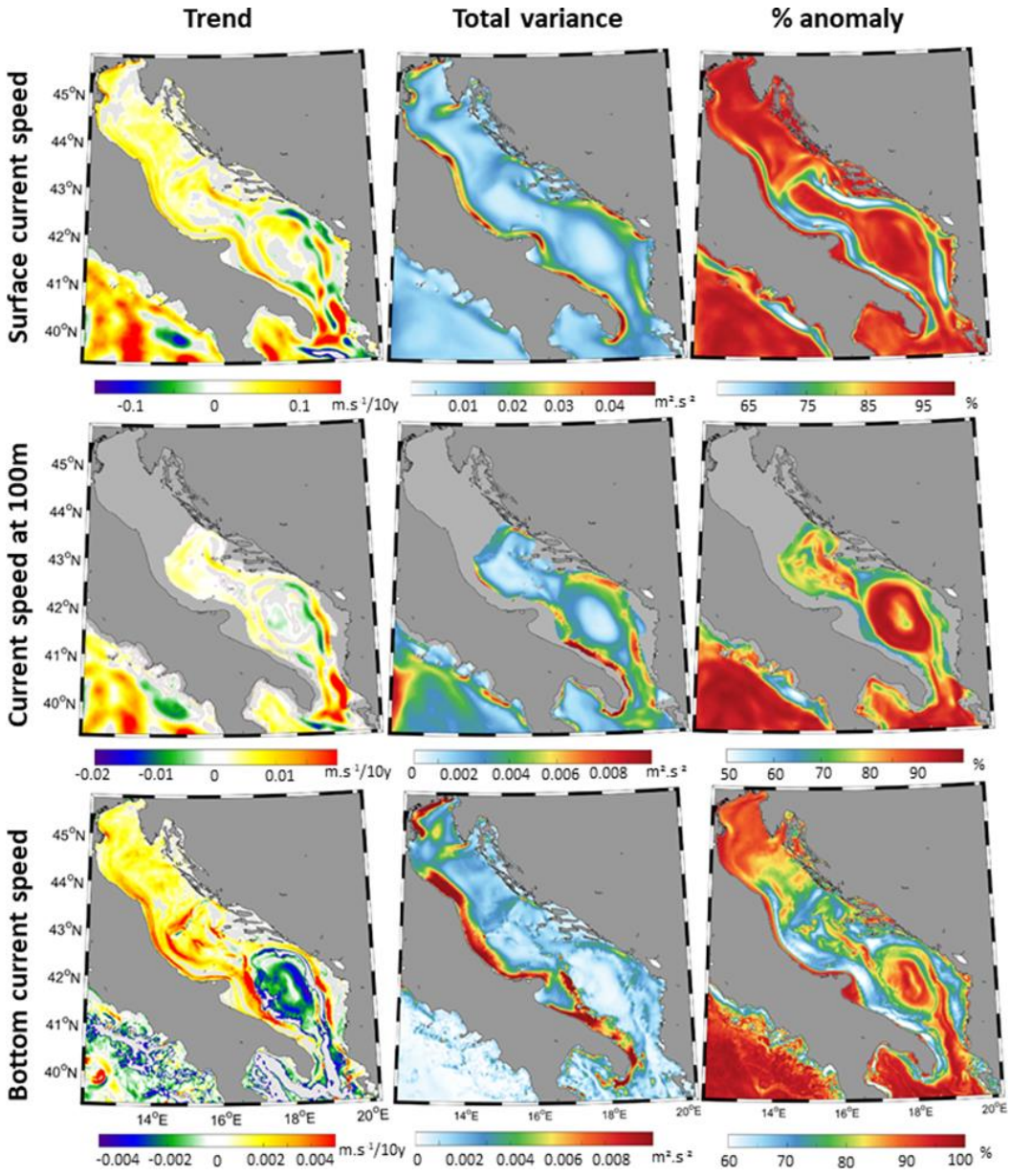

Figure 41. Trends (left panels), total variances (middle panels) and percentage anomalies (right panels) for current speed at the surface, 100m depth and the bottom of the sea. Insignificant trends (significance < 0.95) are shown in light–grey in the left panels.

At 100 m depth, trends reach up to 0.1 per decade in shallow areas but are below 0.05 per decade in the Deep Adriatic region, again presumably due to effects of upwelling from deeper layers at which salinity is lower (Lipizer et al. 2014). Total variance on the surface is, as expected, the highest along the Po River plume and in areas with freshwater flowing into the

sea, like the Albanian and eastern middle Adriatic rivers, with values up to 40. At 100 m depth and at the bottom, variance values are the lowest in deepest areas, around 0.002, and are increasing with sea depth decreasing. The highest variances on the bottom are found along the west Adriatic coast, and in the middle and southern parts of the east coast along river plumes with the highest discharges (Raicich 1996; Vilibić et al. 2016).

Current speed trends and variabilities also contrast with the temperature and salinity results (Fig. 41). First, it should be noted that areas with insignificant trends exist and are marked by light–grey colour on the plots. Second, for the middle and northern Adriatic, surface current speed is increasing with decadal trend values mostly around 0.05 m/s and up to 0.1 m/s per decade. In the southern Adriatic and Otranto Strait, there are pronounced patchy patterns in trends all over the water column, indicating that the major dynamic features there – the southern Adriatic cyclonic gyre and the water mass exchanges through the Otranto Strait – are exhibiting spatial changes in time. For example, the negative current speed trend near the eastern coast of the southern Adriatic conjoined with positive trends off the coast are indicating shrinking of the gyre and offshore displacements of the Eastern Adriatic Coastal Current (Orlić et al. 1992) in the 2000s and 2010s. Further, the negative current speed trend at the bottom of the southern Adriatic cyclonic gyre may indicate a lower advection of dense waters from the northern Adriatic, which are indeed reflected in the observed decrease in dissolved oxygen content (Vilibić et al. 2011). This is also in agreement with the mostly negative current speed trends at the bottom of the Otranto Strait, which resemble lower production of dense waters in the southern Adriatic (Li & Tanhua 2020). In contrast, the current speed is increasing in surface and intermediate layers of the strait, indicating larger advection of saline surface and Levantine Intermediate Water to the Adriatic, following recent salinization of the Levantine Basin (Kassis & Korres 2020). Total variances of current speeds on the surface are the highest (up to 0.06 m^2/s^2) along the west and southwest coasts of the Adriatic Sea, following the seasonal variability of the Western Adriatic Coastal Current (Zavatarelli et al. 2002; Burrage et al. 2009). At 100 m depth, total variances are an order of magnitude lower than on the surface, being the lowest in deep waters and higher at the perimeter of the southern Adriatic cyclonic gyre and surface coastal outflow in the Otranto Strait. At the bottom, variances are of the same order of magnitude as at 100 m depth, being again the lowest in the deep Adriatic, and higher (up to 0.012 m^2/s^2) along the west coast. Percentage anomalies at surface are over 95 % everywhere but on two stripes along the west and east coast, going from the mid Adriatic to the Otranto strait, where values stay below 65 %. These strips are indicating seasonal

pulsations of the along–Adriatic transport, where the Western Adriatic Coastal Current is widened in summer and thereafter provoking the inflow of waters from the southeast along the eastern Adriatic coast (Poulain, 2001). Similar patterns are observed at the bottom, with slightly lower percentages, varying between 75 and 95 % in the rest of the domain, and being the highest in the northernmost and deep areas of the Adriatic. At 100 m depth, percentages are high, above 90 % in deep Adriatic area, indicating the stability of the southern Adriatic cyclonic gyre, and are dropping to around 70 % when approaching shallower areas.

To better investigate the vertical trends and variabilities of sea temperature, salinity, and current speed in the Adriatic Sea, two transects are analysed: (1) the Otranto transect where all the exchanges between the Adriatic and Ionian seas take place and (2) the Alongshore transect representative of the spatial variability of the Adriatic basin.

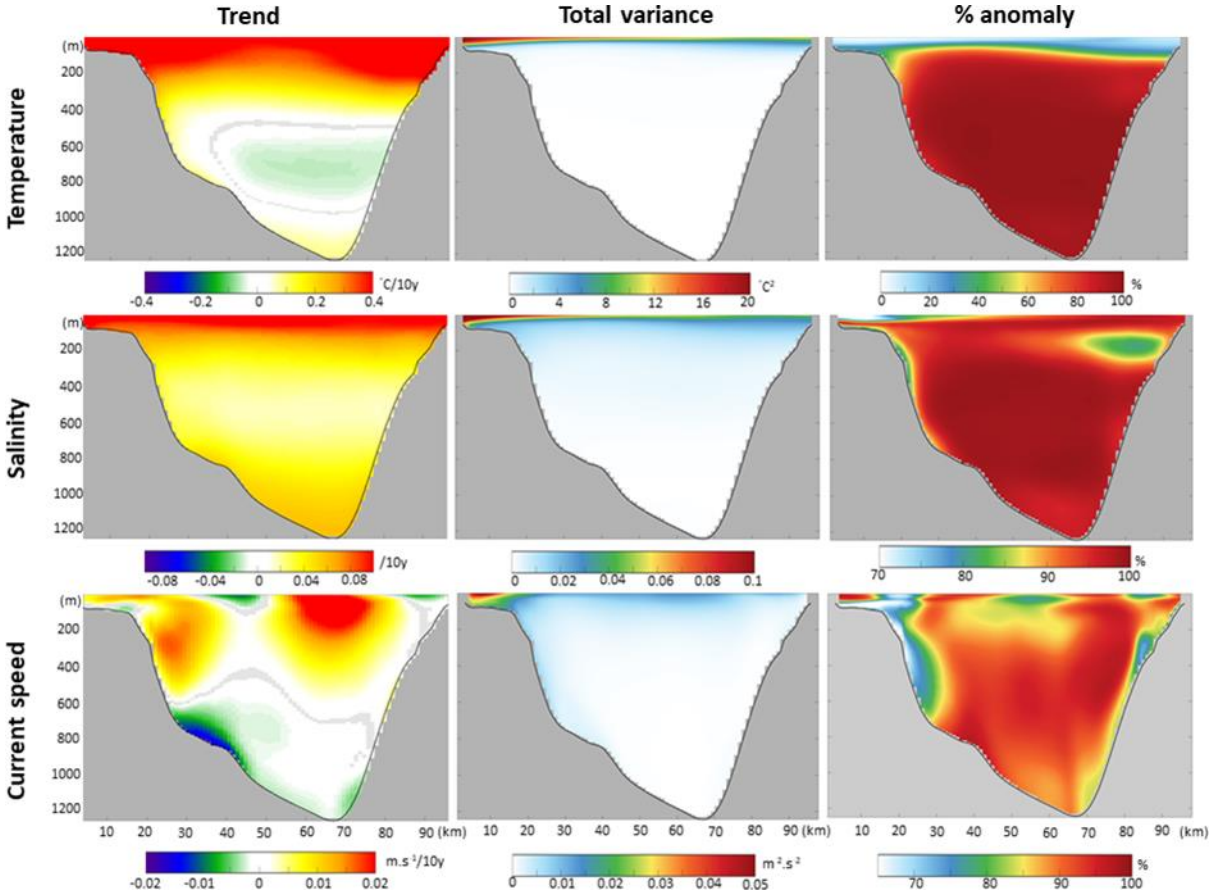

Figure 42. Trends (left panels), total variances (middle panels) and percentage anomalies (right panels) for temperature, salinity and current speed along the Otranto transect. Insignificant trends (significance < 0.95) are shown in light–grey in the left panels.

For the Otranto transect, as seen in Fig. 42, trends in temperature are generally positive, with the highest values (up to 0.4 ºC per decade) in surface, but with an elliptic area of negative trends, of up to –0.1 ºC per decade, between 500 and 900 m depth. Such a distribution of

temperature trends — large positive trends at surface, negative trends in intermediate and deeper layers and a weak positive trend at the bottom — is already documented on long–term measurements along the Palagruža Sill transect (Vilibić et al. 2013). Although the Palagruža Sill transect is much shallower than the Otranto Strait, the temperature trends highlight similar processes: (1) strong heating of the surface layer due to an increase in vertical stratification in upper layers, (2) decrease in transport in deeper layers, seen also in current speed trends, which is decreasing the transport of warmer waters from the Ionian Sea towards the southern Adriatic at the lower section of the inflow and therefore resulting in negative temperature trends, and (3) weak warming near the bottom, where the Adriatic dense waters are outflowing (Gačić et al. 1996), indicating generation of warmer waters in the Adriatic. The latter (i.e. the positive near–bottom temperature trends) are conjoined with positive salinity and strong negative current speed trends, reflecting a decrease in dense water production in the Adriatic which is known to generate more saline waters in 2000s and 2010s than in 1980s and 1990s (Mihanović et al. 2021). Total temperature variance is the highest on the surface (up to 20 $^{o}C^{2}$) and almost 0 below 200 m. Percentages of the non–seasonal variability are, as expected, below 10 % near the surface and gradually increasing up to more than 80 % below 200 m depth. Salinity trends are also overall positive, with values up to 0.1 per decade in the surface layer and down to around 0.04 per decade in the deeper areas. Variance is generally low, with the highest values (up to 0.1) on the western surface area. Percentage anomalies are over 95 % almost everywhere except in the (1) west surface area inhabited by Western Adriatic Coastal Current and near–bottom between 100 and 800 m, where the dense water is outflowing, and (2) on the eastern areas between 150 and 300 m depth, where they fall to 80 % exhibiting seasonality in the inflow of saline waters to the Adriatic (Yari et al. 2012). Current speed trends are positive on the western and eastern parts of the transect up to 600 m depth, indicating a strengthening of water mass exchange in surface and intermediate layers, and negative below that depth and in the surface layer between areas of positive trends. Indeed, these trends are indicating a shallowing of the Adriatic–Ionian thermohaline circulation, as projected for the future climate (Somot et al. 2006). Variance of current speed is generally low, with higher values up to 0.05 m^2/s^2 only in the westernmost surface layer. Percentage anomalies mostly stay above 80 %, falling below that value on the western boundary of the transect, up to 700 m depth.

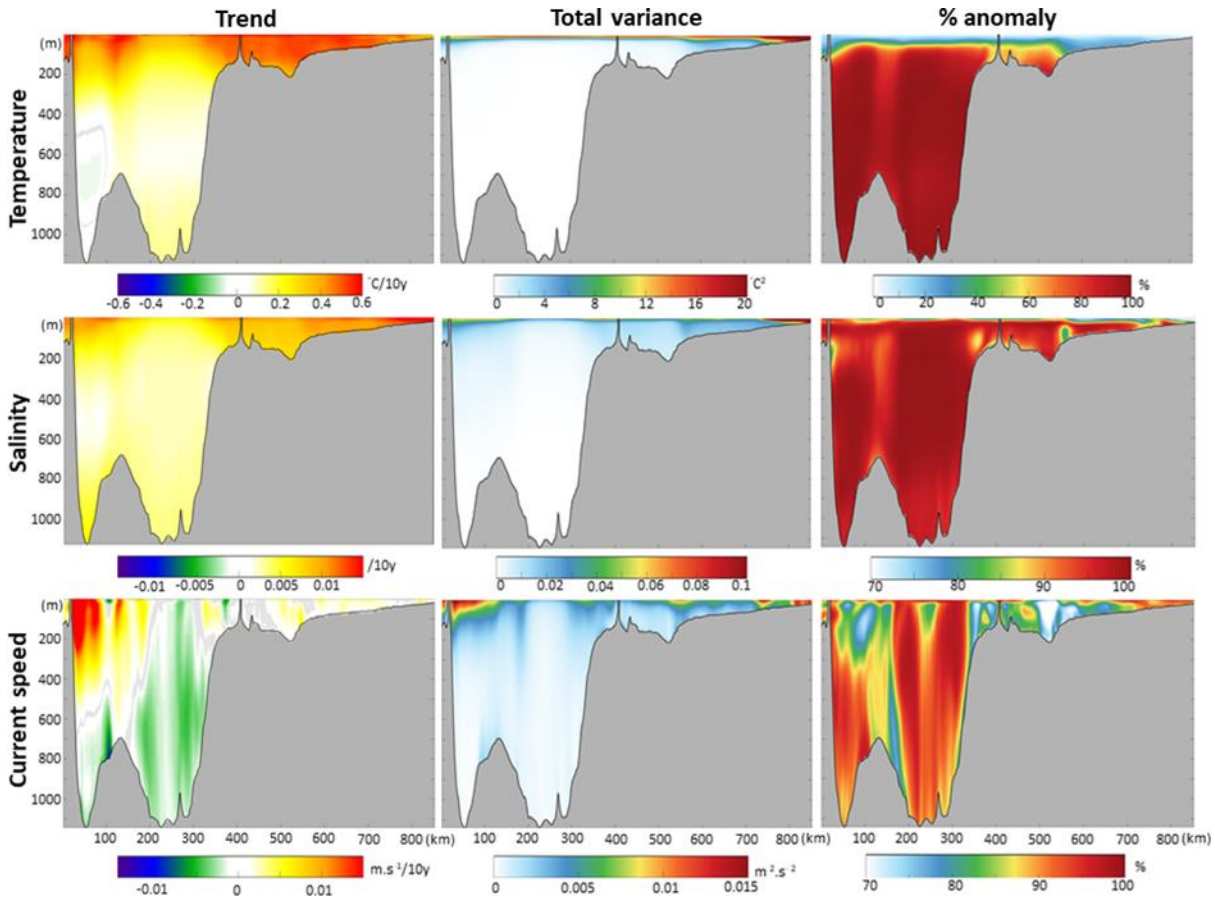

Figure 43. Trends (left panels), variances (middle panels) and percentage anomalies (right panels) for temperature, salinity, and current speed along the Alongshore transect. Insignificant trends (significance < 0.95) are shown in light–grey in the left panels.

The Alongshore transect results (Fig. 43) display the differences between trends and variances in the shallow and deep–sea areas of the Adriatic Sea. Both temperature and salinity trends are much stronger in the shallow northern Adriatic than in the deep Adriatic, going up to 0.6 ºC per decade for temperature, and 0.02 per decade for salinity in shallow areas. The temperature trends correspond to the one recorded in measurements along the northern Adriatic well surveyed transect (Vilibić et al. 2019), while salinity trends are somehow overestimated by the AdriSC model. However, the latter is following the documented overestimation in salinity of the AdriSC model off the Po River delta (Pranić et al. 2021), while the trend estimates are also found sensitive to sampling (i.e. different trends have been found at two stations off the Po River) indicating the change in plume dynamics in the last 30 years (Vilibić et al. 2019). Negative temperature trends are found in the first 150 km of the transect between 600 and 900 m depth, in agreement with the Otranto transect estimates. However, the temperature trends are positive (around 0.1 °C per decade) in the deepest part of the southern Adriatic, indicating a warming of the Adriatic deep waters coming from the northern Adriatic

shelf (Cardin et al. 2020). Salinity trends at these depths are also positive (around 0.005 per decade), stretching also at the bottom of the Otranto Strait and south of it, thus indicating an increase in salinity of the deep Adriatic outflow observed recently. In the upper layers, up to 200 m, salinity trends are much larger, around 0.01 per decade (except at the centre of the southern Adriatic cyclonic gyre). Still, these salinity trends are about two times lower than observed in the 1952–2010 period over the Palagruža Sill transect (Vilibić et al. 2013) probably due to the different sampling periods of the analyses. Current speed trends are mostly insignificant or slightly positive in the shallow northern Adriatic area, and strongly positive in the first 200 km of the transect, up to 500 m depth, indicating stronger water mass exchange in the Otranto Strait. In the same area but in greater depths, trends are negative, that resemble a weakening of the deep Adriatic water outflow. The weakening of the outflow is the result of weakening of the deep–water production in the southern Adriatic cyclonic gyre, as between 200 and 350 km (i.e. in the middle of the gyre) the trends are negative over the entire water column. Variances are mostly low for both temperature and salinity, with expectedly higher values in the northernmost, and shallowest, part of the transect, and near the surface. Current speed variances are also mostly low (up to 0.005 m^2/s^2) with values up to 0.015 m^2/s^2 in the northern Adriatic area and in the first 150 km of the transect, near the Otranto strait. Further, percentage anomalies caused by non–seasonal variations reach almost 100 % for the entire transect for the salinity and for the temperature below 100 to 200 m depth (i.e. below the seasonal thermocline; Buljan & Zore–Armanda 1976; Artegiani et al. 1997a). The temperature percentage anomalies are gradually dropping below 20 % when getting closer to the surface. Interestingly, percentage values are less homogeneous for current speed than for salinity and temperature but are also high, above 70 % almost everywhere. The first exception is the centre of the Jabuka Pit (between 480 and 550 km of the transect), where more than 30 % of the variance is ascribed by the seasonal changes, resembling the seasonal non–stationarity of the middle Adriatic cyclonic gyre that is driven by both seasonal changes in the Western Adriatic Coastal Current and the near–bottom dense water outflow (Martin et al. 2009). Another exception is the southern edge of the Palagruža Sill, where the exchange of water masses is also seasonally modulated (Martin et al. 2009; Vilibić et al. 2015). The last exception is the Otranto Strait, in particular, its upper 300 m, where exchanges of surface and intermediate waters are taking place and are known to have strong seasonal pulsations (Mihanović et al. 2021).

5.1.2 Subdomain analysis

The results of the subdomain monthly analyses are presented as tables with columns representing each month and rows representing mean, maximum and minimum daily data grouped by subdomains (Fig. 44 for the atmospheric variables for four subdomains and Figs. 45–47 for the oceanic variables for five subdomains). The minimum for rain is not presented as, within the Adriatic basin, monthly rain minimums are always equal to zero. Further, insignificant trends are represented with black diagonal lines in the monthly square where they occur.

5.1.2.1 Atmosphere

In the atmosphere, monthly trends of temperature at 2 m, rain, wind speed at 10 m and relative humidity at 2 m are mostly insignificant (Fig. 44), implying that the atmospheric variability is much higher than the estimated trends over this 31–year period in the Adriatic basin. However, temperature trends in June are significant and high, with values up to 0.6 ºC per decade for the mean over all the subdomains and for the maximum only over the Dinarides subdomain. For the Adriatic Sea subdomain, months of March, April and July also have high and significant trends for both mean and maximum temperatures, from 0.3 ºC per decade in spring up to 0.6 ºC per decade in summer. High and significant trends for mean temperature are also found in April for the Apennines and Velebit subdomains (up to 0.5 ºC per decade), in July for the Velebit and Dinarides subdomains (up to 0.4 ºC per decade) and in August for the Dinarides subdomain (up to 0.4 ºC per decade). Significant positive trends of temperature maximums are found for August in Velebit and Dinarides subdomains (up to 0.6 ºC per decade). These results are in good agreement with the observed trends found much stronger and significant in summer and spring than during winter and autumn months (Scorzini & Leopardi 2019; Bonacci et al. 2021b; Nimac et al. 2021). This monthly analysis also highlights that summer trends of air temperature at 2 m are generally higher above the sea (up to 0.6 ºC per decade), than in the mountainous areas (up to 0.4 ºC per decade). Also, trends for maximums are mostly higher than those of means, while lowest trends, down to 0.1 ºC per decade, are found for the minimum datasets.

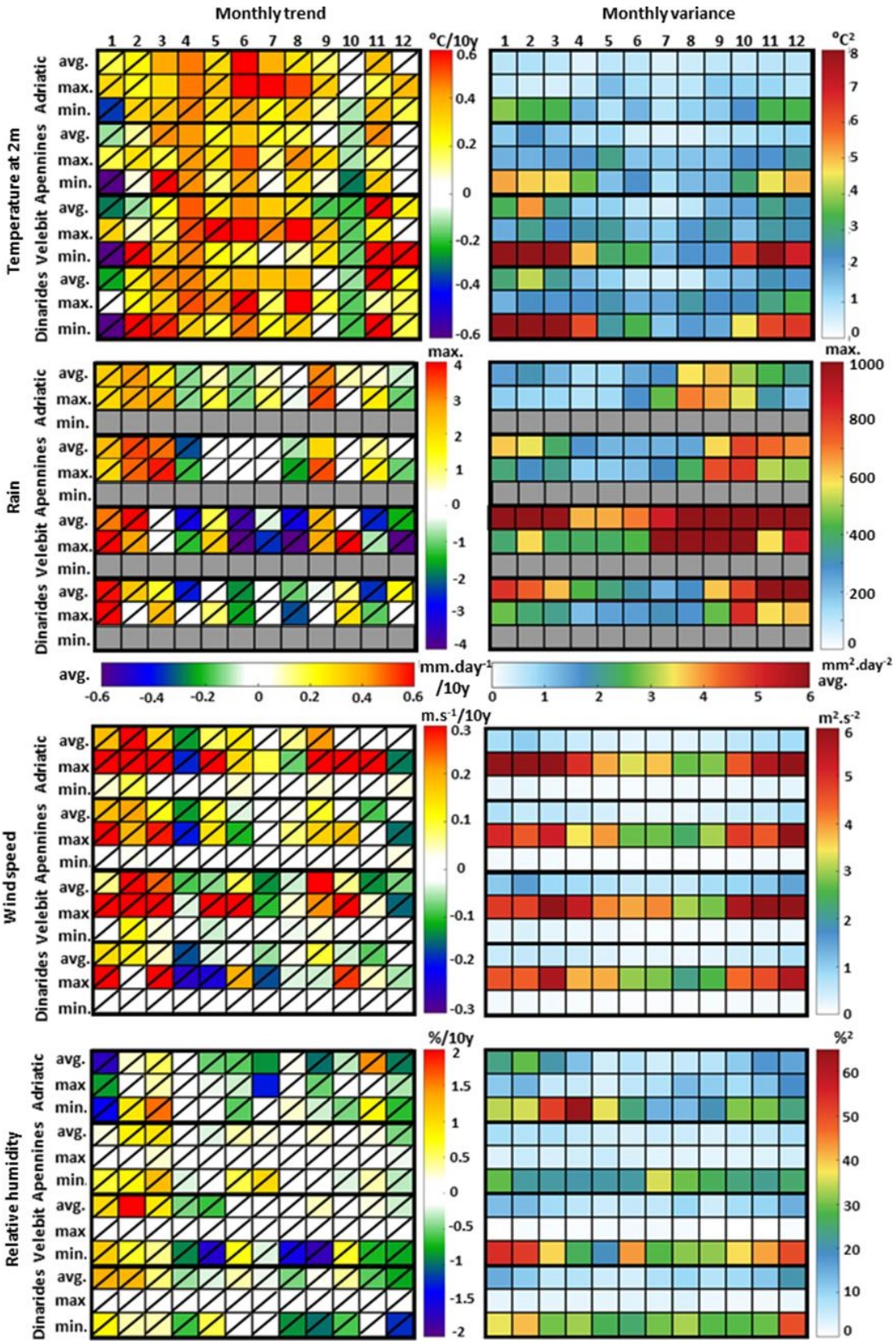

Figure 44. Atmospheric monthly trends (left panels) and variances (right panels) for average (avg.), maximum (max.) and minimum (min.) values of temperature at 2m, rain, wind speed at 10m and relative humidity at 2m for the four subdomains of interest. Black diagonal lines represent insignificant trends for the subdomain.

Interestingly, January trends of minimum temperature are strongly negative, being lower than –0.5 ºC per decade in all four subdomains, while mean temperature trends are negative, down to –0.35 ºC per decade, everywhere but in the Adriatic Sea subdomain, where trends reach 0.2 ºC per decade. This might be explained by cold waves, such as the one in January 2017 (Anagnostopoulou et al. 2017), and the fact that the monthly trends are only calculated with 31 values. In January 2017, several temperature records for the absolute lowest air temperature in the history of meteorological measurements were set. On January 7, 2017, Makarska, Komiža, Split Airport, Dubrovnik Ćilipi, and Imotski recorded these records. In Makarska, the temperature dropped to -5.5°C, in Komiža to -4.5°C, at the Split Airport to -7.2°C, Dubrovnik Ćilipi to -6.3°C, and in Imotski to -12°C. On January 8, 2017, the Dubrovnik Ćilipi station recorded a minimum temperature of -7.4°C, setting a new absolute temperature record for the lowest temperature. On Wednesday, January 11, 2017, at 7 am, 3 cm of snow was measured at the DHMZ meteorological station in Dubrovnik, with a temperature of -3.2°C. Snow continued to fall throughout the day, and by 7 pm, 8 cm of snow was measured in Dubrovnik, setting a record snow depth for the city. It should be noted that January trends of minimum temperature are higher by 0.2 ºC per decade in the 1987−2016 period (but stay negative) compared to the 1987−2017 period due to the absence of one cold spell. Negative temperature trends are found also in October for all subdomains, with values between –0.1 ºC and –0.3 ºC per decade, following observations in the central Mediterranean (Liuzzo et al. 2017). Trends are lower in winter than in summer for the Adriatic Sea and Apennines subdomains. While, for Velebit and Dinarides subdomains, November mean and minimum datasets have strong positive trends with values up to 0.6 ºC per decade. Intuitively, the opposing temperature trends in October and November are associated with the change in dominant synoptic and planetary conditions over Europe, that are resulting in earlier advection of cold air masses in autumn in the 2000s and 2010s which may result from climatic changes over the Arctic (Chripko et al. 2021).

Concerning the rain, only trends from mean dataset in September in Apennines subdomain are significant with values up to 0.25 mm/day per decade. Rain trends are positive for both mean and maximum values for all the subdomains in January, February, March, May, September, and October, but they are negative for April, June, August, and December. Strongest negative trends are found during the summer period in the Velebit subdomain: –0.6 mm/day per decade for the mean and about –4 mm/day per decade for the maximum. These estimates are consistent with observations, which are documenting a redistribution of

precipitation during the year with an overall decrease during summer and an increase in intensity during extreme events (Giorgi & Lionello 2008; Russo et al. 2019; Bonacci et al. 2021a).

As for the rain, insignificant trends are dominating both relative humidity and wind speed variables. However, positive trends for the mean and maximum wind speeds (up to 0.3 m/s per decade) are found for the winter months (January, February, March) in all subdomains and in September–October for some subdomains. Negative trends with values down to –0.3 m/s per decade are found for all subdomains for the mean and maximum wind speeds during April and December, and for the Dinarides and Velebit subdomains during July. Overall, the AdriSC model results are in good agreement with the wind speed increase found over the Adriatic for different periods by different reanalysis products (e.g. 1960–1988, Cavaleri et al. 1997; 1979–2014, Soukissian et al. 2017). Relative humidity trends are mostly negative from August to December, except during November for the Adriatic Sea subdomain and during October for the Velebit subdomain. In contrast, positive relative humidity trends (up to 2 % per decade) are dominating during winter (January–March) in all but the Adriatic Sea subdomain. Overall, relative humidity trends in all subdomains, and particular in the Adriatic Sea subdomain, are generally negative, except for February, March, and November, which is in accordance with the negative trends in relative humidity found in global analysis over most of the Mediterranean Sea (Vicente–Serrano et al. 2018).

Monthly temperature variance is mostly below 2 $^{o}C^{2}$ for mean and maximum values, while it is up to 4 times higher from October to April for minimum values. In more detail, during this period, minimum temperature variances go up to 4 $^{o}C^{2}$ in the Adriatic Sea subdomain, 5.5 $^{o}C^{2}$ in the Apennines subdomain, and 8 $^{o}C^{2}$ in the Velebit and Dinarides subdomains. Convincingly, minimum temperatures are strongly driven by outbreaks of continental and polar air masses that are reaching the Mediterranean during cold periods, but not during warm periods of the year (Saaroni et al. 1996). For the rain, minimum variance is not presented (as minimum rain is always zero) but mean and maximum variances strongly vary between the different subdomains, reflecting the orographically–driven observed patterns (Ivušić et al. 2021). They are (1) the highest for the Velebit subdomain with values over 1000 mm^{2}/day^{2} except during the April–July period, (2) up to 1000 mm^{2}/day^{2} but generally lower than those in the Velebit subdomain for the Apennines and Dinarides subdomains during the August–March period and (3) the lowest in the Adriatic Sea subdomain (about 2 mm^{2}/day^{2} for the mean and 300 mm^{2}/day^{2} for the maximum) during the August–December period. The maximum

wind speed variances (over 6 m^2/s^2) are found for the maximum datasets all year except during the summer, when values vary between 2 m^2/s^2 and 4 m^2/s^2. Their highest values are reached within the Adriatic Sea and Velebit subdomains. Mean wind speed variances are the highest in the Velebit subdomain (1–2 m^2/s^2), then over the Adriatic Sea subdomain, while over the Apennines and Dinarides subdomains they are generally below 0.5 m^2/s^2. In contrast to the wind speed, relative humidity variances are the highest for the minimum values (up to 55 $\%^2$), particularly during the winter months for the Velebit and Dinarides subdomains, presumably reflecting the strong difference in humidity between two major Adriatic winter regimes, bora and sirocco (Belušić Vozila et al. 2021). This difference is not so large in the Apennines, as the dry bora wind is gaining moisture when crossing the Adriatic Sea (Davolio et al. 2017). For the Adriatic Sea subdomain, the relative humidity variances are largest during the spring months, with values up to 65 $\%^2$. This might be attributed to the large difference between air and sea temperatures, where the cold sea has no capacity to feed the dry and warm atmosphere (relative humidity minimum is reached in March–April, Zaninović et al. 2008), while still being affected with sirocco–driven humid periods.

To summarise the monthly analysis in the atmosphere, air temperature trends are generally the strongest over the Adriatic Sea where variances are the lowest in comparison to the other subdomains. Rain trends are insignificant but positive during winter and weakly negative over land during summer only, particularly over the Velebit subdomain. Relative humidity trends are positive during winter overland but not over the Adriatic Sea, while mostly negative during the rest of the year. Wind speed is also following the rain trends during winter. Generally, no great difference exists between the land domains. However, the Velebit subdomain does stand out in several cases: (1) rain variances are much higher and rain trends are more negative, (2) wind speed trends in wintertime are stronger, and (3) relative humidity variances are higher, and trends are stronger.

5.1.2.2 Ocean

Contrarily to the atmosphere, monthly trends of sea temperature and salinity (Figs. 45–47) are almost exclusively significant for all subdomains and all depths, but current speed trends remain generally less significant. It should be noted that only Deep Adriatic and Jabuka Pit subdomain results are presented at 100 m depth (Fig. 46), since other subdomains are shallower than 100 m depth.

Trends in sea surface temperature (Fig. 45) are positive in all five analysed subdomains, being the highest in June and July with values over 0.6 ºC per decade, but also being over 0.4 ºC per decade from April to August. The lowest trends are found in November and October when trends are mostly insignificant everywhere except within the Kvarner Bay subdomain. These values agree with observational studies, either along the long–term monitored transect such as in the northern Adriatic (Vilibić et al. 2019) or with satellite–derived sea surface temperature trends (Shaltout & Omstedt 2014a; Pastor et al. 2018; Grbec et al. 2018). Trends of maximum temperatures are lower than those of mean or minimum temperatures during May and November, while they are significantly higher during September.

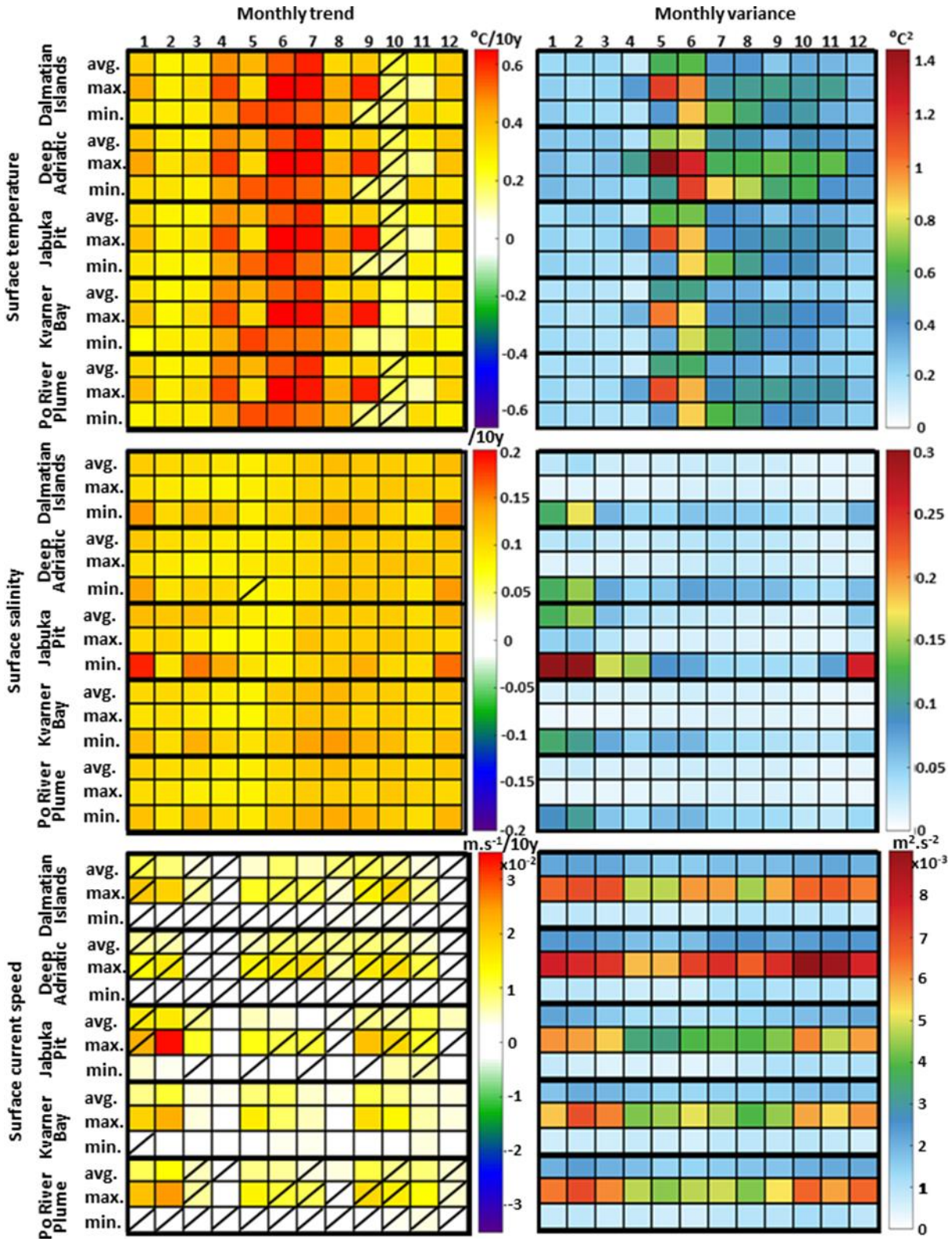

Figure 45. Ocean monthly trends (left panels) and variances (right panels) for average (avg.), maximum (max.) and minimum (min.) values of temperature, salinity and current speed at the surface for the five subdomains of interest. Black diagonal lines represent insignificant trends for the subdomain.

Surface temperature variances are the lowest from January to April, and the highest in May and June. Interestingly, the highest variance values (up to 1.4 ºC^2) are found during May for the maximum dataset in the Deep Adriatic subdomain. Generally, variances in the Deep Adriatic subdomain stay higher than the ones in other subdomains until November. This might be due to vertical processes in the southern Adriatic cyclonic gyre, which may occasionally bring or block the uplift of deep waters through upwelling, depending on its intensity and embedded mesoscale features (Cushman–Roisin et al. 2007). The lowest variances of sea surface temperature are found in the Kvarner Bay, with a maximum barely reaching 1 ºC^2 in May. Indeed, the transport of waters between the Kvarner Bay and the open Adriatic is restricted by a chain of islands, while these islands are also prohibiting strong sea–breeze and Etesian wind during the warm season (Prtenjak et al. 2006; Klaić et al. 2009). Consequently, both horizontal advection and vertical mixing are presumably lower in the summer season and are not strongly affecting the surface temperature within the Kvarner Bay.

Temperature trends at 100 m depth (Fig. 46) differ from those at surface, being mostly around 0.3 ºC per decade for mean, maximum and minimum datasets in the two subdomains, slightly higher in December and the highest in January. Indeed, the 100 m depth analysis has been chosen as saline Levantine Intermediate Water is known to inflow in these depths (Buljan & Zore–Armanda 1976; Artegiani et al. 1997a), and to increase in temperature and salinity in recent decades (Fedele et al. 2022). Trends in the Deep Adriatic subdomain are slightly higher than those in the Jabuka Pit subdomain. This relation between the subdomains is similar for the variance values that are generally lower than at the surface. High variance values in both subdomains are found from October until March, being the highest for November and December when the destruction of the seasonal thermocline is taking place (Buljan & Zore–Armanda 1976), followed by convection processes and a decrease in temperature acting in both deep ocean subdomains (Gačić et al. 2002; Querin et al. 2013).

Results of bottom data analysis (Fig. 47) show that the situation at the bottom highly differs from the surface. The highest temperature trends are found in the Jabuka Pit subdomain (up to 0.2 ºC per decade) indicating that the northern Adriatic dense water that are collected at the bottom of the pit (Vilibić & Supić 2005; Mihanović et al. 2013) are rapidly warming. The warming is much smaller in the other dense water collector, the Deep Adriatic subdomain.

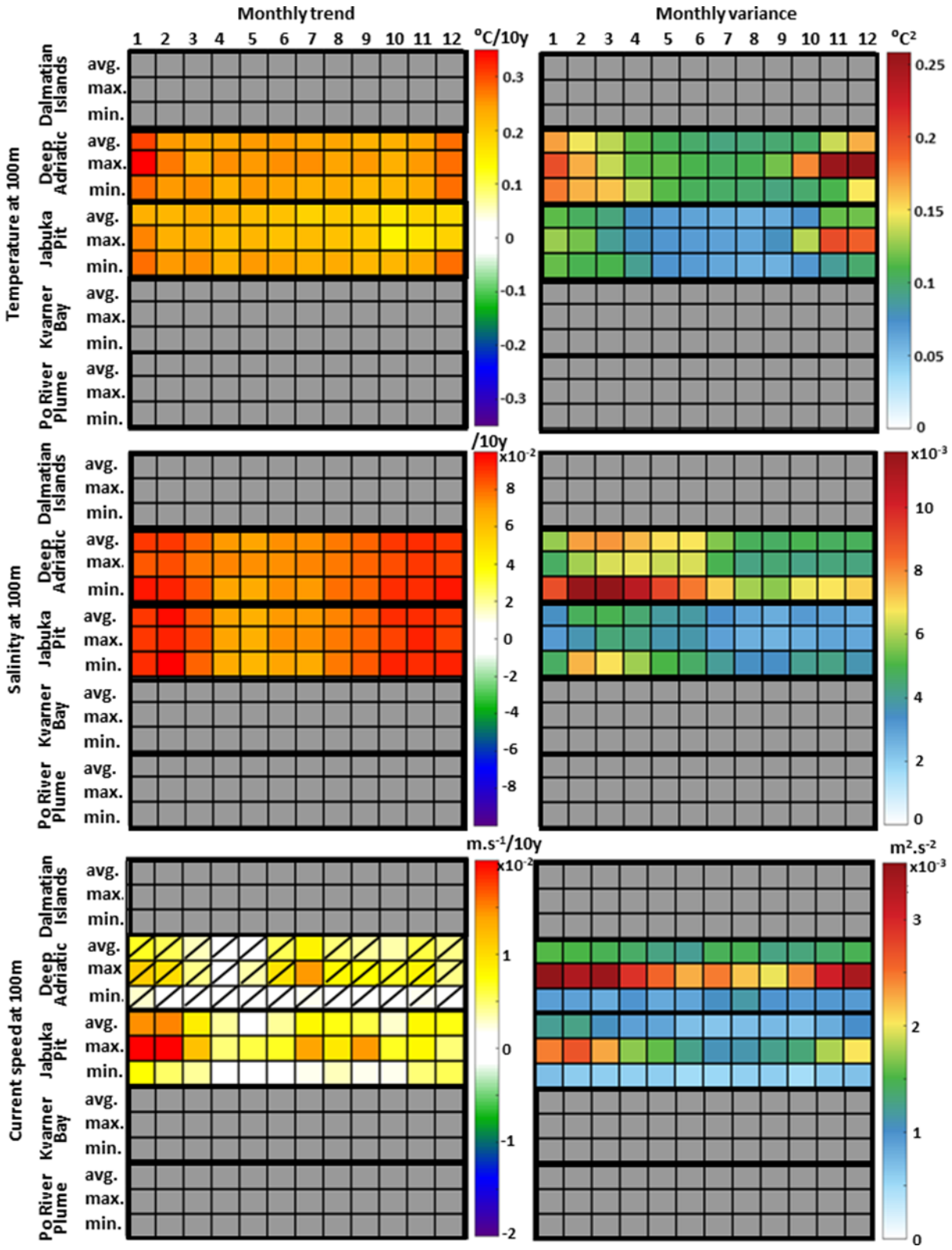

Figure 46. Ocean monthly trends (left panels) and variances (right panels) for average (avg.), maximum (max.) and minimum (min.) values of temperature, salinity and current speed at 100 m depth for the two subdomains deeper than 100m depth. Black diagonal lines represent insignificant trends for the subdomain.

Trends in the Deep Adriatic subdomain are also positive throughout the year (above 0.1 ºC per decade) with slightly higher trends for the minimum datasets, especially in February, March, and April. Variances are also the highest in the Jabuka Pit subdomain. For all subdomains, (1) mean variances are lower than maximum and minimum variances and (2) variances are the lowest in April and the highest between May and November for the maximum datasets.

Surface salinity (Fig. 45) presents positive trends for all the subdomains, with values mostly between 0.1 and 0.15 per decade. These values are higher than the values observed along the Palagruža Sill transect during the 1952–2010 period (Vilibić et al. 2013) but 2 to 3 times lower than observed between 2001 and 2019 (Fedele et al. 2022). Therefore, salinification of the Adriatic is found to rapidly increase in the last decades. Highest trends are found for minimums of salinity, especially for December, January, and March, with these trends in the Jabuka Pit subdomain being the highest. May and June trends are lower than average for all datasets and for all subdomains. Slightly higher trends are found between July and October, indicating that higher evaporation with increased stratification may keep saline waters closer to the surface. Such a process is commonly observed in the Levantine Basin (Kassis & Korres 2020) and is frequently occurring in the Adriatic (Mihanović et al. 2021) in recent decades. Variances reach high values (up to 0.3) during wintertime for minimums, especially in the Jabuka Pit subdomain, while mostly staying below 0.05 for means and maximums (except for winter in the Jabuka Pit subdomain).

At 100 m depth (Fig. 46), salinity variances are higher for the Deep Adriatic subdomain than for the Jabuka Pit subdomain. The highest variances at this depth are found for February and March, when open ocean convection is taking place while the lowest ones occur in August and September. The pattern is shifted for two months in comparison to surface data. Trends in both subdomains are the lowest during spring and summer when the Adriatic–Ionian thermohaline circulation is normally at its maximum (Orlić et al. 2007), thus indicating its weakening. The trends are much higher from October until March, with values up to 0.1 per decade. No difference can be seen between mean, maximum, and minimum datasets, neither between the different subdomains.

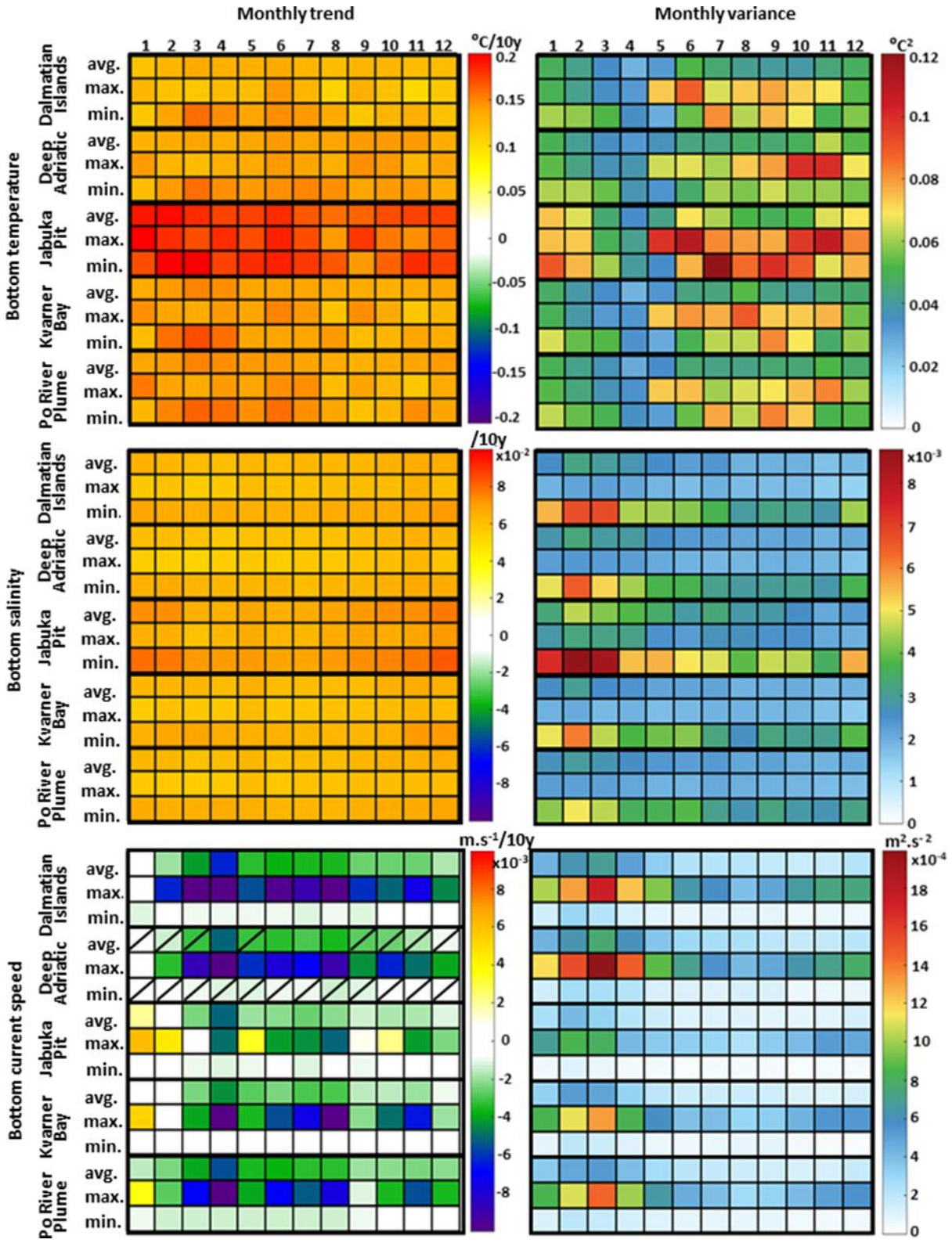

Figure 47. Ocean monthly trends (left panels) and variances (right panels) for average (avg.), maximum (max.) and minimum (min.) values of temperature, salinity, and current speed at the bottom for the five subdomains of interest. Black diagonal lines represent insignificant trends for the subdomain.

At the bottom (Fig. 47), variances are again the highest for the minimum datasets, from December until March, when either vertical mixing is reaching the bottom (for all but the Deep Adriatic subdomain) or the dense water outflow is transported downslope (for both Jabuka Pit and Deep Adriatic subdomains, Vilibić and Supić, 2005; Rubino et al. 2012). Maximum dataset variances are generally the lowest with no great difference between months or subdomains. Trends are positive overall, with values mostly around 0.06 per decade, being the highest for winter months in the Jabuka Pit subdomain. Generally, at the bottom, trends for minimum and mean datasets are higher than those for maximum datasets.

Current speed variances and trends at surface are the highest for maximum datasets (Fig. 45). Variances are generally the highest in the Deep Adriatic and Dalmatian Islands subdomains during the October–March period when the cyclonic activity and wind–driven circulation is the strongest (Poulain 2001). The trends are mostly insignificant in the Deep Adriatic, Dalmatian Islands and Po River Plume subdomains, presumably related to higher variability. In March, April, August, and December trends are generally much weaker, while they reach 0.02 m/s in the rest of the year. Some similarities between the surface current speed trends and wind speed at 10 m (Fig. 44) may be seen, indicating that surface currents are strengthening in some months largely due to the increase of wind forcing at the surface.

At 100 m depth (Fig. 46), current speed variances are the highest for maximum datasets in wintertime and are higher in the Deep Adriatic subdomain than in the Jabuka Pit subdomain. Values are up to 3 times lower than on the surface. Trends are the highest for maximum current speeds, in particular in January, February and July, resembling stronger advection of saline waters during these months.

At the bottom, negative current speed trends prevail in all the domains and for all data series (Fig. 47). Trends obtained from maximum current speeds have much higher values than those obtained from the mean current speeds, surpassing 0.005 m/s for some months, in particular during spring and summer. This indicates much lower intensity in pulsation of waters near the bottom, which are largely coming from bottom dense currents, being in line with the decrease and shallowing of thermohaline circulation and dense water production, in particular on the northern Adriatic shelf (Somot et al. 2006; Vilibić et al. 2013).

In brief, trends of temperature and salinity are strongly significant and positive over all domains, while current speeds are less significant but positive in the surface and intermediate layers, but strongly negative at the bottom. Specifically, the trends are resembling (1)

summertime extensive warming by the atmosphere at the surface, affecting both temperature and salinity (through evaporation), (2) strong salinization by Levantine Intermediate Water inflow in the intermediate layer (at about 100 m depth), (3) stronger circulation in the upper layer of the ocean due to strengthening of the vertical stratification which presumably lead to stronger baroclinicity, and (4) substantial weakening of the near–bottom circulation, which may indicate a weakening of the dense water dynamics and, consequently, of the deep thermohaline circulation in the Adriatic Sea.

5.2 Far–future extreme warming conditions (RCP 8.5, 2070–2100)

Hereafter, the trends, variability, and frequency of extreme events under far–future extreme warming conditions (RCP 8.5; 2070–2100) are compared to the historical conditions presented in section 5.1.

5.2.1 Atmosphere

Decadal temperature trends in the Adriatic region indicate that significant warming continues during the 2070–2100 period (Fig. 48, upper panels). Temperature trends at 2 m are higher over sea (up to 0.4–0.5 °C per decade) than over land (up to 0.3 °C per decade) similarly to the trends found in the historical run. The percentage of temperature trend shows that far–future warming is generally expected to be less intense compared to the historical conditions. This is particularly visible over most of the Adriatic Sea (up to a 10 % decrease) and southern Italy and Dinarides (15 % decrease). However, trends are projected to increase in the southern Pannonian plains (around 7 %). Variance of temperature at 2 m above 35 $°C^2$ is observed over land, with lower variability along the coast due to the influence of the sea and roughly two times less variability over the deep Adriatic Sea. Compared to the historical conditions, a general 5–10 % increase in temperature variability is projected for this extreme warming scenario. Monthly analysis of the change in number of extreme air temperatures extreme events (Fig. 48, lower panels) aligns with the spatial analysis, indicating more significant changes over sea, with over 20 more days per month over the historical maximum threshold and not a single day below the historical minimum threshold (i.e. about 3 less days per month than in the historical run), than over land. In particular, July–August exhibits nearly continuous extreme high temperatures over sea. Overland, around 10 days per month are projected to exceed the historical maximum threshold throughout the year, with over 20 days in July–August while no day below the minimum historical threshold is expected.

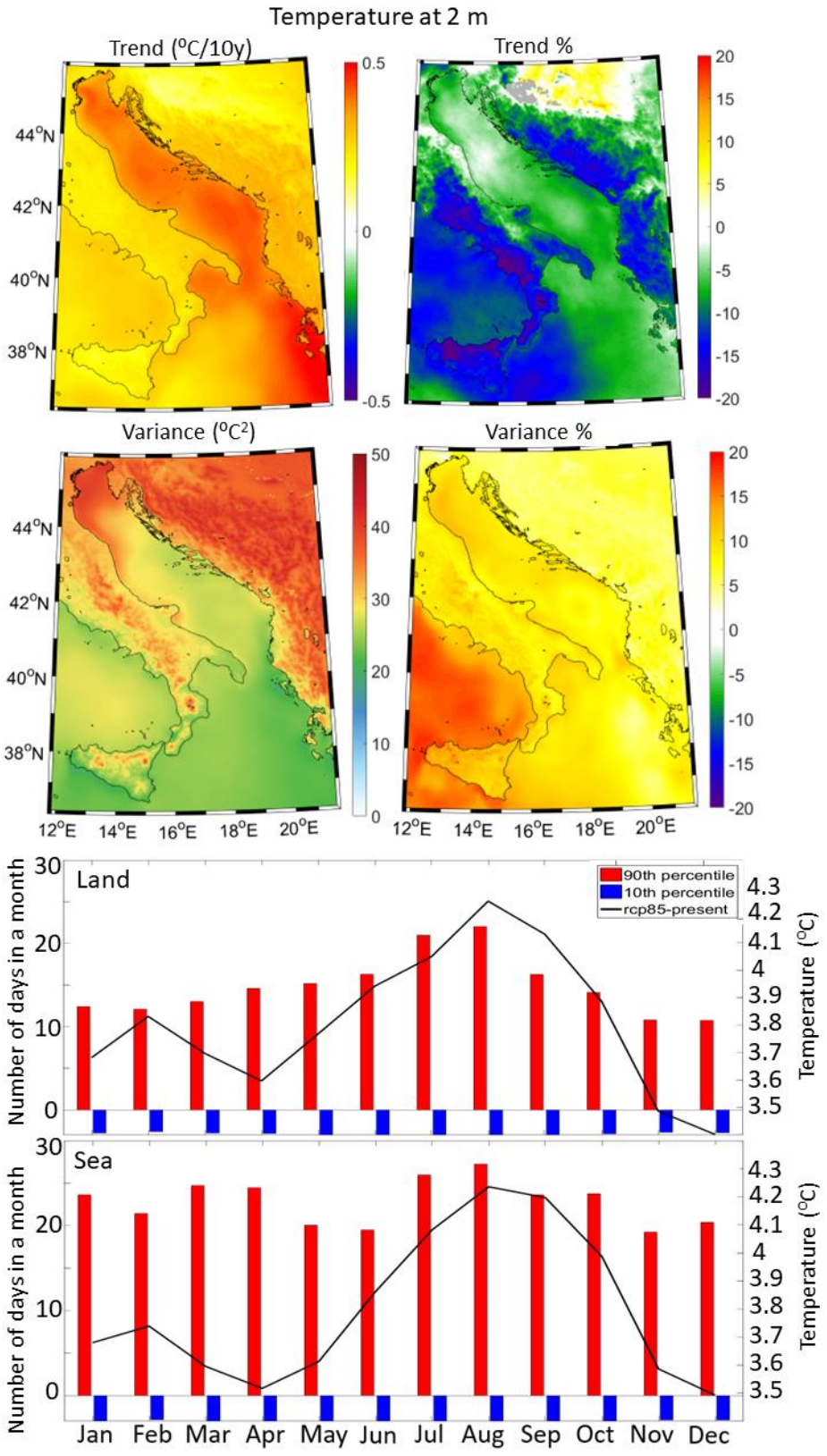

Figure 48. Spatial plots show trends, trend percentages, variances, and variance percentages during the 2070–2100 period (top panels), alongside changes between future (2070-2100) and present (1987-2017) periods in both monthly average conditions (black line) and the number of daily extreme events per month calculated below/above the historical minimum (10th percentile)/maximum (90th percentile) thresholds (bar plots) over land and sea

subdomains (bottom panels) for 2-meter air temperature. Additionally, the percentages of trends/variances represent the impact of climate change, obtained from the difference between future (2070-2100) and present (1987-2017) values.

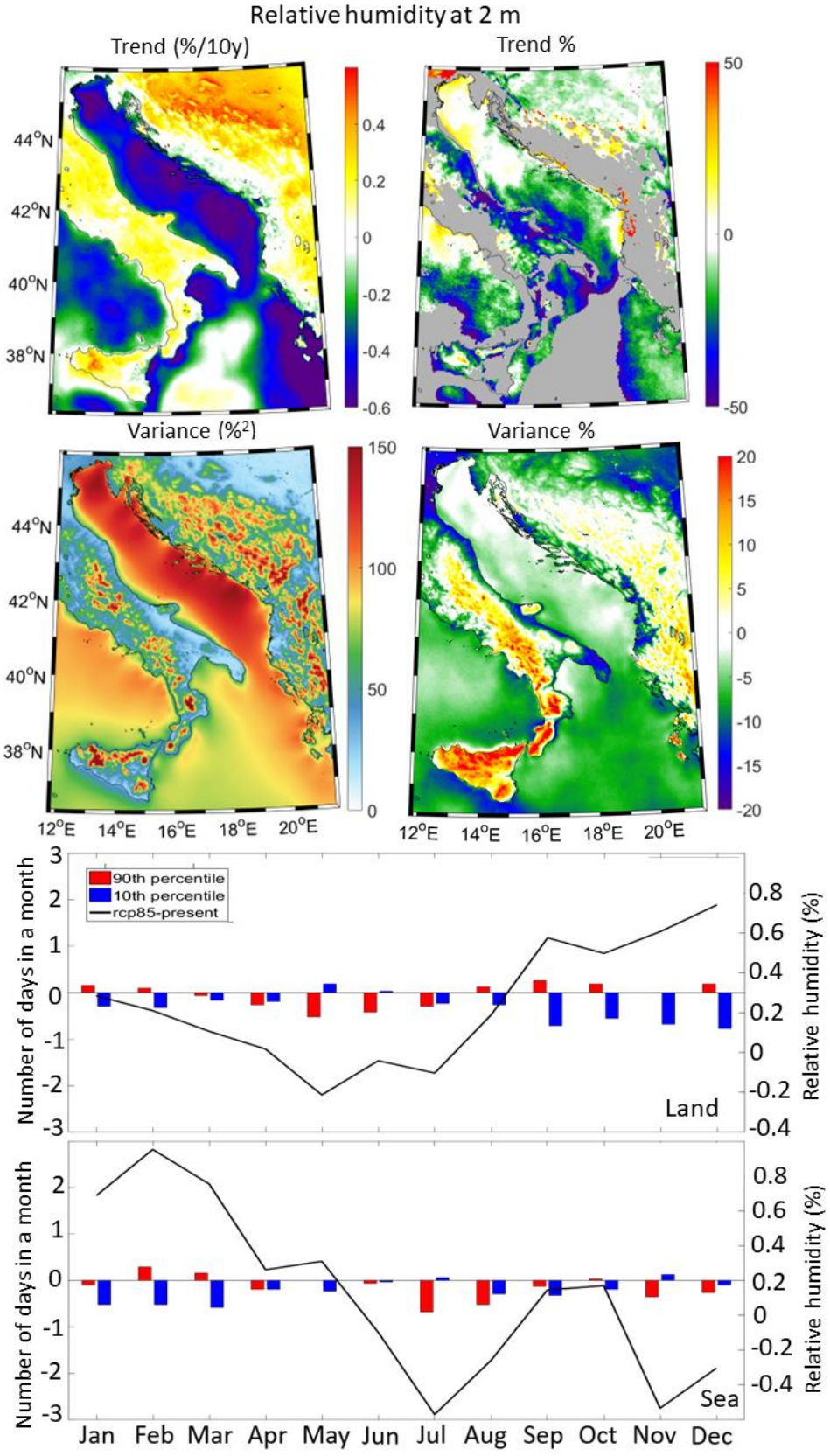

Figure 49. Same as Figure 48 but for the relative humidity at 2 m.

Relative humidity trends at 2 m (Fig. 49, upper panels) are negative over sea (–0.6 % to –0.4 % per decade) and positive over land (0.3–0.5 % per decade), mirroring present climate trends. These results probably originate from boundary condition forcing, as negative trends in relative humidity have been previously found in regional analysis over most of the Mediterranean Sea (Vicente-Serrano et al. 2018). Negative trends are expected to intensify over the southern Adriatic Sea and most of the coastal areas but to decrease over the middle Adriatic Sea. Mountainous regions, like the Apennines and the Dinarides, exhibit patchy distributions, reflecting local effects of mountain ridges on humidity trends. Variability of relative humidity is expected to decrease in the far–future climate, ranging from 5 % over sea to 15 % in northern Italy, Istria, and central Dalmatia coastal areas. Exceptions include mountainous regions like the Apennines, Sicily, and southeastern Dinarides. Monthly analysis for extreme relative humidity in the far–future climate (Fig. 49, lower panels) reveals a decrease (less than a day per month) in dry days (below the minimum historical threshold) over land in September–December. This decrease is accompanied by an overall increase in mean relative humidity (up to 0.8 %). Over sea, the decrease (less than one day per month) occurs in January–March. Moist days (above the maximum historical threshold) are expected to slightly decrease (less than a day per month) during the warm season over both land and sea subdomains. The land-sea contrasts in terms of relative humidity are defined as positive climatology differences over land and negative ones over sea, except in May-August when both are negative.

Rain decadal trends in the far–future climate (Fig. 50, upper panels) are positive over sea and the coastal regions, except in the Rijeka area where large negative trends are projected (below –0.2 mm/day). Coastal regions along the eastern coast and the northern Adriatic present larger decadal rain trends (up to 0.2 mm/day) than in the rest of the domain (around 0.1 mm/day). South of the Adriatic, trends are lower and mostly decreasing. Rain variance percentages indicate an overall increase of more than 50 % in variability. Monthly analysis of rain (Fig. 50, lower panels) reveals an increase in days with extreme rainfall in the far–future climate, particularly in October–January. The number of days with extreme rainfall decreases (up to a day per month) during the warm season (May–September) over both land and sea subdomains, accompanied by an increase in mean rain intensity over the land and sea subdomains varying between 0.2 to 0.8 mm/day during the cold season (September–January).

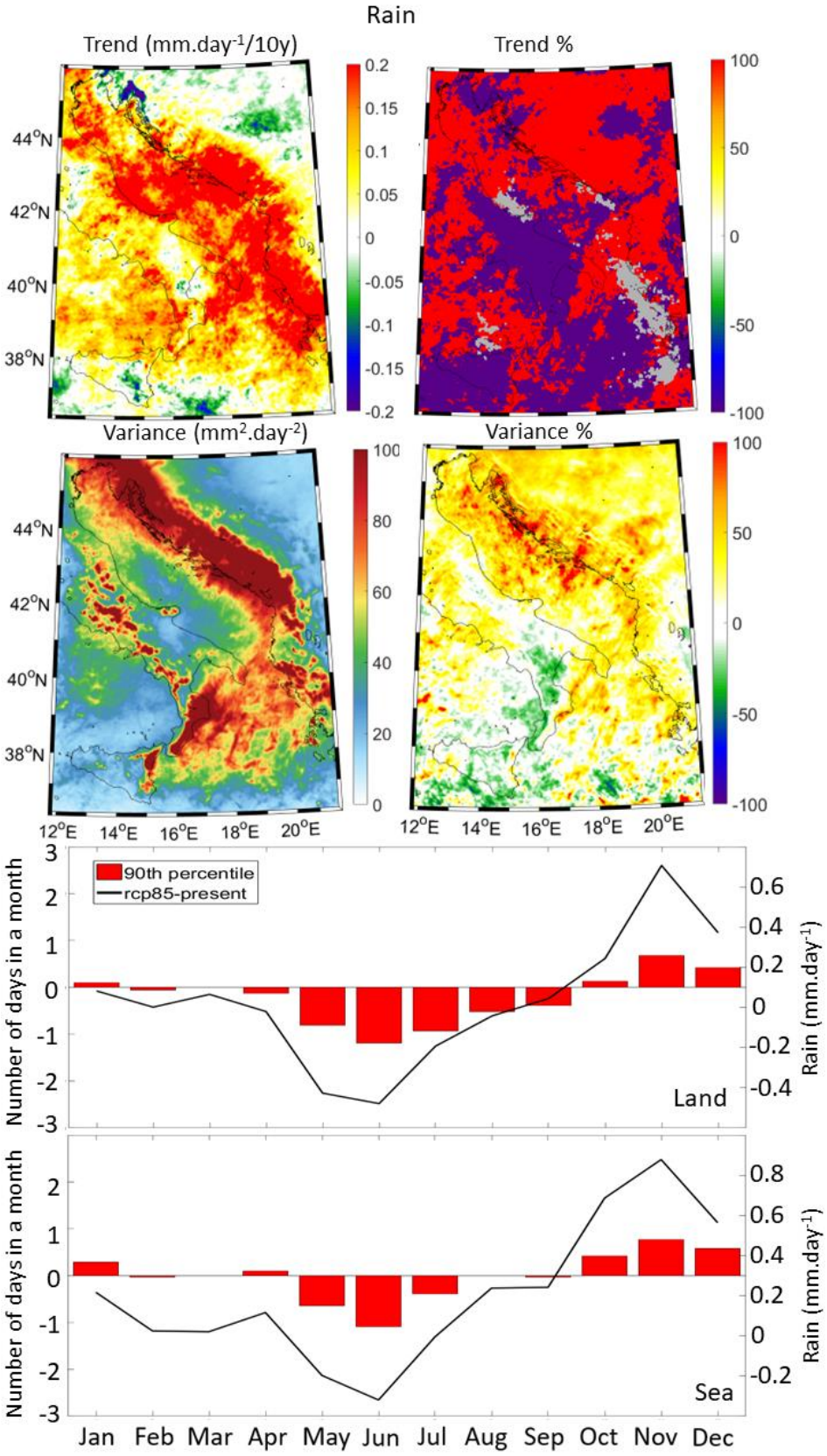

Figure 50. Same as Figure 48 but for the surface rain. The changes in the number of daily extreme events per month below the historical minimum threshold equal to 0 mm/day are not presented.

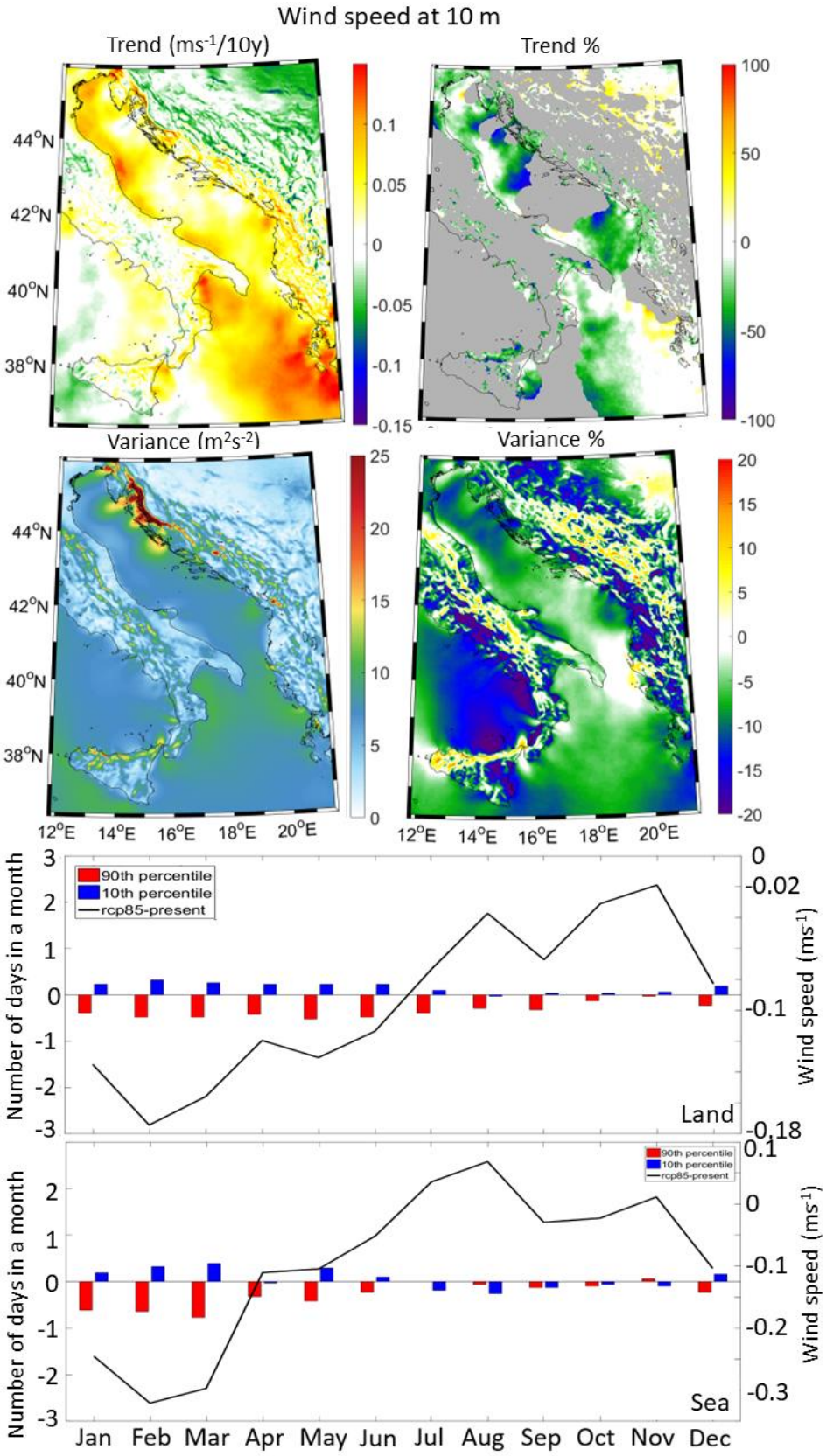

Figure 51. Same as Figure 48 but for the wind speed at 10 m.

For the wind speed at 10 m (Fig. 51, upper panels), positive decadal trends are mostly observed over the sea and coastal regions (mostly between 0.05 and 0.1 m/s), except along the bora wind jets, where trends are slightly negative (between –0.025 and 0 m/s). Mountainous regions and the Pannonian plains show mostly negative trends (around –0.05 m/s). Variability in wind speed is projected to decrease over most of the domain, reflecting greater persistence of wind regimes. Exceptions are mountainous regions, where variability is expected to increase by approximately 10 %. Highest total variances, reaching up to 25 m^2/s^2, in wind speed at 10 m are found along the Velebit mountain, known for its strong bora wind events. Monthly wind speed analysis (Fig. 51, lower panels) indicates a decrease in strong wind events throughout the year over the land domain, except in October–November. Over sea, a decrease is noted between January and March. Winter sees the most significant decrease in mean wind speed over both land and sea domains (up to –0.3 m/s), while July–August experiences a small increase over sea.

5.2.2 Ocean

Sea surface temperature trends (Fig. 52) predominantly range from 0.25 to 0.35 °C per decade, with slightly higher values in the southern than in the northern Adriatic and maximum values at the perimeter of the Southern Adriatic Pit (SAP). Trend percentages (Fig. 52) indicate a decrease in sea surface temperature trends in the far–future climate compared to the historical results, mostly around 30 %, with higher values of approximately 50 % in the central Adriatic and along the western coastal current but lower values below 10 % in the SAP.

Sea temperature trends at 100 m depth (Fig. 53, upper panels) show an increase of approximately 0.4 °C per decade. The Otranto Strait experiences the highest warming rates (around 0.5 °C per decade), while the SAP shows the lower values (about 0.35 °C per decade). Trend percentages indicate a decrease in temperature trends of 25–40 % in the central Adriatic and an increase of 25–50 % in the SAP and the Otranto Strait compared to the historical results.

Decadal trends of sea bottom temperature (Fig. 54, upper panels) demonstrate contrasting behaviour between the SAP and the rest of the Adriatic Sea. The SAP exhibits negative trends (0.1–0.2 °C per decade), while positive trends (up to 0.5 °C per decade) are observed elsewhere, with the highest values along the eastern coast and the Dalmatian islands.

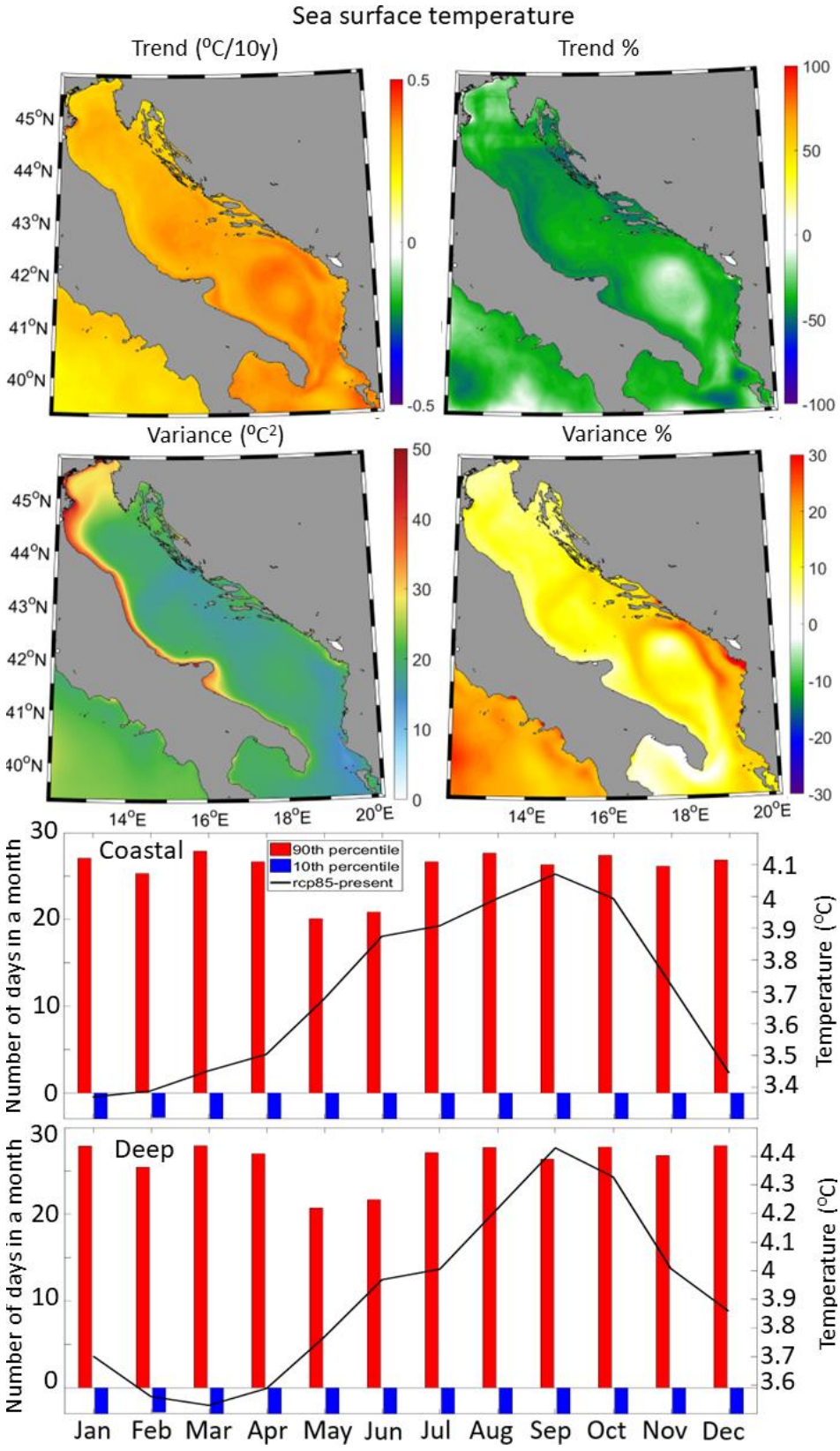

Figure 52. Trend, trend percentage, variance and variance percentage spatial plots (top panels) as well as changes in both monthly average conditions (black line) and number of daily extreme events per month calculated below/above the historical minimum (10th percentile)/maximum (90th percentile) thresholds (bar plots) over the coastal and deep subdomains (bottom panels), for the sea surface temperature.

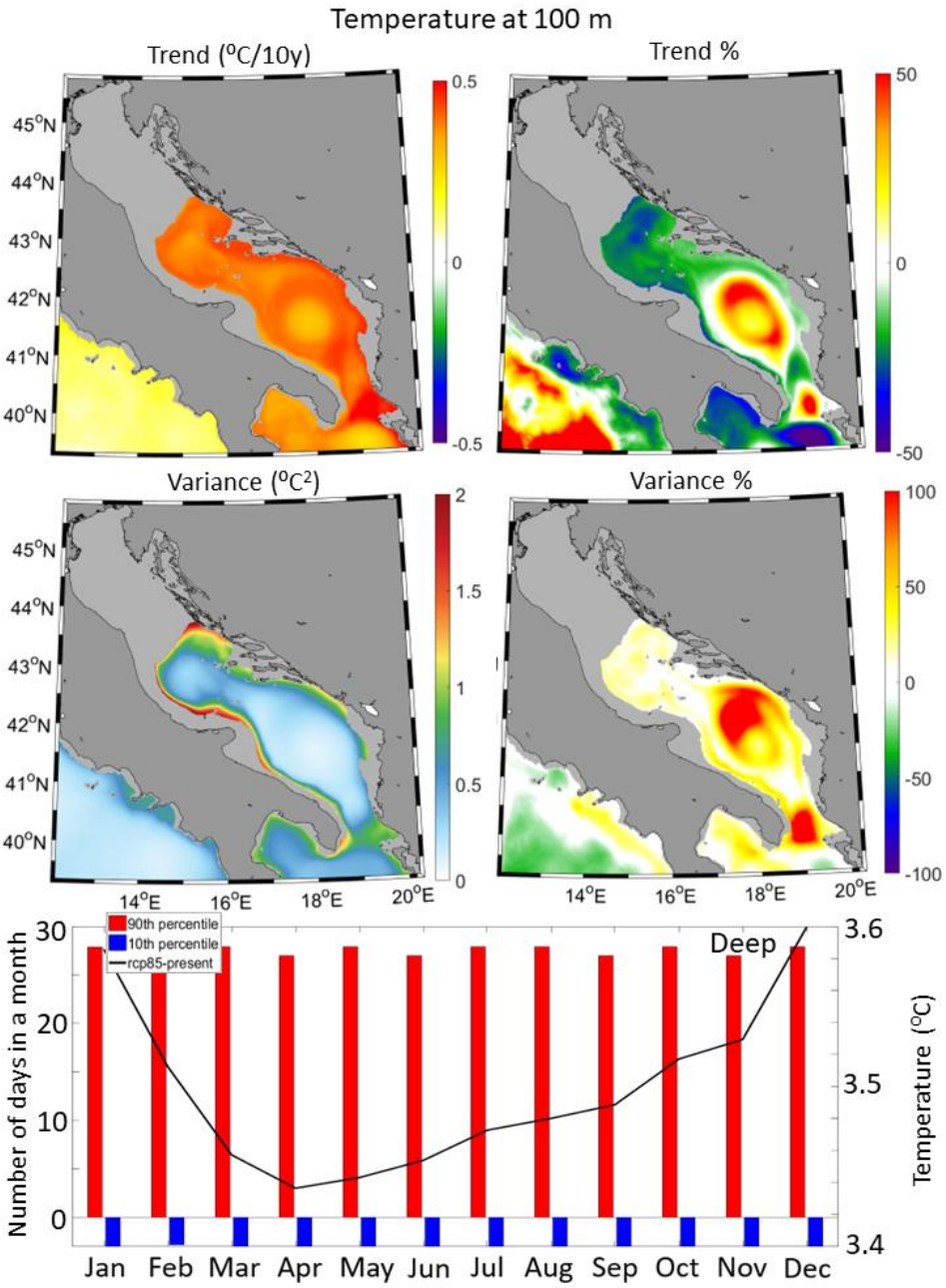

Figure 53. Same as Figure 52 but for the sea temperature at 100 m. The monthly results for the coastal subdomain are not presented.

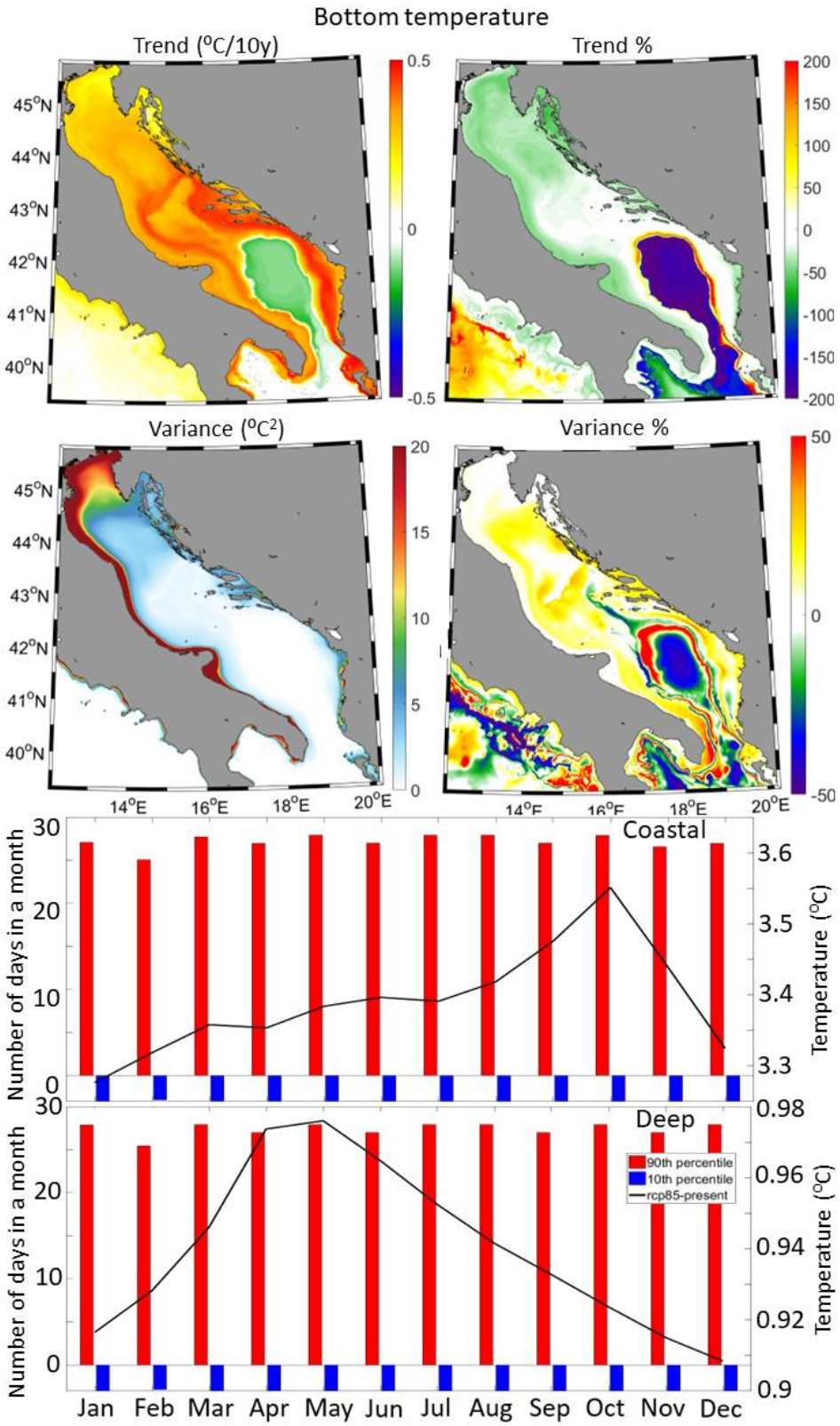

Figure 54. Same as Figure 52 but for the sea bottom temperature.

Trend percentages indicate a general decrease in future sea bottom temperature trends, with the lowest values in the central Adriatic and along the Dalmatian coast and islands, dropping below 20 %. Higher percentages are found in the SAP and the Otranto Strait, with trends up to 200 % lower than for the historical results. Far–future temperature variability is expected to increase compared to the historical results, by 10–20 % at the surface and up to 100 % at 100 m in the SAP and the Otranto Strait.

Monthly analysis reveals significant changes in sea temperature extremes in the far–future climate. Temperatures below the minimum historical threshold in the historical run no longer occur but temperatures above the maximum historical threshold persist in all months, except May–June when 5–8 days do not exceed this threshold. Differences in monthly climatologies show a sea surface temperature increase in the coastal Adriatic regions ranging from 3.4–3.5 °C in winter to 4.1–4.4 °C in summer. At 100 m, the increase is 3.4–3.6 °C, more pronounced in winter and less in spring and summer due to seasonal conditions. At the bottom, temperature differences also vary, with coastal areas experiencing similar values to those at 100 m, but significantly lower values in the deep subdomain, ranging from 0.9 to 1 °C.

Surface salinity trends (Fig. 55 upper panels) generally vary around 0.1, with slightly lower values in the Kvarner Bay and Dalmatian Island regions (0.05). Higher salinity trends are observed off the Po River delta (exceeding 0.15 per decade) and in the Otranto Strait. Compared to the historical trends, salinity is expected to increase by approximately 25% in the SAP and the eastern side of the Otranto Strait. Lower salinity trend differences are projected for the rest of the Adriatic, particularly along the Po River plume, the Kvarner Bay coastal area, and the Neretva River delta.

At a depth of 100 m (Fig. 56), salinity trends range between 0.05 and 0.1 per decade while, compared to the historical trends, far–future trends are expected to decrease by approximately 20% in the western Adriatic region but to increase in the eastern part, especially in the SAP. Variability at 100 m is generally low but is expected to be much larger than in the present climate.

Bottom salinity trends (Fig. 57 upper panels) are positive, with lower values in deeper regions and higher values in shallower areas, such as the northern Adriatic shelf. Salinity trends decrease along the Po River plume, in the northern Adriatic, and the Kvarner Bay, while they increase in the Southern Adriatic Pit and the Otranto Strait. Bottom salinity variability is projected to decrease in the Southern Adriatic Pit but increase in the rest of the Adriatic.

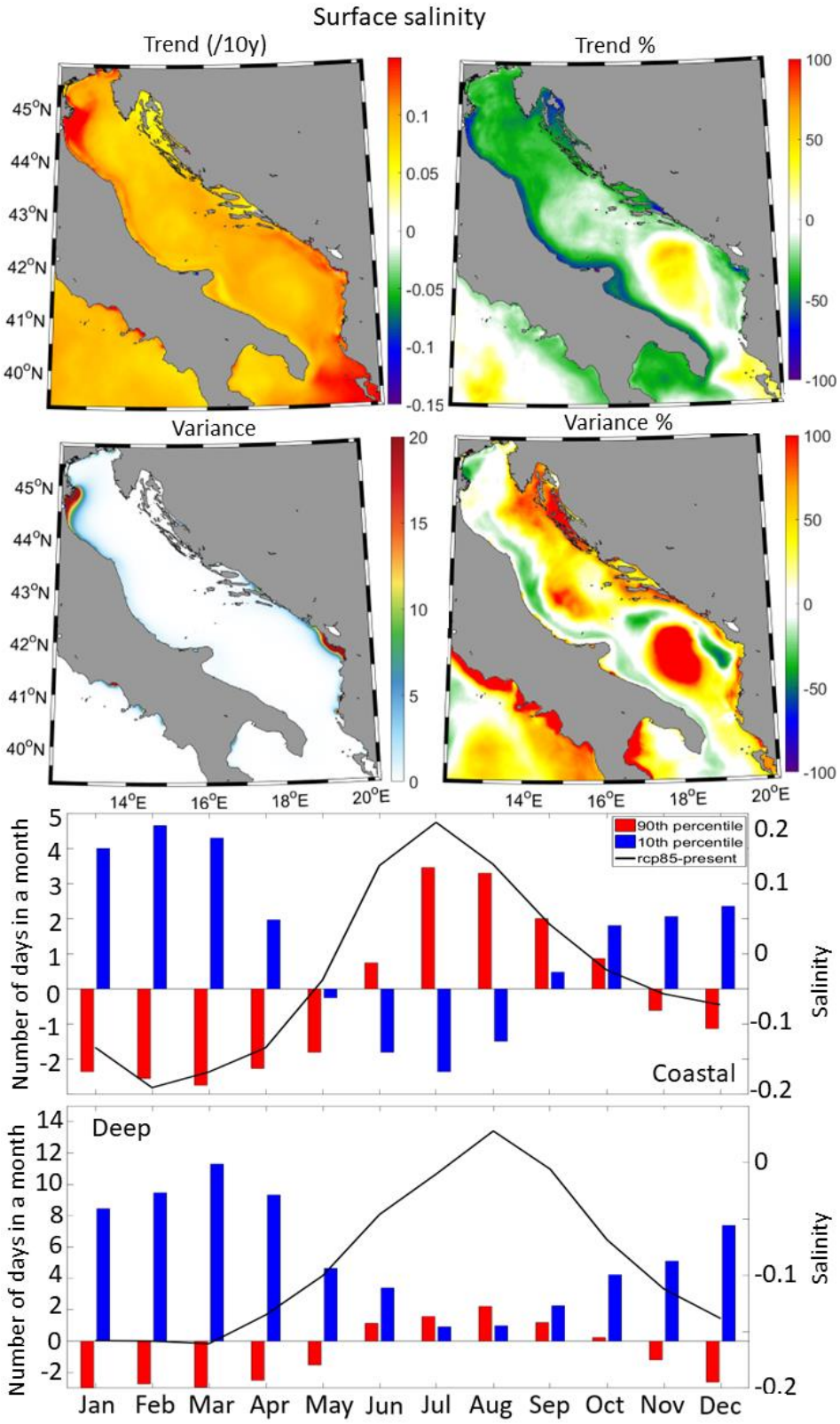

Figure 55. Same as Figure 52 but for the sea surface salinity.

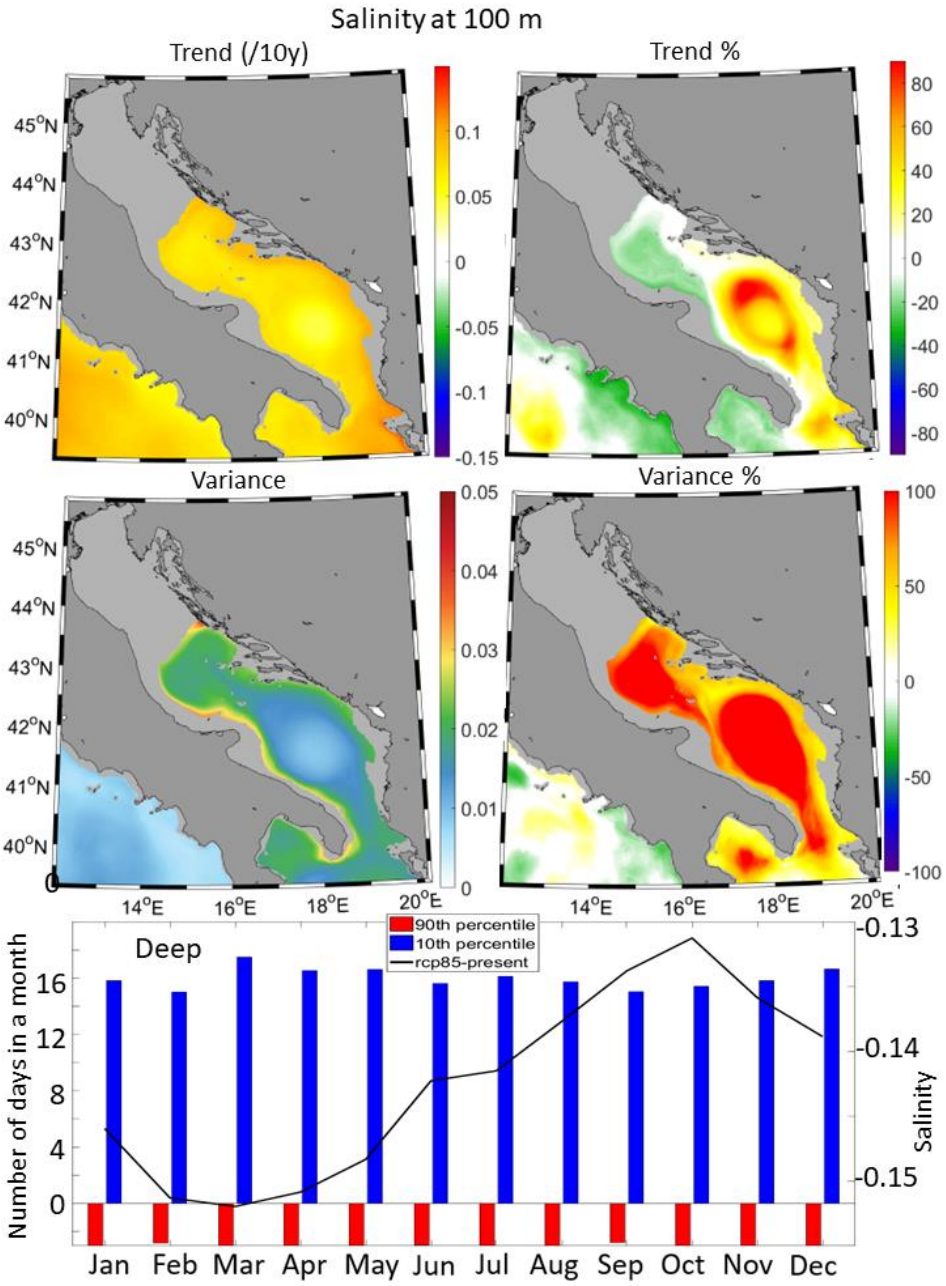

Figure 56. Same as Figure 52 but for the sea salinity at 100 m. The monthly results for the coastal subdomain are not presented.

At the surface, differences in the number of days of extreme high salinity events reveal positive changes during summer (up to 3 and 2 days more in the coastal and deep domains, respectively), but negative changes, associated with an average decrease in salinity of up to 0.2, otherwise. At 100 m depth, all differences are negative throughout the year with at least 14 days more of extreme low salinity events than under the historical conditions associated with a decrease in salinity up to 0.15. This clearly indicates lower salinity in the far–future climate, especially during the winter months. At the bottom, differences are negative in the

coastal subdomain leading to at least 4 days more of extreme low salinity events, while in the deep domain, they are positive leading to at least 18 days more of extreme high salinity events.

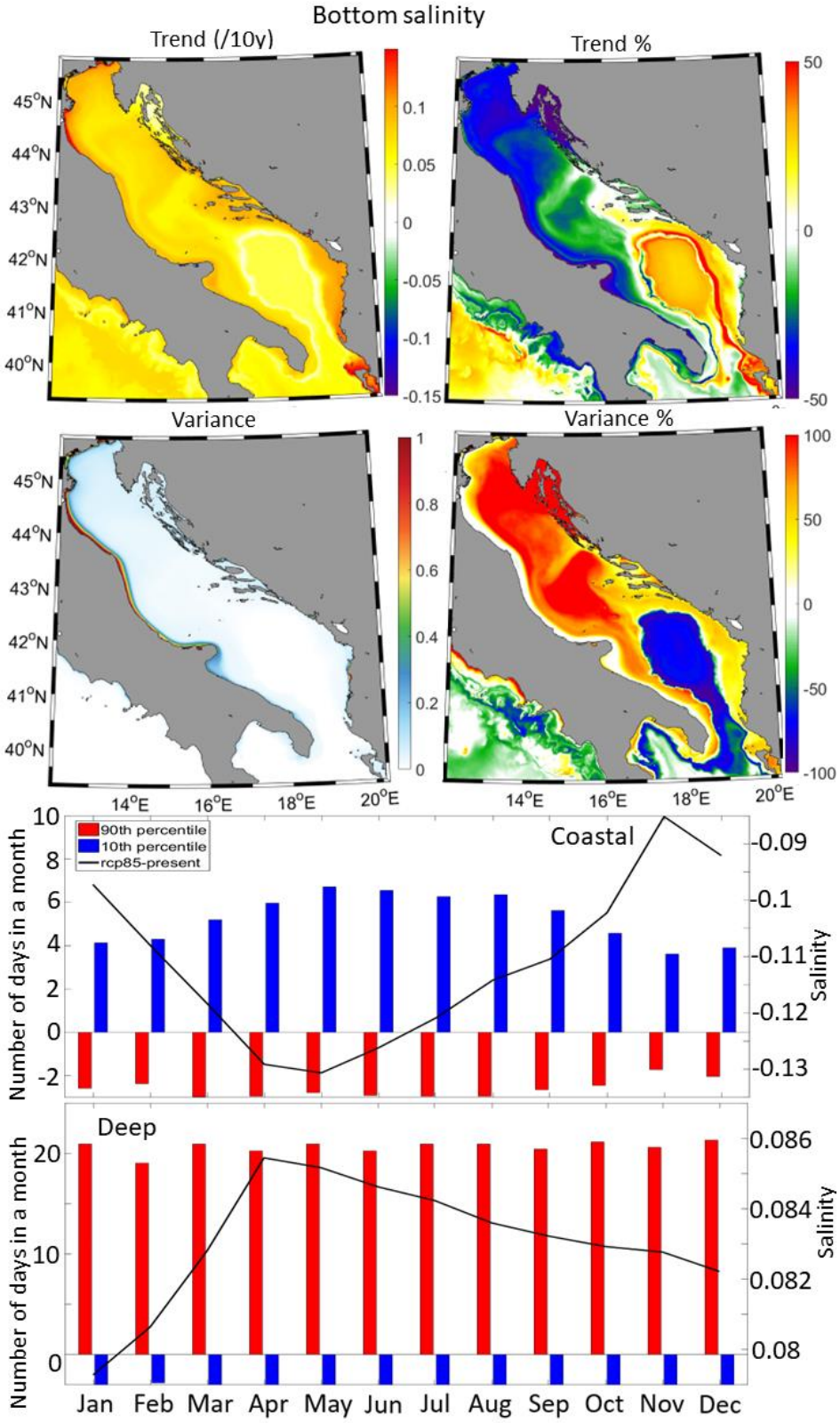

Figure 57. Same as Figure 52 but for the sea bottom salinity.

Far–future current speeds in the Adriatic Sea (Figs. 58–60) show positive trends across all depths, like it has been documented for the present climate. At the surface (Fig. 58), trends range from 0.005 to 0.01 m/s per decade in most areas, except for the SAP, where they reach up to 0.02 m/s per decade in the inner part of the cyclonic gyre and around –0.005 m/s per decade in its outer parts. Compared to historical trends, positive changes are observed in the central SAP, transversely over the northern Adriatic, and along the eastern and western coastal regions.

At a depth of 100 m (Fig. 59), current speed trends are similar to surface trends, with positive values up to 0.005 m/s per decade, primarily concentrated in the centre of the SAP where both trends and variability increase by more than 100 %.

At the bottom (Fig. 60), current speed trends remain generally low, below 0.002 m/s per decade, with the lowest values in the SAP. Compared to the historical trends, a strong increase in trends (more than 100 %) associated with a strong decrease in variability (up to 100 %) is expected in the SAP and the Otranto Strait.

Monthly analysis of surface current speeds indicates a significant increase in the deep domain during wintertime, while summer months show lower increases. Consequently, the number of days with extreme high surface current speeds will double or triple in the deep domain in the far–future climate, while weak surface current events will decrease by half. At 100 m depth, mean current speeds will increase, particularly in January–May, with almost half of the month characterised by extreme high current speeds. At the bottom, the deep domain will experience a weakening of the currents, particularly in summer when up to 11 days more of extreme weak events per month are expected to occur compared to the historical conditions. In the coastal domain, the changes in current speed are mostly negligible.

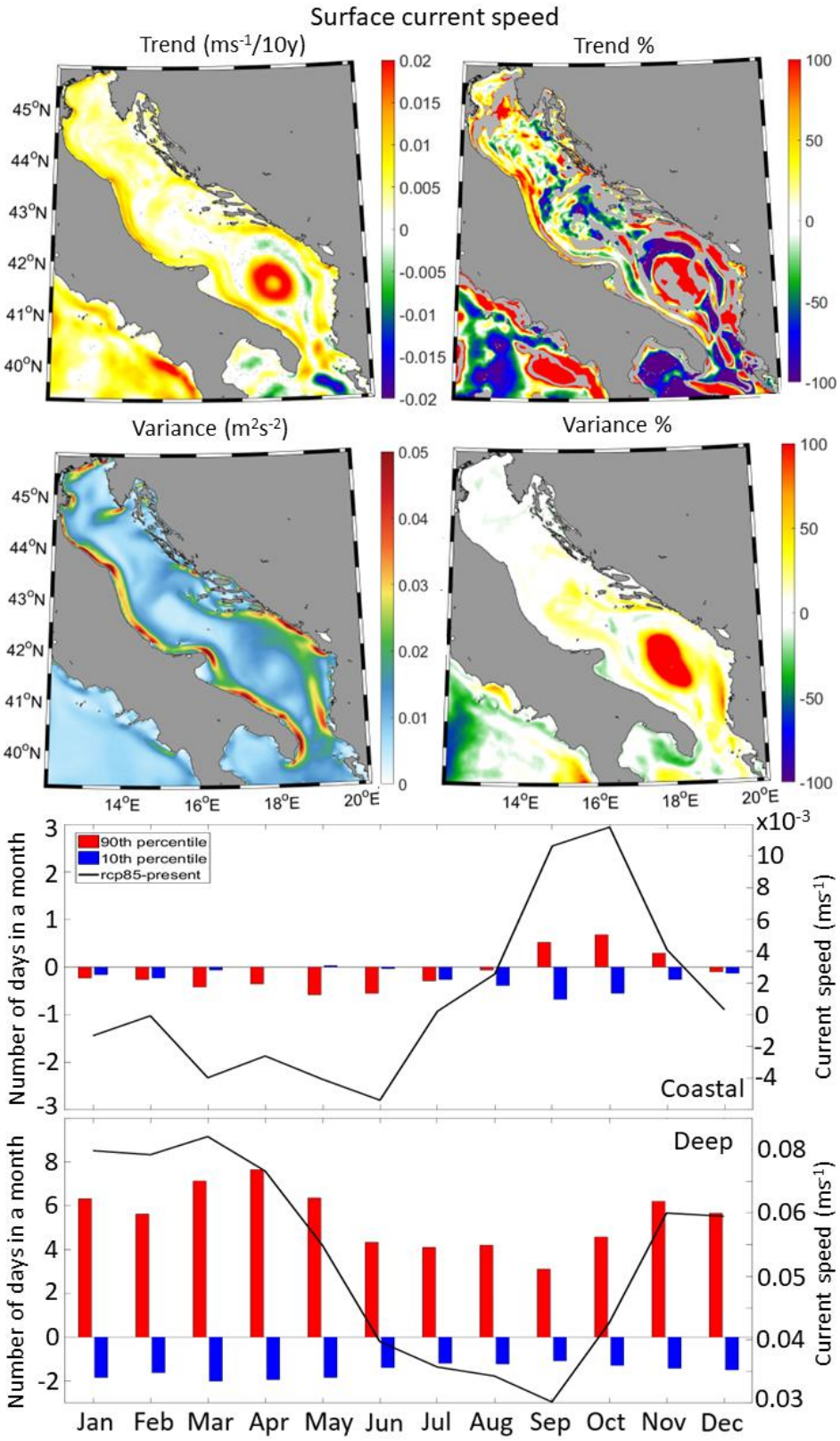

Figure 58. Same as Figure 52 but for the sea surface current speed.

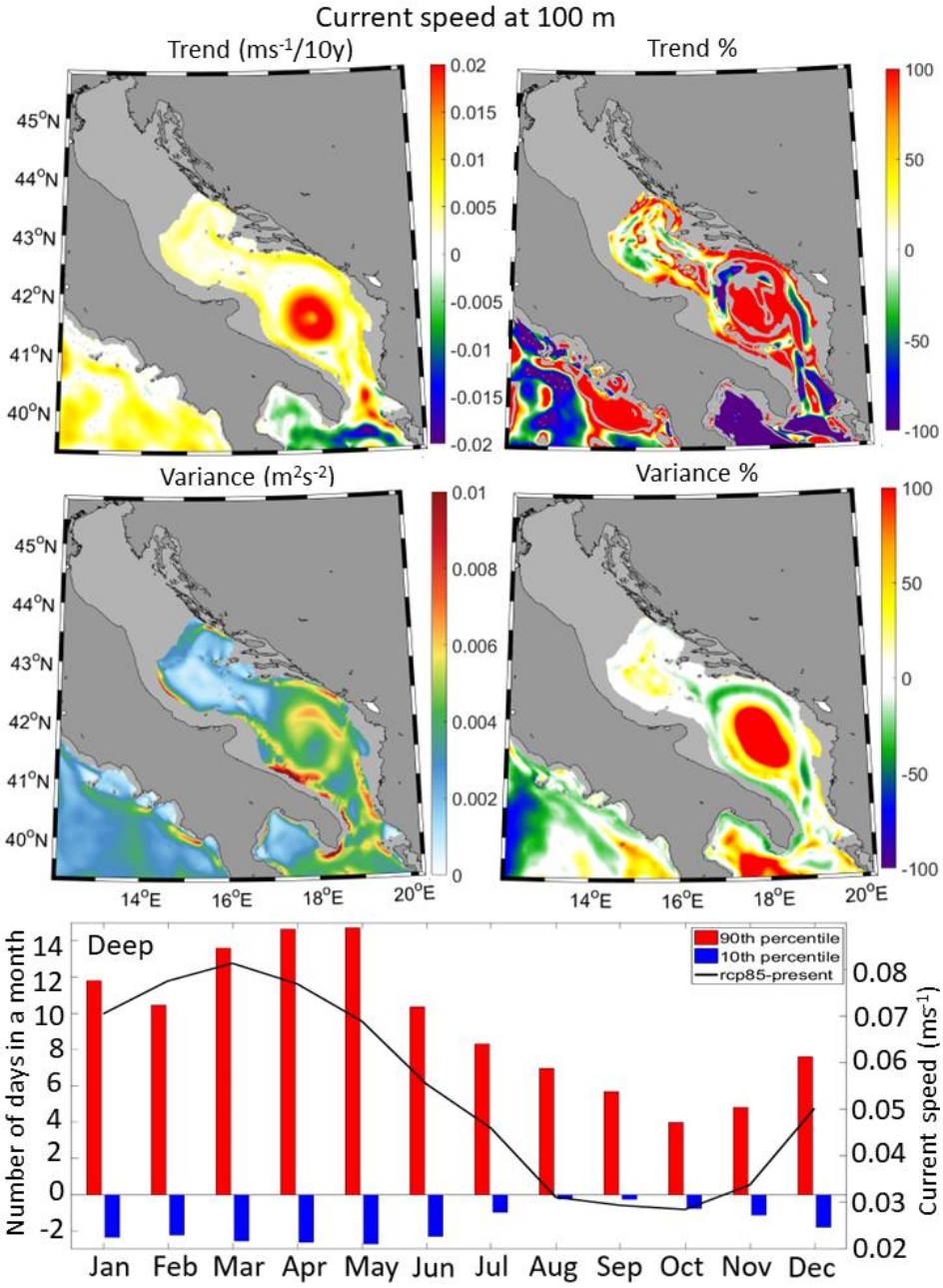

Figure 59. Same as Figure 52 but for the current speed at 100 m. The monthly results for the coastal subdomain are not presented.

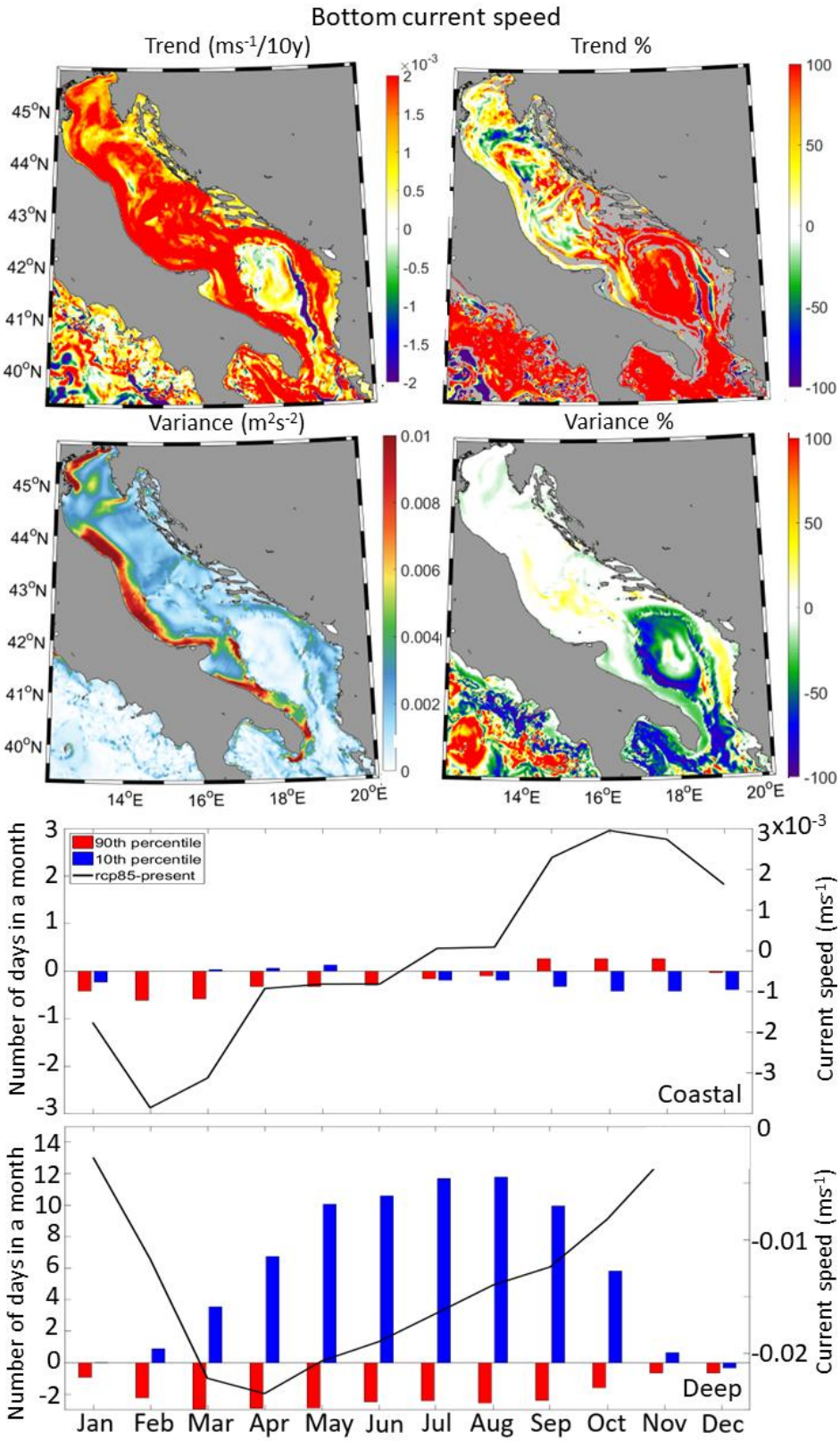

Figure 60. Same as Figure 52 but for the sea bottom current speed.

5.3 Discussion

The analysis of the Adriatic climate, including historical and far–future projections of trends, variability and frequency of extremes, was conducted in this chapter. Through short simulations, the AdriSC model has already been proven to successfully capture the fine–scale dynamics in both the atmosphere (e.g. the bora wind, see previous chapters) and the ocean (e.g. surface cooling, dense water generation, BiOS regimes, see previous chapters and Pranić et al. 2023) under the historical conditions (1987–2017). However, this is the first analysis of the full AdriSC far–future long–term projections which should capture the impact of climate change on events not well represented in regional climate models with coarser resolutions. The following discussion is thus presenting the relevance of these results with the aim to, first, explain their potential implications for the Adriatic atmosphere–ocean dynamics, and second, compare them with the Mediterranean regional climate models.

5.3.1 Implications for the atmosphere–ocean dynamics

The presented AdriSC results reveal several changes that can impact the atmosphere–ocean dynamics across the Adriatic region. These changes are presented below for four different categories: (1) heatwaves, extreme rainfalls, and droughts, (2) dense water formation, (3) salinity budget and (4) Southern Adriatic dynamics.

5.3.1.1 Heatwaves, extreme rainfalls, and droughts

In the atmosphere, findings suggest a continuous warming during the 2070–2100 period (up to 0.5 °C per decade) which leads to at least 10 more days per month of extreme heat over land than under the historical conditions. This suggests an increase in the number of heatwaves, as defined in the present climate by Robinson (2001), which will be particularly intense and prolonged during July–August with 20 more days of extreme heat associated with an average increase in temperatures of 4.3 °C. Over the sea, not only the air but also the ocean temperatures are warming at an even faster rate than inland. This leads to at least 20 more days per month of extreme heat than under the historical conditions from the surface to the bottom of the Adriatic Sea, with an average temperature increase ranging from 0.9–1 °C at the bottom of the deepest part of the Adriatic to more than 4 °C at the surface in the coastal areas. Under these conditions, marine heatwaves, as defined in the present climate by Hobday et al. (2016), would be nearly constant. In addition to the heatwaves, the warming conditions projected by the AdriSC model show an increase in rain variability of over 50 % across the entire studied

region, and up to 100 % along the eastern Adriatic coast, compared to the historical conditions. Further, in average, the number of extreme precipitations projected with the AdriSC model will be reduced by up to 33 % in May–July, associated with a decrease in relative humidity of 0.2–0.4 %, and increased by up to 25 % in October–December, associated with an increase in relative humidity of up to 0.8 %. Considering the complexity of interactions between changes in relative humidity and rainfall occurrence (Denson et al. 2021), these results suggest potential implications for expected increases in extreme rainfall in winter (Zittis et al. 2021) and droughts in summer, since in a warmer world, the intensification of the hydrological cycle is anticipated (Allen & Ingram 2002; Giorgi et al. 2019).

5.3.1.2 Dense water formation

In the Adriatic, the primary driver of the dense water formation is the cooling of surface waters during the winter season by cold northerly bora winds. These winds enhance surface heat loss and evaporation, causing surface waters to cool rapidly and sink to the deeper layers (Pullen et al. 2006; Janeković et al. 2014; Ličer et al. 2016). The AdriSC far–future results project less intense and less frequent winds over the entire Adriatic region with both a decrease in speed (up to 0.18 m/s over land and 0.3 m/s over sea) and a decrease in the number of extreme high events over the sea (up to 25 %) during January–April which is the period during which strong bora events occur. However, several other factors also influence the dense water formation. First, warmer waters during the winter season may slow down the cooling required for dense water formation, potentially reducing the intensity of the process. In the coastal areas of the Adriatic Sea, the AdriSC results show an increase in sea surface temperatures above 4 °C during February–March when the dense water formation is known to occur under the historical conditions. Second, new precipitation patterns and river discharges due to climate change may affect the surface salinity values. During January–April, the AdriSC results show an increase in both precipitations over sea (ranging from 2.6 to 3.4 mm/day) and river discharge forcing (compared to the historical conditions, increase by 40–50 % in January–February, no increase in March and decrease by less than 10 % in April; see Fig. 4 in Denamiel et al. 2020a). Providing that the extreme bora events occur during the same period for historical and far–future conditions, the sea surface salinity is thus likely to be decreased during the far–future bora events which is confirmed by the increase (decrease) of extreme low (high) sea surface salinity events in the coastal areas by up to 5 days (2 days) per month during this period. Consequently, the density of the dense waters generated by sea surface cooling will also decrease. Third, a decrease in relative humidity during bora events can produce an increase in

latent heat losses despite the decrease in bora wind speeds (Denamiel et al. 2020b). The AdriSC results, however, show an increase of the relative humidity over sea by up to 0.8 %. Consequently, following these preliminary results the dense water formation within the Adriatic Sea is likely to be largely reduced under far–future extreme warming conditions.

5.3.1.3 Salinity budget

Several noticeable changes in salinity are seen in the AdriSC far–future projections. First, the increase in salinity in the surface and intermediate layers during summer (up to 0.2 associated with 3 more days per month of extreme high salinity events) signals the prevalence of evaporation over precipitation and river runoff. This phenomenon is already observed in the present climate as surface saline "lakes" (Mihanović et al. 2021). Second, strong surface salinity trends (more than 0.11 per decade) and variability (more than 20) are expected in the vicinity of the Po and Drini river plumes which have the highest discharges in the Adriatic Sea. Further, within the coastal subdomain, surface salinity is expected to decrease in October–April when the river discharge forcing has been increased by 10–50 % under RCP 8.5 conditions and when there is an increase in precipitation over land and sea. As the northern Adriatic is strongly influenced by local freshwater discharges (Raicich, 1996), the salinity budget in this region is mostly following the imposed changes in river discharges in the AdriSC model extreme warming run.

5.3.1.4 Southern Adriatic dynamics

Over the SAP, the AdriSC results show a decrease in salinity by at least 0.13–0.15 and an increase in temperatures by 3.4–3.6 °C of the intermediate waters associated with higher current speeds (up to 0.08 m/s and at least 14 more days per month above the extreme high speeds compared to historical conditions) particularly during the January–May period. These results, which contrast with the coastal areas of the Adriatic Sea, suggest the intensification and shrinking of the southern Adriatic cyclonic gyre in the middle of which, under the historical conditions, upwelling of deep waters can occur (Gačić et al. 2002). Further, at the bottom, the increase in salinity by 0.08–0.09 and the increase in temperatures by 2.5 °C less than in the intermediate layer associated with far less variability than under historical conditions (up to 200 %) suggest a strengthening of the vertical stratification over the SAP. As the same patterns are observed over the Otranto Strait, this strengthening of the vertical stratification may result from the Adriatic–Ionian exchanges. This weakening and shallowing of the Adriatic–Ionian thermohaline circulation has also been simulated with coarse

atmosphere–ocean models (Somot et al. 2006) and likely results from an increased stratification and a decrease in dense water production in the southern Adriatic (Parras–Berrocal et al. 2023). The peculiar behaviour of the SAP compared to the coastal areas of the Adriatic could also be linked to boundary issues. However, the AdriSC open boundary is positioned well south of the strait of Otranto and the AdriSC historical simulation didn't exhibit such behaviour. Further, the regional climate model used in the PGW approach, the LMDZ4–NEMOMED8 model, doesn't display systematic issues and is regularly used in the Med–CORDEX ensembles. The SAP behaviour might thus be the consequence of an excessive warming of the Adriatic Sea compared to the central Mediterranean under the far–future climate conditions but the sensitivity to the density interplay at the strait of Otranto should be further studied to reach any firm conclusion.

All the processes discussed above need to be further investigated as trends, variability and extreme events averaged over large subdomains are not appropriate methodologies to understand the atmosphere–ocean dynamical properties.

5.3.2 Comparison to previous studies and limitations

As trends and variability are generally well reproduced by RCMs, the EURO– (Coppola et al. 2021) and Med–CORDEX (Ruti et al. 2016) ensembles are used to perform a comparative evaluation of the far–future AdriSC projections.

Ivušić et al. (2021) analysed the EURO–CORDEX ensemble precipitations over the Adriatic region for the far–future period (2071–2100) with respect to the historical period (1971–2000). They found a considerable reduction of the total precipitation during the summer months associated with a decrease of the number of rainy days over the entire region and strong south–north gradients particularly during the winter months when the precipitation intensity could increase. Baronetti et al. (2022) analysed both EURO– and Med– CORDEX simulations in northern Italy for the same periods and also found a north–south spatial gradient as well as an intensification of the droughts. Under the far–future AdriSC projections, the number of days with extreme precipitation is also expected to decrease during summer and to increase during winter over both the land and sea domains. In terms of south–north gradients, the most intense positive precipitation trends are mostly located over the Adriatic Sea and below 44 °N of latitude, while the negative trends cover the Pannonian plain mostly above 44 °N of latitude. However, following the trends and variability analyses, the land–sea contrasts also highlighted

in Coppola et al. (2021) are much more pronounced than the south–north gradients in the AdriSC results.

Belušić Vozila et al. (2019) used two members of the EURO–CORDEX ensemble to analyse the far–future near–surface winds over the Adriatic region. They found a reduction in the number of bora events, an increase in the number of sirocco events in the northern Adriatic during the winter season, and a decrease of the intensity of both bora and sirocco events, except in the northern Adriatic for the bora events. The AdriSC far–future results also project a decrease in the intensity of the wind speeds over the entire Adriatic region particularly during winter time as well as a decrease in the number of extreme events above the maximum historical threshold over the sea subdomain particularly during January–April which is the period during which strong bora events occur. The increase in sirocco events cannot be seen in the presented AdriSC results which average the wind speed conditions over the entire sea subdomain.

Parras–Berrocal et al. (2023) analysed the REMO–OASIS–MPIOM model results (Sein et al. 2015) of the Med–CORDEX ensemble and found that the projected dense water formation could be reduced by 75 % in the Adriatic Sea (84 % in the Aegean Sea, 83 % in the Levantine Sea) by the end of the century due to hydrographic changes in surface and intermediate water that strengthen the vertical stratification, hampering vertical mixing and thus convection. As documented by Soto-Navarro et al. (2020), the changes will manifest in an increase of temperature over the whole water column, more at the surface and less in deep layers, while most Med-CORDEX models are projecting an increase in salinity of the whole Adriatic for the RCP8.5 scenario. The AdriSC results are mostly aligned with these findings. First, the northern Adriatic dense water formation is expected to be reduced due to local changes (increased sea surface temperatures, decreased sea surface salinity, decreased wind speeds). Second, the changes in properties of the intermediate (decreased salinity and increased temperatures) and bottom (increased salinity and increased temperatures by 2.5 °C less than in the intermediate layer) layers over the Southern Adriatic Pit (SAP) seen by the AdriSC model also confirm a strengthening of the vertical stratification potentially linked to the Ionian–Adriatic exchanges.

Finally, the limitations of the AdriSC far–future projections are twofold. First, the PGW method uses the same synoptic forcing in both historical and extreme warming runs which implies that potential changes in intra– and interannual variability might be missed. Second, as the results of only one RCM are used in the AdriSC PGW approach, the climate uncertainty,

derived by running ensembles of simulations forced by multiple global climate models under multiple warming scenarios (Semenov and Stratonovitch, 2010), is ignored.

6. CONCLUSIONS

The detailed analyses presented in this thesis underscore the feasibility and the unique benefits of using an ultra–high–resolution atmosphere–ocean model to simulate the Adriatic basin climate at various temporal and spatial scales. Such an approach is novel as the implementation of the new generation of ultra–high–resolution, kilometre–scale, coupled climate models within the World Climate Research Programme (WCRP) started in 2022 (WCRP 2022). Further, as highlighted by the WCRP kilometre–scale research group, running and analysing such models creates enormous (exascale) challenges in particular concerning the handling of the enormous data volumes (i.e. higher spatial resolution and higher frequency in time of the model output than in regional climate models) generated by such climate simulations. Despite these challenges, and thanks to the generous allocation of numerical resources on the ECMWF HPC — through several Special Projects and Croatian national quota with the support of DHMZ — the Adriatic Sea and Coast (AdriSC) climate model has now been implemented and analysed for an ensemble of extreme windstorms, as well as, for two 31–year–long climate simulations.

This thesis has demonstrated that the AdriSC climate model is capable to offer a more precise representation of the Adriatic climate — particularly in the coastal areas of the semi–enclosed basin — than the RCMs of the CORDEX experiment. In these coastal areas, complex local processes, like the bora and dense water dynamics, play important roles in shaping the regional climate which RCMs struggle to capture adequately due to their coarser resolutions in both atmosphere and ocean. This leads to large biases and, generally, the underrepresentation of these critical processes. In contrast, the kilometre–scale atmosphere–ocean AdriSC climate model effectively replicates the most important processes specific to the Adriatic coastal region, including the bora dynamics and the decadal thermohaline variability of the Adriatic Sea. In particular, this thesis highlighted that the proper representation of the bora–driven sea surface cooling within the Kvarner Bay may be critical to the accurate modelling of the dense water formation in the northern Adriatic shelf. For that, the AdriSC model resolutions of 3 km in the atmosphere and 1 km in the ocean are found appropriate for leveraging balance between model accuracy and efficiency. The AdriSC model was also found to be the first climate model capable to capture the impact of the BiOS regimes within the Adriatic Sea. Convincingly, the enhanced precision offered by kilometre–scale climate modelling allows for more accurate representations and, hence, projections of many extreme climate events (e.g. heatwaves, extreme rainfalls, droughts, wind–waves, storm surges).

The added value of kilometre–scale modelling also lies in its ability to uncover trends and variations that were previously unknown. In particular, this thesis underscores the extensive and profound changes in trends, variability and extremes expected in the Adriatic region due to ongoing and projected future climate variations. These changes occur in both the atmosphere and the ocean, suggesting substantial implications for the environment, the society, and the regional economy. Key conclusions from the thesis encompass several main processes like heatwaves, extreme rainfall, droughts, ocean salinity, etc., but also the importance of using kilometre–scale climate models in order to adequately simulate and prepare for these changes in the Adriatic basin. Concerning the heatwaves, extreme rainfalls, and droughts, a consistent warming trend is already felt across the Adriatic basin over the recent decades. This notable rise in temperatures is evident in both the atmosphere and the ocean. Projections under extreme warming suggest the persistence and potential intensification of these trends, particularly during summer months, indicating an increased frequency and duration of heatwaves. This is foreseen to bring an increased number of days of extreme heat and substantial temperature rises, coupled with altered precipitation patterns. In particular, the results suggest intensified winter rainfall and summer droughts due to changes in humidity and the hydrological cycle. Changes in the timing and intensity of rainfall across different seasons are also expected, potentially heightening the risks of droughts or floods. These changes hold significance for agricultural practices, water resource management, and infrastructure resilience. In the Adriatic Sea, changes in salinity patterns signal increased evaporation over precipitation and river runoff, particularly notable during summer. Salinity variations near river plumes and distinct impacts across different regions and layers within the Adriatic Sea are anticipated. When it comes to the important process of dense water formation, the trend, variability, and extreme results show that factors contributing to dense water formation in the Adriatic are expected to undergo significant shifts. Decreased wind speeds, changes in sea surface temperatures, precipitation patterns, river discharges, and alterations in relative humidity during bora events collectively suggest a decrease in the formation of dense waters. In contrast, the analysis of the short–term extreme bora simulations and the associated sea surface cooling, shows that despite the decreased bora wind speeds, the decrease in relative humidity is expected to amplify sea surface cooling during bora events. Though these insights differ from past findings, they emphasise the need for further research and validation.

In light of the projected climate changes described in this thesis, it is now crucial to establish informed policy strategies, undertake regional planning, and formulate adaptive

measures to mitigate the potential adverse effects on the environment, society, and the economy in the Adriatic region. The use of kilometre–scale models, exemplified by the AdriSC model, greatly advances our understanding of the local climate dynamics, enabling a more comprehensive assessment of the Adriatic's unique climatic characteristics and their implications for various sectors and communities. Consequently, the AdriSC experiment should now be generalised by implementing and running more kilometre–scale atmosphere–ocean models forced by more regional models under more climate scenarios in the Adriatic region. This ensemble of simulations could then be used to derive robust climate hazard assessments at the local scale, with higher reliability of reproduction of extreme values and more reliable quantification and projections of the most extreme events in both atmosphere and ocean (e.g. coastal flooding, flash floods, droughts, wildfires, etc.) than the available ensembles of coarser resolution models.

7. PROŠIRENI SAŽETAK

Posljedice globalnog zagrijavanja nisu samo perspektiva daleke budućnosti, već i sadašnja stvarnost. Ubrzani porast temperature utjecao je na mnoge aspekte svijeta u kojem živimo, poput otapanja morskog leda, ubrzanog rasta razine mora te duljih i intenzivnijih toplinskih valova. Klimatske promjene su prostorno nehomogene i različito utječu na različite regije svijeta, dok je sposobnost tih regija da se prilagode i ublaže klimatske rizike ključna za dobrobit lokalnih zajednica. Zbog tih promjena na regionalnoj razini i s njima povezanih rizika, potreba donositelja politika i njihovih savjetnika za točnim regionalnim i lokalnim informacijama o globalnom zatopljenju veća je nego ikada. Stoga klimatske studije moraju pružiti razumijevanje fizičkih procesa koji upravljaju trendovima i promjenama klime na regionalnoj i lokalnoj razini. To posebno vrijedi za Sredozemno more, koje je prepoznato kao "žarište" vrlo osjetljivo na klimatske promjene, sa zagrijavanjem u prosjeku 20% bržim nego u ostatku svijeta. Njegov najsjeverniji bazen, Jadransko more, duboko je urezan u europsko kopno, te je stoga njegova klima snažno definirana kompleksnom orografijom, kontrastom između kopna i mora, intenzivnom interakcijom atmosfere i mora i nizom složenih dinamičkih procesa različitih razmjera koji predstavljaju izazove za adekvatno modeliranje klime. Budući da združeni atmosfersko-oceanski klimatski modeli na globalnoj i regionalnoj razini (GCM-ovi, RCM-ovi) imaju relativno grubu prostornu razlučivost (u rasponu od stotina do desetaka kilometara), uglavnom nisu prikladni za procjenu utjecaja klimatskih promjena na lokalnoj razini. Stoga je potrebno premostiti jaz između tih studija i utjecaja klimatskih promjena na lokalnoj razini. Atmosferski klimatski modeli s prostornom razlučivošću od kilometra već neko vrijeme su u mogućnosti uključivati precizniju topografiju i obale, te vjerodstojnije reproducirati interakcije atmosfere i mora u usporedbi s GCM-ovima i RCM-ovima u jadranskom području. Oni bolje prikazuju fenomene poput orografski uvjetovanih varijacija u oborinama, vjetru i ravnoteži površinske energije (Gutowski et al. 2020), što je izuzetno važno u obalnim (Estournel et al. 2021) i planinskim (Prein et al. 2016) regijama poput jadranske.

Klimatski model Jadranskog mora i obale (AdriSC) s razlučivošću od kilometra nedavno je razvijen kako bi precizno reproducirao atmosferske i oceanske procese na različitim vremenskim i prostornim skalama iznad Jadranskog mora i sjevernog Jonskog mora, obuhvaćajući utjecaj klimatskih promjena na ekstremne događaje te operativnu prognozu ekstremnih razina mora duž hrvatske obale. Klimatska komponenta AdriSC modela usmjerena je na proučavanje dugoročnih atmosferskih i oceanskih procesa u jadranskom području s razlučivošću od kilometra. Korištena su dva pristupa: (1) dugoročne simulacije obuhvatile su

razdoblje od 1987. do 2017. za sadašnju klimu, te su projicirale klimu daleke budućnosti s visokim emisijama stakleničkih plinova prema scenariju Representative Concentration Pathway (RCP) 8.5 za razdoblje od 2070. do 2100. (2) Kratkoročne simulacije obuhvatile su razdoblje od 1977. do 2017. za sadašnju klimu i projicirale buduće klime (RCP4.5, RCP8.5) za razdoblje od 2060. do 2100., fokusirajući se na brojne ekstremne događaje. Simulacije daleke budućnosti koristile su metodu pseudo-globalnog zagrijavanja (PGW), nedavno proširenu na združene atmosfersko-oceanske modele.

Zbog kompleksne orografije i batimetrije Jadranske regije, glavna teza ove disertacije je da se utjecaj klimatskih promjena u ovom području može opisati samo pomoću kompleksnih atmosfersko-oceanskih modela s razlučivošću od kilometra ili manje, poput AdriSC modela. Budući da je ovaj model već uspješno validiran na cijelom jadranskom području na temelju velikog skupa *in situ* i daljinskih mjerenja (Denamiel et al. 2021b; Pranić et al. 2021), cilj ovog doktorskog istraživanja je analizirati rezultate AdriSC simulacija za povijesne uvjete (1987.–2017.) i uvjete umjerenog i ekstremnog zagrijavanja u dalekoj budućnosti (RCP 4.5 i RCP 8.5; 2070.–2100.) kako bi se procijenio lokalni utjecaj klimatskih promjena na obalna područja Jadranskog mora.

Dokumentirane su prednosti modeliranja s razlučivošću kilometra u jadranskom području kroz istraživanja dvaju fenomena: (1) ekstremnih bura, pri čemu se istraživala osjetljivost na horizontalnu razlučivost atmosferskog modela te prostorna svojstva bure, te (2) varijacije termohalinih svojstava Jadrana uzrokovane BiOS-om. Procijenjen je i utjecaj klimatskih promjena na ekstremne bure u dalekoj budućnosti, kao i na hlađenje morske površine pri čemu se stvara sjevernojadranska voda visoke gustoće. Napravljena je detaljna analiza trendova, varijabilnosti i ekstrema u atmosferi i oceanu pod sadašnjim (1987.–2017.) i budućim (RCP 8.5, 2070.–2100.) klimatskim uvjetima. Razmotrene su implikacije tih promjena, posebice njihov utjecaj na dinamiku atmosfere i mora u jadranskom području, a rezultati analiza uspoređeni su s prethodnim istraživanjima.

Pri analizi ekstremnih bura zaključeno je da pravilno modeliranje ohlađivanja morske površine pod utjecajem bure u Kvarnerskom zaljevu igra ključnu ulogu u preciznom simuliranju formacije gustih voda na sjevernom dijelu jadranskog šelfa. Ovaj rezultat postignut je zahvaljujući visokoj rezoluciji AdriSC modela od 3 km u atmosferi i 1 km u moru. Pri analizi varijacija termohalinih svojstava uzrokovanih BiOS-om pokazano je da je AdriSC model prvi klimatski model koji uspješno bilježi utjecaj BiOS-a na svojstva Jadranskog mora. Ove

činjenice naglašavaju vrijednost poboljšane preciznosti koju pruža kilometarsko modeliranje klime, omogućujući tako preciznije reprezentacije i prognoze ekstremnih klimatskih događaja poput toplinskih valova, ekstremnih oborina, suša, vjetrova, valova te oluja. Također, identificirane su i kvantificirane sveobuhvatne i značajne promjene u trendovima, varijabilnosti i ekstremima u Jadranskom području zbog aktualnih i predviđenih budućih klimatskih varijacija i u atmosferi i u moru, što ukazuje na potencijano značajne implikacije za okoliš, društvo i regionalno gospodarstvo. Pri analizi toplinskih valova, ekstremnih oborina i suša, već je primjećen trend porasta temperature u atmosferi i moru u posljednjim desetljećima širom jadranskog područja. Projekcije pod utjecajem ekstremnog zagrijavanja sugeriraju postojanost i potencijalno pojačanje tih trendova, posebno tijekom ljetnih mjeseci, što ukazuje na povećanu učestalost i trajanje toplinskih valova. Očekuje se da će doći do povećanja broja dana s ekstremnom toplinom i značajnog porasta temperature, uz promijenjen uzorak oborina. Konkretno, rezultati sugeriraju intenziviranje zimskih oborina i ljetnih suša zbog promjena u vlažnosti i hidrološkom ciklusu. Očekuju se promjene u intenzitetu oborina tijekom različitih godišnjih doba, što može povećati rizik od suša ili poplava. Ove promjene imaju potencijalno značajne posljedice za poljoprivredu, upravljanje vodnim resursima i otpornost infrastrukture. U Jadranskom moru, promjene u uzorcima saliniteta ukazuju na povećano isparavanje u odnosu na oborine i riječni dotok, posebno tijekom ljeta. Očekuju se varijacije saliniteta blizu ušća rijeka i različiti utjecaji na različite regije i slojeve unutar Jadranskog mora. Što se tiče važnog procesa formiranja voda visoke gustoće, rezultati pokazuju da faktori koji doprinose formiranju tih voda u Jadranskom moru očekuju značajne promjene. Smanjenje brzine vjetra, promjene u temperaturi morske površine, obrasci oborina, dotok rijeka i promjene u relativnoj vlažnosti tijekom događaja snažne bure sugeriraju smanjenje formiranja voda visoke gustoće. Nasuprot tome, analiza kratkoročnih simulacija ekstremnih bura i povezanog hlađenja morske površine pokazuje da će, unatoč smanjenju brzine bure, smanjenje relativne vlažnosti pojačati hlađenje morske površine tijekom tih događaja snažne bure. Iako ovi rezultati odstupaju od prethodnih saznanja, ističu potrebu za daljnjim istraživanjem i provjerom.

S obzirom na negativne učinke navedenih klimatskih promjena na ljude i različite gospodarske sektore, razumijevanje i predviđanje ovih promjena ključno je za donositelje odluka i lokalne zajednice kako bi razvili učinkovite strategije prilagodbe i ublažavanja. Stoga bi simulacije AdriSC modelom trebale biti proširene pokretanjem ansambla atmosfersko-

oceanskih modela visoke razlučivosti, uzimajući u obzir više scenarija klimatskih promjena u jadranskom području.

8. REFERENCES

Adloff F, Jordà G, Somot S, Sevault F, Arsouze T, Meyssignac B, et al. (2018) Improving sea-level simulation in Mediterranean regional climate models. Clim Dyn 51:1167–1178. https://doi.org/10.1007/s00382-017-3842-3

Allen M, Ingram W (2002) Constraints on future changes in climate and the hydrologic cycle. Nature 419, 224–232. https://doi.org/10.1038/nature01092

Alpers W, Ivanov A, Horstmann J (2009) Observations of Bora events over the Adriatic Sea and Black Sea by spaceborne synthetic aperture radar. Mon Weather Rev 137:1150-1161. https://doi.org/10.1175/2008MWR2563.1

Amante C, Eakins BW (2009) ETOPO1 1 arc–minute global relief model: procedures, data sources and analysis, NOAA Technical Memorandum NESDIS NGDC–24.

Anagnostopoulou C, Tolika K, Lazoglou G, Maheras P (2017) The exceptionally cold January of 2017 over the Balkan Peninsula: a climatological and synoptic analysis. Atmosphere 8:252. https://doi.org/10.3390/atmos8120252

Argueso D, Evans JP, Fita L, Bormann KJ (2014) Temperature response to future urbanization and climate change. Clim Dyn 42:2183–2199. https://doi.org/10.1007/s00382-013-1789-6

Artegiani A, Salusti E (1987) Field observation of the flow of dense water on the bottom of the Adriatic Sea during the winter of 1981. Oceanol Acta 10:387–391

Artegiani A, Bregant D, Paschini E, Pinardi N, Raicich, F, Russo A (1997a) The Adriatic Sea general circulation, 1: Air–Sea Interactions and Water Mass Structure. J Phys Oceanogr 27:1492–1514.

Artegiani A, Bregant D, Paschini E, Pinardi N, Raicich F, Russo A (1997b) The Adriatic Sea general circulation, 2: Baroclinic circulation structure. J Phys Oceanogr 27:1515–1532.

Ban N, Schmidli J, Schär C (2015) Heavy precipitation in a changing climate: Does short-term summer precipitation increase faster?. Geophys Res Lett 42:1165– 1172. https://doi.org/10.1002/2014GL062588

Bajo M, Međugorac I, Umgiesser G, Orlić M (2019) Storm surge and seiche modelling in the Adriatic Sea and the impact of data assimilation. Q J Roy Meteorol Soc 145:2070–2084. https://doi.org/10.1002/qj.3544

Baronetti A, Dubreuil V, Provenzale A et al. (2022) Future droughts in northern Italy: high-resolution projections using EURO-CORDEX and MED-CORDEX ensembles. Clim Change 172:22. https://doi.org/10.1007/s10584-022-03370-7

Batistić M, Garić R, Molinero JC (2014) Interannual variations in Adriatic Sea zooplankton mirror shifts in circulation regimes in the Ionian Sea. Clim Res 61:231–240. https:// doi. org/ 10. 3354/cr012 48

Béranger K, Drillet Y, Houssais M-N, Testor P, Bourdallé-Badie R, Alhammoud B et al. (2010) Impact of the spatial distribution of the atmospheric forcing on water mass formation in the Mediterranean Sea. J Geophys Res 115:C12041. https://doi.org/10.1029/2009JC005648

Beg Paklar G, Isakov V, Koračin D, Kourafalou V, Orlić M (2001) A case study of bora-driven flow and density changes on the Adriatic Shelf (January 1987). Cont Shelf Res 21:1751-1783. https://doi.org/10.1016/S0278-4343(01)00029-2

Bellafiore D, Bucchignani E, Gualdi S, Carniel S, Djurdjević V, Umgiesser G (2012) Assessment of meteorological climate models as inputs for coastal studies. Ocean Dyn 62:1-14. 10.1007/s10236-011-0508-2.

Belušić D, Klaić, ZB (2004) Estimation of bora wind gusts using a limited area model, Tellus A 56:296–307. https://doi.org/10.1111/j.1600–0870.2004.00068.x

Belušić D, Klaić ZB (2006) Mesoscale dynamics, structure and predictability of a severe Adriatic bora case. Meteorol Z 15:157–168.

Belušić D, Žagar M, Grisogono B (2007) Numerical simulation of pulsations in the bora wind, Q J Roy Meteorol. Soc 133:1371–1388. https://doi.org/10.1002/qj.12

Belušić D, Hrastinski M, Večenaj Ž, Grisogono B (2013) Wind regimes associated with a mountain gap at the northeastern Adriatic coast. J Appl Meteorol Clim 52:2089–2105. https://doi.org/10.1175/JAMC–D–12–0306.1

Belušić A, Prtenjak MT, Güttler I, Ban N, Leutwyler D, Schär C (2017) Near–surface wind variability over the broader Adriatic region: Insights from an ensemble of regional climate models. Clim Dyn 50:4455–4480. https://doi.org/10.1007/s00382–017–3885–5

Belušić Vozila A, Güttler I, Ahrens B, Obermann-Hellhund A, Telišman Prtenjak M (2019) Wind over the Adriatic region in CORDEX climate change scenarios. J Geophys Res Atmos 124:110–130. https://doi.org/10.1029/2018JD028552

Belušić Vozila A, Telišman Prtenjak M, Güttler I (2021) A weather-type classification and its application to near-surface wind climate change projections over the Adriatic region. Atmosphere 12:948. https://doi.org/10.3390/atmos12080948

Benetazzo A, Fedele F, Carniel S, Ricchi A, Bucchignani E, Sclavo M (2012) Wave climate of the Adriatic Sea: a future scenario simulation. Nat Hazards Earth Syst Sci 12:2065–2076. https://doi.org/10.5194/nhess-12-2065-2012

Bergamasco A, Oguz T, Malanotte-Rizzoli P (1999) Modeling dense water mass formation and winter circulation in the Northern and Central Adriatic Sea. J Mar Syst 20:279–300.

Bernstein L, Bosch P, Canziani O, Chen Z, Christ R, Riahi K (2008) IPCC, 2007: Climate Change 2007: Synthesis Report. Geneva: IPCC. ISBN 2-9169-122-4

Bessières L, Rio MH, Dufau C, Boone C, Pujol MI (2013) Ocean state indicators from MyOcean altimeter products. Ocean Sci 9(3):545–560.

Beuvier J, Sevault F, Herrmann M, Kontoyiannis H, Ludwig W, Rixen M et al. (2010) Modeling the Mediterranean Sea interannual variability during 1961–2000: Focus on the Eastern Mediterranean Transient. J Geophys Res Atmos 115:C08017. https://doi.org/10.1029/2009JC005950

Biolchi S, Furlani S, Devoto S, Scicchitano G, Korbar T, Vilibić I, Šepić J (2019a) The origin and dynamics of coastal boulders in a semi–enclosed shallow basin: a northern Adriatic case study. Mar Geol 411:62–77. https://doi.org/10.1016/j.margeo.2019.01.008

Biolchi S, Denamiel C, Devoto S, Korbar T, Macovaz V, Scicchitano G et al. (2019b) Impact of the October 2018 Storm Vaia on coastal boulders in the northern Adriatic Sea. Water 11:2229. https://doi.org/10.3390/w11112229

Blasnig M, Riedel B, Schiemer L, Zuschin M, Stachowitsch M (2013) Short-term post-mortality scavenging and longer term recovery after anoxia in the northern Adriatic Sea. Biogeosciences 10:7647–7659. https://doi.org/10.5194/bg-10-7647-2013

Bonacci O, Andrić I, Vrsalović A, Bonacci D (2021a) Precipitation regime changes at four Croatian meteorological stations. Atmosphere 12:885. https://doi.org/10.3390/atmos12070885

Bonacci O, Bonacci D, Patekar M, Pola M (2021b) Increasing trends in air and sea surface temperature in the central Adriatic Sea (Croatia) J Mar Sci Eng 9:358. https://doi.org/10.3390/jmse9040358

Booij N, Holthuijsen LH, Ris RC (1996) The SWAN wave model for shallow water, Proc. 25th Int. Conf. Coastal Engng, Orlando, USA, Vol. 1, pp. 668-676.

Borzelli GL, Gačić M, Cardin V, Civitarese G (2009) Eastern Mediterranean transient and reversal of the Ionian Sea circulation. Geophys Res Lett. 36, L15108, https://doi.org/10.1029/2009GL039261

Brogli R, Sørland SL, Kröner N, Schär C (2019a) Causes of future Mediterranean precipitation decline depend on the season. Environ Res Lett 14:114017. https://doi.org/10.1088/1748-9326/ab4438

Brogli R, Kröner N, Sørland SL, Lüthi D, Schär C (2019b) The role of Hadley circulation and lapse-rate changes for the future European summer climate. J Clim 32:385–404. https://doi.org/10.1175/JCLI-D-18-0431.1

Brzović N, Strelec Mahović N (1999) Cyclonic activity and severe jugo in the Adriatic Phys. Chem. Earth, B: Hydrol Oceans & Atmos. 24:653-657, https://doi.org/10.1016/S1464-1909(99)00061-1.

Budillon G, Bue NL, Siena G, Spezie G (2010) Hydrographic characteristics of water masses and circulation in the Northern Ionian Sea. Deep Sea Res II 57:441–457.

Buljan M (1953) Fluctuations of salinity in the Adriatic, Izvještaj Republičke ribarstveno-biološke ekspedicije “Hvar” 1948–1949. Acta Adriat 2:1–64.

Buljan M, Zore-Armanda M (1976) Oceanographic properties of the Adriatic Sea. Oceanogr Mar Biol Annu Rev 14:11–98.

Burrage DM, Book JW, Martin PJ (2009) Eddies and filaments of the Western Adriatic Current near Cape Gargano: analysis and prediction. J Mar Syst 78:S205–S226. https://doi.org/10.1016/j.jmarsys.2009.01.024

Cardin V, Wirth A, Khosravi M, Gačić M (2020) South Adriatic recipes: estimating the vertical mixing in the deep Pit. Front Mar Sci 7:1015. https://doi.org/10.3389/fmars.2020.565982

Carniel S, Benetazzo A, Bonaldo D, Falcieri FM, Miglietta MM, Ricchi A, et al. (2016) Scratching beneath the surface while coupling atmosphere, ocean and waves: Analysis of a dense water formation event. Ocean Model 101:101-112. https://doi.org/10.1016/j.ocemod.2016.03.007

Cavaleri L, Bertotti L, Tescaro N (1997) The modelled wind climatology of the Adriatic Sea. Theor Appl Climatol 56:231–254, https://doi.org/10.1007/BF00866430

Cavaleri L, Bertotti L, Buizza R, Buzzi A, Masato V, Umgiesser G, et al. (2010) Predictability of extreme meteo–oceanographic events in the Adriatic Sea. Q J Roy Meteorol Soc 136:400–413. https://doi.org/10.1002/qj.567

Chapman DC (1985) Numerical treatment of cross–shelf open boundaries in a barotropic coastal ocean model. J Phys Oceanogr 15:1060–1075. https://doi.org/10.1175/1520–0485(1985)0152.0.CO;2.

Chiaudani G, Marchetti R, Vighi M (1980) Eutrophication in Emilia-Romagna coastal waters (North Adriatic Sea, Italy): a case history. Prog. Water Technol., 12

Chripko S, Msadek R, Sanchez-Gomez E, Terray L, Bessieres L, Moine MP (2021) Impact of reduced Arctic Sea ice on Northern Hemisphere climate and weather in autumn and winter. J Clim 34:5847-5867. https://doi.org/10.1175/JCLI-D-20-0515.1

Christensen JH, Hewitson B, Busuioc A, Chen A, Gao X, Held I et al. (2007) Regional climate projections. In: Solomon S, Qin D, Manning M, Chan Z, Marquis M, Averyt KB, Tignor M, Miller HL (eds) Climate Change 2007: The Physical Science Basis. Contribution of Working Group I to the Fourth Assessment Report of the Intergovernmental Panel on Climate Change, Cambridge University Press, Cambridge, 847-940.

Ciglenečki I, Vilibić I, Dautović J, Vojvodić V, Ćosović B, Zemunik P et al. (2020) Dissolved organic carbon and surface active substances in the northern Adriatic Sea: long-term trends, variability and drivers. Sci Total Environ 730:139104. https://doi.org/10.1016/j.scitotenv.2020.13910

Civitarese G, Gačić M, Lipizer M, Eusebi Borzelli GL (2010): On the impact of the Bimodal Oscillating System (BiOS) on the biogeochemistry and biology of the Adriatic and Ionian Seas (Eastern Mediterranean). Biogeosciences 7:3987–3997.

Climate Risk Profile: Croatia (2021): The World Bank Group.

Conan P, Testor P, Estournel C, D'Ortenzio F, Pujo-Pay M, Durrieu de Madron X (2018) Preface to the Special Section: Dense water formations in the northwestern Mediterranean: From the physical forcings to the biogeochemical consequences. J Geophys Res Oceans 123:6983–6995. https://doi.org/10.1029/2018JC014301

Coppola E, Nogherotto R, Ciarlò JM, Giorgi F, van Meijgaard E, Kadygrov N et al. (2021) Assessment of the European climate projections as simulated by the large EURO-CORDEX regional and global climate model ensemble. J Geophys Res Atmos 126:e2019JD032356. https://doi.org/10.1029/2019JD032356

Cushman–Roisin B, Gačić M, Poulain PM, Artegiani A (2001) Physical Oceanography of the Adriatic Sea: Past, Present and Future. Kluwier Academic Publisher, Dordrecht, 2001, pp. 67-109. doi:10.1007/978-94-015-9819-4_3

Cushman–Roisin B, Naimie CE (2002) A 3d finite–element model of the Adriatic tides. J Mar Syst 37:279–297. https://doi.org/10.1016/S0924–7963(02)00204–X

Cushman-Roisin B, Korotenko KA, Galos CE, Dietrich DE (2007) Simulation and characterization of the Adriatic Sea mesoscale variability. J Geophys Res Oceans 112:C03S14. https://doi.org/10.1029/2006JC003515

Darmaraki S, Somot S, Sevault F et al. (2019) Future evolution of Marine Heatwaves in the Mediterranean Sea. Clim Dyn 53, 1371–1392. https://doi.org/10.1007/s00382-019-04661-z

Davolio S, Stocchi P, Benetazzo A, Bohm E, Riminucci F, Ravaioli M et al. (2015) Exceptional bora outbreak in winter 2012: Validation and analysis of high-resolution atmospheric model simulations in the northern Adriatic area. Dyn Atmos Oceans 71:1–20. https://doi.org/10.1016/j.dynatmoce.2015.05.002

Davolio S, Henin R, Stocchi P, Buzzi A (2017) Bora wind and heavy persistent precipitation: atmospheric water balance and role of air-sea fluxes over the Adriatic Sea. Q J Roy Meteorol Soc 143:1165-1177. https://doi.org/10.1002/qj.3002

Dee DP, Uppala SM, Simmons AJ, Berrisford P, Poli P, Kobayashi S et al. (2011) The ERA-Interim reanalysis: configuration and performance of the data assimilation system. Q J Roy Meteorol Soc 137:553–597. https://doi.org/10.1002/qj.828

Denamiel C, Šepić J, Ivanković D, Vilibić I (2019) The Adriatic Sea and Coast modelling suite: evaluation of the meteotsunami fore-cast component. Ocean Model 135:71–93. https://doi.org/10.1016/j.ocemod.2019.02.003

Denamiel C, Pranić, P, Quentin F et al. (2020a) Pseudo–global warming projections of extreme wave storms in complex coastal regions: the case of the Adriatic Sea. Clim Dyn 55:2483–2509. https://doi.org/10.1007/s00382–020–05397–x

Denamiel C, Tojčić I, Vilibić I (2020b) Far future climate (2060–2100) of the northern Adriatic air–sea heat transfers associated with extreme bora events. Clim Dyn 55:3043–3066. https://doi.org/10.1007/s00382-020-05435-8

Denamiel C, Tojčić I, Vilibić I (2021a) Balancing accuracy and efficiency of atmospheric models in the northern Adriatic during severe bora events. J Geophys Res Atmos 126:e2020JD033516. https://doi. org/10.1029/2020JD033516

Denamiel C, Pranić P, Ivanković D, Tojčić I, Vilibić I (2021b) Performance of the Adriatic Sea and coast (AdriSC) climate component—a COAWST V3.3-based coupled atmosphere–ocean modelling suite: atmospheric dataset. Geosci Model Dev 14:3995–4017. https:// doi. org/ 10. 5194/ gmd- 14- 3995- 2021

Denamiel C, Tojčić I, Pranić P et al. (2022) Modes of the BiOS-driven Adriatic Sea thermohaline variability. Clim Dyn 59, 1097–1113. https://doi.org/10.1007/s00382-022-06178-4

Denson E, Wasko C, Peel M (2021) Decreases in relative humidity across Australia. Environ. Res Lett 16, Iss. 7, DOI:10.1088/1748-9326/ac0aca

Dietrich JC, Tanaka S, Westerink JJ et al. (2012) Performance of the unstructured-mesh, SWAN+ADCIRC model in computing hurricane waves and surge. J Sci Comput 52:468–497 https://doi.org/10.1007/s10915-011-9555-6

Djakovac T, Degobbis D, Supić N, Precali R (2012) Marked reduction of eutrophication pressure in the northeastern Adriatic in the period 2000-2009. Estuar Coast Shelf Sci 115:25-32. https://doi.org/10.1016/j.ecss.2012.03.029.

Dorman CE, Carniel S, Cavaleri L, Sclavo M, Chiggiato J, Doyle J et al. (2006) February 2003. Marine atmospheric conditions and the bora over the northern Adriatic. J Geophys Res Oceans 111:C03S03.

Dudhia J (1989) Numerical study of convection observed during the winter monsoon experiment using a mesoscale two–dimensional model. J Atmos Sci 46:3077–3107.

Dudhia J (1996) A Multi–Layer Soil Temperature Model for MM5, Sixth PSU/NCAR Mesoscale Model Users' Workshop, Boulder, 22–24 July 1996, 49–50

Dunić N, Vilibić I, Šepić J, Somot S, Sevault F (2018) Dense water formation and BiOS-induced variability in the Adriatic Sea simulated using an ocean regional circulation model. Clim Dyn 51(3):1211–1236.

Dunić N, Vilibić I, Šepić J, Mihanović H, Sevault F, Somot S et al. (2019) Performance of multi-decadal ocean simulations in the Adriatic Sea. Ocean Model 134:84–109. https://doi.org/10.1016/j.ocemod.2019.01.006

Dutour Sikirić M, Janeković I, Kuzmić, M (2009) A new approach to bathymetry smoothing in sigma–coordinate ocean models. Ocean Model 29:128–136. https://doi.org/10.1016/j.ocemod.2009.03.009

Ebisuzaki W (1997) A method to estimate the statistical significance of a correlation when the data are serially correlated. J Clim 10(9):2147–2153. https://doi.org/10.1175/1520-0442(1997)010%3c2147:amtets%3e2.0.co;2

Estournel C, Marsaleix P, Ulses C (2021) A new assessment of the circulation of Atlantic and intermediate waters in the Eastern Mediterranean. Prog Oceanogr 198:102673. https:// doi. org/ 10. 1016/j. pocean. 2021. 102673

Eusebi Borzelli GL, Carniel S (2023) A reconciling vision of the Adriatic-Ionian Bimodal Oscillating System. Sci Rep 13, 2334. https://doi.org/10.1038/s41598-023-29162-2

Fedele G, Mauri E, Notarstefano G, Poulain P-M (2022) Characterization of the Atlantic Water and Levantine Intermediate Water in the Mediterranean Sea using 20 years of Argo data. Ocean Sci 18:129-142. https://doi.org/10.5194/os-18-129-2022

Flather RA (1976) A tidal model of the north–west European continental shelf, Mem. Soc. R. Sci Liege, 6, 141–164

Fosser, G, Khodayar S, Berg P (2016) Climate change in the next 30 years: what can a convection-permitting model tell us that we did not already know? Clim Dyn 48:1987–2003. https//doi.org/10.1007/s00382-016-3186-4

Franco P, Michelato A (1992) Northern Adriatic Sea: Oceanography of the basin proper and of the western coastal zone. In A. Vollenweider, R. Marchetti, & R. Viviani (Eds), Marine and Coastal Eutrophication (pp. 35–62) Amsterdam: Elsevier.

Franic Z (2005) Estimation of the Adriatic Sea water turnover time using fallout 90Sr as a radioactive tracer. Journal of Marine Systems. 57. 1–12. 10.1016/j.jmarsys.2004.11.005.

Furlan D (1977) The climate of southeast Europe. World Surv. Climatol, 6, 185–235

Gačić M, Civitarese G, Miserocchi S, Cardin V, Crise A, Mauri E (2002) The open–ocean convection in the Southern Adriatic: A controlling mechanism of the spring phytoplankton bloom. Cont. Shelf Res, 22, 1897–1908, https://doi.org/10.1016/ S0278–4343(02)00050–X

Gačić M, Borzelli GE, Civitarese G, Cardin V, Yari S (2010) Can internal processes sustain reversals of the ocean upper circulation? The Ionian Sea example, Geophys. Res. Lett, 37(9), doi:10.1029/2010GL043216

Gačić M, Civitarese G, Eusebi Borzelli GL, Kovačević V, Poulain PM, Theocharis A et al. (2011) On the relationship between the decadal oscillations of the northern Ionian Sea and the salinity distributions in the eastern Mediterranean. J Geophys Res. https://doi.org/10.1029/2011JC007280

Gačić M, Civitarese G, Kovačević V, Ursella L, Bensi M, Menna M, et al. (2014) Extreme winter 2012 in the Adriatic: an example of climatic effect on the BiOS rhythm, Ocean Sci, 10, 513–522. https://doi.org/10.5194/os–10–513–2014

Gačić M, Ursella L, Kovačević V, Menna M, Malačič V, Bensi M et al. (2021) Impact of densewater flow over a sloping bottom on open-sea circulation: laboratory experiments and an Ionian Sea (Mediterranean) example. Ocean Sci 17:975–996. https:// doi. org/ 10. 5194/ os-17- 975- 2021

Gajić-Čapka M (1993) Fluctuations and trends of annual precipitation in different climatic regions of Croatia. Theor Appl Climatol 47, 215–221. https://doi.org/10.1007/BF00866242

Gilbert RO (1987) Statistical methods for environmental pollutionmonitoring. Wiley, New York

Gilmartin M, Degobbis D, Revelante N, Smodlaka N (1990), The Mechanism Controlling Plant Nutrient Concentrations in the Northern Adriatic Sea. Int. Revue ges. Hydrobiol. Hydrogr, 75: 425-445. https://doi.org/10.1002/iroh.19900750402

Giorgi F, Lionello P (2008) Climate change projections for the Mediterranean region. Global Planet Change 63:90-104. https://doi.org/10.1016/j.gloplacha.2007.09.005

Giorgi F, Raffaele F, Coppola E (2019) The response of precipitation characteristics to global warming from climate projections, Earth Syst. Dynam, 10, 73–89, https://doi.org/10.5194/esd-10-73-2019

Gohm A, Mayr GJ, Fix A, Giez A (2008) On the onset of bora and the formation of rotors and jumps near a mountain gap. Q J R Meteorol Soc 134:21–46. https://doi.org/10.1002/qj.206

Grbec B, Matić F, Paklar GB, Morović M, Popović R, Vilibić I (2018) Long-term trends, variability and extremes of in situ sea surface temperature measured along the eastern Adriatic coast and its relationship to hemispheric processes. Pure Appl Geophys 175:4031–4036. https://doi.org/10.1007/s00024-018-1793-1

Grisogono B, Belušić D (2009) A review of recent advances in understanding the meso- and micro-scale properties of the severe Bora wind. Tellus, 61A, 1-16.

Grubišić V (2004) Bora-driven potential vorticity banners over the Adriatic. Q J Roy Meteor Soc 130:2571–2603. https://doi.org/10.1256/qj.03.71

Gualdi S, Somot S, Li L, Artale V, Adani M, Bellucci A et al. (2013) The CIRCE simulations: Regional climate change projections with realistic representation of the Mediterranean Sea. Bull Am Meteor Soc 94:65–81. https://doi.org/10.1175/BAMS-D-11-00136.1

Gutowski WJ Jr, Ullrich PA, Hall A, Leung LR, O'Brien TA, Patricola CM et al. (2020) The ongoing need for high-resolution regional climate models: process understanding and stakeholder information. Bull Am Meteorol Soc 101:E664–E683. https:// doi. org/ 10. 1175/BAMS-D- 19- 0113.1

Güttler I, Stepanov I, Branković Č, Nikulin G, Colin J (2015) Impact of Horizontal resolution on precipitation in complex orography simulated by the regional climate model RCA3. Mon Weather Rev 143:3610–3627. https:// doi. org/ 10. 1175/ MWR-D- 14- 00302.1

Hannachi A, Jolliffe IT, Stephenson DB (2007) Empirical orthogonal functions and related techniques in atmospheric science: a review. Int J Climatol 27:11191152

Hawkins E, Sutton R (2007) Variability of the Atlantic thermohaline circulation described by three-dimensional empirical orthogonal functions. Clim Dyn 29:745–762. https:// doi. org/ 10. 1007/s00382- 007- 0263-8

Hersbach H, de Rosnay P, Bell B, Schepers D, Simmons A, Soci C et al. (2018) Operational global reanalysis: Progress, future directions and synergies with NWP. ECMWF ERA Report Series 27.

Hobday A, Alexander LV, Perkins SE, Smale DA, Straub SC, Oliver ECJ et al. (2016) A hierarchical approach to defining marine heatwaves, Progress in Oceanography, Volume 141, Pages 227-238, ISSN 0079-6611, https://doi.org/10.1016/j.pocean.2015.12.014.

Hourdin F, Musat I, Bony S, Braconnot P, Codron F, Dufresne JL et al. (2006) The LMDZ4 general circulation model: climate performance and sensitivity to parametrized physics with emphasis on tropical convection. Clim Dyn 27:787–813. https://doi.org/10.1007/s00382-006-0158-0

Hurrell JW (1995) Decadal trends in the North Atlantic Oscillation index and relationship to regional temperature and precipitation. Science, 269, 676 – 679

IPCC (2007) Climate Change 2007: Impacts, Adaptation and Vulnerability. Contribution of Working Group II to the Fourth Assessment Report of the Intergovernmental Panel on Climate Change

IPCC (2022) Climate Change 2022: Impacts, Adaptation, and Vulnerability. Contribution of Working Group II to the Sixth Assessment Report of the Intergovernmental Panel on Climate Change

Ivanov VV, Shapiro GI, Huthnance JM, Aleynik DL (2004) Cascades of dense water around the world ocean. Prog Oceanogr 60:47-98.

Ivušić S, Güttler I, Horvath K (2021) Future precipitation changes over the eastern Adriatic and Dinaric Alps areas in the latest EURO-CORDEX ensemble, EMS Annual Meeting 2021, online, 6–10 Sep 2021, EMS2021-12, https://doi.org/10.5194/ems2021-12

Janeković I, Kuzmić M (2005) Numerical simulation of the Adriatic Sea principal tidal constituents, Ann. Geophys, 23, 3207–3218, https://doi.org/10.5194/angeo–23–3207–2005.

Janeković I, Mihanović H, Vilibić I, Tudor M (2014), Extreme cooling and dense water formation estimates in open and coastal regions of the Adriatic Sea during the winter of 2012, J. Geophys. Res. Oceans, 119, 3200–3218, doi:10.1002/2014JC009865.

Janeković I, Mihanović, H, Vilibić I, Grčić B, Ivatek-Šahdan S, Tudor M, Djakovac T (2020) Using multi-platform 4D-Var data assimilation to improve modeling of Adriatic Sea dynamics. Ocean Modelling. 146. 101538. 10.1016/j.ocemod.2019.101538.

Janjić Z (1994) The Step–Mountain eta Coordinate Model: Further developments of the convection, viscous sublayer, and turbulence closure schemes, Mon. Weather Rev, 122, 927–945, https://doi.org/10.1175/1520– 0493(1994)1222.0.CO;2

Jeffries MA, Lee C (2007) A mode-based climatology of the northern Adriatic Sea. J Geophys Res 112:C03S02. doi:10.1029/2006JC003664

Jenkins SR, Coleman RA, Della Santina P, Hawkins SJ, Burrows MT, Hartnoll RG (2005) Regional scale differences in the determinism of grazing effects in the rocky intertidal. Mar Ecol Prog Ser 287:77–86

Jiang Q, Doyle JD (2005) Wave breaking induced surface wakes and jets observed during a bora event. Geophys Res Lett 32:L17807. https//doi.org/10.1029/2005GL022398

Jolliffe IT (2002) Principal component analysis, 2nd edn. Springer, New York

Jordà G, Gomis D (2013) On the interpretation of the steric and mass components of sea-level variability: The case of the Mediterranean basin. J Geophys Res Oceans 118:953– 963. https//doi.org/10.1002/jgrc.20060

Josipović L, Obermann-Hellhund A, Brisson E, Ahrens B (2018) Bora in regional climate models: Impact of model resolution on simulations of gap wind and wave breaking. Croatian Meteorological Journal, 53, 31–42. https://hrcak.srce.hr/231266

Kassis D, Korres G (2020) Hydrography of the Eastern Mediterranean basin derived from Argo floats profile data. Deep-Sea Res II 171:104712. https://doi.org/10.1016/j.dsr2.2019.104712

Kehler–Poljak G, Telišman Prtenjak M, Kvakić M, Šariri K, Večenaj Ž (2017) Interaction of sea breeze and deep convection over the northeastern Adriatic Coast: An analysis of sensitivity experiments using a high–resolution mesoscale model, Pure Appl. Geophys, 174, 4197–4224, https://doi.org/10.1007/s00024–017–1607–x.

Kendall MG (1975) Rank correlation methods, 4th edn. Charles Grif-fin, London

Kendon EJ, Fowler HJ, Roberts MJ, Chan SC, Senior CA (2014) Heavier summer downpours with climate change revealed by weather forecast resolution model. Nat Clim Change 4:570–576. https//doi.org/10.1038/nclimate2258

Kendon EJ, Ban N, Roberts NM, Fowler HJ, Roberts MJ, Chan SC et al. (2017) Do convection-permitting regional climate models improve projections of future precipitation change?. Bull Am Meteor Soc 98:79–93. https://doi.org/10.1175/BAMS-D-15-0004.1

Klaić ZB, Prodanov AD, Belušić D (2009) Wind measurements in Senj—Underestimation of true bora flows. Geofizika, 26, 245–252.

Klemp JB, Durran DR (1987) Numerical modelling of Bora winds. Meteor Atmos Phys 36:215–227. https://doi.org/10.1007/BF01045150

Kokkini Z, Gerin R, Poulain P-M, Mauri E, Pasarić Z, Janeković I et al. (2017) A multiplatform investigation of Istrian Front dynamics (north Adriatic Sea) in winter 2015. Medit Mar Sci 18:344–354.

Komen GJ, Hasselmann S, Hasselmann K (1984) On the existence of a fully developed wind-sea spectrum, J. Phys. Oceanogr, 14, 1271-1285

Kotlarski S, Keuler K, Christensen OB, Colette A, Déqué M, Gobiet A et al. (2014) Regional climate modeling on European scales: a joint standard evaluation of the EURO-CORDEX RCM ensemble, Geosci. Model Dev, 7, 1297–1333, https://doi.org/10.5194/gmd-7-1297-2014, 2014.

Kourafalou VH (1999) Process studies on the Po River plume, NorthAdriatic Sea. J Geophys Res 104(C12):29963–29985. https:// doi.org/ 10. 1029/ 1999J C9002 17

Kozmar H, Butler K, Kareem A (2012) Transient cross-wind aerodynamic loads on a generic vehicle due to bora gusts. Journal of Wind Engineering and Industrial Aerodynamics, 111, 73–84. https://doi.org/10.1016/j.jweia.2012.09.001

Krasakopoulou E, Souvermezoglou E, Minas HJ, Scoullos M (2005) Organic matter stoichiometry based on oxygen consumption-nutrients regeneration during a stagnation period in Jabuka Pit (middle Adriatic Sea) Cont Shelf Res 25(1):127–142.

Krokos G, Velaoras D, Korres G, Perivoliotis L, Theocharis A (2014) On the continuous functioning of an internal mechanism that drives the Eastern Mediterranean thermohaline circulation: the recent activation of the Aegean Sea as a dense water source area. J Mar Syst 129:484–489

Kröner N, Kotlarski S, Fischer E, Lüthi D, Zubler E, Schär C (2017) Separating climate change signals into thermodynamic, lapse-rate and circulation effects: theory and application to the European summer climate. Clim Dyn 48:3425–3440. https://doi.org/10.1007/s00382-016-3276-3

Kuzmic M, Janekovic I, Book JW, Martin PJ, Doyle JD (2007) Modeling the northern Adriatic double-gyreresponse to intense bora wind: a revisit. J Geophys Res 112:C03S13. doi:10.1029/2005JC003377

Kuzmić M, Grisogono B, Li X, Lehner S (2015) Examining deep and shallow Adriatic bora events. Q J Roy Meteor Soc 141:3434-3438. https://doi.org/10.1002/qj.2578

Laprise R (1992) The Euler Equations of motion with hydrostatic pressure as independent variable, Mon. Weather Rev, 120, 197–207, https://doi.org/10.1175/1520–0493(1992)1202.0.CO;2

Larnicol G, Ayoub N, Le Traon P-Y (2002) Major changes in Mediterranean Sea level variability from 7 years of TOPES/Poseidon and ERS-1/2 data. J Mar Syst 33–34:63–89

Larson J, Jacob R, Ong E (2005) The model coupling toolkit: a new fortran90 toolkit for building multiphysics parallel coupled models, Int. J. High Perform. Comput. Appl, 19, 277–292, https://doi.org/10.1177/1094342005056115

Lavigne H, Civitarese G, Gačić M, D'Ortenzio F (2018) Impact of decadal reversals of the north Ionian circulation on phytoplankton phenology. Biogeosciences 15:4431–4444. https://doi.org/10.5194/bg-15-4431-2018

Lazar M, Pavić M, Pasarić Z, Orlić M (2007) Analytical modelling of wintertime coastal jets in the Adriatic Sea. Cont Shelf Res 27:275–285. https://doi.org/10.1016/j.csr.2006.10.007

Lepri P, Večaj Ž, Kozmar H, Grisogono B (2017) Bora wind characteristics for engineering applications. Wind and Structures, 24, 579–611. https://doi.org/10.12989/was.2017.24.6.579

Li PY, Tanhua T (2020) Recent changes in deep ventilation of the Mediterranean Sea; evidence from long-term transient tracer observations. Front Mar Sci 7:594. https://doi.org/10.3389/fmars.2020.00594

Ličer M, Smerkol P, Fettich A, Ravdas M, Papapostolou A, Mantziafou A et al. (2016) Modeling the ocean and atmosphere during an extreme bora event in northern Adriatic using one-way and two-way atmosphere–ocean coupling, Ocean Sci, 12, 71–86, https://doi.org/10.5194/os-12-71-2016

Lionello P, Malanotte-Rizzoli, P, Boscolo, R, Alpert, P, Artale, V, Li, L et al. (2006) The Mediterranean climate: an overview of the maincharacteristics and issues, in P.Lionello, P.Malanotte-Rizzoli, R.Boscolo (eds) Mediterranean ClimateVariability. Amsterdam: Elsevier (NETHERLANDS), 1-26

Lionello P, Cavaleri L, Nissen KM, Pino C, Raicich F, Ulbrich U (2012a) Severe marine storms in the Northern Adriatic: Characteristics and trends. Phys Chem Earth 40(41):93–105. https://doi.org/10.1016/j.pce.2010.10.002

Lionello P, Galati MB, Elvini E (2012b) Extreme storm surge and wind wave climate scenario simulations at the Venetian littoral. Phys Chem Earth 40(41):86–92. https://doi.org/10.1016/j.pce.2010.04.001

Lipizer M, Partescano E, Rabitti A, Giorgetti A, Crise A (2014) Qualified temperature, salinity and dissolved oxygen climatologies in a changing Adriatic Sea. Ocean Sci 10:771-797. https://doi.org/10.5194/os-10-771-2014

Liu F, Mikolajewicz U, Six KD (2021) Drivers of the decadal variability of the North Ionian Gyre upper layer circulation during 1910–2010: a regional modelling study. Clim Dyn. https://doiorg/10.1007/s00382-021-05714-y

Liuzzo L, Bono E, Sammartano V, Freni G (2017) Long-term temperature changes in Sicily, Southern Italy. Atmos Res 198:44-55. https://doi.org/10.1016/j.atmosres.2017.08.007

Ljubenkov I (2015) Hydrodynamic modeling of stratified estuary: case study of the Jadro River (Croatia), J. Hydrol. Hydromech, 63, 29–37, https://doi.org/10.1515/johh–2015–0001

Ludwig W, Dumont E, Meybeck M, Heussner S (2009) River discharges of water and nutrients to the Mediterranean Sea: major drivers for ecosystem changes during past and future decades?, Prog. Oceanogr, 80, 199–217, https://doi.org/10.1016/j.pocean.2009.02.001

Luettich RA, Birkhahn RH, Westerink JJ (1991) Application of ADCIRC-2DDI to Masonboro Inlet, North Carolina: A brief numerical modeling study, Contractors Report to the US Army Engineer Waterways Experiment Station, August 1991

Macias D, Stips A, Garcia-Gorriz E, Dosio A (2018) Hydrological and biogeochemical response of the Mediterranean Sea to freshwater flow changes for the end of the 21st century. PLoS ONE 13(2): e0192174. https://doi.org/10.1371/journal.pone.0192174

Madsen OS, Poon YK, Graber HC (1988) Spectral wave attenuation by bottom friction: Theory, Proc. 21th Int. Conf. Coastal Engineering, ASCE, 492-504

Malačić V, Petelin B (2009) Climatic circulation in the Gulf of Trieste (northern Adriatic), J. Geophys. Res, 114, C07002, https://doi.org/10.1029/2008JC004904

Malanotte-Rizzoli P et al (1997) A synthesis of the Ionian Sea hydrography, circulation and water mass pathways during POEM Phase I. Prog Oceanogr 39:153–204

Manca B, Giorgetti A (1999) Flow patterns of the main water masses across transversal areas in the southern Adriatic Sea: Seasonal variability. In: Malanotte – Rizoli,P, Eremeev, V.N. (eds), The eastern Mediterranean asa laboratory basin for the assessment of contrasting ecosystems, 495 – 506. Kluwer Academic Publ, Amsterdam

Mann HB (1945) Non-parametric tests against trend. Econometrica13:163–171

Mantziafou A, Lascaratos A (2004) An eddy resolving numerical study of the general circulation and deep-water formation in the Adriatic Sea, Deep Sea Research Part I: Oceanographic Research Papers, Volume 51, Issue 7, Pages 921-952, ISSN 0967-0637, https://doi.org/10.1016/j.dsr.2004.03.006.

Mantziafou A, Lascaratos A (2008) Deep-water formation in the Adriatic Sea: interannual simulations for the years 1979- 1999. Deep-Sea Res. I 55, 1403–1427. https://doi.org/10.1016/j.dsr.2008.06.005

Manzo C, Braga F, Zaggia L, Brando VE, Giardino C, Bresciani M, et al. (2018) Spatio-temporal analysis of prodelta dynamics by means of new satellite generation: the case of Po river by Landsat-8 data. Int J Appl Earth Obs Geoinf 66:210–225. https://doi.org/10.1016/j.jag.2017.11.012

Marchesiello P, McWilliams JC, Shchepetkin A (2001) Open boundary conditions for long–term integration of regional oceanic models, Ocean Model, 3, 1–20, https://doi.org/10.1016/S1463–5003(00)00013–5

Marini M, Russo A, Paschini E, Grilli F, Campanelli A (2006) Shortterm physical and chemical variations in the bottom water of middle Adriatic depressions. Clim Res 31(2/3):227–237. http://www.jstor.org/stable/24869280

Martin PJ, Book JW, Burrage DM, Rowley CD, Tudor M (2009) Comparison of model-simulated and observed currents in the central Adriatic during DART. J Geophys Res 114:C01S05. https://doi.org/10.1029/2008JC004842

Mihanović H, Vilibić I, Carniel S, Tudor M, Russo A, Bergamasco A et al. (2013) Exceptional dense water formation in the Adriatic shelf in the winter of 2012. Ocean science, 9, 561–572

Mihanović H, Vilibić I, Dunić N, Šepić J (2015) Mapping of decadal middle Adriatic oceanographic variability and its relation to the BiOS regime. J Geophys Res 120(8):5615–5630

Mihanović H, Janeković I, Vilibić I, Kovačević V, Bensi M (2018) Modelling interannual changes in dense water formation on the northern Adriatic shelf. Pure and Applied Geophysics, 175, 4065–4081. https://doi.org/10.1007/s00024-018-1935-5

Mihanović H, Vilibić I, Šepić J, Matić F, Ljubešić Z, Mauri E, et al. (2021) Observation, preconditioning and recurrence of exceptionally high salinities in the Adriatic Sea. Front Mar Sci 8:672210. https://doi.org/10.3389/fmars.2021.672210

Milliman J, Bonaldo D, Carniel S (2016) Flux and fate of river–discharged sediments to the Adriatic Sea. Advances in Oceanography and Limnology. 7. 10.4081/aiol.2016.5899

Mlawer EJ, Taubman SJ, Brown PD, Iacono MJ, Clough SA (1997) Radiative transfer for inhomogeneous atmospheres: RRTM, a validated correlated–k model for the longwave, J. Geophys. Res, 102, 16663, https://doi.org/10.1029/97JD00237

Monahan AH, Fyfe JC, Ambaum MHP, Stephenson DB, North GR (2009) Empirical orthogonal functions: the medium is the message. J Clim 22:65016514

Mondal A, Kundu S, Mukhopadhyay A (2012) Rainfall trend analysisby Mann-Kendall test: a case study of north-eastern part of Cut-tack district, Orissa. Int J Geol Earth Environ Sci 2:70–78

Morrison H, Curry JA, Khvorostyanov VI (2005) A New Double-Moment Microphysics Parameterization for Application in Cloud and Climate Models. Part I: Description. J. Atmos. Sci, 62, 1665–1677, https://doi.org/10.1175/JAS3446.1.

Navarra A, Simoncini V (2010) The canonical correlation analysis. A guide to empirical orthogonal functions for climate data analysis. Springer, Dordrecht. https://doi.org/10.1007/978-90-481-3702-2_7

Newman M, Compo GP, Alexander MA (2003) ENSO-forced variability of the Pacific Decadal Oscillation. J Clim 16(23):3853–3857

Nimac I, Herceg-Bulić I, Kalin Cindrić K, Perčec Tadić M (2021) Changes in extreme air temperatures in the mid-sized European city situated on southern base of a mountain (Zagreb, Croatia) Theor Appl Clim 146:429-441. https://doi.org/10.1007/s00704-021-03689-8

Niziol TA, Snyder WR, Waldstreicher JS (1995) Winter weather forecasting throughout the Eastern United States. Part IV: Lake effect snow. Weather and Forecasting, 10, 61–77. https://doi.org/10.1175/1520-0434(1995)010<0061:WWFTTE>2.0.CO;2

Obermann-Hellhund A, Ahrens B (2018) Mistral and tramontane simulations with changing resolution of orography. Atmospheric Science Letters, 19, e848. https://doi.org/10.1002/asl.848

Ogrin D (2015) Long-term air temperature changes in Ljubljana (Slovenia) in comparison to Trieste (Italy) and Zagreb (Croatia) Moravian Geographical Reports, Vol.23 (Issue 3), pp. 17-26. https://doi.org/10.1515/mgr-2015-0014

Oplanić M, Marić AČ, Goreta Ban S, Čop T, Njavro M (2023) Horticultural Farmers' Perceived Risk of Climate Change in Adriatic Croatia. Sustainability, 15(1):539. https://doi.org/10.3390/su15010539

Orlanski I (1976) A simple boundary condition for unbounded hyperbolic flows, J. Comput. Phys, 21, 251–269, https://doi.org/10.1016/0021–9991(76)90023–1

Orlić M, Gačić M, Laviolette P (1992) The currents and circulation of the Adriatic Sea. Oceanologica Acta, 15, 109–124

Orlić M, Dadić V, Grbec B, Leder N, Marki A, Matić F et al. (2007) Wintertime buoyancy forcing, changing seawater properties, and two different circulation systems produced in the Adriatic. J. Geophys. Res. 111, C03S07. https://doi.org/10.1029/2005JC003271.

Pan L-L, Chen S-H, Cayan D, Lin M-Y, Hart Q, Zhang M-H, et al. (2011) Influences of climate change on California and Nevada regions revealed by a high-resolution dynamical downscaling study. Clim Dyn 37:2005–2020. https://link.springer.com/article/10.1007/s00382-010-0961-5

Pano N, Abdyli B (2002) Maximum floods and their regionalization on the Albanian hydrographic river network, in: International Conference on Flood Estimation, 6–8 March 2002, CHR. Report II,17, Bern, Switzerland, 379–388

Pano N, Frasheri A, Avdyli B (2010) The climatic change impact in water potential processe on the Albanian hydrographic river network, in: International Congress on Environmental Modelling and Software, 5–8 July 2010, Ottawa, Ontario, Canada, available at: https://scholarsarchive.byu.edu/iemssconference/2010/all/266

Parras-Berrocal IM, Vazquez R, Cabos W, Sein DV, Álvarez O, Bruno M, et al. (2023) Dense water formation in the Eastern Mediterranean under global warming scenario, EGUsphere [preprint], https://doi.org/10.5194/egusphere-2023-159

Pasarić M, Orlić M (2004) Meteorological forcing of the Adriatic: present vs. projected climate conditions. Geofizika, 21 (1), 69-87. https://hrcak.srce.hr/17008

Pasarić Z, Belušić D, Klaic Z (2007) Orographic influences on the Adriatic sirocco wind. Annales Geophysicae. 25. 10.5194/angeo-25-1263-2007.

Pastor F, Valiente JA, Palau JL (2018) Sea surface temperature in the Mediterranean: Trends and spatial patterns (1982–2016) Pure Appl Geophys 175:4017–4029. https://doi.org/10.1007/s00024-017-1739-z

Pašičko R, Branković Č, Šimić Z (2012) Assessment of climate change impacts on energy generation from renewable sources in Croatia. Renewable Energy, 46, 224–231. https://doi.org/10.1016/j.renene.2012.03.029

Peharda M, Vilibić I, Black BA, Markulin K, Dunić N, Džoić T et al. (2018) Using bivalve chronologies for quantifying environmental drivers in a semi-enclosed temperate sea. Sci Rep 8(1):1–9

Peters H, Lee CM, Orlić M, Dorman CE (2007): Turbulence in the wintertime northern Adriatic Seaunder strong atmospheric forcing. Journal of geophysical research oceans, 112, C03S09

Pinardi N, Zavatarelli M, Adani M, Coppini G, Fratianni C, Oddo P et al. (2015) Mediterranean Sea large-scale low-frequency ocean variability and water mass formation rates from 1987 to 2007: a retrospective analysis. Prog Oceanogr 132:318–332

Pomaro A, Cavaleri L, Lionello P (2017) Climatology and trends of the Adriatic Sea wind waves: Analysis of a 37–year long instrumental data set. International Journal of Climatology. 37. 10.1002/joc.5066.

Poulain PM, Raicich F (2001) Forcings. In: Cushman-Roisin, B, Gačić, M, Poulain, P.M, Artegiani, A. (Eds), Physical Oceanography of the Adriatic Sea: Past, Present and Future. Kluwer Academic Pub, pp. 45–65.

Powley HR, Krom MD, Van Cappellen P (2016) Circulation and oxygen cycling in the Mediterranean Sea: Sensitivity to future climate change. J Geophys Res Oceans 121:8230–8247. https://doi.org/10.1002/2016JC012224

Pranić P, Denamiel C, Vilibić I (2021) Performance of the Adriatic Seaand coast (AdriSC) climate component—a COAWST V3.3-basedone-way coupled atmosphere–ocean modelling suite: Oceanresults. Geosci Model Dev 14:5927–5955. https://doi.org/10.5194/gmd-14-5927-2021

Pranić P, Denamiel C, Janeković I, Vilibić I (2023) Multi-model analysis of the Adriatic dense-water dynamics. 19. 649-670. 10.5194/os-19-649-2023.

Prein AF, Langhans W, Fosser G, Ferrone A, Ban N, Goergen K et al. (2015), A review on regional convection-permitting climate modeling: Demonstrations, prospects, and challenges, Rev. Geophys, 53, 323–361. doi:10.1002/2014RG000475

Prtenjak MT, Grisogono B, Nitis T (2006) Shallow mesoscale flows at the north-eastern Adriatic coast. Q J Roy Meteorol Soc 132:2191-2215. https://doi.org/10.1256/qj.05.41

Prtenjak MT, Belušić D (2009) Formation of reversed lee flow over the north eastern Adriatic during bora. Geofizika 26:145–155.

Prtenjak MT, Viher M, Jurkovic J. (2010) Sea-land breeze development during a summer bora event along the north-eastern Adriatic coast. Q. J. R. Meteorol. Soc. 136: 1554–1571, DOI: 10.1002/qj.649

Pujol M-I, Larnicol G (2005) Mediterranean sea eddy kinetic energy variability from 11 years of altimetric data. J Mar Syst 58(3–4):121–142

Pullen J, Doyle JD, Signell RP (2006) Two-way air–sea coupling: a study of the Adriatic. Mon Weather Rev 134:1465–1483. https://doi.org/10.1175/MWR3137.1

Pullen J, Doyle JD, Haack T, Dorman C, Signell RP, Lee CM (2007) Bora event variability and the role of air-sea feedback. J. Geophys. Res. 112, C03S18. https://doi.org/10.1029/2006JC003726

Qian C, Zhang X, Li Z (2019) Linear trends in temperature extremes in China, with an emphasis on non-Gaussian and serially dependent characteristics. Clim Dyn 53:533–550. https://doi.org/10.1007/s00382-018-4600-x

Querin S, Cossarini G, Solidoro C (2013) Simulating the formation and fate of dense water in a midlatitude marginal sea during normal and warm winter conditions. J Geophys Res Oceans 118:885-900. https://doi.org/10.1002/jgrc.20092

Querin S, Bensi M, Cardin V, Solidoro C, Bacer S, Mariotti L, et al. (2016) Saw-tooth modulation of the deep-water thermohaline properties in the southern Adriatic Sea. J Geophys Res Oceans 121:4585–4600. https://doi.org/10.1002/2015J C011522

Radić J, Savor Z, Puz G (2003) Report: Extreme wind and salt influence on Adriatic bridges. Structural Engineering International, 13(4), 242–245. https://doi.org/10.2749/101686603777964487

Radilović S, Koračin D, Denamiel C, Belušić D, Güttler I, Vilibić I (2020) Simulated and observed air temperature trends in the eastern Adriatic. Atmos Sci Lett. 21:e951. https://doi.org/10.1002/asl.951

Raicich F (1996) On the fresh water balance of the Adriatic Sea. J Mar Syst 9:305-319. https://doi.org/10.1016/S0924-7963(96)00042-5

Raicich F, Malačič V, Celio M, Giaiotti D, Cantoni C, Colucci RR, et al. (2013) Extreme air-sea interactions in the Gulf of Trieste (North Adriatic) during the strong Bora event in winter 2012. J Geophys Res Oceans 118:5238– 5250. https://doi.org/10.1002/jgrc.20398

Ramieri E (2000) : An overview of the vulnerability of Venice to the impacts of climate change and sea level rise, Nota di Lavoro, No. 22. 2000, Fondazione Eni Enrico Mattei (FEEM), Milano

Rasmussen R, Liu C, Ikeda K, Gochis D, Yates D, Chen F et al. (2011) High-resolution coupled climate runoff simulations of seasonal snowfall over Colorado: A process study of current and warmer climate. J Clim 24:3015–3048. https://doi.org/10.1175/2010JCLI3985.1

Rasmussen R, Ikeda K, Liu C, Gochis D, Clark M, Dai A et al. (2014) Climate change impacts on the water balance of the Colorado headwaters: High-resolution regional climate model simulations. J Hydrometeor 15:1091–1116. https://doi.org/10.1175/JHM-D-13-0118.1

Reale M, Salon S, Crise A, Farneti R, Mosetti R, Sannino G (2017) Unexpected covariant behavior of the Aegean and Ionian Seas in the period 1987–2008 by means of a nondimensional sea surface height index. J Geophys Res 122(10):8020–8033

Ricchi A, Miglietta MM, Falco PP, Benetazzo A, Bonaldo D, Bergamasco A et al. (2016) On the use of a coupled ocean–atmosphere–wave model during an extreme cold air outbreak over the Adriatic Sea. Atmos. Res, 172–173, 48–65

Robinson PJ (2001) On the Definition of a Heat Wave. J. Appl. Meteor. Climatol, 40, 762–775, https://doi.org/10.1175/1520-0450(2001)040<0762:OTDOAH>2.0.CO;2

Roether W, Klein B, Manca BB, Theocharis A, Kioroglou S (2007) Transient Eastern Mediterranean deep waters in response to the massive dense-water output of the Aegean Sea in the 1990's. Prog Oceanogr 74:540–571. https://doi.org/10.1016/j.pocean.2007.03.001

Rubino A, Romanenkov D, Zanchettin D, Cardin V, Hainbucher D, Bensi M et al. (2012) On the descent of dense water on a complex canyon system in the southern Adriatic basin. Cont Shelf Res 44:20-29. https://doi.org/10.1016/j.csr.2010.11.009

Rubino A, Gačić M, Bensi M, Kovačević V, Malačič V, Menna M et al. (2020) Experimental evidence of long-term oceanic circulation reversals without wind influence in the North Ionian Sea. Sci Rep 10(1):1–9

de Ruggiero P, Zanchettin D, Bensi M et al. (2018) Water masses in the Eastern Mediterranean Sea: An analysis of measured isotopic oxygen. Pure Appl Geophys 175:4047–4064. https://doi.org/10.1007/s00024-018-1850-9

Rummukainen M (2016) Added value in regional climate modeling. Wires Clim Change 7:145–459. https://doi.org/10.1002/wcc.378

Russo A, Gouveia CM, Dutra E, Soares PMM, Trigo RM (2019) The synergy between drought and extremely hot summers in the Mediterranean. Environ Res Lett 14:014011. https://doi.org/10.1088/1748-9326/aaf09e

Ruti P, Somot S, Giorgi F, Dubois C, Flaounas E, Obermann A et al. (2016) Med-CORDEX initiative for Mediterranean climate studies. Bull Am Meteorol Soc 97:1187–1208. https://doi.org/10.1175/BAMS-D-14-00176.1

Saaroni H, Bitan A, Alpert P, Ziv B (1996) Continental polar outbreaks into the Levant and eastern Mediterranean. Int J Clim 16:1175-1191. https://doi.org/10.1002/(SICI)1097-0088(199610)16:10<1175::AID-JOC79>3.0.CO;2-#

Scorzini AR, Leopardi M (2019) Precipitation and temperature trends over central Italy (Abruzzo Region): 1951-2012. Theor Appl Clim 135:959-977. https://doi.org/10.1007/s00704-018-2427-3

Schär C, Frei C, Luthi D, Davies HC (1996) Surrogate climate-change scenarios for regional climate models. Geophys Res Lett 23:669–672. https://doi.org/10.1029/96GL00265

Schär C, Fuhrer O, Arteaga A, Ban N, Charpilloz C, Di Girolamo S et al. (2020) kilometre-Scale Climate Models: Prospects and Challenges. Bull. Amer. Meteor. Soc, 101, E567–E587, https://doi.org/10.1175/BAMS-D-18-0167.1.

Sein DV, Mikolajewicz U, Gröger M, Fast I, Cabos W, Pinto JG et al. (2015), Regionally coupled atmosphere-ocean-sea ice-marine biogeochemistry model ROM: 1. Description and validation, J. Adv. Model. Earth Syst, 7, 268–304, doi:10.1002/2014MS000357.

Semenov M, Stratonovitch, P (2010) Use of multi-model ensembles from global climate models for assessment of climate change impacts. Climate Research - CLIMATE RES. 41. 1-14. 10.3354/cr00836.

Shaltout M, Omstedt A (2014a) Recent sea surface temperature trends and future scenarios for the Mediterranean Sea. Oceanologia 56:411–443. https://doi.org/10.5697/oc.56-3.411

Shaltout M, Omstedt A (2014b) Recent precipitation trends and future scenarios over the Mediterranean Sea. Geofizika 31:127-150. https://doi.org/10.15233/gfz.2014.31.7

Shchepetkin AF, McWilliams JC (2009) Correction and commentary for "Ocean forecasting in terrain–following coordinates: Formulation and skill assessment of the regional ocean modeling system" by Haidvogel et al, J. Comput. Phys, 227, pp. 3595–3624, J. Comp. Phys. 228, 8985–9000, https://doi.org/10.1016/j.jcp.2009.09.002

Signell RP, Chiggiato J, Horstmann J, Doyle JD, Pullen J, Askari F (2010) High-resolution mapping of bora winds in the northern Adriatic Sea using synthetic aperture radar. Journal of Geophysical Research, 115, C04020. https://doi.org/10.1029/2009JC005524

Simoncelli S, Fratianni C, Pinardi N, Grandi A, Drudi M, Oddo P, et al. (2019) Mediterranean Sea Physical Reanalysis (CMEMS MED–Physics)_ (Version 1) [Data set]. Copernicus Monitoring Environment Marine Service (CMEMS) https://doi.org/10.25423/MEDSEA_REANALYSIS_PHYS_006_004

Skamarock WC, Klemp JB, Dudhia J, Gill DO, Barker DM, Wang W, et al. (2005) A description of the Advanced Research WRF Version 2, NCAR Technical Note NCAR/TN468+STR, http://dx.doi.org/10.5065/D6DZ069T

Smith V, Devane D, Begley CM et al. (2011) Methodology in conducting a systematic review of systematic reviews of healthcare interventions. *BMC Med Res Methodol* **11**, 15 https://doi.org/10.1186/1471-2288-11-15

Smolarkiewicz PK, Grabowski WW (1990) The multidimensional positive definite advection transport algorithm: nonoscillatory option, J. Comput. Phys, 86, 355–375, https://doi.org/10.1016/0021–9991(90)90105–A

Somot S, Sevault F, Déqué M (2006) Transient climate change scenario simulation of the Mediterranean Sea for the twenty-first century using a high-resolution ocean circulation model. Clim Dyn 27:851-879. https://doi.org/10.1007/s00382-006-0167-z

Soto-Navarro J, Jordá G, Amores A, Cabos W, Somot S, Sevault F, et al. (2020) Evolution of Mediterranean Sea water properties under climate change scenarios in the Med-CORDEX ensemble. Climate Dynamics, 54, 2135–2165. https://doi.org/10.1007/s00382-019-05105-4

Soukissian T, Karathanasi F, Axaopoulos P, Voukouvalas E, Kotroni V (2017) Offshore wind climate analysis and variability in the Mediterranean Sea. Int J Climatol 38:384–402. https://doi.org/10.1002/joc.5182

Stiperski I, Ivančan-Picek B, Grubišić V, Bajić A (2012) Complex bora flow in the lee of Southern Velebit. Q J Roy Meteor Soc 138:1490-1506. https://doi.org/10.1002/qj.1901

Stocchi P, Davolio S (2017) Intense air-sea exchanges and heavy orographic precipitation over Italy: The role of Adriatic Sea surface temperature uncertainty. Atmospheric Research, 196, 62–82. https://doi.org/10.1016/j.atmosres.2017.06.004

Škreb S et al. (1942) Climate of Croatia (in Croatian) Geophysical lnstitute, Zagreb, 140 pp.

Theocharis A, Krokos G, Velaoras D, Korres G (2014) An internal mechanism driving the alternation of the Eastern Mediterranean dense/deep water sources. Mediterr Sea 10:113–137

Tojčić I, Denamiel C, Vilibić I (2023) Kilometre–scale trends and variability of the Adriatic present climate (1987–2017), Clim. Dyn., vol. 61, no. 5–6, Springer, pp. 2521–2545, DOI: 10.1007/s00382–023–06700–2

Tojčić I, Denamiel C, Vilibić I (2024) Kilometre-scale trends, variability, and extremes of the Adriatic far-future climate (RCP 8.5, 2070−2100), Frontiers in Marine Science

Tolle MH, Gutjahr O, Busch G, Thiele JC (2014) Increasing bioenergy production on arable land: Does the regional and local climate respond? Germany as a case study. J Geophys Res Atmos 119:2711–2724. https://doi.org/10.1002/2013JD020877

Torresan S, Gallina V, Gualdi S, Bellafiore D, Umgiesser G, Carniel S et al. (2019) Assessment of Climate Change Impacts in the North Adriatic Coastal Area. Part I: A Multi-Model Chain for the Definition of Climate Change Hazard Scenarios. Water, 11(6):1157. https://doi.org/10.3390/w11061157

Totti C, Romagnoli T, Accoroni S, Coluccelli A, Pellegrini M, Campanelli A, et al. (2019) Phytoplankton communities in the northwestern Adriatic Sea: Interdecadal variability over a 30-years period (1988–2016) and relationships with meteoclimatic drivers. J Mar Syst 193:137-153. https://doi.org/10.1016/j.jmarsys.2019.01.007

Trigo IF, Davies TD (2002) Meteorological conditions associated with sea surges in Venice: a 40 year climatology. Int J Climatol 22:787–803. https://doi.org/10.1002/joc.719

Trošić T, Trošić Z (2010) Numerical simulation and observational analysis of the wrinkles of Pag's ribs. Boundary-Layer Meteorology, 134, 353–366. https://doi.org/10.1007/s10546-009-9439-6

Tsimplis M, Marcos M, Somot S, Barnier B (2008) Sea-level forcing in the Mediterranean Sea between 1960 and 2000. Global Planet. Change 63(4):325–332. https://doi.org/10.1016/j.gloplacha.2008.07.004

Umgiesser G, Ferrarin C, Bajo M, Bellafiore D, Cucco A, De Pascalis F et al. (2022) Hydrodynamic modelling in marginal and coastal seas — The case of the Adriatic Sea as a permanent laboratory for numerical approach, Ocean Model, 179, 102123, 1463-5003, https://doi.org/10.1016/j.ocemod.2022.102123.

Umlauf L, Burchard H (2003) A generic length–scale equation for geophysical turbulence models, J. Mar. Res, 61, 235–265, https://doi.org/10.1357/002224003322005087

Vargas-Yanez M, Garcia-Martinez MC, Moya F, Balbin R, Lopez-Jurado JL, Serra M et al. (2017) Updating temperature and salinity mean values and trends in the Western Mediterranean: The RADMED project. Prog Oceanogr 157:27-36. https://doi.org/10.1016/j.pocean.2017.09.004

Vautard R, Gobiet A, Jacob D, Belda M, Colette A, Déqué M et al. (2013) The simulation of European heat waves from an ensemble of regional climate models within the EURO-CORDEX project. Clim Dyn 41:2555–2575. https://doi.org/10.1007/s00382-013-1714-z

Velaoras D, Krokos G, Nittis K, Theocharis A (2014) Dense intermediate water outflow from the Cretan Sea: a salinity driven, recurrent phenomenon, connected to thermohaline circulation changes. J Geophys Res 119(8):4797–4820

Vicente-Serrano SM, Nieto R, Gimeno L, Azorin-Molina C, Drumond A, El Kenawy A, et al. (2018) Recent changes of relative humidity: regional connections with land and ocean processes. Earth Syst Sci 9:915-937. https://doi.org/10.5194/esd-9-915-2018

Vilibić I, Orlić M (2002): Adriatic water masses, their rates of formation and transport through the OtrantoStrait. Deep–sea research, I 49, 1321 – 1340

Vilibić I, Grbec B, Supić N (2004) Dense water generation in the north Adriatic in 1999 and its recirculation along the Jabuka Pit. Deep Sea Res Part I 51:1457–1474. https://doi.org/10.1016/j. dsr.2004.07.012

Vilibić I, Supić N (2005) Dense water generation on a shelf: the case of the Adriatic Sea. Ocean Dynamics 55,403–415.

Vilibić I, Book JW, Beg Paklar G, Orlić M, Dadić V, Tudor M et al. (2009) West Adriatic coastal water excursions into the East Adriatic. Journal of Marine Systems 78:S132–S156.

Vilibić I, Mihanović H, Šepić J, Matijević S (2011) Using Self-Organising Maps to investigate long-term changes in deep Adriatic water patterns. Cont Shelf Res 31:695-711. https://doi.org/10.1016/j.csr.2011.01.007

Vilibić I, Šepić J, Proust N (2013) Weakening thermohaline circulation in the Adriatic Sea. Climate Research. 55. 217-225. 10.3354/cr01128.

Vilibić I Pištalo D, Šepić J (2015) Long-term variability and trends of relative geostrophic currents in the middle Adriatic. Cont Shelf Res 93:70-80. https://doi.org/10.1016/j.csr.2014.12.003

Vilibić I, Mihanović H, Janeković I, Šepić J (2016) Modelling the formation of dense water in the northern Adriatic: Sensitivity studies, Ocean Modelling, Volume 101, Pages 17-29, ISSN 1463-5003, https://doi.org/10.1016/j.ocemod.2016.03.001.

Vilibić I, Mihanović H, Janeković I, Denamiel C, Poulain PM, Orlić M et al. (2018) Dense water formation in the coastal northeastern Adriatic Sea: The NAdEx 2015 experiment. Ocean Science, 14, 237–258. https://doi.org/10.5194/os-14-237-2018

Vilibić I, Zemunik P, Šepić J, Dunić N, Marzouk O, Mihanović H et al. (2019) Present climate trends and variability in thermohaline properties of the northern Adriatic shelf, Ocean Sci, 15, 1351–1362, https://doi.org/10.5194/os–15–1351–2019

Vilibić I, Zemunik P, Dunić N, Mihanović H (2020) Local and remote drivers of the observed thermohaline variability on the northern Adriatic shelf (Mediterranean Sea) Cont Shelf Res 199:104110. https://doi.org/10.1016/j.csr.2020.104110

Vilibić I, Pranić P, Denamiel C (2023), North Adriatic Dense Water: lessons learned since the pioneering work of Mira Zore–Armanda 60 years ago, Acta Adriatica, Vol. 64 No. 1, https://doi.org/10.32582/aa.64.1.11

Viličić D (2014) Specific oceanological characteristics of the Croatian part of the Adriatic. Hrvatske Vode. 22. 297–314

Vosper S, Ross A, Renfrew I, Sheridan P, Elvidge A, Grubišić V (2018) Current challenges in orographic flow dynamics: Turbulent exchange due to low-level gravity-wave processes. Atmosphere, 9, 361. https://doi.org/10.3390/atmos9090361

Vörösmarty C, Fakers B, Tucker B (1996) River discharge database, version 1.0 (RivDIS vLO), volumes 0 through 6, in: A contribution to IHP–V Theme 1, Technical Documents Series, Technical report, UNESCO, Paris, France

Wang XH, Oddo P, Pinardi N (2006) On the bottom density plume on coastal zone off Gargano (Italy) in the southern Adriatic Sea and its interannual variability. J Geophys Res 111:C03S17. https://doi.org/10.1029/2005JC003110

Warner JC, Armstrong B, He R, Zambon JB (2010) Development of a Coupled Ocean–Atmosphere–Wave–Sediment Transport (COAWST) Modeling System. Ocean Model. 35, 230–244. https://doi.org/10.1016/j.ocemod.2010.07.010

Weatherall P, Marks KM, Jakobsson M, Schmitt T, Tani S, Arndt JE et al. (2015) A new digital bathymetric model of the world's oceans, Earth and Space Science, 2, 331–345, https://doi.org/10.1002/2015EA000107

World Climate Research Programme (2022) Report of the WCRP km–scale modeling workshop, 8/2022, 3–7 October 2022, hybrid format

Yari S, Kovačević V, Cardin V, Gačić M, Bryden HL (2012) Direct estimate of water, heat, and salt transport through the Strait of Otranto. J Geophys Res Oceans 117:C09009. https://doi.org/10.1029/2012JC007936

Yoshino MM (1976) Local wind bora (289pp) Tokyo, Japan: University of Tokyo Press.

Zaninović K, Gajić-Čapka M, Perčec Tadić M, Vučetić M, Milković J, Bajić A et al. (2008) Klimatski atlas Hrvatske / Climate atlas of Croatia 1961–1990, 1971–2000. Meteorological and Hydrological Service of the Republic of Croatia, Zagreb, 200 pp

Zavatarelli M, Pinardi N, Kourafalou VH, Maggiore A (2002) Diagnostic and prognostic model studies of the Adriatic Sea general circulation: Seasonal variability. J Geophys Res Oceans 107:3004. https://doi.org/10.1029/2000JC000210

Zängl G, Hornsteiner M (2007) Can trapped gravity waves be relevant for severe foehn windstorms? A case study. Meteorol Z 16:203–212. https://doi.org/10.1127/0941-2948/2007/0199

Zhang Y, Wallace JM, Battisti DS (1997) ENSO-like interdecadal variability. J Clim 10:1004–1020

Zittis G, Bruggeman A, Lelieveld J (2021) Revisiting future extreme precipitation trends in the Mediterranean, Weather and Climate Extremes, Volume 34, 100380, ISSN 2212-0947, https://doi.org/10.1016/j.wace.2021.100380

Zore M (1963) Les masses d'eau de la mer Adriatique. Acta Adriat 10:5–88

Zore–Armanda Mira (1969) Water exchange between the Adriatic and the Eastern Mediterranean, Deep Sea Research and Oceanographic Abstracts, Volume 16, Issue 2, Pages 171–178, ISSN 0011–7471, https://doi.org/10.1016/0011-7471(69)90072-2

Zore-Armanda M, Gačić M (1987) Effects of Bora on the circulation in the north Adriatic. Ann Geophys 5B:93–102

9. CURRICULUM VITAE

Iva Tojčić, born on July 2nd 1995 in Split, Croatia, graduated in September 2019 from the Faculty of Science at the University of Split, with a specialisation in Environmental Physics. She is a recipient of two dean's awards from the Faculty of Science in Split and the rector's award for excellence from the University of Split. After obtaining a master's degree in physics, she was employed at the Institute of Oceanography and Fisheries in Split on the Interreg project "Change We Care" and enrolled in the Interdisciplinary PhD Programme in Oceanology at the University of Zagreb in October 2020. In November 2021, she started working as a research assistant at the Ruđer Bošković Institute in Zagreb, in the Laboratory for physical oceanography and chemistry of aquatic systems. Additionally, for two consecutive academic years, she taught courses in Physics in Forensic Sciences and Applied Physics in Forensic Sciences as part of the undergraduate programme at the University Department of Forensic Sciences in Split. Since June 2024, she is employed as an assistant in the Department of Physics at the Faculty of Science in Split. She is also active in promoting science among children and the general population as the founder and president of the Association for the Popularisation of Science, Eureka. In this role, she led two national and participated in coordinating activities in two international projects aimed at developing competencies in STEM areas for children and teachers.

Her area of scientific research includes analysing the results of simulations of a coupled atmosphere-ocean model with ultra-high resolution in the Adriatic Sea, coastal modelling in the Adriatic, identifying climate trends, variability, and extremes, as well as biogeochemical modelling in the Adriatic Sea.

In her scientific career so far, Iva Tojčić has published nine scientific papers indexed in CC. She is the first author of three of these papers, and eight have been published in Q1 and Q2-ranked international journals with high impact factors. She has orally presented her research at seven international scientific conferences as the first author of the abstract. She completed an international scientific school organised by the European Space Agency and is a recipient of the British Scholarship Trust scholarship for professional specialisation in the United Kingdom, where she spent two months at the Plymouth Marine Laboratory. Iva has actively participated as a researcher in five scientific projects and is currently the principal investigator of the ECMWF Special Project “Adriatic Sea Climate: Towards Kilometre-Scale Biogeochemical Modelling”.

10. PUBLISHED SCIENTIFIC PAPERS

1. **Tojčić I**, Denamiel C and Vilibić I (2024) Kilometre-scale trends, variability, and extremes of the Adriatic far-future climate (RCP 8.5, 2070−2100), Front. Mar. Sci. 11:1329020, doi: 10.3389/fmars.2024.1329020
2. **Tojčić I**, Denamiel C, Vilibić I (2023) Kilometre–scale trends and variability of the Adriatic present climate (1987–2017), Clim. Dyn., vol. 61, no. 5–6, Springer, pp. 2521–2545, DOI: 10.1007/s00382–023–06700–2
3. Marušić M, **Tojčić I**, Alešković LM (2023) Onečišćenje bukom i svjetlošću na području grada Splita – sadašnje stanje i vizija budućnosti. Kemija u industriji: časopis kemičara i tehnologa Hrvatske, 72, 5-6; 331-338, DOI: https://doi.org/10.15255/KUI.2022.070
4. Denamiel C, **Tojčić I**, Pranić P et al. (2022) Modes of the BiOS-driven Adriatic Sea thermohaline variability. Clim Dyn 59, 1097–1113. https://doi.org/10.1007/s00382-022-06178-4
5. Denamiel C, **Tojčić I,** Vilibić I (2022) Meteotsunamis in Orography–Free, Flat Bathymetry and Warming Climate Conditions. J Geophys Res Ocn, 127, e2021JC017386, DOI:10.1029/2021JC017386
6. Denamiel C, **Tojčić I**, Vilibić I (2021) Balancing accuracy and efficiency of atmospheric models in the northern Adriatic during severe bora events. J Geophys Res Atmos 126:e2020JD033516. https://doi. org/10.1029/2020JD033516
7. Denamiel C, Pranić P, Ivanković D, **Tojčić I**, Vilibić I (2021) Performance of the Adriatic Sea and coast (AdriSC) climate component—a COAWST V3.3-based coupled atmosphere–ocean modelling suite: atmospheric dataset. Geosci Model Dev 14:3995–4017. https:// doi. org/ 10. 5194/ gmd- 14- 3995- 2021
8. **Tojčić I**, Denamiel C, Vilibić I (2021) Performance of the Adriatic early warning system during the multi–meteotsunami event of 11–19 May 2020: an assessment using energy banners, Nat. Hazards Earth Syst. Sci., 21, 2427–2446, https://doi.org/10.5194/nhess-21-2427-2021
9. Denamiel C, **Tojčić I**, Vilibić I (2020) Far future climate (2060–2100) of the northern Adriatic air–sea heat transfers associated with extreme bora events. Clim Dyn 55:3043–3066. https://doi.org/10.1007/s00382-020-05435-8